

2015 | Faculty of Sciences

DOCTORAL DISSERTATION

Pathways toward increased efficiency and lifetime of organic photovoltaics

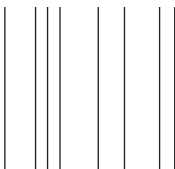
Doctoral dissertation submitted to obtain the degree of
Doctor of Science: Chemistry, to be defended by

Jurgen Kesters

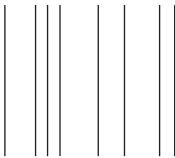
Promoter: Prof. Dr Wouter Maes | UHasselt

Co-promoters: Prof. Dr Jean Manca | UHasselt

Prof. Dr Dirk Vanderzande | UHasselt



D/2015/2451/8



Chairman:	Prof. Dr. Karin Coninx
Promoter:	Prof. Dr. Wouter Maes
Copromoters:	Prof. Dr. Jean Manca Prof. Dr. Dirk Vanderzande
Members of the jury:	Dr. Laurence Lutsen, IMO-IMOMEC Prof. Dr. Peter Adriaensens, UHasselt Dr. Eva Bundgaard, Technical University of Denmark Prof. Dr. Bruno Van Mele, Vrije Universiteit Brussel

DANKWOORD

Eindelijk, het dankwoord, een stukje tekst waar ik niet moet letten op spelling, zinsbouw, taalgebruik, etc. De afgelopen vier jaren zijn wel zeer snel voorbijgevlogen en de vele mensen die ik gedurende die periode heb mogen leren kennen hebben het op z'n minst uiterst plezant gemaakt. Daarom dat ik ook de volgende pagina's wil spenderen om een dikke merci over te dragen aan iedereen voor de vele toffe momenten, evenals voor een succesvolle afwerking van dit onderzoekswerk, ervan uitgaande dat ik hier dus hopelijk niemand vergeet te vermelden ...

Allereerst zou ik mijn promotor, Prof. dr. Wouter Maes, willen bedanken. Ook al was het startschot van mijn doctoraat een beetje stroef (projectgewijs), toch denk ik dat we best tevreden mogen zijn met het eindresultaat en wat we voorlopig hebben kunnen bereiken. Al vanaf het begin was het mij duidelijk dat je zeer gedreven was in wat je deed. Tijdens het verbeteren van de artikels was je dan ook zeer kritisch en ging je gedetailleerd te werk, wat me toch wel geholpen heeft om een niveautje verder te geraken op dit vlak. Natuurlijk moest er af en toe eens afgereageerd kunnen worden, maar gelukkig hebben we daar een tennisnet tussen kunnen plaatsen, en de introductie in Zelem was uiterst aangenaam. Dus bij deze, voor alles, thanks!!!

Mijn eerste copromotor, Prof. dr. Jean Manca, zou ik uiteraard ook willen bedanken. Aangezien de meeste van mijn activiteiten plaatsvonden aan de kant van de fysica, is het natuurlijk ook duidelijk dat jij deel zou uitmaken van dit doctoraatsavontuur. Hetgeen mij het meest opviel vanaf het moment dat ik in je

Dankwoord

bureau binnenstapte was je vrolijkheid en motivatie voor het wetenschappelijke veld, en het gemak waarop je mensen kan motiveren. De bijnaam 'mister cool' zal ik waarschijnlijk ook niet meer kunnen afschudden? Bedankt voor de kans die je mij gegeven hebt en me in je groep hebt toegelaten.

Vervolgens verdient mijn tweede copromotor, Prof. dr. Dirk Vanderzande, ook een dank-je-wel. Ik was best wel aangenaam verrast door je sociaal en open karakter (en dat gevoel werd ook wel eens bevestigd op één van de BPG-feestjes), en dat is een prachtig kenmerk voor iemand in jouw positie. Hetgeen me altijd is bijgebleven is ons preliminair sollicitatie-telefoontje 4 jaar geleden, waardoor jij eigenlijk aan de bakermat stond van dit doctoraat, waarvoor dank. Natuurlijk mag ik ook onze zeiltrip van eerder dit jaar niet vergeten. Het was werkelijk een super ervaring, en hopelijk kunnen we volgende keer effectief Engeland bereiken.

Not to forget, dr. Laurence Lutsen, thank you very much for everything. Through our small discussions, you were always able to show me a different side to every story. Also, thank you for giving me the opportunities to visit various conferences, allowing me to meet a lot of new people in our field of research.

Of course, I would also like to thank the other members of the jury for taking the time to evaluate this work.

Het volgende stukje zou ik willen toewijden aan mijn directe collega's, die natuurlijk voor een groot deel voor alle fijne tijden die we hier samen hebben beleefd hebben ingestaan. Laten we er dan ook maar geen doekjes om draaien, dit is waarschijnlijk het enige wat de meesten gaan lezen (☺). Aangezien ik met hun nog het meeste contact heb gehad, en zij het hebben uitgehouden met mij

al die jaren, verdienen zij toch ook wel een dank-je-wel. Als lid van twee verschillende groepen loopt dit aantal wel een beetje op, dus laten we hopen dat ik hier nu niemand ga vergeten ... Allereerst een klein woordje voor het vaste personeel. Iris, dank je wel voor de plezante babbeltjes. Huguette, bedankt voor je onmiddellijke paraatheid als het op metingen aankwam. Je kennis van bepaalde technieken was zeer behulpzaam, en je verdient zeker alle lof hiervoor. Gunther, je was altijd zo een beetje een vaderfiguur voor de groep, een zeer harde werker en toch ook altijd klaar voor een lach en babbel. I wish you the best of luck with everything! Prof. dr. Jan D'Haen, bedankt voor de TEM metingen, die de verhalen toch elke keer een stukje specialer maakten. Christel, Hilde, bedankt voor het goede opvolgen van de bestellingen, zodat wij arme doctoraatsstudentjes altijd voort konden met ons onderzoek. Johnny man, ik vermoed dat ik je vaak genoeg het bloed onder de nagels uit heb gehaald met mijn 'plezante' opmerkingen, maar bij deze ga ik dat meteen rechtzetten. Merci voor de snelle ingrepen die (vaak) voor kwamen bij het gebruik van de gloveboxen. Zonder jouw aanwezigheid zou het onderzoek 100 keer trager zijn verlopen. Ik denk dat het IMO misschien wel letterlijk uit elkaar zou kunnen vallen zonder alles wat je daar 'fixed'. Ook de 'oude' garde mag ik natuurlijk niet vergeten in dit plaatje. Sarah, vanaf het moment dat ik jouw motivatie zag, wist ik dat je een soort rolmodel zou zijn voor komende doctoraatsstudenten, waaronder mezelf. Ans, de chille bureaugenoot aan ons eilandje, veel succes met je dochttertje, je doet dat waarschijnlijk super. Toon, ook al lukt het me momenteel niet meer echt om te komen opdagen, merci om mij te introduceren tot het klimmen, en natuurlijk niet te vergeten, de plezante samenwerking. Inge, mijn bureaubuur gedurende toch wel een lange periode, veel succes met je nieuwe job. Tommeke, mister festival of mister PhD-presentation (ik kon niet

Dankwoord

kiezen), veel succes nog met het afronden van je doctoraat. Wouter V., bedankt voor de meerdere, mooie en zeer succesvolle samenwerkingen. Je was hier maar 2 jaar aanwezig als post-doc, maar ik denk dat je een zeer goed voorbeeld bent geweest voor een heel aantal mensen. Ook jij veel succes met je nieuwe job, ook al is het waarschijnlijk een beetje aanpassen met het aanmaken van kg'en in plaats van mg'en. Natuurlijk, de huidige generatie van collega's mogen we ook niet vergeten. Pieter, ik kende je al een beetje voor onze tijd hier in Hasselt, maar de afgelopen vier jaren hebben me laten inzien wat voor een goede gast je bent, en hoe fel je gegroeid bent in de onderzoekswereld. Ik weet ook dat ik wel vaak achter je veren aanzat, dus bedankt dat je mij al die tijd hebt getolereerd. Jeroen D., AFM-superman, merci voor de 10000'den metingen te doen waarmee ik je heb opgezadeld. Ook al bleef ik de stalen maar opstapelen, ik hoorde je (bijna) nooit klagen, wat dan toch ook gelukkig heeft uitgedraaid tot een aantal mooie publicaties. Geert, Joris, "Mingeh!!" wie heeft die gasten hier losgelaten. Buiten plezante collega's zijn jullie dan ook uiteraard nog eens goei kameraden. Het afgelopen jaar was al super, maar ik denk dat we zo nog wel eventjes kunnen doorgaan. "Schol hé boys!" Tim, de happy man, altijd zo enthousiast en opgewekt (na half 10 dan toch), bedankt voor de snelheid van de verschillende metingen, en voor het helpen nadenken over die vervelende probleempjes die we tegenkwamen. Ook nog veel succes met de muziek, maar dat komt wel in orde. Joke, tennis dubbelpartner van het jaar, merci voor de mooie matches (en overwinningen)! Natuurlijk ook Rafaël niet vergeten, bedankt voor de hulp toen ik even het noorden kwijt was met al die sectie- en pagina-eindes ... Of course, I would also like to thank all the other colleagues for all the fun times; Julija (small molecules yeah!), Yasmine, Sanne, Mathias (laat die porfyrines maar lopen), Jeroen, Vero, Evelien, Joachim,

Benjamin, Stephan, Kayte, Ya-Mi, Rebekka, Brecht, David, Tien, Bert, Sabine, Wim, Lien, Wouter D., Ilaria, Dieter, Mirco, Koen, Sien, Jeroen S., Inge V., I wish you all the best of luck in everything you do!

Nu (denk ik) dat ik nog maar één iemand aan dit lijstje moet toevoegen, maar ze verdient wel een apart paragraafje. Neomy, je bent een fantastische steun en toeverlaat geweest het afgelopen jaar. Je begreep elke keer opnieuw als er me iets dwars zat, en je tolereerde ook dat ik sommige periodes, zeker naar het einde toe, iets minder tijd had. Je gaat dit zelf nog allemaal fantastisch doen. Ik zie je graag!

Next I would also like to thank all the people I was able to collaborate with. To start off, thank you to everyone from Solliance. Attending the regular meetings showed me the high potential of our field of research. Afshin, Eszter, David, Bregt, Tom, and all the others from IMEC, thank you for everything that you taught me. Of course, I cannot forget to thank you as well for your amazing hospitality during our troubling times without the glovebox at the UHasselt. Especially to Afshin, thank you for taking your time to teach me pretty much everything on OPV processing. To the people from Eindhoven (Alice, Serkan, Koen, Gijs, Hans, ...), thanks for the wonderful times at the HOPV conference in Sevilla (I still keep thinking about that one tapas bar).

De mensen van de Vrije Universiteit Brussel, Prof. dr. Bruno Van Mele, Niko, Maxime, jullie bijdrage inzake thermische analyses leverde altijd een grote meerwaarde aan al de verschillende projecten die we hebben kunnen afleveren. Niko, dank je wel voor alle metingen, interpretaties en je gastvrijheid om me alles eens in detail te tonen tijdens een rondleiding.

Dankwoord

Prof. dr. Benoît Champagne (Laboratoire de Chimie Théorique, Namur), thank you for the theoretical calculations. They showed to be an added value to our work for several articles.

Tenslotte mag ik nog drie belangrijke mensen zeker niet vergeten te bedanken. Als eerste, mijn ouders, voor alle steun en kansen die ze me ooit hebben gegeven. Twee jaren geleden zijn we begonnen aan ons eigen grote zijproject, het huis, en daarvoor wil ik jullie nogmaals zeer hard bedanken. Zonder jullie had ik dit nooit allemaal kunnen verwezenlijken in combinatie met een doctoraat. Nancy, 'grote' zus, bedankt voor al je steun over al die jaren. De vele telefoontjes zijn altijd al een goede uitlaatklep geweest voor als er me iets dwarszat, en je stond altijd wel klaar om te luisteren (tenzij je weer eens niet opnam ☺).

THANKS!!!

Jurgen

CONFERENCE PRESENTATIONS

J. Kesters, T. Ghooos, H. Penxten, J. Drijkoningen, T. Vangerven, L. Lutsen, D. Vanderzande, J. Manca, W. Maes, *Efficiency enhancement by incorporation of imidazolium-substituted polythiophenes as electron transport layers in organic photovoltaics*, Hybrid and Organic Photovoltaics Conference (HOPV) 2013, 05.05.2013 – 08.05.2013, Sevilla, Spain.

J. Kesters, T. Ghooos, J. Drijkoningen, T. Vangerven, L. Lutsen, D. Vanderzande, W. Maes, *Imidazolium-substituted polythiophenes as efficient electron transport materials improving photovoltaic performance*, Belgian Polymer Group (BPG) Meeting 2013, 16.05.2013 – 17.05.2013, Houffalize, Belgium.

*** **Best Presentation Award** ***

J. Kesters, J. Drijkoningen, B. Conings, S. Clément, L. Lutsen, D. Vanderzande, J. Manca, W. Maes, *Efficiency enhancement of organic photovoltaics by incorporation of interfacial layers*, Koninklijke Vlaamse Chemische Vereniging (KVCV), ChemCYS (Chemistry Conference for Young Scientists) 2014, 27.02.2014 – 28.02.2014, Blankenberge, Belgium.

*** **Best Presentation Award** ***

J. Kesters, J. Drijkoningen, B. Conings, S. Clément, L. Lutsen, D. Vanderzande, J. Manca, W. Maes, *Efficiency enhancement of organic photovoltaics by incorporation of interfacial layers*, Materials Research Society (MRS) Spring Meeting 2014, 21.04.2014 – 25.04.2014, San Francisco, US.

LIST OF PUBLICATIONS

J. Vandenberg, B. Conings, S. Bertho, J. Kesters, D. Spoltore, S. Esiner, J. Zhao, G. Van Assche, M.M. Wienk, W. Maes, L. Lutsen, B. Van Mele, R.A.J. Janssen, J. Manca, D. Vanderzande, *Thermal stability of poly[2-methoxy-5-(2'-phenylethoxy)-1,4-phenylene vinylene] (MPE-PPV):fullerene bulk heterojunction solar cells*, *Macromolecules*, **2011**, *44*, 8470.

- Device preparation, degradation studies, characterization and analysis

S. Van Mierloo, A. Hadipour, M.-J. Spijkman, N. Van den Brande, B. Ruttens, J. Kesters, J. D'Haen, G. Van Assche, D.M. de Leeuw, T. Aernouts, J. Manca, L. Lutsen, D. Vanderzande, W. Maes, *Improved photovoltaic performance of a semicrystalline narrow bandgap copolymer based on 4H-cyclopenta[2,1-b:3,4-b']dithiophene donor and thiazolo[5,4-d]thiazole acceptor units*, *Chem. Mater.*, **2012**, *24*, 587.

- Device optimization, characterization and data analysis

N. Nevil, Y. Ling, S. Van Mierloo, J. Kesters, F. Piersimoni, P. Adriaensens, L. Lutsen, D. Vanderzande, J. Manca, W. Maes, S. Van Doorslaer, E. Goovaerts, *Charge transfer in the weak driving force limit in blends of MDMO-PPV and dithienylthiazolo[5,4-d]thiazoles towards organic photovoltaics with high Voc*, *Phys. Chem. Chem. Phys.*, **2012**, *14*, 15774.

- Device optimization, characterization and data analysis

Publications

B.J. Campo, D. Bevk, J. Kesters, J. Gilot, H. Bolink, J. Zhao, J.-C. Bolsée, W.D. Oosterbaan, S. Bertho, J. D'Haen, J. Manca, L. Lutsen, G. Van Assche, W. Maes, R.A.J. Janssen, D. Vanderzande, *Ester-functionalized poly(3-alkylthiophene) copolymers: Synthesis, physicochemical characterization and performance in bulk heterojunction organic solar cells*, Org. Electron., **2013**, 14, 523.

- Device optimization, characterization and data analysis

J. Kesters, T. Ghooos, H. Penxten, J. Drijkoningen, T. Vangerven, D.M. Lyons, B. Verreert, T. Aernouts, L. Lutsen, D. Vanderzande, J. Manca, W. Maes, *Imidazolium-substituted polythiophenes as efficient electron transport materials improving photovoltaic performance*, Adv. Energy Mater., **2013**, 9, 1180.

- Article writing
- Device optimization, characterization and data analysis

D.M. Lyons, J. Kesters, W. Maes, C.W. Bielawski, J.L. Sessler, *Improving efficiencies by modulating the central metal ion in porphyrin-oligothiophene-mediated P3HT/PCBM organic solar cells*, Synth. Metals, **2013**, 178, 56.

- Supervision
- Device preparation, characterization and data analysis

J. Kesters, S. Kudret, S. Bertho, N. Van den Brande, M. Defour, B. Van Mele, H. Penxten, L. Lutsen, J. Manca, D. Vanderzande, W. Maes, *Enhanced intrinsic stability of the bulk heterojunction active layer blend of polymer solar cells by varying the polymer side chain pattern*, Org. Electron., **2014**, 15, 549.

- Article writing
- Device optimization, degradation studies, characterization and analysis

S. Kudret, J. Kesters, S. Janssen, N. Van den Brande, M. Defour, B. Van Mele, J. Manca, L. Lutsen, D. Vanderzande, W. Maes, *Facile synthesis of 3-(ω -acetoxyalkyl)thiophenes and derived copolythiophenes using Rieke zinc*, *React. Funct. Polym.*, **2014**, *75*, 22.

- Device optimization, characterization and data analysis

J. Drijkoningen, J. Kesters, T. Vangerven, L. Lutsen, D. Vanderzande, W. Maes, J. D'Haen, J. Manca, *Investigating the role of efficiency enhancing interlayers for bulk heterojunction solar cells by scanning probe microscopy*, *Org. Electron.*, **2014**, *15*, 1282.

- Device optimization, characterization and data analysis

W. Vanormelingen, J. Kesters, P. Verstappen, J. Drijkoningen, J. Kudrjasova, S. Koudjina, V. Liégeois, B. Champagne, J. Manca, L. Lutsen, D. Vanderzande, W. Maes, *Enhanced open-circuit voltage in polymer solar cells by dithieno[3,2-*b*:2',3'-*d*]pyrrole *N*-acylation*, *J. Mater. Chem. A*, **2014**, *2*, 7535.

- Device optimization, characterization and data analysis

I. Cardinaletti, J. Kesters, S. Bertho, B. Conings, F. Piersimoni, J. D'Haen, L. Lutsen, M. Nesladek, B. Van Mele, G. Van Assche, K. Vandewal, A. Salleo, D. Vanderzande, W. Maes, J. Manca, *Toward bulk heterojunction polymer solar cells with thermally stable active layer morphology*, *J. Photon. Energy*, **2014**, *4*, 040997.

- Article revision & contribution to writing

Publications

S.A. Gevorgyan, R. Pacios, J. Ajuria, I. Etxebarria, J.P. Kettle, N.D. Bristow, M. Neophytou, S.A. Choulis, L.S. Roman, T. Yohannes, A. Cester, P. Cheng, X. Zhan, J. Wu, Z. Xie, W.-C. Tu, J.-H. He, C.J. Fell, K. Anderson, M. Hermenau, D. Bartesaghi, L.J.A. Koster, F. Machui, I. Gonzalez-Valls, M. Lira-Cantu, P.P. Khlyabich, B.C. Thompson, R. Gupta, K. Shanmugam, G.U. Kulkarni, Y. Galaghan, A. Urbina, J. Abad, R. Roesch, H. Hoppe, P. Morvillo, E. Bobeico, E. Panaitescu, L. Menon, Q. Luo, Z. Wu, C. Ma, A. Hambarian, V. Melikyan, M. Hamsch, P.L. Burn, P. Meredith, R. Rath, S. Dunst, G. Trimmel, G. Bardizza, H. Mülleijans, A.E. Goryachev, R.K. Misra, E.A. Katz, K. Takagi, S. Magaino, H. Saito, D. Aoki, P.M. Sommeling, J.M. Kroon, T. Vangerven, J. Manca, J. Kesters, W. Maes, O.D. Bobkova, V.A. Trukhanov, D.Y. Paraschuk, F.A. Castro, J. Blakesley, S.M. Tuladhar, J.A. Röhr, J. Nelson, J. Xia, E.A. Parlak, T.A. Tumay, H.-J. Egelhaaf, D.M. Tanenbaum, G.M. Ferguson, R. Carpenter, H. Chen, B. Zimmermann, L. Hirsch, G. Wantz, Z. Sun, P. Singh, C. Bapat, T. Offermans, F.C. Krebs, *Worldwide outdoor round robin study of organic photovoltaic devices and modules*, Sol. Energy Mater. Sol. Cells, **2014**, 130, 281.

- Outdoor measurements @Hasselt University

J. Kesters, P. Verstappen, W. Vanormelingen, J. Drijkoningen, T. Vangerven, D. Devisscher, L. Marin, B. Champagne, J. Manca, L. Lutsen, D. Vanderzande, W. Maes, *N-Acyl-dithieno[3,2-b:2',3'-d]pyrrole-based low bandgap copolymers affording improved open-circuit voltages and efficiencies in polymer solar cells*, Sol. Energy Mater. Sol. Cells, **2015**, DOI: 10.1016/j.solmat.2014.12.037.

- Article writing

- Device optimization, characterization and data analysis

P. Verstappen, J. Kesters, W. Vanormelingen, G.H.L. Heintges, J. Drijkoningen, T. Vangerven, L. Marin, S. Koudjina, B. Champagne, J. Manca, L. Lutsen, D. Vanderzande, W. Maes, *Fluorination as an effective tool to increase the open-circuit voltage and charge carrier mobility of organic solar cells based on poly(cyclopenta[2,1-b;3,4-b']dithiophene-alt-quinoxaline) copolymers*, J. Mater. Chem. A, **2015**, DOI: 10.1039/C4TA06054G.

- Device optimization, characterization and data analysis

J. Kesters, P. Verstappen, M. Kelchtermans, L. Lutsen, D. Vanderzande, W. Maes, *Porphyrin-based bulk heterojunction organic photovoltaics: the rise of the colors of life*, manuscript submitted.

- Article writing

J. Kesters, P. Verstappen, J. Raymakers, W. Vanormelingen, J. Drijkoningen, J. D'Haen, J. Manca, L. Lutsen, D. Vanderzande, W. Maes, *Enhanced organic solar cell stability by polymer (PCPDTBT) side chain functionalization*, manuscript submitted.

- Article writing

- Device optimization, degradation studies, characterization and analysis

P. Verstappen, J. Kesters, L. D'Olieslaeger, J. Drijkoningen, T. Vangerven, I. Cardinaletti, J. D'Haen, J. Manca, L. Lutsen, D. Vanderzande, W. Maes, *Simultaneous enhancement of polymer solar cell efficiency and stability by reducing the side chain density on fluorinated PCPDTQx copolymers*, manuscript submitted.

- Device optimization, characterization and data analysis

TABLE OF CONTENTS

Dankwoord	i
Conference Presentations	vii
List of Publications	ix
Table of Contents	xv
Chapter 1: Introduction	
1.1: General Introduction	2
1.2: Photovoltaics	3
1.3: Organic Photovoltaics	5
1.4: Working Principle of Organic Solar Cells	8
1.5: Construction and Performance Features of Organic Solar Cells	10
1.6: Overview of OPV Active Layer Materials	14
1.7: OPV Applications	27
1.8: Outline of the Thesis	29
1.9: References	32
Chapter 2: Enhanced Intrinsic Stability of the Bulk Heterojunction Active Layer Blend of Polymer Solar Cells by Varying the Polymer Side Chain Pattern	
2.1: Introduction	41
2.2: Experimental Section	46
2.3: Results and Discussion	54
2.4: Conclusions	77
2.5: References	78
2.6: Acknowledgements	87
2.7: Supporting Information	88

Table of Contents

Chapter 3: Enhanced Organic Solar Cell Stability by Polymer (PCPDTBT) Side Chain Functionalization

3.1: Introduction	97
3.2: Results and Discussion	100
3.3: Conclusions	116
3.4: Experimental Section	118
3.5: References	122
3.6: Acknowledgements	130
3.7: Supporting Information	131

Chapter 4: Enhanced Open-Circuit Voltage in Polymer Solar Cells by Dithieno[3,2-*b*:2',3'-*d*]pyrrole N-Acylation

4.1: Introduction	145
4.2: Results and Discussion	147
4.3: Conclusions	160
4.4: Experimental Section	161
4.5: References	170
4.6: Acknowledgements	177
4.7: Supporting Information	178

Chapter 5: N-Acyl-Dithieno[3,2-*b*:2',3'-*d*]pyrrole-Based Low Bandgap Copolymers Affording Improved Open-Circuit Voltages and Efficiencies in Polymer Solar Cells

5.1: Introduction	185
5.2: Experimental Section	188
5.3: Results and Discussion	192
5.4: Conclusions	204
5.5: References	206
5.6: Acknowledgements	217
5.7: Supporting Information	218

Chapter 6: Imidazolium-Substituted Polythiophenes as Efficient Electron Transport Materials Improving Photovoltaic Performance

6.1: Introduction	229
6.2: Results and Discussion	232
6.3: Experimental Section	240
6.4: Conclusions	242
6.5: References	243
6.6: Acknowledgements	246
6.7: Supporting Information	247

Chapter 7: Exploring the Scope of Polythiophene-Based Conjugated Polyelectrolytes as Cathode Interlayer Materials for Polymer Solar Cells

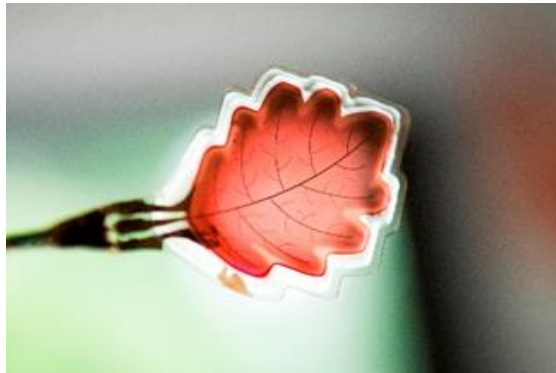
7.1: Introduction	260
7.2: Results and Discussion	262
7.3: Conclusions	268
7.4: Experimental Section	269
7.5: References	271
7.6: Supporting Information	274

Chapter 8: Summary and Outlook

8.1: Summary	280
8.2: Outlook	283
8.3: Nederlandse Samenvatting	287

Chapter 1

Introduction



1.1 GENERAL INTRODUCTION

Sustainable energy has been gaining large attention over the past decade and currently wind turbines and solar panels are decorating our every day scenery. With a global population of 7 billion people and an estimated population of over 9 billion people by 2050, the call for alternative renewable energy sources is one that needs to be answered rather sooner than later.^[1] At the moment, the predominating sources for our energy supply are fossil fuels (coal, crude oil and gas), but as these are finite and considering the continuous economic growth and industrialization across the world, alternative possibilities have to be explored. Additionally, during the last decade, the problem of 'global warming' has arisen, with various climate change conferences discussing the issues and possible solutions. The main challenge originates from the fact that the combustion of fossil fuels leads to the production of CO₂, the primary malefactor for climate change. To step away from these polluting processes, an intensification of research and development toward **renewable and clean energy** sources (wind, biomass, geothermal, hydropower and solar) is required. In 2011, 11% of the total energy supply in the U.S. arose from renewable energy, and it is prospected to rise to 15% by 2040.^[2] As illustrated in Figure 1, before 2010, most of the renewable energy (in the U.S.) was gathered from sources such as hydropower, biomass and wind power. However, solar energy has the capacity to become the main renewable energy source, as the amount of solar irradiation upon earth in one hour is equivalent to the world's annual energy demand. The figures and prospects from 2011 to 2015 already show a clear increase in the contribution of solar energy to the total renewable energy

pallet (Figure 1). With only a share of 0.6% in 2011, there was a growth to 2.7% in the U.S. in 2012, illustrating the rise in popularity of solar energy.^[3]

U.S. Renewable Energy Supply

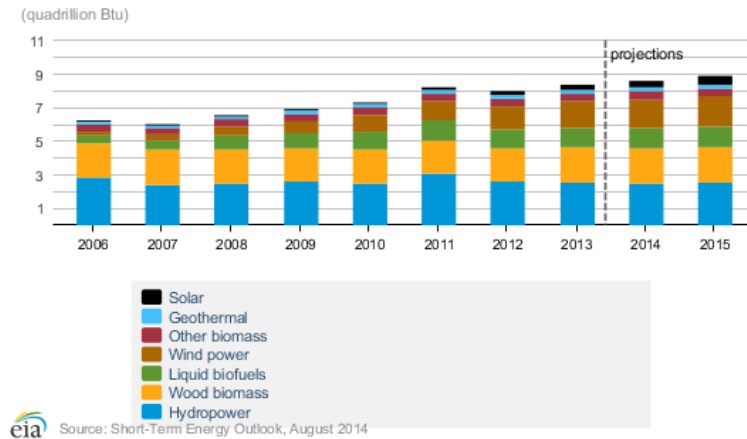


Figure 1: Distribution of renewable energy sources (figures for the U.S.) showing an increase in the contribution of solar energy.^[4]

1.2 PHOTOVOLTAICS

The rapid development of photovoltaic (PV) technologies is clearly visible nowadays when looking at the change in rooftop appearance over the past few years. Despite the difficult economic situation, the worldwide PV market doubled in 2010, showed a consecutive growth of 30% in 2011 and took another leap forward (11%) in 2012.^[5] Starting from the first silicon based solar cells achieving 6% power conversion efficiency (PCE), as reported in 1954 by Chapin *et al.*,^[6] present PV modules are reaching PCE's of approximately 25% and they are guaranteed to have a continuous energy output for at least 25 years. These current generation PV modules mainly consist out of mono- or polycrystalline Si and are generally considered to be the **first generation** solar cell technology.^[7]

Even though at present day the cost of this technology is decreasing, the production costs still remain rather high. To reduce these costs, a **second generation** of solar cells has been developed, based on thin-film technologies.^[7] This second generation PV comprises mainly of cells based on amorphous silicon, copper-indium-gallium-selenide (CIGS) or cadmium-telluride (CdTe), materials characterized by high absorption coefficients, hence reducing the required material quantities. Recently, a CIGS based solar cell with a PCE of 20.8% was reported, only slightly lagging behind the current PCE's obtained from crystalline Si solar cells.^[8] However, the technology still faces difficulties in scalability. In an attempt to simplify the large-scale production processes, enormous efforts are directed toward a **third generation** solar cell technology, consisting of organic and hybrid organic/inorganic solar cells, with current record efficiencies of 10.8%,^[9] 9.95%,^[10] and 12.2%^[11] for single junction polymer, small molecule and liquid dye-sensitized solar cells (DSSC), respectively. This novel generation of solar cells is attractive for particular applications due to additional appealing features such as aesthetics, semi-transparency, flexibility, improved low-light performance, cost-effectiveness, and large area printability. In DSSC's, the liquid electrolyte causes issues toward long-term applicability and toxicity. Very recently, the appearance of perovskite based solid state DSSC's and their high performance provided a way to circumvent these challenges. These types of solar cells utilize a light harvesting material taking the form of the perovskite crystal structure (generally $\text{CH}_3\text{NH}_3\text{MX}_3$, with M a metal cation and X an oxide or halide anion). The group of Yang Yang recently reported a planar perovskite based solar cell (in contrast to the mesoporous TiO_2 or AlO_3 architecture) with an astonishing PCE of 19.3%,^[12] and in November 2014, the

Korean Research Institute of Chemical Technology (KRICT) produced a certified perovskite solar cell with a PCE of 20.1%.^[13]

Figure 2 summarizes the efficiency roadmap for solar cell technologies over the past 40 years. As can be observed, organic solar cells have only been emerging as a promising technology for approximately 15 years, starting with certified PCE's of 2.5% in 2001, and they have shown a strong growth to 10.8% in the last couple of years.^[9]

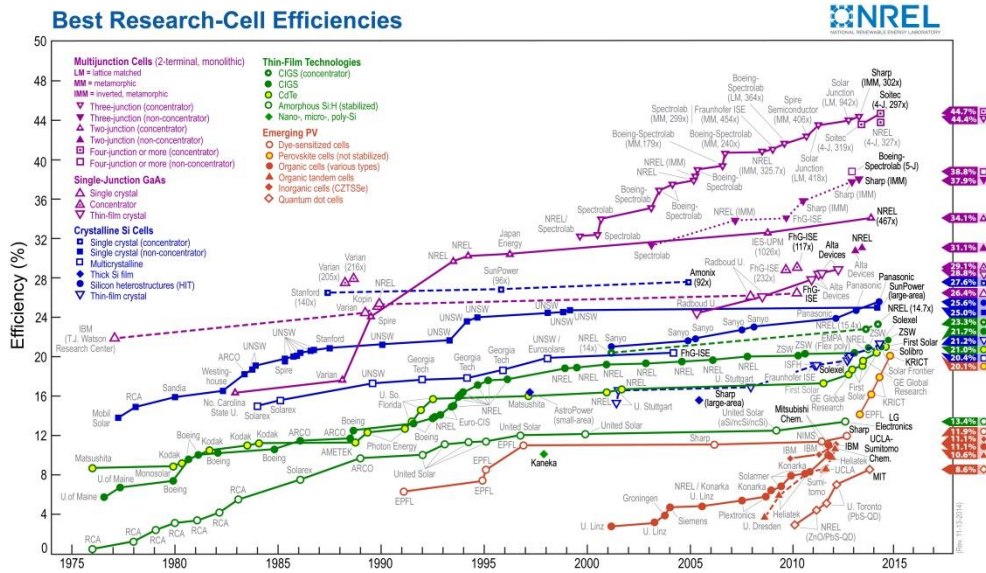


Figure 2: Evolution of the best research-cell efficiencies over the last 40 years

(source: NREL, version November 2014).^[13]

1.3 ORGANIC PHOTOVOLTAICS

The cradle of organic photovoltaics (OPV) is situated in the 1970's when Alan Heeger, Alan MacDiarmid and Hideki Shirakawa discovered the high conductivity of polyacetylene after doping with chlorine, iodine or bromine. The result was a

material that approached the conductivity of copper or silver (10^5 vs 10^8 S/m), resulting in the Nobel Prize for Chemistry for 'the discovery and development of conductive polymers'.^[14,15] Inspired by these findings, the quest toward efficient organic solar cells started, comprising the use of conjugated polymers. However, due to the little available knowledge, the first results were rather discouraging. Tang *et al.* came up with a proper approach for establishing organic photovoltaic cells in 1986, and by utilizing a **bilayer** stack approach, PCE's of up to 1% could be achieved by thermal evaporation of an n-type material (a perylenetetracarboxylic acid derivative) on top of a p-type material (Cu-phthalocyanine), sandwiched between two electrodes.^[16] To further improve the performance, a search for alternative acceptor layers commenced. It was only in 1992 that Sariciftci and coworkers discovered the photoinduced electron transfer from conducting polymers to buckminsterfullerenes, conceiving the concept of **polymer-fullerene solar cells**.^[17] As the bilayer architecture was still the predominant cell structure, the limited maximum thickness of the polymer donor material became the new focus point. Upon illumination of the donor polymer, bound hole-electron pairs (**excitons**) are formed, which need to dissociate at the donor/acceptor interface. These excitons have binding energies ranging from 0.4 to 0.5 eV, limiting the distance they can travel to 5–10 nm (exciton dissociation length) before undergoing radiative or non-radiative recombination.^[18] A possible approach to lower exciton dissociation is to increase the interfacial area between the donor and the acceptor. In order to do so, Hummelen and Wudl in 1995 synthesized a more soluble C_{60} -methanofullerene derivative, [6,6]-phenyl- C_{61} -butyric acid methyl ester (**PC₆₁BM**), hence laying the foundation for the **bulk heterojunction** (BHJ) organic solar cells.^[19] In these devices, the organic materials are blended

together and upon film formation a BHJ interpenetrating network of the donor and acceptor components, intermixed at a length scale less than the exciton diffusion length, is accomplished. Up to date, the BHJ structure is still the dominant OPV device architecture, as can be seen by the evolution in PCE's, starting at ~1% before 2000 and amounting to 10.8% in 2014.^[9] Obviously, the evolution of the BHJ organic solar cells does not stop here. Due to the limited absorption of most polymer materials, only a portion of the solar spectrum is harvested. Therefore, research efforts are focused on establishing highly efficient **multi-junction** photovoltaics, compiling two or even more **single-junction** solar cells, separated by a recombination layer. Via this approach, a broader window of the solar spectrum can be absorbed, resulting in enhanced performance. Earlier this year, a new record efficiency of 11% was obtained within the group of Yang Yang by optimization of a triple junction organic solar cell.^[20]

The fact that organic photovoltaics have been gaining popularity over the years can clearly be observed from Figure 3, showing the number of publications appearing on the topic each year. Whereas 20 years ago, less than 20 articles per year were published covering the topic of organic solar cells, this number has increased to ~3500 publications in 2013.^[21] Obviously, this interest in the development of OPV technologies has also attracted the attention of various industrial partners, amongst which established industries such as BASF, Solvay, Merck, Belectric, Heliatek and ThyssenKrupp.

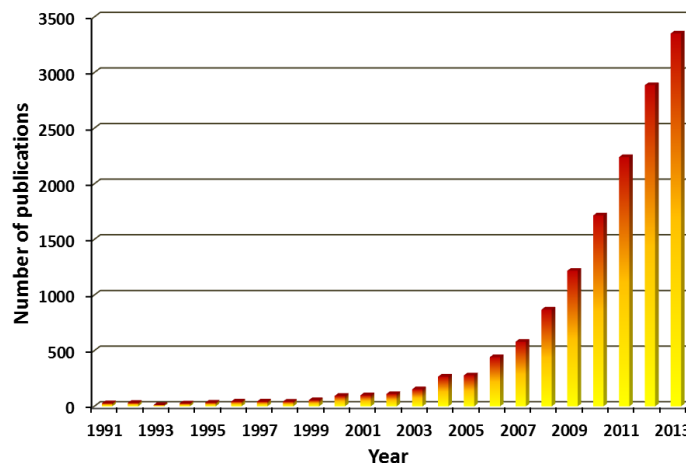


Figure 3: Number of publications on organic solar cells per year (source: Web of Science, search term "organic solar cells").

1.4 WORKING PRINCIPLE OF ORGANIC SOLAR CELLS

As illustrated in Figure 4, generation of current in organic solar cells occurs through a series of steps. Upon absorption of incident solar light by the photoactive layer (PAL) materials (mostly by the donor material), electrons are excited from the highest occupied molecular orbital (HOMO) to the lowest unoccupied molecular orbital (LUMO), resulting in the creation of Coulombically bound excitons (**exciton formation**). In contrast to the inorganic PV counterparts, in which immediate dissociation in free charge carriers is achieved upon photoexcitation, the bound hole-electron pairs first have to diffuse to the donor/acceptor interface (**exciton diffusion**). As mentioned before, the distance these excitons can travel without decaying to the ground state is limited by the exciton diffusion length, and in this respect the concept of the BHJ solar cell is of importance. In a subsequent step, electrons will be transferred to the acceptor material with high electron affinity, e.g. methanofullerenes (**charge**

transfer). To achieve a successful forward charge transfer, a proper energy offset between the LUMO's of the donor and acceptor material must be established. As a rule of thumb, a minimum energy difference of ~ 0.3 eV is required for effective exciton splitting and charge dissociation. Energy differences larger than this will lead to energetic loss-mechanisms, lowering the device performance.^[18,22-27] After charge transfer, recombination processes can still occur, either under the form of geminate (recombination of one electron and one hole originating from the same bound hole-electron pair after charge transfer) or non-geminate (bimolecular) recombination of free charge carriers during transport to the electrodes (**charge separation and charge transport**). The presence of efficient percolated pathways is required to reduce the risk of recombination.

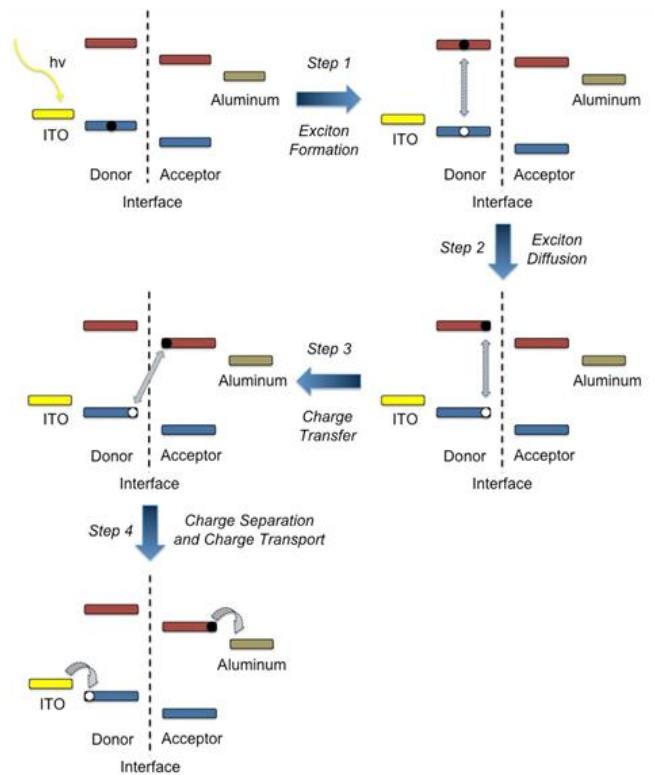


Figure 4: General mechanism of photoconversion in organic solar cells.

1.5 CONSTRUCTION AND PERFORMANCE FEATURES OF ORGANIC SOLAR CELLS

Typical organic solar cells, as illustrated in Figure 5, are constructed on a transparent glass substrate coated with a high work function anode material such as indium tin oxide (ITO). On top of the ITO, a thin hole conducting layer, such as poly(3,4-ethylenedioxythiophene):poly(styrenesulfonate) (PEDOT:PSS) is deposited. The presence of this layer ensures a proper ohmic contact between the anode and the photoactive layer by smoothing out the surface of the anode material, as well as provides a good wettability for the photoactive layer.

In a next step, the photoactive donor-acceptor blend is deposited from solution. Various deposition techniques such as spincoating, screen printing, spray coating, inkjet printing or blade coating have been established to ensure conversion from lab scale to industrial needs. To obtain the final device, a low work function cathode, often consisting of calcium and aluminum (or calcium and silver), is deposited on top of the photoactive layer by thermal evaporation.

As research grew, a more stable device platform was developed as well, which is generally referred to as the **inverted** solar cell architecture (Figure 5). This layer stack is constructed starting from ITO (now serving as the low work function electrode), followed by the deposition of an electron transporting material such as zinc oxide (ZnO) and the active layer. Finally, the device is finished off by the deposition of a small layer of molybdenum oxide and a high work function top electrode. PEDOT:PSS and Ca are eliminated from the device layout. It is known that PEDOT:PSS is responsible for the extraction of indium from the ITO electrode, whereas Ca is prone to oxidize to calcium oxide, both delicate factors when foreseeing long term use of OPV devices.

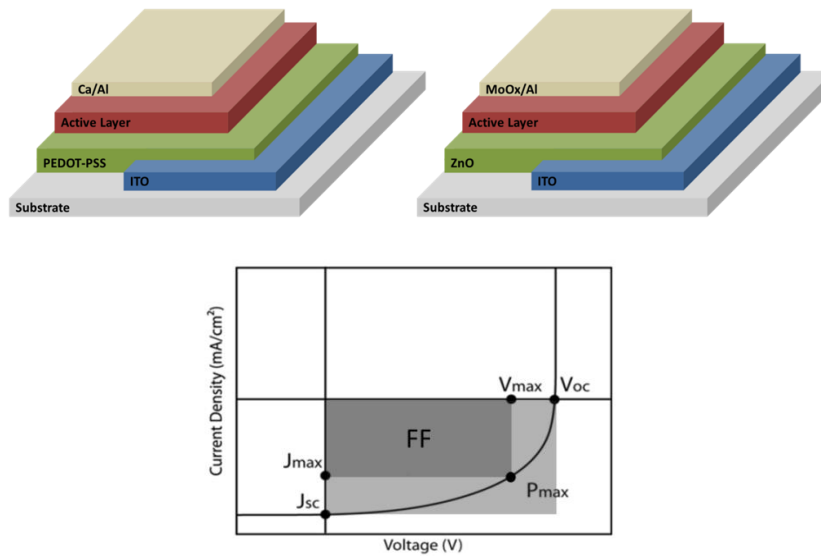


Figure 5: (top-left) Configuration of a standard architecture organic bulk heterojunction solar cell, (top-right) Inverted architecture, (bottom) Current density-voltage curve of a solar cell under illumination with the most important parameters indicated.

The operation of organic solar cells can be evaluated by a series of parameters, such as the short-circuit current density (J_{sc}), the open-circuit voltage (V_{oc}), the fill factor (FF) and the power conversion efficiency, illustrated in Figure 5. All these parameters can be extracted from the fourth quadrant of a current density-voltage plot when performing J - V measurements. The J_{sc} is the current density flowing through an illuminated device when applying a 0 V bias, which is the maximum current the device is able to produce. This current is largely dependent on the overlap between the absorption spectrum, and thus the bandgap, of the organic material and the solar spectrum. Additionally, factors such as active layer thickness, intensity of sunlight and charge collection efficiency will also determine the final J_{sc} . The V_{oc} shows the maximum voltage

attainable when no current is flowing through the device. A general approximation for the value of the V_{oc} can be determined by inspection of the energy level alignment of the HOMO of the donor and the LUMO of the acceptor component.^[28] Additionally, the V_{oc} can be influenced by features such as the presence of impurities, non-optimal interfaces in the solar cell stack and non-optimal phase separation of the donor and acceptor materials. The FF is determined by the device series resistance and the charge recombination rate and extraction efficiency, and quantifies the solar cells actual maximum power output (P_{max}) to its theoretical maximum power output ($P_{theor\ max}$). $P_{theor\ max}$ can be determined constructing a rectangle in the fourth quadrant of the J - V curve starting from J_{sc} and V_{oc} (Figure 5) and can readily be calculated by the product of these two parameters ($P_{theor\ max} = J_{sc} \times V_{oc}$). The actual maximum power output P_{max} from a solar cell under operation is given by the product of the current and voltage at the corresponding maximum power point, i.e. J_{max} and V_{max} . Hence, the FF can be calculated by the following equation:

$$FF = \frac{P_{max}}{P_{theor\ max}} = \frac{J_{max} V_{max}}{J_{sc} V_{oc}} \quad (1)$$

Finally, the performance of a solar cell is expressed by its power conversion efficiency (PCE or η). The PCE corresponds to the ratio of the power that comes out of the device (P_{out} or P_{max}) to the total power input of photon irradiation. The efficiency of a solar cell can thus be calculated according to the following equation:

$$PCE (\eta) = \frac{P_{max}}{P_{in}} = \frac{J_{max} V_{max}}{P_{in}} = FF \frac{J_{sc} V_{oc}}{P_{in}} \quad (2)$$

In order to report and compare solar cell results amongst different laboratories, it is necessary that certain standard testing conditions are established. In general, these include a temperature of 25 °C and an irradiation of 1000 W/m² with an air mass 1.5 (AM 1.5 G) spectrum. The AM 1.5 G spectrum corresponds to the solar irradiation with the sun at 45° above the horizon.

1.6 OVERVIEW OF OPV ACTIVE LAYER MATERIALS

1.6.1 Conjugated polymers

The polymer donor materials developed for organic photovoltaics can be divided into three main generations. As mentioned above, the OPV story started off with the discovery of the high conductivity of polyacetylene via doping the polymer with halides in the 1970's. Inspired by the possibility to create renewable energy applications, research on the fabrication of organic solar cells commenced. However, it was only in 1995 by the introduction of the BHJ concept, using a polymer as a donor component and a buckminsterfullerene as an acceptor, that there was a real chance for application of the technology. The **first generation** of OPV donor materials consisted mainly of poly(*p*-phenylene vinylene) (PPV) type materials. Initial results were obtained by Heeger *et al.*, who successfully generated the first solution-processed BHJ polymer solar cell, consisting of a blend of poly[2-methoxy-5-(2'-ethylhexyloxy)-1,4-phenylene vinylene] (**MEH-PPV**) mixed with PC₆₁BM (Figure 6).^[29] Even though a PCE of only 0.04% could be obtained, mainly attributed to a non-optimal active layer (nano)morphology hindering efficient charge separation, this result demonstrated the photoinduced electron transfer between the donor and the acceptor material. Six years later, in 2001, Shaheen *et al.* utilized a more processable PPV derivative, namely

poly[2-methoxy-5-(3',7'-dimethyloctyloxy)-1,4-phenylene vinylene] (**MDMO-PPV**) (Figure 6), and through substantial efforts in blend morphology optimization, the PCE of the OPV cell could be increased to 2.5%.^[30] A few years later, in 2003, Janssen and coworkers replaced PC₆₁BM with [6,6]-phenyl-C₇₁-butyric acid methyl ester (PC₇₁BM) (Figure 6), enhancing the solar cell performance to 3.0% due to the significantly higher absorption of PC₇₁BM in the visible range up to 700 nm.^[31]

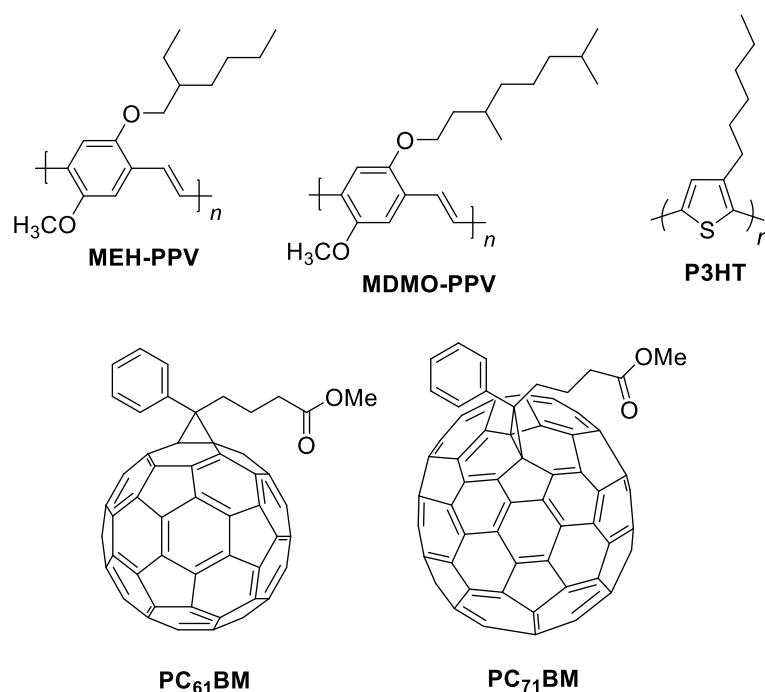


Figure 6: (top) First and second generation conjugated polymers for OPV devices, (bottom) Fullerene acceptors.

Even though considerable knowledge was gathered from the PPV:PC₆₁BM based devices, the interest in this material class was slowly fading, mainly due to the rather low potential of the polymer materials, as they exhibit a quite large

bandgap (~ 2 eV). Simultaneously, a **second generation** polymer class was gaining a lot of attention, poly(alkylthiophene)s, with poly(3-hexylthiophene) (**P3HT**) as the most prominent example (Figure 6). In 2002, Brabec *et al.* published the first promising results for P3HT:PC₆₁BM solar cells with external quantum efficiencies (EQE's) up to 76% at 550 nm.^[32] Further investigations quickly revealed the influence of thermal annealing on the photovoltaic performance, directed by an enhancement in charge carrier mobility.^[33] Soon thereafter, the crystallinity of the material was found to be a key parameter, and through synthesis of regioregular P3HT, PCE's around 5% were established.^[34] From there on out, the P3HT:PC₆₁BM material system was investigated very extensively, and it would remain the benchmark system for several years to follow. Most significant findings came from increasing the regioregularity of P3HT,^[35] optimizing the annealing temperature in combination with the molar mass of the polymer,^[34a,36] slowing down the drying kinetics of the wet films^[34b] and using processing additives to support phase separation between P3HT and PC₆₁BM.^[37] However, P3HT has one big issue that cannot be overcome, being its inherently limited absorption, resulting from a relatively large bandgap of ~ 1.9 eV. Another disadvantage is the limited V_{oc} (0.66 V) of the P3HT:PC₆₁BM system. In 2010, a PCE of 6.48% was reported when replacing PC₆₁BM with an alternative fullerene derivative, indene-C₆₀ bis-adduct. The device showed an improved V_{oc} of 0.84 V, a J_{sc} of 10.61 mA/cm² and a FF of 72.7%.^[38]

It was already stated that conjugated polymers with lower bandgaps could be more beneficial, allowing a more optimal light harvesting of the solar spectrum. With the V_{oc} being proportional to the energy difference between the polymer HOMO level and the acceptor LUMO level, an alternative strategy in the design

of the polymer material was required to lower both the HOMO and LUMO levels while affording increased light absorption through a reduced bandgap well below 2 eV (**low bandgap polymers**). The design of low bandgap polymers is generally based on a donor-acceptor (push-pull) approach, in which electron-rich and electron-poor (heterocyclic) units are coupled in an alternating fashion to form the polymer backbone. These types of polymers are considered to be part of the **third generation** polymer solar cell materials. Obviously, the amount of combinations is nearly endless and tremendous efforts have been put into the discovery of high-performance OPV materials. On the other hand, fine-tuning of established polymer materials is also very important to optimize their performance. In this introduction, we will only mention some of the most well-known examples amongst the low bandgap copolymer materials. Poly[2,6-(4,4-dialkyl-4*H*-cyclopenta[2,1-*b*;3,4-*b'*]-dithiophene)-*alt*-4,7-(2,1,3-benzothiadiazole)] (**PCPDTBT**) (Figure 7) was one of the first push-pull type materials that gained quite some attention as a possible candidate toward higher-performance BHJ OPV devices, with a nearly ideal bandgap of 1.46 eV and excellent charge transport properties. Unfortunately, with a PCE of 3.2%, initial results were somewhat disappointing.^[39] The main reason behind this rather unsatisfying performance was found to be originating from an unfavorable, very intimate nanomorphology of the active layer blend. To tackle this problem, Bazan and Heeger experimented with the blend solution and they found that the morphology could be optimized through the addition of alkanedithiols, leading to efficiencies surpassing 5%.^[40] The key parameters that were influenced were the J_{sc} (from 11 to 16.2 mA/cm²) and FF (from 47% to 55%), clearly indicating an enhancement in morphology and hence charge carrier extraction. Despite a high J_{sc} , the material system was still limited by a

disappointing V_{oc} value (0.6 V). In 2007, a particular carbazole-based copolymer, poly[2,7-(*N*-9-alkyl-2,7-carbazole)-*alt*-5,5-(4',7'-di(2-thienyl)-2',1',3'-benzothiadiazole)] (**PCDTBT**) (Figure 7), was reported by Leclerc *et al.*, with an initial solar cell performance of 3.6% when blended with PC₆₁BM.^[41] With a high V_{oc} of 0.88 V, it was found that the J_{sc} of barely 6.8 mA/cm² was limiting the final device performance. Shortly thereafter, Heeger *et al.* were able to enhance the J_{sc} to 10.6 mA/cm² and hence set a record efficiency of 6.1% for the same material by simply exchanging PC₆₁BM for PC₇₁BM, enlarging the light absorption of the active layer blend in the visible range. In this way, an internal quantum efficiency (IQE) close to 100% could be reached, meaning that almost every absorbed photon results in a separated pair of charge carriers and that all photogenerated carriers are collected at the electrodes.^[42] Consequently, with more than 250 publications by the end of 2013, PCDTBT:PC₇₁BM has become a new benchmark system for various studies involving active layer morphology, device architecture and the influence of the molar mass on the photovoltaic performance. Especially the enhancement in performance through optimization of the interfaces between the separate layers in the BHJ device stack has become a popular topic in recent years. In 2013, the group of Heeger was able to revise its record efficiency of 6.1% to 7.5% by insertion of a very thin (~ 1 nm) graphene oxide layer between the active layer and the top electrode.^[43] The exact working principle of this electron transporting material remained unclear, but it was observed that its insertion led to a reduction in the series resistance (R_s), an enhancement in the shunt resistance (R_{sh}), an improvement in the surface roughness, and the occurrence of a shift in the vacuum level, affected by the magnitude of the interfacial dipole.^[43b] The main concern governing the further applicability of PCDTBT lies in the necessity of using rather thin films.

Optimized devices processed from PCDTBT:PC₇₁BM utilize layer thicknesses in the range of 60–80 nm and a rapid decrease in PCE is observed for thicknesses above 100 nm. Due to this limitation, a lower amount of light can be absorbed, leading to a relatively modest *J*_{sc} (as compared to e.g. PCPDTBT). Additionally, the current is also hindered to a certain extent by the rather wide bandgap of the material (~ 1.88 eV), restricting the portion of the solar spectrum that can be absorbed.

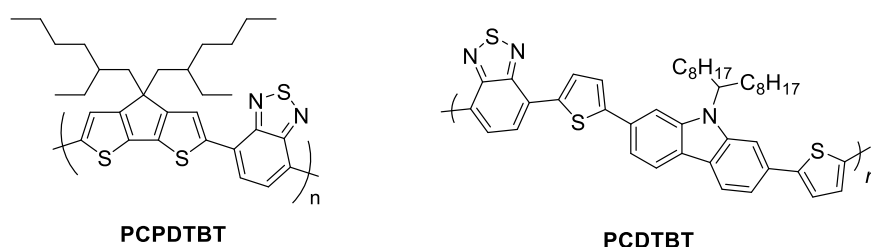


Figure 7: Low bandgap polymers with bridged bithiophene (left) or carbazole (right) electron rich building blocks.

Motivated by the upward trend in OPV device efficiencies, further research led to the discovery of several new state-of-the-art low bandgap copolymers affording polymer solar cells with PCE's exceeding 7%, amongst which poly(thieno[3,4-*b*]thiophene-*co*-benzodithiophene) (**PTB7**) (Figure 8) as one of the most popular representatives. The motivation to investigate the PTB family came from the fact that the thienothiophene (TT) unit is able to stabilize the quinoidal structure of the benzodithiophene (BDT) monomer unit, hence producing polymers with lower bandgaps (1.6–1.8 eV). Moreover, this quinoidal structure enhances the planarity along the polymer backbone, providing more rigidity. Additionally, the nature of the polymer enabled an improved π - π stacking, instigating a shorter distance between different polymer backbones and leading to a high hole

mobility.^[44] The actual synthesis of PTB7 was preceded by the investigation of various other PTB derivatives (PTB1–6) (Figure 8), for which side chain optimization and the effect of fluorination were investigated. Side chain variation can lead to differences in solubility and miscibility with the fullerene acceptor, in its turn influencing the (nano)morphology of the active layer blend, which may lead to more optimal charge extraction.^[45] On the other hand, fluorination has been shown to lower the HOMO level of the donor polymer, possibly enlarging the V_{oc} of the polymer:PCBM solar cells.^[46] In this way, it was found that the PTB derivative containing a fluorine atom on the thienothiophene part (PTB4) resulted in a PCE of 7.1%, encouraging further optimization. With these insights, the synthesis of PTB7 resulted in high performance photovoltaic devices with a V_{oc} of 0.74 V, a relatively high J_{sc} up to 14.5 mA/cm² and an astonishing FF of almost 70%, resulting in a final PCE of 7.5%.^[47] Further optimization of the molar mass and polydispersity (128 kg/mol and 1.12, respectively) of the polymer resulted in device performances up to 8.5%.^[48] Via the use of suitable interfacial layers, similarly as for PCDTBT, the highest reported efficiency for a PTB7 based OPV device is currently set at 9.2%.^[9a]

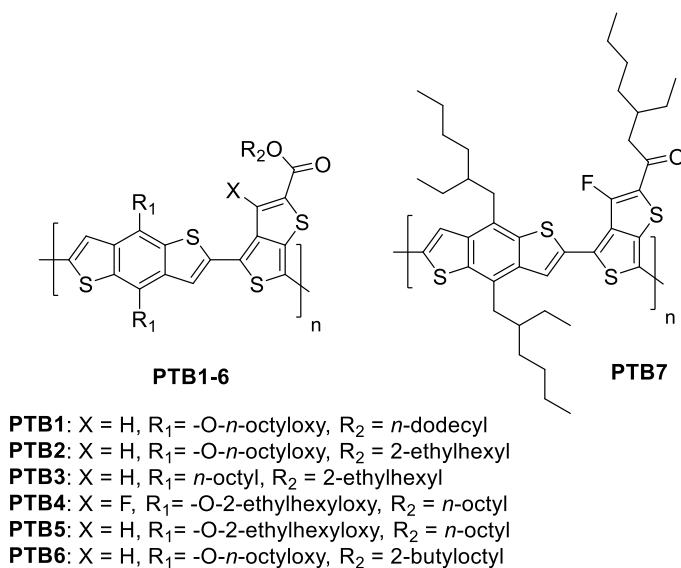


Figure 8: Benzo[1,2-*b*:4,5-*b'*]dithiophene-based low band gap copolymers.

1.6.2 Small molecules

Following the success achieved with conjugated polymer donor materials, the development of analogous small molecules has also seen a strong growth. In this paragraph, a few examples of the top performing small molecules are gathered. Even though the use of small molecules in OPV is found to be a more tedious process, mainly due to their specific active layer film formation, they contain certain advantages over their polymer-based counterparts. Due to their uniform and defined molecular structures, they show less batch-to-batch variations^[49] and they can attain higher hole mobilities than the corresponding polymer materials due to their enhanced stacking properties.^[50]

Since the appearance of P3HT and its general success, it was only natural that thiophene based small molecules would be explored as possible candidates for small molecule organic solar cells. Consistent with most first attempts on

polymer solar cells, initial results on these oligothiophenes were rather depressing, with PCE's of 0.3% when using a tetrahedral silicon core-based three-dimensional oligothiophene as the donor material.^[51] Further improvements to efficiencies just below 2% were obtained by exploration of various branched and star-shaped oligothiophenes.^[52] The main issue behind the disappointing performance is the limited light absorption in the visible and near-infrared region due to a rather large bandgap (>2.2 eV). An important breakthrough was realized in 2006, when Bäuerle *et al.* reported on the vacuum-evaporated quinquethiophene derivative (**DCV5T**) (Figure 9) with a lower bandgap due to the insertion of strongly electron withdrawing dicyanovinyl (DCV) units on both ends of the oligothiophene.^[53] Further optimization of the structure and dimethylation of the central thiophene unit (**DCV5T-Me**) (Figure 9) resulted in a device with a PCE of 6.9%.^[54]

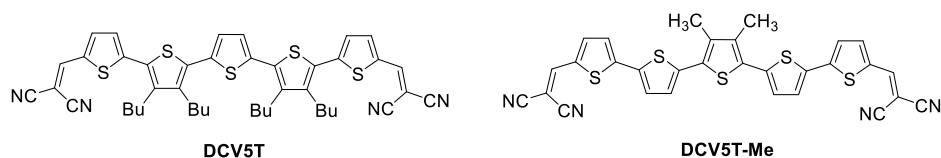


Figure 9: Quinquethiophene-based small molecules for vacuum-evaporated organic solar cells.

In 2013, the group around Heeger and Bazan reported on a new small molecule, 7,7'-[4,4-bis(2-ethylhexyl)-4*H*-silolo[3,2-*b*:4,5-*b'*]dithiophene-2,6-diyl]-bis(6-fluoro-4-(5'-hexyl[2,2'-bithiophen]-5-yl)benzo[*c*][1,2,5]-thiadiazole) (**DTS(FBTTh₂)₂**) (Figure 10), affording a PCE of 8.01% with a very high FF of 73%.^[55] The strength of this material lies in its high mobility, attributed to the high crystallinity, clearly evidenced by fibrillar structures persisting over

distances of almost 1 μm .^[55] Shortly afterwards, Heeger *et al.* revised their top efficiency. Through insertion of an optical spacer (a thin ZnO layer), a new record PCE of 8.94% could be established.

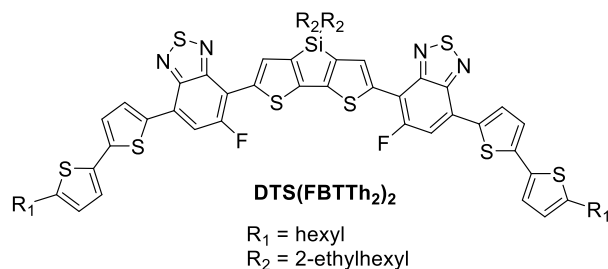


Figure 10: Dithienosilole-based small molecule (DTS(FBTTh₂)₂) for high-performance organic solar cells.

Based on the success of the PTB family of polymer donor materials, some of the top performing all solution-processed small molecules were also constructed from the benzo[1,2-*b*:4,5-*b'*]dithiophene building block. As reported by Chen *et al.* earlier this year, a small molecule comprising of a central BDT donor unit and ethylrhodanine acceptor units on both sides, linked by terthiophene spacers (Figure 11, denoted as **DR3TSBDT**), resulted in solar cells with PCE's up to 9.95% (certified 9.938%).^[10]

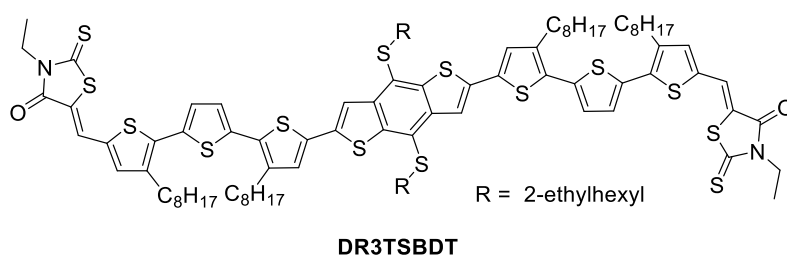


Figure 11: Benzo[1,2-*b*:4,5-*b'*]dithiophene-based small molecule DR3TSBDT.

1.6.3 Non-fullerene acceptors

Even though fullerene derivatives are very attractive due to their high electron mobilities, considerable advances have recently been made toward alternative acceptor materials. Polymers and non-fullerene small molecules exhibit certain advantages over fullerenes, such as higher absorption coefficients, which are a limiting factor for both PC₆₁BM and PC₇₁BM.^[56] Moreover, the use of alternative acceptors allows for reduced production costs as well as an easier tuning of the energy levels, hence providing a means to enhance the photoinduced charge separation at the donor/acceptor interface.^[57] In the next sections, a few examples of polymer-polymer and polymer-small molecule photovoltaic devices are provided.

1.6.3.1 Polymer-polymer OPV

Interestingly, one of the first satisfying results on all-polymer solar cell devices was achieved by combination of a P3HT derivative, poly[3-(4-*n*-octyl)-phenylthiophene] (**POPT**), and a PPV derivative, poly[2-methoxy-5-(2'-ethylhexyloxy)-1,4-(1-cyanovinylene)phenylene] (**MEH-CN-PPV**) (Figure 12), as donor and acceptor material, respectively. Even though the BHJ approach provided evidence of effective charge dissociation between various PPV derivatives, with device performances up to 0.04%,^[58] it was the construction of an optimized bilayer device consisting of Au/PEDOT/[POPT:MEH-CN-PPV (19:1)]/[MEH-CN-PPV:POPT (19:1)]/Ca that provided significant progress toward a PCE of 1.9%.^[59] Fréchet *et al.* in 2009 published new results obtained from GRIM-polymerized POPT as a donor layer and MEH-CN-PPV as an acceptor layer, acquiring a PCE of 2% in a bilayer architecture, the highest recorded efficiency for an all-polymer based photovoltaic device at that time.^[60]

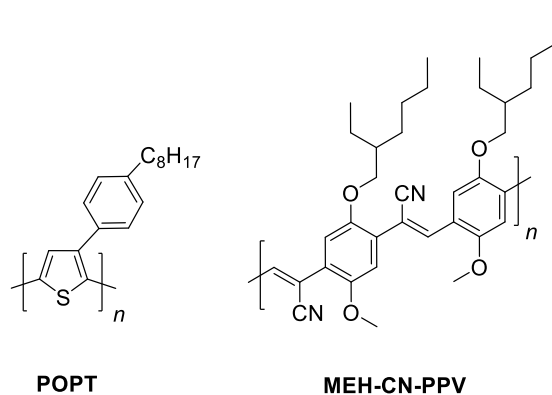


Figure 12: POPT (donor) and MEH-CN-PPV (acceptor) materials for all-polymer solar cells.

In 2009, a PCE of 1.67% was reported for BHJ all-polymer solar cells by using a perylenediimide (**PDI**)-phenylene vinylene copolymer (**P(PDI-PEPEP)**) (Figure 13) as electron acceptor and poly(3-phenylhydrazone-thiophene) (**PPHT**) (Figure 13) as electron donor.^[61] Upon annealing the photoactive blend film at 80 °C for 10 minutes, the more balanced charge transport and improved (nano)morphology increased the efficiency to 2.3%.

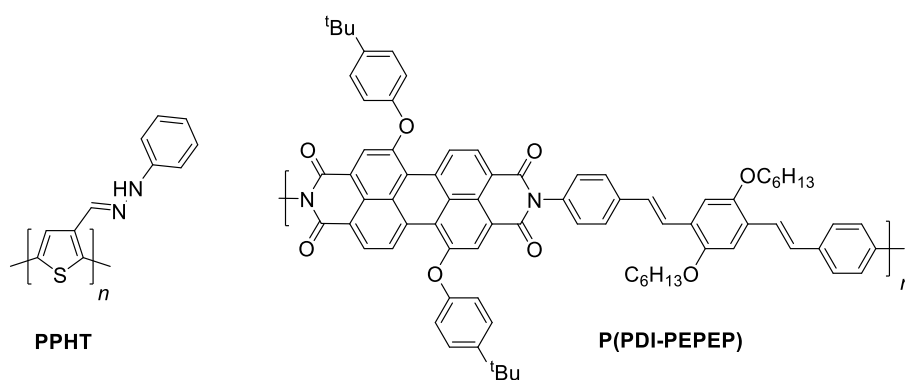


Figure 13: PPHT (donor) and P(PDI-PEPEP) (acceptor) for all-polymer solar cells.

In more recent years, the field of all-polymer based solar cells has been dominated by the Polyera Corporation team. In 2012, Polyera demonstrated polymer-polymer solar cell devices with PCE's exceeding 5%, and only 1 year later a new top efficiency of 6.4% (with Polyera's ActivInk® PV2700) was reported.^[62]

1.6.3.2 Polymer-small molecule OPV

The success of the PDI-based polymers inspired the development of analogous small molecule acceptors. In 2013, a PCE of 4.03% was reported for a polymer-small molecule OPV device comprising of an active layer blend of **PBDTTT-C-T** and 1,1'-bis(2-methoxyethoxy)-7,7'-(2,5-thienyl)-bis-PDI (**bis-PDI-T-EG**) (Figure 14) upon the use of 5% of 1,8-diiodoctane (**DIO**) as a processing additive.^[63] A year later, the same group reported a PCE of 4.34% through fine-tuning of the molecular structure of the PDI acceptor, affording 1,1'-bis(2-methoxy)-7,7'-(2,5-thienyl)-bis-PDI (**bis-PDI-T-MO**) (Figure 14).^[64] A large influence on the PCE was observed for small differences in additive usage. Addition of 2% or 3% of DIO to the active layer blend resulted in PCE's of 3.65% and 4.34%, respectively.^[64] From these results, it becomes apparent that precise optimization of the (nano)morphology is of absolute importance when investigating polymer-small molecule based devices.

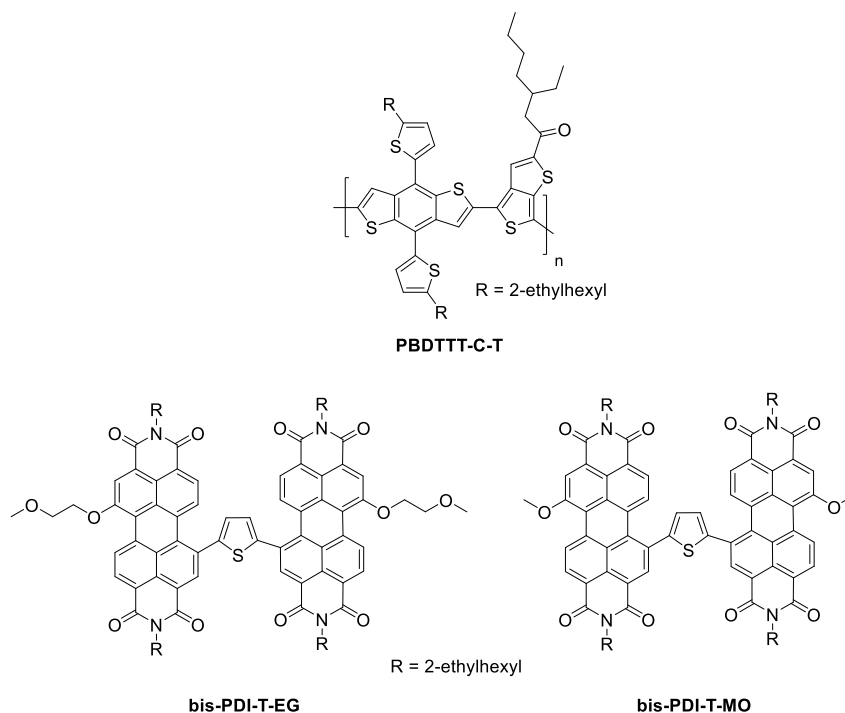


Figure 14: Small molecule acceptors (bottom) combined with a donor polymer (top) for polymer-small molecule BHJ organic solar cells.

1.7 OPV APPLICATIONS

"Can OPV grow toward a commercially viable technology?" This question has come to the forefront many times over the past years. In 2004, Brabec suggested that three key pillars, namely cost, efficiency and stability (Figure 15), need to be addressed in order for OPV to become a competitive player.^[65] As organic solar cells with for instance low cost and high efficiency, but moderate lifetime will receive little attention, all three of these components will have to be optimized.

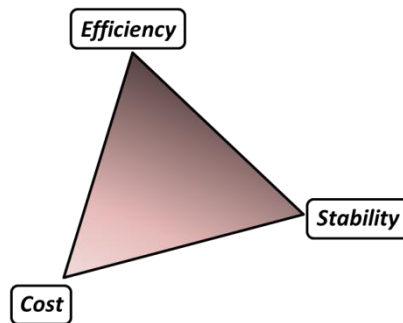


Figure 15: 'Brabec triangle' showing the interdependence of cost, solar cell efficiency and lifetime.

It is generally accepted that OPV will not replace the silicon based solar panels currently installed on many rooftops. The OPV market will most likely be one in which its niche characteristics are important, with the flexibility and semi-transparency of the devices as the most significant features. Adaptation to flexible surfaces such as tents, canopies, clothing, lamella, backpacks, etc. offers many possibilities for 'plug-and-power' applications (Figure 16). Recently, OPV has also gained interest from a number of designers, as the technology can be used both as a decorative object and power supply. Additionally, as organic photovoltaics are not limited by the need of perpendicularly incident light and also function well with indirect light sources, the integration into, for example, windows offers favorable perspectives toward (energy neutral) building and automotive applications.

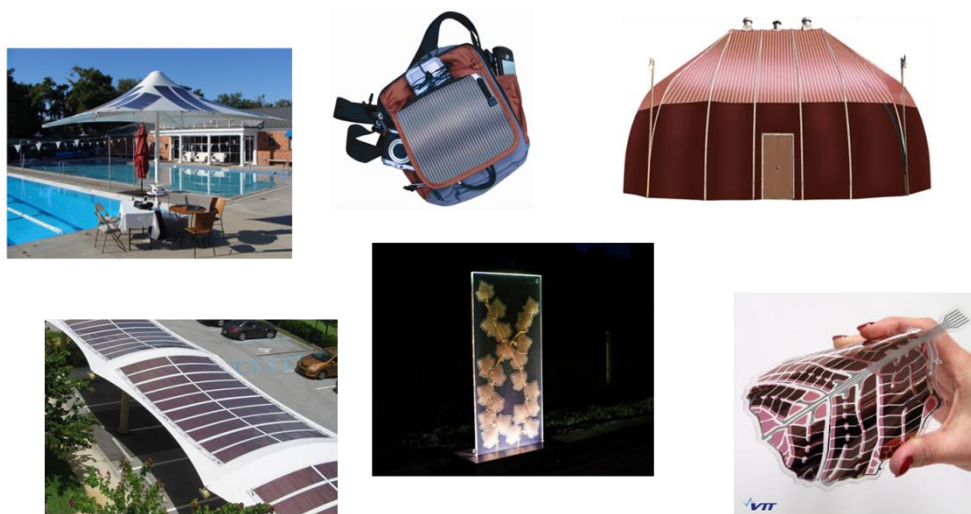


Figure 16: Applications showing the commercialization potential of organic photovoltaics.^[66]

1.8 OUTLINE OF THE THESIS

As indicated by Brabec and illustrated in Figure 15, OPV technology can only become viable for commercialization when complying to three important aspects, i.e. cost, efficiency and stability. The goal of this thesis was to focus on two of these components, i.e. stability and efficiency. In the next two chapters, the focus will be on the (thermal) stabilization of the (nano)morphology of the active layer blend. The subsequent chapters will deal with improvements on efficiency, and in order to do so, two different routes were investigated, i.e. new or fine-tuned donor polymer materials and optimization of electron transporting interlayers.

Chapter 2 focuses on a series of P3HT derivatives on which the hexyl side chains have been modified with functional moieties. The lifetime of the resulting polymer:fullerene solar cell devices was evaluated by accelerated lifetime tests

under thermal stress. Due to the presence of the functional moieties, the behavior of the active layer (nano)morphology upon heating changed. By a combination of continuous *J-V* measurements and TEM imaging, clear differences between the reference P3HT and the modified components have become apparent.

Chapter 3 continues from the work reported in Chapter 2. As the focus of the OPV donor materials has shifted from P3HT to low bandgap polymer systems, it was reasoned to be of interest to translate the findings for P3HT-type materials to a new generation of OPV donor materials. For this purpose, the PCPDTBT:PC₇₁BM system was chosen.

Chapter 4 describes the synthesis and photovoltaic performance of a new donor polymer (**PDTPTPD**). N-alkylated dithieno[3,2-*b*:2',3'-*d*]pyrroles (DTP's) were already known as electron-rich donor building blocks. However, their OPV performance was mainly limited by disappointing *V*_{oc}'s. In this chapter, we present DTP N-acylation as an effective way to enhance the *V*_{oc}, and consequently the PCE, of DTP-based polymer solar cells.

Chapter 5 continues the work on N-acylated DTP's, but now in combination with (fluorinated) electron-deficient quinoxaline (Qx) building blocks. Three different PDTPQx copolymers containing 0, 1 or 2 fluorine atoms on the Qx unit were prepared. Fluorination can serve as an additional way to lower the HOMO level of the donor polymer and thereby improve the *V*_{oc}.

Chapter 6 describes the initial work performed on polythiophene-based cathodic interlayers. By replacing calcium with a conjugated polyelectrolyte layer in the solar cell stack, a significant enhancement in PCE (from ~5.7% to ~6.7%) was

observed for the PCDTBT:PC₇₁BM system. The topographical influence of the addition of the interlayer was investigated. Furthermore, similar observations were made when translating this method to another polymer:fullerene device, i.e. PCPDT-DTTzTz:PC₇₁BM.

Chapter 7 continues the work on ionic (co)polythiophene-based interlayer materials. Four different CPE materials were investigated PBDTPD:PC₇₁BM devices and a record efficiency of 9.08% (7.91% reference device) was obtained for one of these materials. When applied in PCDTBT:PC₇₁BM devices, this specific CPE interlayer was found to give differentiating results in respect to the different *I-V* parameters. Also the topography images revealed a difference in compatibility of the CPE material and the underlying polymer:fullerene active layers.

Finally, in **Chapter 8**, a general summary is given (in English and Dutch) and an outlook is postulated.

1.9 REFERENCES

- [1] <http://www.shell.com/global/future-energy.html>
- [2] http://www.eia.gov/forecasts/ieo/more_highlights.cfm
- [3] <http://www.nrel.gov/docs/fy14osti/60210.pdf>
- [4] http://www.eia.gov/forecasts/steo/report/renew_co2.cfm
- [5] http://iet.jrc.ec.europa.eu/remea/sites/remea/files/pv_status_report_2013.pdf
- [6] Chapin, D.M.; Fuller, C.S.; Pearson, G.L. *J. Appl. Phys.*, **1954**, *25*, 676.
- [7] <http://www.heliatek.com/technologie/organische-photovoltaik/?lang=en>
- [8] Jackson, P.; Hariskos, D.; Wuerz, R.; Wischmann, W.; Powalla, M., *Phys. Status Solidi-R*, **2014**, *8*, 219.
- [9] (a) He, Z.C.; Zhong, C.M.; Su, S.J.; Xu, M.; Wu, H.B.; Cao, Y., *Nat. Photonics*, **2012**, *6*, 591; (b) Zhang, W.; Wu, Y.; Bao, Q.; Gao, F.; Fang, J., *Adv. Energy Mater.*, **2014**, *4*, 1400359; (c) Liu, Y.; Zhao, J.; Li, Z.; Mu, C.; Ma, W.; Hu, H.; Jiang, K.; Lin, H.; Ade, H.; Yan, H., *Nat. Commun.*, **2014**, *5*, 5293.
- [10] Kan, B.; Zhang, Q.; Li, M.; Wan, X.; Ni, W.; Long, G.; Wang, Y.; Yang, X.; Feng, H.; Chen, Y. *J. Am. Chem. Soc.* **2014**, *136*, 15529.
- [11] Yunfang, Z.; Fengshuo, Z.; Shuit-Tong, L.; Liangsheng, L.; Ni, Z.; Baoquan, S., *Adv. Energy Mater.*, **2014**, *4*, 1300923.
- [12] Huanping, Z.; Qi, C.; Gang, L.; Song, L.; Tze-bing, S.; Hsin-Sheng, D.; Ziruo, H.; Jingbi, Y.; Yongsheng, L.; Yang, Y., *Science*, **2014**, *345*, 542.
- [13] <http://www.nrel.gov/ncpv/index.html>
- [14] (a) Shirakawa, H.; Louis, E.J.; MacDiarmid, A.G.; Chiang, C.K.; Heeger, A.J., *J. Chem. Soc., Chem. Commun.*, **1977**, 578; (b) Chiang, C.K.;

- Fischer, C.R.; Park, Y.W.; Heeger, A.J.; Shirakawa, H.; Louis, E.J.; Gau, S.C.; MacDiarmid, A.G., *Phys. Rev. Lett.*, **1977**, *39*, 1098.
- [15] Shirakawa, H. *Nobel lecture Chemistry 1996-2000*, World Scientific Publishing Co., Singapore, **2003**.
- [16] Tang, C.W., *Appl. Phys. Lett.*, **1986**, *48*, 183.
- [17] Sariciftci, N.S.; Smilowitz, L.; Heeger, A.J.; Wudl, F., *Science*, **1992**, *258*, 1474.
- [18] Kroon, R.; Lenes, M.; Hummelen, J.C.; Blom, P.W.M.; de Boer, B., *Polym. Rev.*, **2008**, *48*, 531.
- [19] (a) Wudl, F., *Acc. Chem. Res.*, **1992**, *25*, 15716; (b) Hummelen, J.C.; Knight, B.W.; Lepeq, F.; Wudl, F.; Yao, J.; Wilkins, C.L., *J. Org. Chem.*, **1995**, *60*, 532.
- [20] Chen, C-C.; Chang, W-H.; Yoshimura, K.; Ohya, K.; You, J.; Gao, J.; Hong, Z.; Yang, Y., *Adv. Mater.*, **2014**, *26*, 5670.
- [21] Web of Science, search term "organic solar cells", requested information on 29/08/14.
- [22] (a) Brabec, C.J., *Sol. Energy Mater. Sol. Cells*, **2004**, *83*, 273; (b) Xue, J., *Polym. Rev.*, **2010**, *50*, 411.; (c) Deibel, C.; Dyakonov, V., *Rep. Prog. Phys.*, **2010**, *73*, 096401; (d) Chidichimo, G.; Filippelli, L., *Int. J. Photoenergy*, **2010**, 123534; (e) Nielsen, T.D.; Cruickshank, C.; Foged, S.; Thorsen, J.; Krebs, F.C., *Sol. Energy Mater. Sol. Cells*, **2010**, *94*, 1553; (f) Helgesen, M.; Sondergaard, R.; Krebs, F.C., *J. Mater. Chem.*, **2010**, *20*, 36; (g) Bundgaard, E.; Hagemann, O.; Manceau, M.; Jorgensen, M.; Krebs, F.C., *Macromolecules*, **2010**, *43*, 8115; (h) Krebs, F.C., *Polymeric Solar Cells: Material, Design, Manufacture*; DEStech Publications, Inc., Lancaster Pennsylvania, **2010**; (i) Arias, A.C.;

- Mackenzie, J.D.; McCulloch, I.; Rivnay, J.; Salleo, A., *Chem. Rev.*, **2010**, *110*, 3; (j) Brabec, C.J.; Gowrisanker, S.; Halls, J.J.M.; Laird, D.; Jia, S.; Williams, S.P., *Adv. Mater.*, **2010**, *22*, 3839; (k) Boudreault, P.-L.T.; Najari, A.; Leclerc, M., *Chem. Mater.*, **2011**, *23*, 456; (l) Hübner, A.; Trnovec, B.; Zillger, T.; Ali, M.; Wetzold, N.; Mingebach, M.; Wagenpfahl, A.; Deibel, C.; Dyakonov, V., *Adv. Energy Mater.*, **2011**, *1*, 1018; (m) Teichler, A.; Eckardt, R.; Hoepfner, S.; Friebe, C.; Perelaer, J.; Senes, A.; Morana, M.; Brabec, C.J.; Schubert, U.S., *Adv. Energy Mater.*, **2011**, *1*, 105.
- [23] Mayer, A.C.; Scully, S.R.; Hardin, B.E.; Rowell, M.W.; McGehee, M.D., *Mater. Today*, **2007**, *10*, 28.
- [24] Bundgaard, E.; Krebs, F.C., *Sol. Energy Mater. Sol. Cells*, **2007**, *91*, 954.
- [25] Thompson, B.C.; Fréchet, J.M.J., *Angew. Chem. Int. Ed.*, **2008**, *47*, 58.
- [26] Peet, J.; Heeger, A.J.; Bazan, G.C., *Acc. Chem. Res.*, **2009**, *42*, 1700.
- [27] Brédas, J.-L.; Norton, J.E.; Cornil, J.; Coropceanu, V., *Acc. Chem. Res.*, **2009**, *42*, 1691.
- [28] (a) Brabec, C.J.; Cravino, A.; Meissner, D.; Sariciftci, N.S.; Fromherz, T.; Rispen, M.T.; Sanchez, L.; Hummelen, J.C., *Adv. Funct. Mater.*, **2001**, *11*, 374; (b) Scharber, M.C.; Mülbacher, D.; Koppe, M.; Denk, P.; Waldauf, C.; Heeger, A.J.; Brabec, C.J., *Adv. Mater.*, **2006**, *18*, 789.
- [29] Yu, G.; Gao, J.; Hummelen, J.C.; Wudl, F.; Heeger, A.J., *Science*, **1995**, *270*, 1789.
- [30] Shaheen, S.; Brabec, C.J.; Sariciftci, N.S.; Padinger, F.; Fromherz, T.; Hummelen, J.C., *Appl. Phys. Lett.*, **2001**, *78*, 841.

-
- [31] Wienk, M.M.; Kroon, J.M.; Verhees, W.J.H.; Knol, J.; Hummelen, J.C.; van Hal, P.A.; Janssen, R.A.J., *Angew. Chem. Int. Ed.*, **2003**, *42*, 3371.
- [32] Schilinsky, P.; Waldauf, C.; Brabec, C.J., *Appl. Phys. Lett.*, **2002**, *81*, 3885.
- [33] Mihailetchi, V.D.; Xie, H.; de Boer, B.; Koster, L.J.A.; Blom, P.W.M., *Adv. Funct. Mater.*, **2005**, *15*, 1260.
- [34] (a) Ma, W.; Yang, C.; Gong, X.; Lee, K.; Heeger, A.J., *Adv. Funct. Mater.*, **2005**, *15*, 1617; (b) Li, G.; Shrotriya, V.; Huang, J.; Yao, Y.; Moriarty, T.; Emery, K.; Yang, Y., *Nat. Mater.*, **2005**, *4*, 864.
- [35] Kim, Y.; Cook, S.; Tuladhar, S.M.; Choulis, S.A.; Nelson, J.; Durrant, J.R.; Bradley, D.D.C.; Giles, M.; McCulloch, I.; Ha, C.-S.; Ree, M., *Nat. Mater.*, **2006**, *5*, 197.
- [36] (a) Kline, R.J.; McGehee, M.D.; Kadnikova, E.N.; Liu, J.; Fréchet, J.M.J., *Adv. Funct. Mater.*, **2003**, *15*, 1519; (b) Zen, A.; Pflaum, J.; Hirschmann, S.; Zhuang, W.; Jaiser, F.; Asawapirom, U.; Rabe, J.P.; Scherf, U.; Neher, D., *Adv. Funct. Mater.*, **2004**, *14*, 757; (c) Schilinsky, P.; Asawapirom, U.; Scherf, U.; Biele, M.; Brabec, C.J., *Chem. Mater.*, **2005**, *17*, 2175; (d) Kline, R.J.; McGehee, M.D.; Kadnikova, E.N.; Liu, J.; Fréchet, J.M.J.; Toney, M.F., *Macromolecules*, **2005**, *38*, 3312; (e) Ma, W.; Kim, J.Y.; Lee, K.; Heeger, A.J., *Macromol. Rapid. Commun.*, **2007**, *28*, 1776.
- [37] (a) Peet, J.; Soci, C.; Coffin, R.C.; Nguyen, T.Q.; Mikhailovsky, A.; Moses, D.; Bazan, G.C., *Appl. Phys. Lett.*, **2006**, *89*, 252105; (b) Wang, W.; Wu, H.; Yang, C.; Luo, C.; Zhang, Y.; Chen, J.; Cao, Y., *Appl. Phys. Lett.*, **2007**, *90*, 183512; (c) Moulé, A.J.; Meerholz, K., *Adv. Mater.*, **2008**, *20*, 240.
-

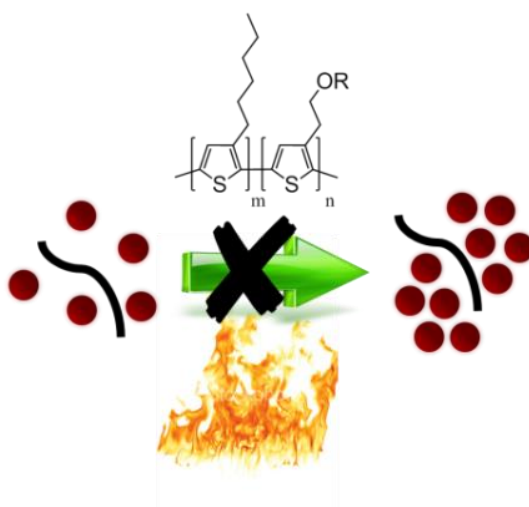
- [38] Zhao, G.; He, Y.; Li, Y., *Adv. Mater.*, **2010**, *22*, 4355.
- [39] (a) Mühlbacher, D.; Scharber, M.; Morana, M.; Zhu, Z.; Waller, D.; Gaudiana, R.; Brabec, C., *Adv. Mater.*, **2006**, *18*, 2884; (b) Soci, C.; Hwang, I.-W.; Moses, D.; Zhu, Z.; Waller, D.; Gaudiana, R.; Brabec, C.J.; Heeger, A.J., *Adv. Funct. Mater.*, **2007**, *17*, 632; (c) Zhang, M.; Tsao, H.N.; Pisula, W.; Yang, C.; Mishra, A.K.; Müllen, K., *J. Am. Chem. Soc.*, **2007**, *129*, 3472; (d) Coffin, R.C.; Peet, J.; Rogers, J., *Nat. Chem.*, **2009**, *1*, 657.
- [40] Peet, J.; Kim, J.U.; Coates, N.E.; Ma, W.L.; Moses, D.; Heeger, A.J.; Bazan, G.C., *Nat. Mater.*, **2007**, *6*, 497; (b) Lee, J.K.; Ma, W.L.; Brabec, C.J.; Yuen, J.; Moon, J.S.; Kim, J.Y.; Lee, K.; Bazan, G.C.; Heeger, A.J., *J. Am. Chem. Soc.*, **2008**, *130*, 3619.
- [41] (a) Blouin, N.; Michaud, A.; Leclerc, M., *Adv. Mater.*, **2007**, *19*, 2295; (b) Blouin, N.; Michaud, A.; Gendron, D.; Wakim, S.; Blair, E.; Neagu-Plesu, R.; Belletête, M.; Durocher, G.; Tao, Y.; Leclerc, M., *J. Am. Chem. Soc.*, **2008**, *130*, 732.
- [42] Park S.H.; Roy, S.; Beaupré, S.; Cho, S.; Coates, N.; Moon, J.S.; Moses, D.; Leclerc, M.; Lee, K.; Heeger, A.J., *Nat. Photonics*, **2009**, *3*, 297.
- [43] (a) Beaupré, S.; Leclerc, M., *J. Mater. Chem. A*, **2013**, *1*, 11097; (b) Wang, D.W.; Kim, J.K.; Seo, J.H.; Park, I.; Hong, B.H.; Park, J.H.; Heeger, A.J., *Angew. Chem. Int. Ed.*, **2013**, *52*, 2874.
- [44] Lu, L.; Yu, L., *Adv. Mater.*, **2014**, *26*, 4413.
- [45] Cabanetos, C.; Labban, A.E.; Bartelt, J.A.; Douglas, J.D.; Mateker, W.R.; Fréchet, J.M.J.; McGehee, M.D.; Beaujuge, P.M., *J. Am. Chem. Soc.*, **2013**, *135*, 4656.

- [46] (a) Chen, H.-C.; Chen, Y.-H.; Liu, C.-H.; Hsu, Y.-H.; Chien, Y.-C.; Chuang, W.-T.; Cheng, C.-Y.; Liu, C.-L.; Chou, S.-W.; Tung, S.-H.; Chou, P.-T., *Polym. Chem.*, **2013**, *4*, 3411; (b) Kim, J.-H.; Song, C.E.; Kim, H.U.; Grimsdale, A.C.; Moon, S.-J.; Shin, W.S.; Choi, S.K.; Hwang, D.-H., *Chem. Mater.*, **2013**, *25*, 2722; (c) Zhang, M.; Guo, S.; Zhang, S.; Hou, J., *Adv. Mater.*, **2013**, *26*, 1118.
- [47] Liang, Y.Y.; Xu, Z.; Xia, J.B.; Tsai, S.T.; Wu, Y.; Li, G.; Ray, C.; Yu, L.P., *Adv. Mater.*, **2010**, *22*, E135.
- [48] Liu, C.; Wang, K.; Hu, X.; Yang, Y.; Hsu, C.-H.; Zhang, W.; Cio, S.; Gong, X.; Cao, Y., *ACS Appl. Mater. Interfaces*, **2013**, *117*, 12628.
- [49] Walker, B.; Kim, C.; Nguyen, T.Q., *Chem. Mater.*, **2011**, *23*, 470.
- [50] Welch, G.C.; Perez, L.A.; Hoven, C.V.; Zhang, Y.; Dang, X.D.; Sharenko, A.; Toney, M.F.; Kramer, E.J.; Thuc-Quyen, N.; Bazan, G.C., *J. Mater. Chem.*, **2011**, *21*, 12700.
- [51] Roquet, S.; de Bettignies, R.; Leriche, P.; Cravino, A.; Roncali, J., *J. Mater. Chem.*, **2006**, *16*, 3040.
- [52] (a) Karpe, S.; Cravino, A.; Frère, P.; Allain, M.; Mabon, G.; Roncali, J., *Adv. Funct. Mater.*, **2007**, *17*, 1163; (b) Ma, C.Q.; Fonrodona, M.; Schikora, M.C.; Wienk, M.M.; Janssen, R.A.J., *Adv. Funct. Mater.*, **2008**, *18*, 3323.
- [53] Schulze, K.; Uhrich, C.; Schüppel, R.; Leo, K.; Pfeiffer, M.; Brier, E.; Reinold, E.; Bäuerle, P., *Adv. Mater.*, **2006**, *18*, 2872.
- [54] Fitzner, R.; Mena-Osteritz, E.; Mishra, A.; Schulz, G.; Reinold, E.; Weil, M.; Körener, C.; Ziehlke, H.; Elschner, C.; Leo, K.; Riede, M.; Pfeiffer, M.; Uhrich, C.; Bäuerle, P., *J. Am. Chem. Soc.*, **2012**, *134*, 11064.

- [55] Kyaw, A.K.K.; Wang, D.H.; Wynands, D.; Zhang, J.; Nguyen, T.-Q.; Bazan, G.C.; Heeger, A.J., *Nano Lett.*, **2013**, *13*, 3796.
- [56] (a) Li, C.-Z.; Yip, H.-L.; Jen, A.K.-Y., *J. Mater. Chem.*, **2012**, *22*, 4161; (b) Umeyama, T.; Imahori, H., *J. Phys. Chem. C.*, **2013**, *117*, 3195.
- [57] Lizin, S.; Van Passel, S.; De Schepper, E.; Maes, W.; Lutsen, L.; Manca, J.; Vanderzande, D., *Energy Environ. Sci.*, **2013**, *6*, 3136.
- [58] (a) Yu, G.; Heeger, A.J., *J. Appl. Phys.*, **1995**, *78*, 4510; (b) Halls, J.J.M.; Walsh, C.A.; Greenham, N.C.; Marseglia, E.A.; Friend, R.H.; Moratti, S.C.; Holmes, A.B., *Nature*, **2002**, *376*, 498.
- [59] Granström, M.; Petritsch, K.; Aria, A.C.; Lux, A.; Andersson, M.R.; Friend, R.H., *Nature*, **1998**, *395*, 257.
- [60] Holcombe, T.W.; Woo, C.H.; Kavulak, D.F.J.; Thompson, B.C.; Fréchet, J.M.J., *J. Am. Chem. Soc.*, **2009**, *131*, 14160.
- [61] Mikroyannidis, J.A.; Stylianakis, M.M.; Sharma, G.D.; Balraju, P.; Roy, M.S., *J. Phys. Chem. C.*, **2009**, *113*, 7904.
- [62] Facchetti, A., *Mater. Today*, **2013**, *16*, 123.
- [63] Zhang, X.; Lu, Z.; Ye, L.; Zhan, C.; Hou, J.; Zhang, S.; Jiang, B.; Liu, Y.; Shi, Q.; Liu, Y.; Yao, J., *Adv. Mater.*, **2013**, *25*, 5791.
- [64] Lu, Z.; Jiang, B.; Zhang, X.; Tang, A.; Chen, L.; Zhan, C.; Yao, J., *Chem. Mater.*, **2014**, *26*, 2907.
- [65] Brabec, C.J., *Sol. Energy Mater. Sol. Cells*, **2004**, *83*, 273.
- [66] (a) <http://www.textileworld.com>; (b) <http://www.solarmer.com>; (c) <http://clinmba2010.blogspot.nl>; (d) <http://www.solarserver.com>; (e) <http://www.solarte.de>; (f) <http://www2.imec.be>.

Chapter 2

Enhanced Intrinsic Stability of the Bulk Heterojunction Active Layer Blend of Polymer Solar Cells by Varying the Polymer Side Chain Pattern



J. Kesters, S. Kudret, S. Bertho, N. Van den Brande, M. Defour, B. Van Mele, H. Penxten, L. Lutsen, J. Manca, D. Vanderzande, W. Maes, *Org. Electron.*, **2014**, *15*, 549.

ABSTRACT

Organic photovoltaics (OPV) have acquired huge attention over the past years as potential renewable energy sources, adding attractive features such as aesthetics, semi-transparency, flexibility, large area printability, improved low-light performance, and cost-effectiveness to the well-known Si-based photovoltaics. Steady improvements in OPV power conversion efficiencies are continuously reported, notably for bulk heterojunction solar cells based on conjugated polymer:fullerene blends. However, apart from efficiency and cost, the stability of organic solar cell devices is of particular concern. Among the different factors contributing to OPV instability, gradual loss of the optimum phase-separated nanomorphology of the photoactive layer blend is a critical parameter. In this paper, we present the results of 'shelf-life' accelerated lifetime tests performed for devices containing a range of functionalized poly(3-alkylthiophene) donor polymers upon prolonged thermal stress. By the incorporation of functional moieties on the side chains of P3HT-based copolymers, a remarkable improvement of the intrinsic stability of the active layer blend morphology is accomplished, even for fairly low built-in ratios (5–15%) and without crosslinking to covalently anchor the polymer and/or fullerene molecules. Moreover, these alterations do not influence the initial power conversion efficiencies to a large extent. As such, the presented approach can be regarded as an attractive paradigm for OPV active layer stability.

2.1 INTRODUCTION

As the introduction of alternative (non-fossil-based) abundant energy sources is becoming more and more important, organic/polymer bulk heterojunction (BHJ) solar cells have gained considerable interest as a means to produce green energy^[1]. BHJ polymer solar cells show desirable properties, as they combine a number of unique features such as solution processability enabling low cost large-area thin film fabrication (by R2R printing), improved low-light performance, aesthetics, reduced weight and mechanical flexibility, making them ideal candidates for a multitude of (niche) applications, including portable/wearable chargers, building-integrated photovoltaics (BIPV) and automotive integration. As record efficiencies are constantly being reported from various research facilities around the world^[1,2], the idea of commercialization is now becoming more and more realistic. However, additional to low production costs and high power conversion efficiencies (PCEs), it is obligatory for these solar cell devices to show long-term stability, which is the Achilles heel of state-of-the-art BHJ organic photovoltaics (OPVs)^[3]. Successful commercialization of OPV rests on 3 key parameters, i.e. cost, efficiency and lifetime (the 'Brabec triangle')^[4]. As moderate cost is a parameter rather inherent to this type of printable thin-layer (carbon-based) technology, and novel materials leading to increased performances are constantly on the horizon, it is OPV lifetime that urgently needs to be addressed.

At present, the most efficient light harvesting electron donor materials employed in BHJ polymer solar cells all belong to the class of donor-acceptor or low bandgap copolymers^[1,2,5]. These materials are combined in photoactive layer

blends with a fullerene derivative, most often PC₆₁BM ([6,6]-phenyl-C₆₁ butyric acid methyl ester), PC₇₁BM ([6,6]-phenyl-C₇₁ butyric acid methyl ester) or ICBA (indene-C₆₀ bisadduct), as the electron accepting component. Nevertheless, the well-established P3HT(poly-3-hexylthiophene):PC₆₁BM blend is still a very successful and widely employed workhorse system, perfectly suitable for fundamental studies^[6]. Solar cells based on these blends have afforded reasonably high efficiencies^[6,7], up to ~5%, and both materials are readily available in reproducible purity and/or molar mass (distribution) for everyone interested in studying and/or applying OPV blends, which is a serious drawback of the more recent low bandgap materials.

Degradation studies on the reference system P3HT:PC₆₁BM have identified lifetimes of approximately 1500 hours when applying continuous illumination (under a sulphur plasma lamp with a light intensity of ca. 1000 W/m²), corresponding with lifetimes of ~1.5 years under exposure to direct sunlight^[8,9]. Translating this to real-world applications, this will add up to lifetimes of 3–4 years, which is still not sufficient for many large-scale market applications. A number of degradation pathways are responsible for the moderate operational lifetimes of OPV devices, acting on either the encapsulating materials, the electrodes, the interconnections or the photoactive layer^[3], and thorough understanding of the various failure mechanisms clearly provides the key to improve OPV reliability. Looking specifically at the photoactive layer blend, the heart of the OPV device, the limited intrinsic stability of the intimately mixed BHJ donor:acceptor blend under light (photo-oxidation^[10]) and heat (degradation and phase demixing^[11]) stress is an important drawback posing challenges to material chemists^[3,12]. It is commonly accepted that the fullerene material

diffuses into microcrystals upon heating the blend, leading to a near-to-complete phase separation of P3HT and PC₆₁BM^[3,13]. As a consequence, the total amount of contact area between donor and acceptor material decreases, charge separation will not occur optimally and less favorable pathways for efficient charge transport to the electrodes are available.

Several strategies have been proposed to improve the thermal stability of BHJ polymer:fullerene blends, such as lowering the regioregularity of the polymer backbone, the use of compatibilizers, anchorage of the fullerene acceptor to the polymer chain, the development of polymers with a higher glass transition temperature (T_g), and crosslinkable fullerene and/or conjugated polymer derivatives^[3,14]. An increase in T_g of the electron donor polymer hampers the demixing process by slowing down molecular diffusion^[11c,14j]. Another way to obtain a more stable blend is to introduce a certain amount of functional groups in the donor polymer that can crosslink and 'freeze in' the ultimate morphology after a thermal or UV treatment. The photocrosslinking approach – which allows decoupling from the thermal annealing step^[14e] – has successfully been demonstrated by Fréchet and co-workers based on bromine-functionalized poly(3-alkylthiophene) (P3AT) copolymers^[14g]. Even though the photocrosslinked devices were much more stable, the effect of the rather harsh crosslinking process on the blend morphology is quite unpredictable and hence presents a serious drawback. In a similar way, an azide-functionalized P3HT copolymer was applied to suppress macroscale phase separation, attributed to the formation of an *in situ* compatibilizer at the polymer:PCBM interface^[14m]. Choi *et al.* extended this approach to 4*H*-cyclopenta[2,1-*b*:3,4-*b'*]dithiophene-based copolymers with appended penta-1,4-diene moieties^[14k], one of the

limited reports applying these principles to low bandgap materials^[14t]. Fréchet and co-workers also extended their photocrosslinking work to thieno[3,4-c]pyrrole-4,6-dione (TPD) based donor-acceptor copolymers^[14l]. Most degradation studies on low bandgap polymer solar cells have focused on PCDTBT (poly{[9-(1-octylnonyl)-9*H*-carbazole-2,7-diyl]-2,5-thiophene-diyl-2,1,3-benzothiadiazole-4,7-diyl-2,5-thiophene-diyl}), for which lifetimes approaching seven years have been projected^[15]. Although this is significantly longer than for P3HT-based devices, the initial 'burn-in loss period' – ascribed by the McGehee group to a photochemical reaction in the active layer^[15] and analyzed in more detail by joint work of the Leclerc and Gardette groups^[16] – is more important. McGehee *et al.* have also demonstrated that material purity of the low bandgap polymers is essential for long-term stability^[17]. Very recently it has been shown that light exposure can enhance the thermal stability of polymer(PCDTBT):PC₆₁BM solar cells, as independently reported by the Manca and Durrant groups^[18]. The photostabilizing effect was linked to light-induced oligomerization of PC₆₁BM, effectively hindering its diffusion and crystallization in the blend.

Previous work within our group has indicated that ester-functionalized random P3AT copolymers (with 10, 30 or 50% functionalized side chains) can readily be synthesized by the Rieke polymerization protocol and that these materials show solar cell performances close to the reference P3HT material^[19,20i]. Moreover, the ester-functionalized copolymers were easily converted into the corresponding hydroxyl- and cinnamoyl-functionalized derivatives^[20a], and the absorption window was broadened by 'click' functionalization with phthalocyanines^[20b]. Within the ISOS-3 inter-laboratory consortium, the stability of seven distinct

sets of state-of-the-art OPV devices, degraded under well-defined conditions, was analyzed by different techniques at different research facilities^[20d-g]. In this general study, the ester-functionalized P3AT copolymer showed better stability and reproducibility features as compared to regular P3HT in the same (semi-encapsulated, flexible and inverted) device setup, assigned to a more stable BHJ morphology within the photoactive layer. It was also shown that the morphology and efficiency of hybrid ZnO:polythiophene solar cells can be effectively controlled via ester side chain functionalization^[20c]. Evaluation of the efficiencies of BHJ solar cells based on copolymer:PC₆₁BM photoactive layers revealed that the performance of the ester-functionalized copolymers is comparable to regular P3HT, as far as the introduced side chains are not too long and the ratio of functionalized units is moderate (below 30%)^[20i].

From an initial lifetime screening (9/1, 7/3 and 1/1 ratios of the building blocks), the copolymers with 10% functionalized side chains seemed most promising in terms of both efficiency and stability^[20h,i]. Hence, in this work, fine-tuning around this ratio was performed for a series of 4 copolymers (Fig. 1) – for which a full description of the synthetic procedures and extensive characterization is provided – aiming to assess the impact of the density and chemical nature of the various side chains on OPV efficiency and stability. The evolution of the active layer morphology upon artificial accelerated aging under thermal stress was visualized by Transmission Electron Microscopy (TEM) with additional information from Selected Area Electron Diffraction (SAED) patterns, and the results were complemented with *in situ* *I-V* measurements at elevated temperatures.

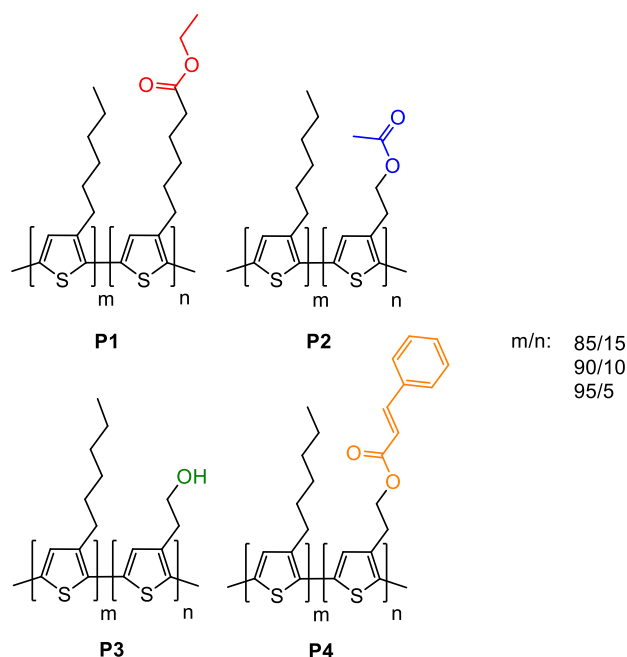


Figure 1: Chemical structures of functionalized P3AT random copolymers **P1-P4**.

2.2 EXPERIMENTAL SECTION

2.2.1 Materials and methods

NMR chemical shifts (δ , in ppm) were determined relative to the residual CHCl_3 absorption (7.26 ppm) or the ^{13}C resonance shift of CDCl_3 (77.16 ppm). Gas chromatography-mass spectrometry (GC-MS) analyses were carried out applying Chrompack Cpsil5CB or Cpsil8CB capillary columns. Polymer molar masses and distributions were determined by size exclusion chromatography (SEC). Analysis was performed on a Tosoh EcoSEC system, comprising of an autosampler, a PSS guard column SDV (50 \times 7.5 mm), followed by three PSS SDV analytical linear XL columns (5 μm , 300 \times 7.5 mm), and a differential refractive index detector (Tosoh EcoSEC RI) and a UV-detector using THF as the eluent at 40 $^\circ\text{C}$ with a flow rate of 1.0 mL min^{-1} . The SEC system was calibrated using linear narrow

polystyrene standards (Polymer Labs) ranging from 474 to 7.5×10^6 g mol⁻¹ ($K = 14.1 \times 10^{-5}$ dL g⁻¹ and $a = 0.70$). Polymer concentrations were in the range of 3–5 mg mL⁻¹. UV-Vis absorption measurements were performed with a scan rate of 600 nm min⁻¹ in a continuous run from 200 to 800 nm. Thin film electrochemical measurements were performed with an Eco Chemie Autolab PGSTAT 30 Potentiostat/Galvanostat using a conventional three-electrode cell under Ar atmosphere (electrolyte: 0.1 M TBAPF₆ in anhydrous CH₃CN). For the measurements, a Ag/AgNO₃ reference electrode (0.01 M AgNO₃ and 0.1 M TBAPF₆ in anhydrous CH₃CN), a platinum counter electrode and a platinum working electrode were used. The polymers were deposited by dipcoating. Cyclic voltammograms were recorded at 100 mV s⁻¹. From the onset potentials of the oxidation and reduction the position of the energy levels could be estimated. All potentials were referenced using a known standard, ferrocene/ferrocenium, which in CH₃CN solution is estimated to have an oxidation potential of -4.98 eV vs. vacuum. DSC measurements were performed at 20 K min⁻¹ in aluminum crucibles on a TA Instruments Q2000 Tzero DSC equipped with a refrigerated cooling system (RCS), using nitrogen (50 mL min⁻¹) as purge gas. TGA experiments were performed at 20 K min⁻¹ in platinum crucibles on a TA Instruments Q5000 TGA using nitrogen (50 mL min⁻¹) as purge gas.

2.2.2 Synthesis

All manipulations were carried out on a dual manifold vacuum/Ar system. Lithium (granular, 99+%) from Acros was stored in a schlenk tube under Ar. Lithium, naphthalene and benzothiophene were weighed in air as needed and transferred to a schlenk tube under a stream of Ar. Naphthalene (Acros, 99+%) and benzothiophene (Sigma-Aldrich, 98%) were stored in a desiccator over

phosphorous pentoxide. Zinc chloride (Acros, analysis grade 98.5%) was transferred into small vials inside a glove box and stored in a separate desiccator over phosphorous pentoxide. Zinc chloride was dried by treating it with thionyl chloride and heating with a Bunsen burner, and subsequently removed under a stream of Ar gas. THF was freshly distilled from Na/benzophenone under a N₂ atmosphere at atmospheric pressure prior to use. Brass cannulas were stored in an (air) oven at 110 °C and cleaned immediately after use with acetic acid (in the case of Zn* remnant), acetone (to clean non-polymeric residues), or hot chloroform and/or chlorobenzene (for polymer-based contaminations). Monomer synthesis was performed according to the procedures previously reported in our manuscript focusing on ester-functionalized copolymers ^[20].

2.2.2.1. Preparation of highly reactive Rieke zinc metal (Zn*)^[21]

Two 120 mL schlenk vessels, A and B, were dried by heating with a bunsen burner under reduced pressure and cooled to rt under a stream of Ar. Schlenk vessel A, filled with Ar, was weighed and then reassembled to the schlenk line. Under a stream of Ar, ZnCl₂ was charged to the vessel. After three Ar/vacuum cycles, ZnCl₂ was wetted with a small amount of SOCl₂. The schlenk was heated by a bunsen burner until the ZnCl₂ salt melted and a white fume was released, and the schlenk was cooled down under an Ar flow. Schlenk flask A was weighed again to determine the exact amount of ZnCl₂ and a stirring bar was added. Dried ZnCl₂ (1.1 equiv) was dissolved in freshly distilled THF (25 mL/g). Li pellets (2.2 equiv), naphthalene (2.25 equiv) and benzothiophene (0.04 equiv) were weighed in air and charged into schlenk B under an Ar stream. Dry THF (the same amount as added to dissolve ZnCl₂) was added (the solution turned

from colorless to dark green within less than 2 min) and the mixture was stirred further for 2 h to dissolve the Li pellets. The ZnCl₂ solution was transferred dropwise via cannula to the lithium naphthalenide solution over 10–15 min. The resulting black suspension can be stirred for 1 more h to consume the undissolved Li or stirring can be stopped right after the addition. The highly reactive zinc was allowed to settle down for a couple of hours. The supernatant was siphoned off via cannula leaving the Zn* powder. Thus prepared Rieke zinc was ready to use.

2.2.2.2. Synthesis of copolymers P1 and P2 (poly{[3-hexylthiophene-2,5-diyl]-co-[3-(6-ethoxy-6-oxohexyl)thiophene-2,5-diyl]} or P[3HT-co-3(EOH)T] and poly{[3-hexylthiophene-2,5-diyl]-co-[3-(2-acetoxyethyl)thiophene-2,5-diyl]} or P[3HT-co-3(AE)T])^[20i]

The monomer mixture, 2,5-dibromo-3-hexylthiophene (**M1**) and either ethyl 6-(2,5-dibromothiophene-3-yl)hexanoate (**M2**) or 2-(2,5-dibromothiophene-3-yl)ethyl acetate (**M3**) (in the corresponding feed ratio: 95/5, 90/10 or 85/15), was added via cannula to freshly prepared Zn*, as prepared by the modified Rieke method^[21], at -78 °C. The mixture was stirred for 1 h at this temperature and then allowed to warm to 0 °C gradually. Unreacted Zn* was allowed to settle down overnight and the organozinc supernatant was filtered via a 0.45 µm acrodisc filter into a flame-dried schlenk vessel. Via a cannula, 0.2 mol% of Ni(dppe)Cl₂ was added to the ice-cooled organozinc solution. The schlenk vessel was immersed into a preheated oil bath at 60 °C and the mixture was stirred at this temperature overnight. It was then poured into a solution of MeOH:HCl (2M) and the resulting dark precipitate was filtered off and washed several times with MeOH. The crude polymer was transferred into an extraction thimble and

purification was performed by sequential soxhlet extractions with MeOH, acetone and hexanes. The polymer was then collected with chloroform and the solvent was removed under reduced pressure. The polymer was redissolved in chloroform and precipitation was again performed upon addition of MeOH. Filtration and drying under high vacuum afforded the pure polymer materials (~50-55% yield). **P1-85/15**: UV-Vis (film, λ_{\max} , nm): 555, 602sh; ^1H NMR (300 MHz, CDCl_3 , δ , ppm): 6.96 (s), 4.10 (q), 2.79 (t), 2.56 (s), 2.31 (t), 1.69 (s), 1.48–1.20 (m), 0.90 (t); FT-IR (NaCl, ν_{\max} , cm^{-1}): 3053, 2955, 2928, 2854, 1738, 1563, 1509, 1455, 1376, 1260, 1179, 820; SEC (THF): $M_w = 25.7 \times 10^3 \text{ g mol}^{-1}$, $M_n = 15.4 \times 10^3 \text{ g mol}^{-1}$, $D = 1.67$; **P1-90/10**: UV-Vis (film, λ_{\max} , nm) 555, 602sh; ^1H NMR (300 MHz, CDCl_3 , δ , ppm): 6.96 (s), 4.11 (q), 2.79 (t), 2.55 (s), 2.31 (t), 1.68 (s), 1.48–1.20 (m), 0.90 (t); SEC (THF): $M_w = 29.0 \times 10^3 \text{ g mol}^{-1}$, $M_n = 17.3 \times 10^3 \text{ g mol}^{-1}$, $D = 1.67$; **P1-95/5**: UV-Vis (film, λ_{\max} , nm): 555, 602sh; ^1H NMR (300 MHz, CDCl_3 , δ , ppm): 6.96 (s), 4.10 (q), 2.79 (t), 2.56 (s), 2.31 (t), 1.69 (s), 1.48–1.20 (m), 0.90 (t); SEC (THF): $M_w = 29.0 \times 10^3 \text{ g mol}^{-1}$, $M_n = 17.9 \times 10^3 \text{ g mol}^{-1}$, $D = 1.62$. **P2-85/15**: UV-Vis (film, λ_{\max} , nm): 551, 600sh; ^1H NMR (300 MHz, CDCl_3 , δ , ppm): 7.00 (s), 6.96 (s), 4.35 (t), 3.14 (t), 2.78 (t), 2.58 (t), 2.06 (s), 1.75–1.60 (m), 1.45–1.34 (m), 0.89 (t); FT-IR (NaCl, cm^{-1}): $\nu_{\max} = 3055, 2954, 2926, 2856, 1744, 1509, 1455, 1378, 1236, 1036, 820$; SEC (THF): $M_w = 37.0 \times 10^3 \text{ g mol}^{-1}$, $M_n = 22.0 \times 10^3 \text{ g mol}^{-1}$, $D = 1.68$; **P2-90/10**: UV-Vis (film, λ_{\max} , nm): 551, 600sh; ^1H NMR (300 MHz, CDCl_3 , δ , ppm): 7.00 (s), 6.96 (s), 4.34 (t), 3.14 (t), 2.78 (t), 2.58 (t), 2.05 (s), 1.75–1.60 (m), 1.45–1.34 (m), 0.89 (t); SEC (THF): $M_w = 29.4 \times 10^3 \text{ g mol}^{-1}$, $M_n = 18.7 \times 10^3 \text{ g mol}^{-1}$, $D = 1.57$; **P2-95/5**: UV-Vis (film, λ_{\max} , nm): 551, 600sh; ^1H NMR (300 MHz, CDCl_3 , δ , ppm): 7.00 (s), 6.96 (s), 4.35 (t),

3.14 (t), 2.78 (t), 2.58 (t), 2.05 (s), 1.75–1.61 (m), 1.48–1.34 (m), 0.90 (t);
SEC (THF): $M_w = 26.6 \times 10^3 \text{ g mol}^{-1}$, $M_n = 17.3 \times 10^3 \text{ g mol}^{-1}$, $D = 1.53$.

2.2.2.3 Synthesis of hydroxyl-functionalized copolymers **P3** (poly{[3-hexylthiophen-2,5-diyl]-co-[3-(2-hydroxyethyl)thiophen-2,5-diyl]} or **P[3HT-co-3(HE)T]**)

Ester-functionalized copolymers **P2**, prepared with different monomer ratios, were dissolved in THF (1 g/100 mL) and a solution of KOH in CH₃OH (6% m/v, 1 g polymer/50 mL solution) was then added dropwise over a period of 1 h at rt. The reaction mixture was heated at reflux for 3 h, cooled down to rt and poured into CH₃OH. After neutralization, the precipitated polymers were recovered by filtration, rinsed with fresh CH₃OH and dried under high vacuum. **P3-85/15**: UV-Vis (film, λ_{max} , nm): 551, 600sh; ¹H NMR (300 MHz, CDCl₃, δ , ppm): 7.03 (s), 6.96 (s), 3.94 (t), 3.11 (t), 2.77 (t), 1.65 (t), 1.45–1.25 (m), 0.87 (t); FT-IR (NaCl, ν_{max} , cm⁻¹): 3055, 2954, 2926, 2856, 1509, 1455, 1377, 1046, 820; SEC (THF): $M_w = 29.3 \times 10^3 \text{ g mol}^{-1}$, $M_n = 16.1 \times 10^3 \text{ g mol}^{-1}$, $D = 1.82$; **P3-90/10**: UV-Vis (film, λ_{max} , nm): 551, 600sh; ¹H NMR (300 MHz, CDCl₃, δ , ppm): 7.03 (s), 6.96 (s), 3.93 (t), 3.09 (t), 2.78 (t), 1.67 (t), 1.45–1.25 (m), 0.89 (t); SEC (THF): $M_w = 34.2 \times 10^3 \text{ g mol}^{-1}$, $M_n = 19.7 \times 10^3 \text{ g mol}^{-1}$, $D = 1.74$; **P3-95/5**: UV-Vis (film, λ_{max} , nm): 551, 600sh; ¹H NMR (300 MHz, CDCl₃, δ , ppm): 7.03 (s), 6.96 (s), 3.94 (t), 3.09 (t), 2.78 (t), 1.70 (t), 1.45–1.25 (m), 0.89 (t); SEC (THF): $M_w = 31.7 \times 10^3 \text{ g mol}^{-1}$, $M_n = 18.7 \times 10^3 \text{ g mol}^{-1}$, $D = 1.69$.

2.2.2.4 Synthesis of copolymers **P4** (poly{[3-hexylthiophene-2,5-diyl]-co-[3-(2-(Z)-(3-phenylacryloyloxy)ethyl)thiophene-2,5-diyl]} or **P[3HT-co-3(PAOE)T]**)

Hydroxyl-functionalized copolymers **P3** were dissolved in THF (1 g/100 mL) at 50 °C. The solutions were cooled down to rt and excess amounts of triethylamine and *trans*-cinnamoyl chloride (10 equiv with regard to the copolymer) were added. The reaction mixtures were warmed to 50 °C and stirred overnight. The mixtures were poured into CH₃OH/HCl (2M) (2/1, v/v) and stirred for 30 min. After neutralization, the precipitated polymers were filtered off and rinsed with water and methanol intensively. The polymers were obtained in pure form after soxhlet extraction with acetone, followed by drying under high vacuum. **P4-85/15**: UV-Vis (film, λ_{\max} , nm): 553, 599sh; ¹H NMR (300 MHz, CDCl₃, δ , ppm): 7.67–7.05 (m), 6.96 (s), 6.42 (d), 4.49 (t), 3.23 (t), 2.79 (t), 1.75–1.60 (m), 1.49–1.25 (m), 0.90 (t); SEC (THF): $M_w = 35.2 \times 10^3 \text{ g mol}^{-1}$, $M_n = 19.2 \times 10^3 \text{ g mol}^{-1}$, $D = 1.83$; **P4-90/10**: UV-Vis (film, λ_{\max} , nm): 553, 599sh; ¹H NMR (300 MHz, CDCl₃, δ , ppm): 7.67–7.05 (m), 6.96 (s), 6.42 (d), 4.49 (t), 3.21 (t), 2.78 (t), 1.75–1.61 (m), 1.49–1.25 (m), 0.90 (t); SEC (THF): $M_w = 31.7 \times 10^3 \text{ g mol}^{-1}$, $M_n = 18.9 \times 10^3 \text{ g mol}^{-1}$, $D = 1.67$; **P4-95/5**: UV-Vis (film, λ_{\max} , nm): 553, 599sh; ¹H NMR (300 MHz, CDCl₃, δ , ppm): 7.67 (d), 7.47–7.05 (m), 6.96 (s), 6.41 (d), 4.49 (t), 3.23 (t), 2.78 (t), 1.75–1.60 (m), 1.50–1.25 (m), 0.90 (t); SEC (THF): $M_w = 33.9 \times 10^3 \text{ g mol}^{-1}$, $M_n = 19.2 \times 10^3 \text{ g mol}^{-1}$, $D = 1.76$.

2.2.3. BHJ OPV devices

Bulk heterojunction solar cells were fabricated using the standard glass/ITO/polymer:PC₆₁BM/Ca/Al architecture. Before processing the devices,

the ITO (100 nm) coated substrates (Kintec, sheet resistivity 20 Ω /sq) were exposed to a standard cleaning procedure using soap, demineralized water, acetone and isopropanol, followed by a UV/O₃-treatment for 15 min. Afterwards, PEDOT-PSS (poly(3,4-ethylenedioxythiophene)-poly(styrenesulfonic acid); Bayer) was spin-coated on top with a thickness of \sim 30 nm. The samples were placed under nitrogen atmosphere in a glove box and an annealing step was performed at 130 °C for 15 min to remove any residual water. This was followed by the deposition of the polymer:PC₆₁BM (Solenne) active layer blends by spin-coating, aiming for a layer thickness of \sim 80 nm. The solutions for the blends were prepared with 10 mg mL⁻¹ of polymer in a 1:1 ratio with PC₆₁BM, using chlorobenzene (CB) as a solvent. Subsequently, these layers were exposed to a post-process annealing at 130 °C for 10 min to optimize the layer morphology, and hence the initial efficiency. The devices were finalized by evaporating the top electrodes, Ca and Al, with layer thicknesses of \sim 20 and 80 nm, respectively, at a pressure of 1×10^{-6} mbar. In this way, complete cells with an active area of 25 mm² were obtained.

After device preparation, the initial efficiencies were measured using a Newport class A solar simulator (model 91195A), calibrated with a silicon solar cell to give an AM 1.5 spectrum. To investigate the thermal degradation behavior, the samples were exposed to an elevated temperature in a nitrogen atmosphere (glove box) for a certain amount of time, while measuring the *I-V* characteristics at particular time intervals, using a White 5500K LED (Lamina). Degradation experiments were always performed on a bulk of substrates. This means for example that the 3 most promising copolymers and the reference P3HT sample (always 4 solar cells at a time) were degraded at the same time in the same setup. Before performing the more detailed study, a rough screening experiment

was performed utilizing a hotplate (280 x 200 mm, type PZ28-2ET, Harry Gestigkeit GmbH, with a PR5 programmer controller). To analyze the layer morphology more into detail, TEM (FEI Tecnai Spirit using an accelerating voltage of 120 kV) samples were prepared. To this end, polymer:PC₆₁BM layers were spin-coated directly on clean glass substrates. Subsequently, the active layers were removed from the substrates by etching in hydrofluoric acid.

2.3 RESULTS AND DISCUSSION

Up until recently, P3HT:PC₆₁BM has been the OPV workhorse system of choice due to the material availability at a reasonable cost, the ease of processing and the relatively high efficiencies that can be obtained from this blend^[6]. However, the intimately mixed donor:acceptor morphology of this heterogeneous blend is not thermodynamically stable over prolonged periods of time, a fact that is easily observable when it is exposed to higher temperatures. To evaluate the BHJ active layer intrinsic (thermal) stability – one of the key factors to improve general OPV stability – experiments monitoring the photovoltaic parameters are generally conducted at elevated temperatures ('accelerated aging' tests).

In previous work we have synthesized a series of regioregular functionalized random P3AT copolymers with different built-in ratios of the functionalized thiophene units (Fig. 1)^[20]. From preliminary studies it is known that both the 'alcohol' and 'cinnamoyl'-substituted 9/1 copolymers (**P3** and **P4**, respectively) have a substantial effect on the thermal stability of the active layer blend morphology^[20h]. For both copolymers, the short-circuit current density (J_{sc}) remained above 90% of its initial value upon thermal annealing at 110 °C for 150 h. In this study, a more general screening of the stability features resulting

from the introduction of functionalized side chains on a polythiophene backbone is presented, varying the amount of functional entities between 5 and 15%.

2.3.1 Synthesis and characterization

As the so-called 'Rieke zinc method' allows the preparation of regioregular polythiophenes with appended ester-functionalized side chains (in contrast to the widely employed GRIM method) directly from the prefunctionalized monomers, this procedure was adopted toward the desired side-chain functionalized random copolymers^[6,22]. Despite the inherent advantages of this method – excellent chemoselectivity and high functional group tolerance and stability of the organozinc reagents^[23] – it has only scarcely been used for the synthesis of conjugated polymer materials so far, and mostly for (co)polythiophenes^[24].[‡] The main reasons for this limited success are the rather unreliable synthesis of the active zinc species and the special precautions that have to be taken. To counter this, we have recently established an efficient and reproducible procedure for the preparation of highly reactive Rieke zinc under standard laboratory conditions^[21]. Rieke zinc is commonly prepared by the reduction of zinc chloride with lithium using a stoichiometric amount of naphthalene. In our hands, it was observed that the reaction outcome was highly dependent on the naphthalene source and purity grade. The presence of benzothiophene seems crucial to avoid coagulation of the zinc particles and the amount of benzothiophene has a large effect on the physical properties and the reactivity of the resulting zinc powder. Accordingly, highly reactive Rieke zinc

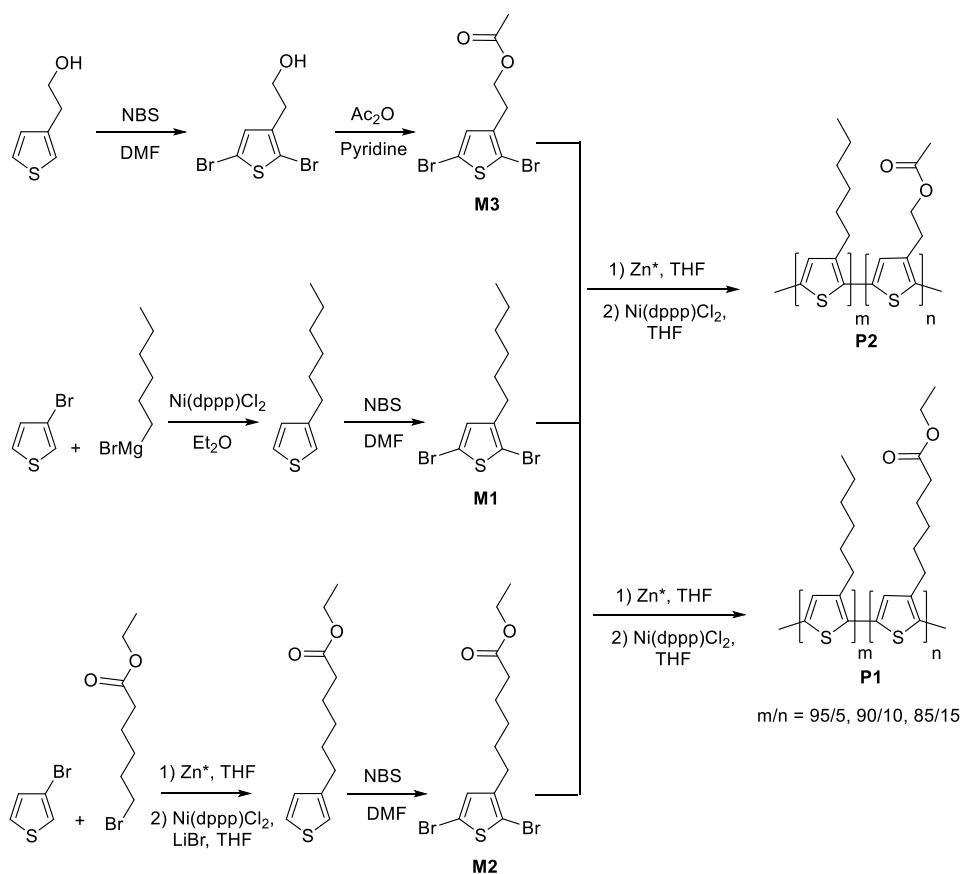
[‡] The importance of the Rieke zinc synthetic method for the OPV field cannot be underestimated though, as a large number of studies are based on the commercially available 'Rieke P3HT'

was easily prepared from zinc chloride by adding an optimum amount (3 mol% with regard to ZnCl_2) of benzothiophene into the lithium naphthalenide solution (prepared *in situ*). The Rieke zinc obtained in this way was previously successfully employed in the synthesis of regioregular P3HT^[21].

The synthetic strategies applied for the requested 2,5-dibromothiophene monomers and ester-functionalized copolymers are shown in Scheme 1. 2,5-Dibromo-3-hexylthiophene (**M1**) was prepared according to a literature procedure via Kumada coupling of 3-bromothiophene and hexylmagnesium bromide and subsequent dibromination with an excess of *N*-bromosuccinimide (NBS) in DMF^[25]. 2-(Thiophene-3-yl)acetic acid was reduced with lithium aluminium hydride in diethyl ether to give 2-(thiophene-3-yl)ethanol, which was then dibrominated and finally reacted with acetic anhydride in pyridine yielding monomer **M3** in high yield. A similar route was followed to prepare ethyl 6-(2,5-dibromothiophene-3-yl)hexanoate (**M2**). Nevertheless, in the first step an organozinc compound was employed instead of the standard organomagnesium reagent. Following the optimized procedure to prepare Rieke zinc in highly reactive form^[21], 6-bromohexanoate was treated with an excess of Rieke zinc at room temperature to afford (6-ethoxy-6-oxohexyl)zinc bromide (by oxidative addition) in excellent (>99%) yield. The coupling reaction with 3-bromothiophene was performed in the presence of 5 mol% of $\text{Ni}(\text{dppe})\text{Cl}_2$ catalyst and LiBr salt to shorten the reaction time^[26].

Ester-functionalized copolymers **P1** and **P2** were then synthesized by the Rieke method (Scheme 1)^[20,21]. Monomer mixtures of **M1**, **M2** and **M3**, in molar compositions 95/5, 85/15 and 90/10, were treated with freshly prepared Rieke zinc to form the corresponding organozinc solutions. Addition of 0.2 mol% of the $\text{Ni}(\text{dppe})\text{Cl}_2$ catalyst then afforded the respective polymers in good yields (~50-

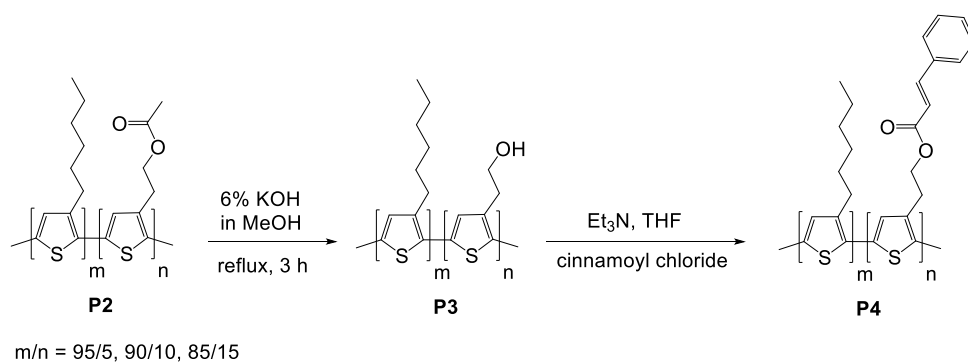
55%) after successive purification by precipitation in methanol, Soxhlet extractions (first with methanol to remove the catalyst, thereafter with hexanes to get rid of the low molar mass species, and finally with acetone to narrow the polydispersity), and reprecipitation.



Scheme 1: Synthetic pathways toward ester-functionalized P3AT copolymers **P1** and **P2**.

The pendant ester moieties can easily be converted to other functionalities by applying post-polymerization protocols (Scheme 2). Hydrolysis was performed by refluxing the **P2** copolymers in methanolic potassium hydroxide^[20h,27]. The success of the reaction was confirmed by the disappearance of the acetoxy

singlet ($\delta = 2.06$ ppm) in the ^1H NMR spectrum and the C=O vibration at ~ 1740 cm^{-1} in the FT-IR spectrum (Fig. S3). Hydrolysis of the ester functions to alcohol moieties reduced the copolymer solubility. Further reaction of the alcohol groups with cinnamoyl chloride in the presence of triethylamine afforded copolymer series **P4** (Scheme 2)^[20h,28]. Full conversion was proven by the appearance of the cinnamon-related signals in the aromatic region of the ^1H NMR spectrum ($\delta = 6\text{--}7$ ppm) and reappearance of an ester-like C=O absorption (~ 1716 cm^{-1}) in FT-IR (Fig. S3).



Scheme 2: Post-polymerization hydrolysis and further functionalization of the **P2** ester copolymers.

Size exclusion chromatography (SEC) was used to determine the molar masses and polymer distributions (Table 1). All copolymers had reasonable average molar masses ($M_n = 15\text{--}20 \times 10^3$ g mol^{-1}) with polydispersity indices of 1.6–1.8. Compared with P3HT synthesized by the same procedure ($M_n = 35.3 \times 10^3$ g mol^{-1} , $D = 1.51$), the molecular weights of the copolymers are slightly lower.

Table 1: Molar masses and distributions of copolymers **P1–P4**, as determined by SEC.

Polymer	M_n ($\times 10^3$ g mol⁻¹)	<i>D</i>
P3HT	35.3	1.51
P1 – 85/15	15.4	1.67
P1 – 90/10	17.3	1.67
P1 – 95/5	17.9	1.62
P2 – 85/15	22.0	1.68
P2 – 90/10	18.7	1.57
P2 – 95/5	17.3	1.53
P3 – 85/15	16.1	1.82
P3 – 90/10	19.7	1.74
P3 – 95/5	18.7	1.69
P4 – 85/15	19.2	1.83
P4 – 90/10	18.9	1.67
P4 – 95/5	19.2	1.76

UV-Vis absorption spectra of the side-chain functionalized copolymers were recorded both in solution and in thin film using chloroform as the (casting) solvent (Fig. S1, S2). The solution UV-Vis spectra show that the four different regioregular copolymers all have a maximum absorption wavelength (λ_{\max}) at approximately 450 nm. The solid-state UV-Vis spectra are red-shifted, suggesting molecular organization in the thin films. All copolymers showed a maximum absorption at ~ 550 nm with a shoulder at ~ 605 nm^[29]. The absorption around 605 nm was in general slightly more intense compared to Rieke P3HT, pointing to a larger degree of ordering (crystallinity and/or supramolecular aggregation).

Cyclic voltammetry (CV) was employed to study the electrochemical characteristics of the polymers and to estimate their highest occupied molecular

orbital (HOMO) and lowest unoccupied molecular orbital (LUMO) energy levels and bandgaps. The results obtained (for unannealed thin films of the respective copolymers) are summarized in Table S1. Rieke P3HT showed a HOMO level of -5.25 eV, a LUMO level of -3.37 eV, and an optical band gap of 1.88 eV. The side-chain functionalized copolymers all showed comparable values with regard to the reference polymer, indicating that the functionalization does not lead to a noticeable impact on the electrochemical characteristics.

Thermogravimetric analysis (TGA) was performed on the 85/15 copolymers to evaluate the thermal stability as a result of the different side-chain functionalities introduced. From Fig. 2, it can clearly be seen that all materials are stable up to a temperature of at least 300 °C.

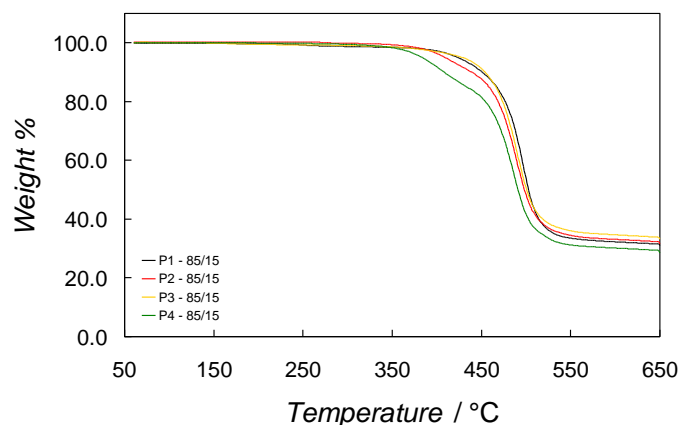
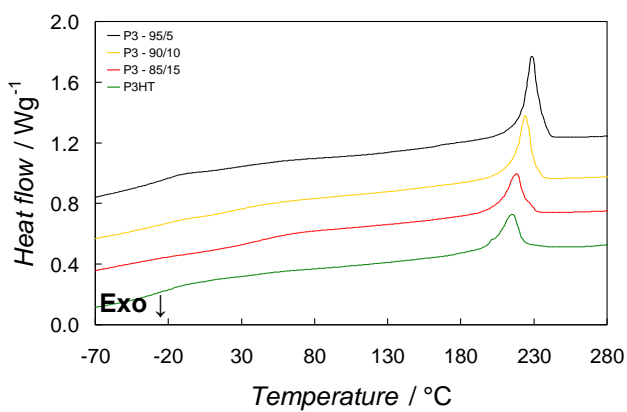
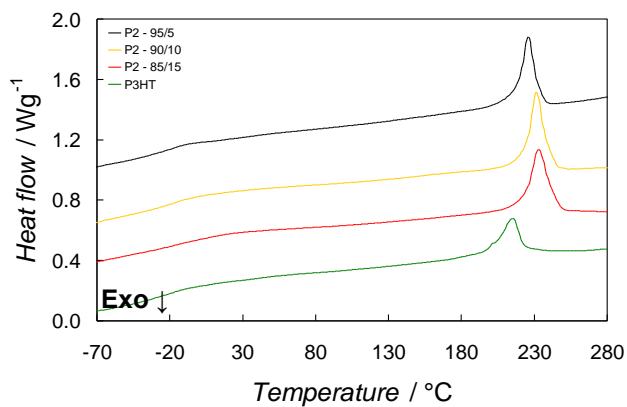
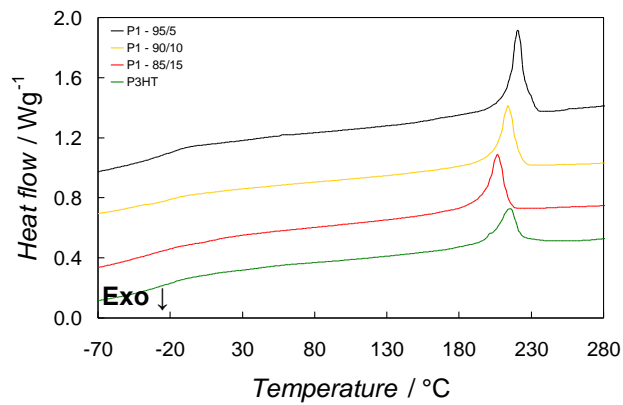


Figure 2: TGA (at 20 K min⁻¹) of the **P1-P4-85/15** copolymers.

DSC thermograms for the different random copolymers are presented in Fig. 3, and the values of the melting peak temperatures and enthalpies are gathered in Table 2. All the polymers analyzed show semi-crystalline behavior. The glass transition temperatures (T_g) were hard to determine due to an unclear step in the heat capacity giving a broad transition. This is consistent with the high

melting enthalpies detected in second heating, indicative for a high degree of crystallinity. In all Figures, a thermogram of pure Rieke P3HT is included for comparison. For the **P2** copolymers, a higher amount of functionalized repeating units leads to higher melting points and higher crystallinity (higher ΔH_m). This trend does not hold for the other copolymers studied. For the **P1**, **P3** and **P4** copolymers, a maximum in both melting point and crystallinity is reached for the 95/5 composition. Further inclusion of functionalized repeating units in these systems probably disturbs crystal formation. These trends might be important for the respective functionalized P3HT:PC₆₁BM state diagrams^[13] and corresponding thermal annealing procedures toward an optimized nanomorphology of the photoactive layer and device performance.



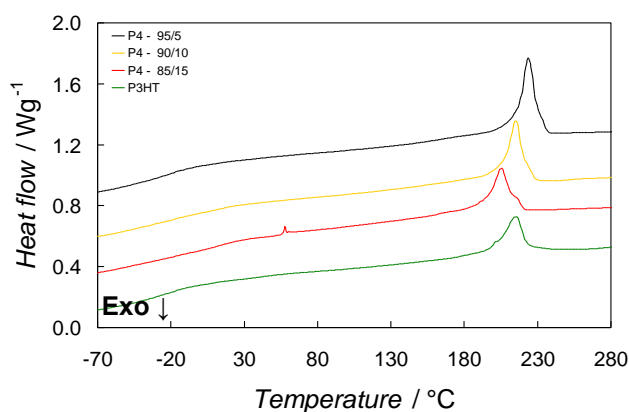


Figure 3: DSC thermograms for the second heating (at 20 K min⁻¹) of the **P1–P4** copolymers. Rieke P3HT is included for comparison. The curves are shifted vertically for clarity.

Table 2: Melting peak temperatures and enthalpies for all copolymers. Rieke P3HT is included for comparison.

Polymer	T_m (°C)	ΔH_m (J g ⁻¹)
P1 – 95/5	221	24.6
P1 – 90/10	214	19.4
P1 – 85/15	207	19.8
P2 – 95/5	226	17.0
P2 – 90/10	232	21.0
P2 – 85/15	233	21.0
P3 – 95/5	228	23.0
P3 – 90/10	224	18.7
P3 – 85/15	218	14.4
P4 – 95/5	224	21.9
P4 – 90/10	215	18.0
P4 – 85/15	205	14.1
P3HT (Rieke) ^a	215	16.2

^a $M_n = 35.3 \times 10^3$ g mol⁻¹, $D = 1.51$.

2.3.2 Bulk heterojunction polymer solar cells

Solar cells were produced using a glass/ITO/PEDOT-PSS/Active layer/Ca/Al architecture, with donor polymers P3HT and **P1–P4** blended in a 1:1 ratio with PC₆₁BM and using chlorobenzene as the active layer spin-coating solvent. The incorporation of functional moieties on the side chains influences both the solubility and the crystallinity of the copolymers^[20a,i], which obviously has an effect on the P3AT:PC₆₁BM blend film morphology, hence also strongly influencing the *I*-*V* characteristics (open circuit voltage *V*_{oc}, short-circuit current density *J*_{sc}, fill factor FF and efficiency η). However, as can be observed in Fig. 4 and Table 3, showing the optimized efficiencies of the copolymers with 5% of appended functionalized side chains, the PCEs are only altered to a minor extent compared to regular P3HT if small amounts of the functionalized comonomers are introduced. In this case, dibromooctane (DBO) was used as an additive in a concentration of 2.5 w/v% to enhance the solar cell performance, rather than performing an annealing step as routinely done for P3HT-based blends [30]. Interestingly, the solar cell output parameters are in the same range as for regular P3HT for the copolymers in which the functionalized side chain is rather small (**P2** and **P3**), whereas the copolymers with larger side chains generally show a slightly lower performance (**P1** and **P4**), which is most notable in the *J*_{sc} (Table 3). In general, *V*_{oc}'s and fill factors are higher for all copolymer devices at the expense of the current (density). The (short) ester-functionalized copolymer **P2** shows even higher efficiency than regular P3HT. As previously shown, larger aberration on the side chains might result in a non-optimal configuration of the crystalline domains, hindering the efficiency of charge separation^[20a,i]. The efficiencies of the 10% and 15% functionalized P3ATs were generally (slightly) lower (Table S2), but it has to be mentioned that the

processing parameters (solvent, concentration, additive, polymer:fullerene ratio) are not individually optimized and these can be expected to deviate more from the standard P3HT processing conditions for larger functionalization degrees.

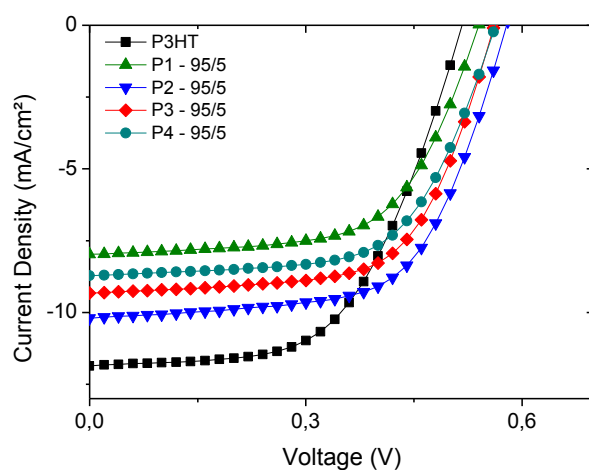


Figure 4: Optimum J - V characteristics for the copolymer:PC₆₁BM systems with a functionalized monomer built-in ratio of 5%.

Table 3: Photovoltaic parameters of optimized solar cells based on P3HT and **P1-P4**.^a

Donor materials	V _{oc} (V)	J _{sc} (mA/cm ²)	FF	η (%)
P3HT ^b	0.52	11.86	0.56	3.48
P1 – 95/5	0.54	7.97	0.62	2.67
P2 – 95/5	0.58	10.20	0.62	3.69
P3 – 95/5	0.56	9.33	0.64	3.34
P4 – 95/5	0.56	8.72	0.63	3.07

^a Glass/ITO/PEDOT-PSS/Active Layer/Ca/Al, using chlorobenzene as a solvent with 2.5 w/v% of DBO added. ^b In-house prepared.

2.3.3 Accelerated (thermal) ageing

Table 4 shows the initial efficiencies for the solar cell devices applied for the thermal degradation experiments. The devices were not annealed prior to the initial lifetime screening tests. However, the first data points, as shown in the Table, are taken after 5 hours of exposure to a temperature of 85 °C. Moreover, the additive was not included to minimize the influence of additional components and/or parameters. It has to be noted that the optimal annealing times are actually different for the various copolymer systems, easily observable by a clear color shift from orange to purple. More in detail, one can observe this shift after 5 min for P3HT, whereas this occurs at slightly longer times (15–20 min) for materials **P1–P4**. For these aging experiments, it should also be mentioned that the applied pristine P3HT material was synthesized in-house, by the same Rieke protocol, to allow optimal comparison with the various copolymer derivatives (enhancing the chances of the presence of similar 'impurities'). This might explain the slightly inferior *I-V* characteristics obtained for the reference system in comparison with literature values^[6].

Table 4: Initial solar cell performance parameters for copolymer series **P1–P4** prior to the thermal degradation experiments.^a

Donor materials	Voc (V)	Jsc (mA/cm²)	FF	η (%)
P3HT	0.56	7.99	0.62	2.77
P1 – 95/5	0.54	5.70	0.61	1.88
P1 – 90/10	0.55	7.49	0.64	2.62
P1 – 85/15	0.54	7.5	0.63	2.55
P2 – 95/5	0.58	8.75	0.60	3.04
P2 – 90/10	0.56	8.38	0.65	3.06
P2 – 85/15	0.59	7.97	0.64	2.99
P3 – 95/5	0.56	8.47	0.65	3.08
P3 – 90/10	0.55	7.15	0.50	1.97
P3 – 85/15	0.60	6.79	0.58	2.33
P4 – 95/5	0.55	8.27	0.62	2.83
P4 – 90/10	0.56	7.91	0.44	1.96
P4 – 85/15	0.56	6.92	0.35	1.29

^a Glass/ITO/PEDOT-PSS/Active Layer/Ca/Al, using chlorobenzene as a solvent. No annealing was performed. Data points were taken after 5 h exposure to 85 °C.

First of all, a preliminary screening experiment was performed to identify the most promising materials for the different copolymer series and conduct a more in-depth lifetime study (up to 700 h) on these derivatives afterwards. Initially, a temperature stress of 85 °C was chosen, as this has become the standard degradation temperature for polymer:PC₆₁BM solar cells (related to the maximum usage T)^[3,20d-g]. Additionally, the experiments were repeated at 100 °C. Solar cell devices of the various materials were prepared as indicated above and placed on a hotplate in the glove box at the specified temperature. At specifically chosen time intervals, the substrates were removed from the hotplate and the *I-V* characteristics were measured. Fig. 5 gathers the data of

the degradation study performed at 85 °C during 700 h (Fig. S4 shows the results at 100 °C for 140 h). The long exposure times are chosen to reveal any possible additional degradation behavior, as it has been shown to be the case for past experiments^[19,31]. The use of relative values (ratio of the values at time t and t_0) is not to hide the lower performance of the copolymers, as the initial efficiencies are comparable to P3HT (as shown above), but to provide an accessible means of comparison between the different material systems. As can clearly be observed, copolymers **P2**, **P3** and **P4** lead to more stable blend systems in comparison with the system containing regular P3HT as the donor material. On the other hand, copolymers **P1** seem to give rise to less stable blends, for each of the three different built-in ratios. Closer inspection of Fig. 5b and 5d, containing the degradation data on copolymers **P2** and **P4**, reveals a particular trend amongst the various functionalization degrees, i.e. an increased stability upon moving from 5% to 15% of functionalized (ester) side chains. On the other hand, for the alcohol-copolymer **P3** series (Fig. 5c), the 10% functionalized copolymer seems to provide the most thermally stable blend. Even though the differences obtained are rather small, the results of the degradation study at 100 °C confirm the observed phenomena (Fig. S4).

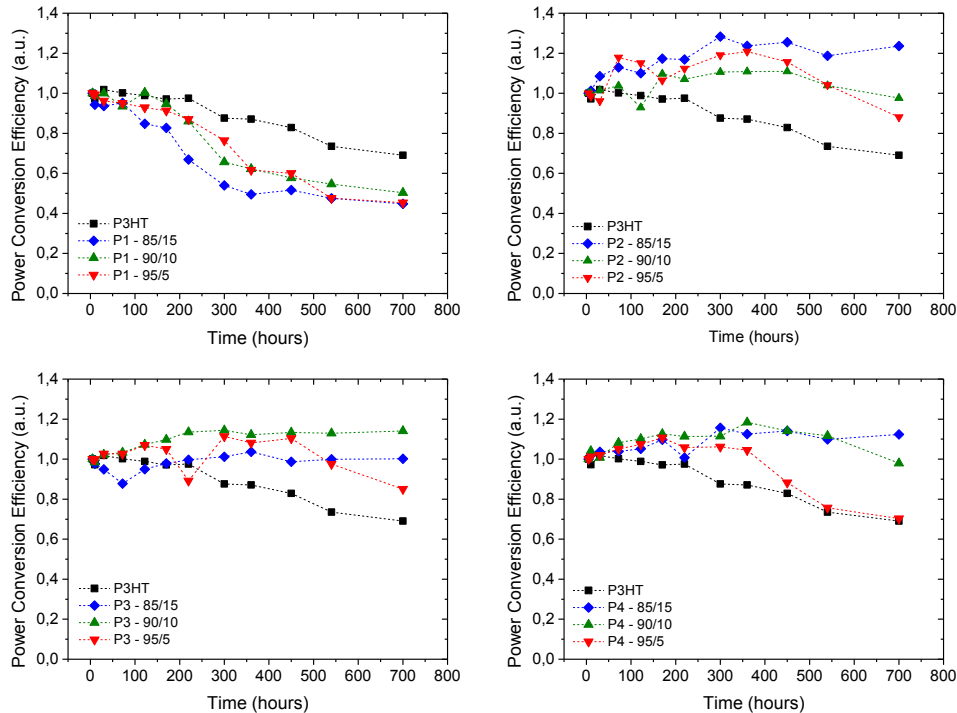


Figure 5: Initial screening of the degradation behavior for all P3AT:PC₆₁BM-based systems at 85 °C. In all cases Rieke P3HT is included for comparison.

Dashed lines serve as a guide to the eye only.

A possible explanation for the differences in stability in comparison with the standard P3HT:PC₆₁BM system obviously has to focus on the presence of the functional groups. For copolymers **P4**, (spontaneous) crosslinking of the vinyl groups could possibly explain the increase in stability^[19]. A simple test consisting of dipping the substrates in the applied spin-coating solvent (chlorobenzene) revealed, however, that the active layer dissolved in the solvent, so no crosslinking has occurred.

Following the initial screening of the large material set for the optimal comonomer ratios, a more thorough degradation study was performed in a more

dedicated setup. Copolymers **P2-85/15**, **P3-90/10** and **P4-85/15** were subjected to a constant heating at 85 °C, and the *I-V* characteristics were measured *in situ* and compared against a reference P3HT:PC₆₁BM solar cell. The results for these experiments are visualized in Fig. 6. It is clear that the *in situ* method reduces the scattering as observed in the 'rough' screening procedure and enhances reproducibility.

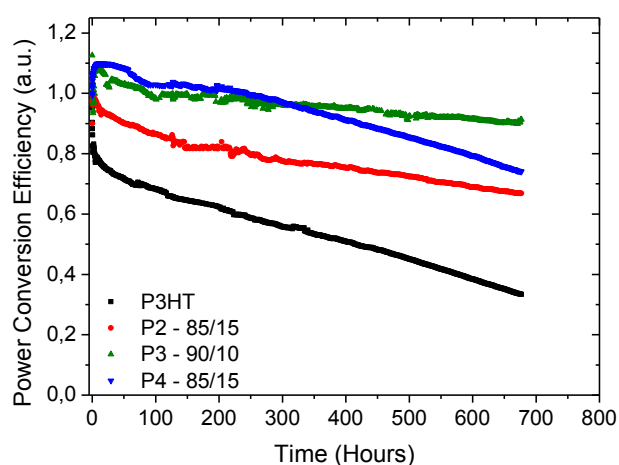


Figure 6: Degradation behavior of BHJ OPV devices with photoactive layers based on P3HT and the best-performing P3AT (**P2-P4**) copolymers. The curves are normalized to the first measurement point at 85 °C.

As can be observed, due to the constant monitoring of the efficiency, additional features come into play (separate degradation curves for the V_{oc} , J_{sc} and FF are shown in Fig. S5). For the **P3** - 90/10 and **P4** - 85/15 copolymers, an initial increase in efficiency (mainly due to J_{sc} , Fig. S5) can be seen, from which we can deduce that the annealing step (130 °C for 10 min) was not sufficient to afford an optimal nanocrystalline interpenetrating network. The most remarkable observation is the steep decrease in efficiency for the reference P3HT:PC₆₁BM

solar cell in less than a couple of hours, which has been identified in literature as the initial 'burn-in'^[15a,b]. Afterwards, the efficiency remains more stable, although the decrease is still more pronounced for the reference system in comparison with the three copolymers. For the functionalized P3ATs the initial burn-in is almost absent and consequently the overall efficiency remains noticeably higher than for the P3HT:PC₆₁BM reference solar cell. As the only different parameter compared to the reference system – assuming a similar purity of all materials, as they are made and purified by the same protocols – is the introduction of functional groups, we can conclude that the increase in stability has to be attributed to the presence of these functions. Among the different copolymers, the ester- and alcohol-functionalized derivatives look somewhat more promising, as a gradual efficiency decrease is noticed for the cinnamoyl derivative after ~300 hours. Obviously, one must note that the exposure of the devices to elevated temperatures for these prolonged periods of time will also have consequences for the electrodes and the interphases, which might lead to (minor) artifacts in the curves.

Optical microscopy images were taken to reveal preliminary information on the film morphology aging process. Fig. 7 shows the films of P3HT:PC₆₁BM and **P2–P4–90/10**:PC₆₁BM blends at 3 different stages upon exposure to a temperature of 125 °C. As can be observed, the P3HT:PC₆₁BM film already contains a multitude of microcrystalline (fullerene) needles after only 15 minutes, whereas the other systems barely show any needle formation. After intense annealing for 24 hours at 125 °C, a small amount of crystallization has occurred, giving a preliminary indication on the increased thermal stability of these BHJ blends in comparison to regular P3HT:PC₆₁BM.

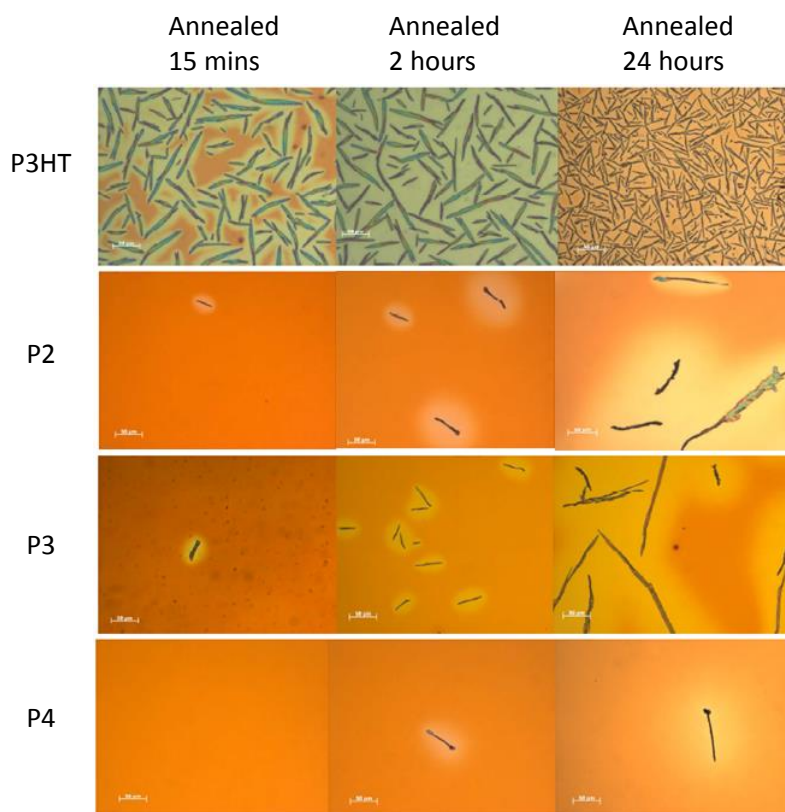


Figure 7: Optical microscopy images of P3HT and **P2-P4-90/10** films when blended with PC₆₁BM, annealed at 125 °C for 15 min, 2 h and 24 h.

To gain a more in-depth view, TEM images were taken to visualize the morphological changes occurring within the active layer blends during the thermal treatment at 85 °C in more detail (Fig. 8). Based on the data obtained from the degradation study, it was opted to have the images taken directly after the post-process annealing step at 130 °C and after 15 and 700 hours of exposure to the thermal stress. TEM images were made at different places within the samples and no differences in morphology were observed, which makes the images representative for the whole sample. After the initial

annealing, some phase-separated needles can already be seen for the reference P3HT:PC₆₁BM system. Lighter colored areas are visible around these needles. SAED patterns (also shown in Fig. 8) at different locations reveal the content of the mixture. For the darker colored areas, the diffraction pattern shows two concentric rings, which can be ascribed to the presence of both P3HT (outer ring) and PC₆₁BM (inner ring) in the blend. When moving toward the lighter area, the inner ring disappears, revealing that this area contains mostly P3HT. The needle-like structures are crystalline and the diffraction patterns show that these structures are indeed PC₆₁BM microcrystals. In other words, once a PC₆₁BM nucleus is formed, the PC₆₁BM surrounding this point will diffuse toward this nucleus and the crystal needle will grow, leaving a depletion area of PC₆₁BM-deficient P3HT around it^[32]. The TEM image of the reference P3HT:PC₆₁BM solar cell exposed to 85 °C for 15 hours shows a substantially higher amount of needles and larger depletion areas. From this, we can conclude that across this timeframe, the surrounding PC₆₁BM has diffused even more toward the already formed crystals, leading to an enhanced phase separation and therefore a decrease in efficiency. Finally, after 700 hours of exposure to 85 °C, the phase separation is almost complete, leading to a system consisting mainly of PC₆₁BM microcrystals embedded in a P3HT-rich layer^[11c,13]. Moving on to the **P3**:PC₆₁BM and **P4**:PC₆₁BM blends, we can observe that along the entire time range of 700 hours no PC₆₁BM microcrystals are formed, which explains the increased thermal stability for these blends. For the copolymer **P2**:PC₆₁BM blend, the TEM images reveal that exposure of the films to 85 °C for 15 hours does not lead to any microcrystal formation. However, after 700 hours, the system is in a similar state as the reference P3HT:PC₆₁BM layer after 15 hours.

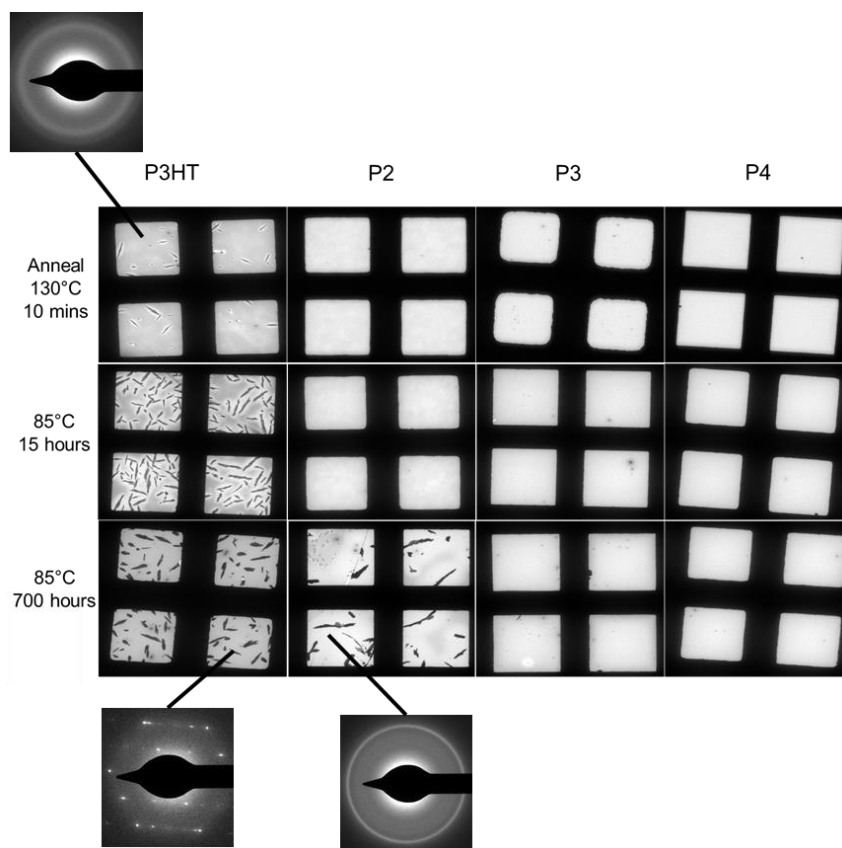


Figure 8: TEM images after annealing (10 min at 130 °C, 15 h at 85 °C, and 700 h at 85 °C) for blends of PC₆₁BM and P3HT or the most stable P3AT copolymers **P2–P4**.

Integration of the SAED patterns of Fig. 8 provides a more accurate picture of the amount of PC₆₁BM left in the matrix in between of the needles after exposure to the thermal stress (Fig. 9). As illustrated in Fig. 9a, the peaks around 3.6 and 4.5 Å are related to P3HT and PC₆₁BM, respectively. The more intense the peak at 4.5 Å, the higher the PC₆₁BM content in the matrix. As can be observed from Fig. 9a, prolonged exposure to 85 °C leads to a strong decrease in PC₆₁BM content for the P3HT:PC₆₁BM reference system, proving that

it is really PC₆₁BM that is diffusing out of the mixture into needle-like structures. On the other hand, the SAED patterns for copolymer **P2** reveal the presence of considerable amounts of PC₆₁BM remaining in the matrix, even after completion of the stability test (Fig. 9b). The intensity of the PC₆₁BM peak somewhat decreased, confirming the results from the TEM images. Finally, Fig. 9c and d show that the PC₆₁BM content in the matrix of the blends based on copolymers **P3** and **P4** remains practically constant, even after exposure to 85 °C for up to 700 hours.

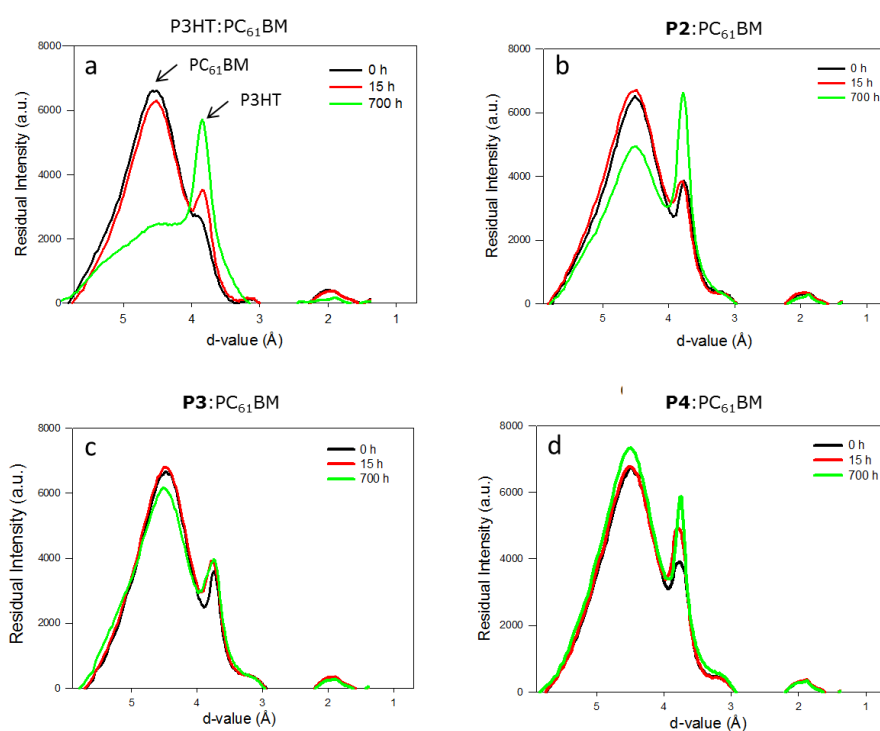


Figure 9: Integrated SAED patterns for P3HT:PC₆₁BM and the various copolymer:PC₆₁BM systems: a) P3HT:PC₆₁BM, b) **P2-85/15**:PC₆₁BM, c) **P3-90/10**:PC₆₁BM, d) **P4-85/15**:PC₆₁BM.

Although the glass transition temperatures of the copolymers were not clearly identifiable by regular DSC, previous scattered results (e.g. $T_g = 30$ °C for **P3-90/10** and $T_g = 19$ °C for **P4-90/10**^[20h]) indicate that these are all in close proximity to the value found for P3HT ($T_g = 12$ °C^[13]). The beneficial effect of the copolymers on blend stability hence does not seem to be merely a T_g effect causing reduced mobility (which is substantiated by the very similar results obtained upon degradation at various temperatures). Noncovalent interactions (e.g. π - π -overlap, hydrogen bonding or dipole-dipole interactions) are likely involved^[14n,33]. In this respect, it is noteworthy to mention that, although the number of functionalized side chains might seem very small (5–15%), a simple calculation of the mol fraction of functionalized side chains compared to PCBM molecules in the blend (1/1 in wt%) reveals that the amount of these functionalities is far from negligible, and hence noncovalent interactions might indeed result in pronounced effects. For instance for the **P2-90/10** copolymer, a functional side chain is available per 1.85 PC₆₁BM molecules in the blend, which means that on average for every two PC₆₁BM molecules, one secondary interaction (polymer side chain-PC₆₁BM) can be present, reducing the diffusion rate. As there is clearly a substantial effect on the diffusion and crystallization behavior of the two components when functionalized P3HT copolymers are blended with PC₆₁BM, advanced thermal analysis seems to be well-suited to gain more insight in the underlying principles causing the increased morphological stability^[13]. Studies in this direction are currently ongoing within our groups, as is the extension of this approach to (low T_g) low bandgap copolymers providing higher solar cell efficiencies.

2.4 CONCLUSIONS

In this work, a set of 12 functionalized poly(3-alkylthiophene) random copolymers was efficiently synthesized by the Rieke protocol and analyzed in bulk heterojunction organic solar cell devices with the general aim to increase the thermal stability of the corresponding P3AT:PC₆₁BM photoactive layers. Morphology development and phase separation were visualized by TEM (and corresponding SAED patterns) at several stages during the aging process, corroborated by electrical *J-V* testing of devices at increasing annealing times. Even though the functionalization approach might lead to a slight decrease - if any - in initial power conversion efficiency, the overall performance in function of time is considerably enhanced due to the increased thermal stability of (some of) the copolymer:PC₆₁BM blends, therefore making this approach a viable option to improve the lifetime of BHJ polymer solar cells. Further work will be directed toward analysis of the photooxidative sensitivity of the copolymer series and the degradation behavior of encapsulated devices in climate chamber conditions, and in-depth analysis of the mechanism governing the stability improvement by dedicated thermal analysis techniques (diffusion and crystallization kinetics/dynamics and phase behavior).

2.5 REFERENCES

¹ a) Thompson, B. C.; Fréchet, J. M. J. *Angew. Chem. Int. Ed.* **2008**, *47*, 58. b) Kippelen, B.; Brédas, J.-L. *Energy Environ. Sci.* **2009**, *2*, 251. c) Brabec, C. J.; Gowrisanker, S.; Halls, J. J. M.; Laird, D.; Jia, S.; Williams, S. P. *Adv. Mater.* **2010**, *22*, 3839. d) Nelson, J. *Mater. Today* **2011**, *14*, 462. e) Service, R. F. *Science* **2011**, *332*, 293. f) Thompson, B. C.; Khlyabich, P. P.; Burkhart, B.; Aviles, A. E.; Rudenko, A.; Shultz, G. V.; Ng, C. F.; Mangubat, L. B. *Green* **2011**, *1*, 29. g) Li, G.; Zhu, R.; Yang, Y. *Nat. Photonics* **2012**, *6*, 153. h) Koster, L. J. A.; Shaheen, S. E.; Hummelen, J. C. *Adv. Energy Mater.* **2012**, *10*, 1246. i) Vandewal, K.; Himmelberger, S.; Salleo, A. *Macromolecules* **2013**, *46*, 6379. j) Lizin, S.; Van Passel, S.; De Schepper, E.; Maes, W.; Lutsen, L.; Manca, J.; Vanderzande, D. *Energy Environ. Sci.* **2013**, *6*, 3136.

² a) Green, M. A.; Emery, K.; Hishikawa, Y.; Warta, W.; Dunlop, E. D. *Prog. Photovolt: Res. Appl.* **2012**, *20*, 12. b) He Z.; Zhong C.; Su S.; Xu M.; Wu H.; Cao Y. *Nat. Photonics* **2012**, *6*, 591. c) Cabanetos, C.; El Labban, A.; Bartelt, J. A.; Douglas, J. D.; Mateker, W. R.; Fréchet, J. M. J.; McGehee, M. D.; Beaujuge, P. M. *J. Am. Chem. Soc.* **2013**, *135*, 4656.

³ a) Jørgensen, M.; Norrman, K.; Krebs, F. C. *Sol. Energy Mater. Sol. Cells* **2008**, *92*, 686. b) Jørgensen, M.; Norrman, K.; Gevorgyan, S. A.; Tromholt, T.; Andreasen, B.; Krebs, F. C. *Adv. Mater.* **2012**, *24*, 580. c) Grossiord, N.; Kroon, J. M.; Andriessen, R.; Blom, P. W. M. *Org. Electron.* **2012**, *13*, 432. d) Manceau, M.; Rivaton, A.; Gardette, J.-L. Photochemical stability of materials for OPV. In *Stability and Degradation of Organic and Polymer Solar Cells*; Krebs, F. C., Ed.;

Wiley, **2012**, 71. e) Lee, J. U.; Jung, J. W.; Jo, J. W.; Jo, W. H. *J. Mater. Chem.* **2012**, 22, 24265. f) Gupta, S. K.; Dharmalingam, K.; Pali, L. S.; Rastogi, S.; Singh, A.; Garg, A. *Nanomaterials and Energy* **2013**, 2, 42. g) Bundgaard, E.; Helgesen, M.; Carlé, J. E.; Krebs, F. C.; Jørgensen, M. *Macromol. Chem. Phys.* **2013**, 214, 1546.

⁴ Brabec, C. J. *Sol. Energy Mater. Sol. Cells* **2004**, 83, 273.

⁵ a) Bundgaard, E.; Krebs, F. C. *Sol. Energy Mater. Sol. Cells* **2007**, 91, 954. b) Heeger, A. J. *Chem. Soc. Rev.* **2010**, 39, 2354. c) Boudreault, P.-L. T.; Najari, A.; Leclerc, M. *Chem. Mater.* **2011**, 23, 456. d) Facchetti, A. *Chem. Mater.* **2011**, 23, 733. e) Zhou, H.; Yang, L.; You, W.; *Macromolecules* **2012**, 45, 607. f) Bian, L.; Zhu, E.; Tang, J.; Tang, W.; Zhang, F. *Prog. Polym. Sci.* **2012**, 37, 1292.

⁶ a) Dang, M. T.; Hirsch, L.; Wantz, G. *Adv. Mater.* **2011**, 23, 3597. b) Marrocchi, A.; Lanari, D.; Facchetti, A.; Vaccaro, L. *Energy Environ. Sci.* **2012**, 5, 8457. c) Dang, M. T.; Hirsch, L.; Wantz, G.; Wuest, J. D. *Chem. Rev.* **2013**, 113, 3734.

⁷ a) Ma, W.; Yang, C.; Gong, X.; Lee, K.; Heeger, A. J. *Adv. Funct. Mater.* **2005**, 15, 1617. b) Li, G.; Shrotriya, V.; Huang, J.; Yao, Y.; Moriarty, T.; Emery, K.; Yang, Y. *Nat. Mater.* **2005**, 4, 864.

⁸ Zimmermann, B.; Würfel, U.; Niggemann, M. *Sol. Energy Mater. Sol. Cells* **2009**, 93, 491.

⁹ Tipnis, R.; Bernkopf, J.; Jia, S.; Krieg, J.; Li, S.; Storch, M.; Laird, D. *Sol. Energy Mater. Sol. Cells* **2009**, *93*, 442.

¹⁰ a) Manceau, M.; Rivaton, A.; Gardette, J.-L.; Guillerez, S.; Lemaitre, N. *Polym. Degrad. Stab.* **2009**, *94*, 898. b) Manceau, M.; Rivaton, A.; Gardette, J.-L.; Guillerez, S.; Lemaitre, N. *Sol. Energy Mater. Sol. Cells* **2011**, *95*, 1315. c) Dupuis, A.; Wong-Wah-Chung, P.; Rivaton, A.; Gardette, J.-L. *Polym. Degrad. Stab.* **2012**, *97*, 366.

¹¹ a) Yang, X.; van Duren, J. K. J.; Rispens, M. T.; Hummelen, J. C.; Janssen, R. A. J.; Michels, M. A. J.; Loos, J. *Adv. Mater.* **2004**, *16*, 802. b) Yang, X.; van Duren, J. K. J.; Janssen, R. A. J.; Michels, M. A. J.; Loos, J. *Macromolecules* **2004**, *37*, 2151. c) Bertho, S.; Janssen, G.; Cleij, T. J.; Conings, B.; Moons, W.; Gadisa, A.; D'Haen, J.; Goovaerts, E.; Lutsen, L.; Manca, J.; Vanderzande, D. *Sol. Energy Mater. Sol. Cells* **2008**, *92*, 753.

¹² Manceau, M.; Helgesen, M.; Krebs, F. C. *Polym. Degrad. Stab.* **2010**, *95*, 2666.

¹³ a) Zhao, J.; Swinnen, A.; Van Assche, G.; Manca, J.; Vanderzande, D.; Van Mele, B. J. *Phys. Chem. B* **2009**, *113*, 1587. b) Demir, F.; Van den Brande, N.; Van Mele, B.; Bertho, S.; Vanderzande, D.; Manca, J.; Van Assche, G. *J. Therm. Anal. Calorim.* **2011**, *105*, 845.

¹⁴ a) Marcos Ramos, A.; Rispens, M. T.; van Duren, J. K. J.; Hummelen, J. C.; Janssen, R. A. J. *J. Am. Chem. Soc.* **2001**, *123*, 6714. b) Sivula, K.; Ball, Z. T.; Watanabe, N.; Fréchet, J. M. J. *Adv. Mater.* **2006**, *18*, 206. c) Zhou, Z.; Chen,

X.; Holdcroft, S. *J. Am. Chem. Soc.* **2008**, *130*, 11711. d) Woo, C. H.; Thompson, B. C.; Kim, B. J.; Toney, M. F.; Fréchet, J. M. J. *J. Am. Chem. Soc.* **2008**, *130*, 16324. e) Miyanishi, S.; Tajima, K.; Hashimoto, K. *Macromolecules* **2009**, *42*, 1610. f) Zhang, Y.; Yip, H.-L.; Acton, O.; Hau, S. K.; Huang, F.; Jen, A. K.-Y. *Chem. Mater.* **2009**, *21*, 2598. g) Kim, B. J.; Miyamoto, Y.; Ma, B.; Fréchet, J. M. J. *Adv. Funct. Mater.* **2009**, *19*, 2273. h) Lee, J. U.; Jung, J. W.; Emrick, T.; Russell, T. P.; Jo, W. H. *J. Mater. Chem.* **2010**, *20*, 3287. i) Hsieh, C.-H.; Cheng, Y.-J.; Li, P.-J.; Chen, C.-H.; Dubosc, M.; Liang, R.-M.; Hsu, C.-S. *J. Am. Chem. Soc.* **2010**, *132*, 4887. j) Vandenberghe, J.; Conings, B.; Bertho, S.; Kesters, J.; Spoltore, D.; Esiner, S.; Zhao, J.; Van Assche, G.; Wienk, M. M.; Maes, W.; Lutsen, L.; Van Mele, B.; Janssen, R. A. J.; Manca, J.; Vanderzande, D. J. M. *Macromolecules* **2011**, *44*, 8470. k) Lee, U. R.; Lee, T. W.; Hoang, M. H.; Kang, N. S.; Yu, J. W.; Kim, K. H.; Lim, K.-G.; Lee, T.-W.; Jin, J.-I.; Choi, D. H. *Org. Electron.* **2011**, *12*, 269. l) Griffini, G.; Douglas, J. D.; Piliago, C.; Holcombe, T. W.; Turri, S.; Fréchet, J. M. J.; Mynar, J. L. *Adv. Mater.* **2011**, *23*, 1660. m) Kim, H. J.; Han, A.-R.; Cho, C.-H.; Kang, H.; Cho, H.-H.; Lee, M. Y.; Fréchet, J. M. J.; Oh, J. H.; Kim, B. J. *Chem. Mater.* **2012**, *24*, 215. n) Lin, Y.; Lim, J. A.; Wei, Q.; Mannsfeld, S. C. B.; Briseno, A. L.; Watkins, J. J. *Chem. Mater.* **2012**, *24*, 622. o) Yun, H. M.; Kim, J.; Yang, C.; Kim, J. Y. *Sol. Energy Mater. Sol. Cells* **2012**, *104*, 7. p) Nam, C.-Y.; Qin, Y.; Park, Y. S.; Hlaing, H.; Lu, X.; Ocko, B. M.; Black, C. T.; Grubbs, R. B. *Macromolecules* **2012**, *45*, 2338. q) He, D.; Du, X.; Zhang, W.; Xiao, Z.; Ding, L. *J. Mater. Chem. A* **2013**, *1*, 4589. r) Ouhib, F.; Tomassetti, M.; Manca, J.; Piersimoni, F.; Spoltore, D.; Bertho, S.; Moons, H.; Lazzaroni, R.; Desbief, S.; Jérôme, C.; Detrembleur, C. *Macromolecules* **2013**, *46*, 785. s) Santo, Y.; Jeon, I.; Yeo, K. S.; Nakagawa,

T.; Matsuo, Y. *Appl. Phys. Lett.* **2013**, *103*, 073306. t) Chen, X.; Chen, L.; Chen, Y. *J. Polym. Sci. A: Polym. Chem.* **2013**, *51*, 4156.

¹⁵ a) Peters, C. H.; Sachs-Quintana, I. T.; Kastrop, J. P.; Beaupré, S.; Leclerc, M.; McGehee, M. D. *Adv. Energy Mater.* **2011**, *1*, 491. b) Peters, C. H.; Sachs-Quintana, I. T.; Mateker, W. R.; Heumueller, T.; Rivnay, J.; Noriega, R.; Beiley, Z. M. *Adv. Mater.* **2012**, *24*, 663.

¹⁶ Tournebize, A.; Bussiere, P.-O.; Wong-Wah-Chung, P.; Thérias, S.; Rivaton, A.; Gardette, J.-L.; Beaupré, S.; Leclerc, M. *Adv. Energy Mater.* **2013**, *3*, 478.

¹⁷ Mateker, W. R.; Douglas, J. D.; Cabanetos, C.; Sachs-Quintana, I. T.; Bartelt, J. A.; Hoke, E. T.; Labban, A. E.; Beaujuge, P. M.; Fréchet, J. M. J.; McGehee, M. D. *Energy Environ. Sci.* **2013**, *6*, 2529.

¹⁸ a) Li, Z.; Wong, H. C.; Huang, Z.; Zhong, H.; Tan, C. H.; Tsoi, W. C.; Kim, J. S.; Durrant, J. R.; Cabral, J. T. *Nat. Commun.* **2013**, *4*, 2227. b) Piersimoni, F.; Degutis, G.; Bertho, S.; Vandewal, K.; Spoltore, D.; Vangerven, T.; Drijkoningen, J.; Van Bael, M. K.; Hardy, A.; D'Haen, J.; Maes, W.; Vanderzande, D.; Nesladek, M.; Manca, J. *J. Polym. Sci.: Polym. Phys.* **2013**, *51*, 1209.

¹⁹ a) Lutsen, L.; Vanderzande, D.; Campo, B. *PCT Int. Appl.* **2010**, WO 2010000504 A1 20100107. b) Lutsen, L.; Vanderzande, D.; Campo, B. *PCT Int. Appl.* **2011**, WO 2011069554 A1 20110616.

²⁰ a) Campo, B. J.; Oosterbaan, W. D.; Gilot, J.; Cleij, T. J.; Lutsen, L.; Janssen, R. A. J.; Vanderzande, D. *Proc. SPIE* **2009**, *7416*, 74161G. b) Campo, B. J.;

Duchateau, J.; Ganivet, C. R.; Ballesteros, B.; Gilot, J.; Wienk, M. M.; Oosterbaan, W. D.; Lutsen, L.; Cleij, T. J.; de la Torre, G.; Janssen, R. A. J.; Vanderzande, D.; Torres, T. *Dalton Trans.* **2011**, *40*, 3979. c) Oosterhout, S. D. L.; Koster, J. A.; van Bavel, S. S.; Loos, J.; Stenzel, O.; Thiedmann, R.; Schmidt, V.; Campo, B.; Cleij, T. J.; Lutsen, L.; Vanderzande, D.; Wienk, M. M.; Janssen, R. A. J. *Adv. Energy Mater.* **2011**, *1*, 90. d) Tanenbaum, D. M.; Hermenau, M.; Voroshazi, E.; Lloyd, M. T.; Galagan, Y.; Zimmermann, B.; Hösel, M.; Dam, H. F.; Jørgensen, M.; Gevorgyan, S. A.; Kudret, S.; Maes, W.; Lutsen, L.; Vanderzande, D.; Würfel, U.; Andriessen, R.; Rösch, R.; Hoppe, H.; Lira-Cantu, M.; Rivaton, A.; Uzunoğlu, G. Y.; Germack, D.; Andreasen, B.; Madsen, M. V.; Norrman, K.; Krebs, F. C. *RSC Adv.* **2012**, *2*, 882. e) Rösch, R.; Tanenbaum, D. M.; Jørgensen, M.; Seeland, M.; Bärenklau, M.; Hermenau, M.; Voroshazi, E.; Lloyd, M. T.; Galagan, Y.; Zimmermann, B.; Würfel, U.; Hösel, M.; Dam, H. F.; Gevorgyan, S. A.; Kudret, S.; Maes, W.; Lutsen, L.; Vanderzande, D.; Andriessen, R.; Teran-Escobar, G.; Lira-Cantu, M.; Rivaton, A.; Uzunoğlu, G. Y.; Germack, D.; Andreasen, B.; Madsen, M. V.; Norrman, K.; Hoppe, H.; Krebs, F. C. *Energy Environ. Sci.* **2012**, *5*, 6521. f) Andreasen, B.; Tanenbaum, D. M.; Hermenau, M.; Voroshazi, E.; Lloyd, M. T.; Galagan, Y.; Zimmermann, B.; Kudret, S.; Maes, W.; Lutsen, L.; Vanderzande, D.; Würfel, U.; Andriessen, R.; Rösch, R.; Hoppe, H.; Teran-Escobar, G.; Lira-Cantu, M.; Rivaton, A.; Uzunoğlu, G. Y.; Germack, D.; Hösel, M.; Dam, H. F.; Jørgensen, M.; Gevorgyan, S. A.; Madsen, M. V.; Bundgaard, E.; Krebs, F. C.; Norrman, K. *Phys. Chem. Chem. Phys.* **2012**, *14*, 11780. g) Teran-Escobar, G.; Tanenbaum, D. M.; Voroshazi, E.; Hermenau, M.; Norrman, K.; Lloyd, M. T.; Galagan, Y.; Zimmermann, B.; Hösel, M.; Dam, H. F.; Jørgensen, M.; Gevorgyan, S.; Kudret, S.; Maes, W.; Lutsen, L.; Vanderzande, D.; Würfel, U.; Andriessen, R.; Rösch,

R.; Hoppe, H.; Rivaton, A.; Uzunođlu, G. Y.; Germack, D.; Andreasen, B.; Madsen, M. V.; Bundgaard, E.; Krebs, F. C.; Lira-Cantu, M. *Phys. Chem. Chem. Phys.* **2012**, *14*, 11824. h) Bertho, S.; Campo, B.; Piersimoni, F.; Spoltore, D.; D'Haen, J.; Lutsen, L.; Maes, W.; Vanderzande, D.; Manca, J. *Sol. Energy Mater. Sol. Cells* **2013**, *110*, 69. i) Campo, B.; Kesters, J.; Bevk, D.; Gilot, J.; Bolink, H. J.; Zhao, J.; Bolsée, J.-C.; Oosterbaan, W. D.; Bertho, S.; Ruttens, B.; D'Haen, J.; Manca, J.; Lutsen, L.; Maes, W.; Van Assche, G.; Janssen, R. A. J.; Vanderzande, D. *Org. Electron.* **2013**, *14*, 523.

²¹ Kudret, S.; Oosterbaan, W.; D'Haen, J.; Lutsen, L.; Vanderzande, D.; Maes, W. *Adv. Synth. Catal.* **2013**, *355*, 569.

²² a) Chen, T. A.; Wu, X. M.; Rieke, R. D. *J. Am. Chem. Soc.* **1995**, *117*, 233. b) Oosterbaan, W. D.; Vrindts, V.; Berson, S.; Guillerez, S.; Douhéret, O.; Ruttens, B.; D'Haen, J.; Adriaensens, P.; Manca, J.; Lutsen, L.; Vanderzande, D. *J. Mater. Chem.* **2009**, *19*, 5424.

²³ a) *Organozinc Reagents, A Practical Approach* (Eds.: Knochel, P.; Jones, P.), Oxford University Press, New York, **1999**. b) *The Chemistry of Organozinc Compounds* (Eds: Rappoport, Z.; Marek, I.), John Wiley & Sons Ltd, West Sussex, England, **2006**. c) Knochel, P.; Schade, M. A.; Bernhardt, S.; Manolikakes, G.; Metzger, A.; Piller, F. M.; Rohbogner, C. J.; Mosrin, M. *Beilstein J. Org. Chem.* **2011**, *7*, 1261; d) Wu, X.-F. *Chem. Asian J.* **2012**, *7*, 2505; e) Wu, X.-F.; Neumann, H. *Adv. Synth. Catal.* **2012**, *354*, 3141.

- ²⁴ a) Chen, T. A.; O'Brien, R. A.; Rieke, R. D. *Macromolecules* **1993**, *26*, 3462.
b) Coppo, P.; Adams, H.; Cupertino, D. C.; Yeates, S. G.; Turner, M. L. *Chem. Commun.* **2003**, 2548.
- ²⁵ Bauerle, P.; Pfau, F.; Schlupp, H.; Wurthner, F.; Gaudl, K.-U.; Caro, M. B.; Fischer, P., *J. Chem. Soc. Perkin Trans 2* **1993**, 489.
- ²⁶ Kim, S.-H.; Kim, J.-G. *Bull. Korean Chem. Soc.* **2009**, *30*, 2283.
- ²⁷ Lanzi, M.; Costa-Bizzarri, P.; Paganin, L.; Cesari, G. *React. Funct. Polym.* **2007**, *67*, 329.
- ²⁸ Iovu, M. C.; Jeffries-El, M.; Sheina, E. E.; Cooper, J. R.; McCullough, R. D. *Polymer* **2005**, *46*, 8582.
- ²⁹ a) Babudri, F.; Colangiuli, D.; Di Bari, L.; Farinola, G. M.; Hassan Omar, O.; Naso, F.; Pescitelli, G. *Macromolecules* **2006**, *39*, 5206; b) Vandeleene, S.; Van den Bergh, K.; Verbiest, T.; Koeckelberghs, G. *Macromolecules* **2008**, *41*, 5123.
- ³⁰ Lee, J. K.; Ma, W. L.; Brabec, C. J.; Yuen, J.; Moon, J. S.; Kim, J. Y.; Lee, K.; Bazan, G. C.; Heeger, A. J. *J. Am. Chem. Soc.* **2008**, *130*, 3619.
- ³¹ Voroshazi, E.; Verreet, B.; Aernouts, T.; Heremans, P. *Sol. Energy Mater. Sol. Cells* **2011**, *95*, 1303.
- ³² Swinnen, A.; Haeldermans, I.; van de Ven, M.; D'Haen, J.; Vanhoyland, G.; Aresu, S.; D'Olieslaeger, M.; Manca, J. *Adv. Funct. Mater.* **2006**, *16*, 760.

³³ a) Chen, Y.-H.; Huang, P.-T.; Lin, K.-C.; Huang, Y.-J.; Chen, C.-T. *Org. Electron.* **2012**, *13*, 283. b) Lobez, J. M.; Andrew, T. L.; Bulovic, V.; Swager, T. M. *ACS Nano* **2012**, *6*, 3044.

2.6 ACKNOWLEDGEMENTS

We are grateful to Hasselt University for providing the PhD grants of J. K. and S. K. We further acknowledge the OPV-Life project from the IWT (Agentschap voor Innovatie door Wetenschap en Technologie; O&O 080368), the POLYSTAR project from PV ERA-NET, the IWT-SBO project POLYSPEC (Nanostructured POLYmer photovoltaic devices for efficient solar SPECTrum harvesting), the project ORGANEXT (EMR. INT4-1.2.-2009-04/054), selected in the frame of the operational program INTERREG IV-A Euregio Maas-Rijn, and Belspo for supporting the IAP P6/27 and IAP 7/05 networks.

2.7 SUPPORTING INFORMATION

2.7.1 Electrochemical analysis

Table S1: Electrochemical characterization of the copolymers.

Polymer	HOMO (eV)	LUMO (eV) ^a	E _g ^(opt) (eV)
Rieke P3HT	-5.25	-3.37	1.88
P1 – 95/5	-5.16	-3.24	1.92
P1 – 90/10	-5.26	-3.34	1.92
P1 – 85/15	-5.12	-3.20	1.92
P2 – 95/5	-5.17	-3.26	1.91
P2 – 90/10	-5.16	-3.26	1.90
P2 – 85/15	-5.19	-3.26	1.93
P3 – 95/5	-5.13	-3.25	1.88
P3 – 90/10	-5.21	-3.32	1.89
P3 – 85/15	-4.84	-2.93	1.91
P4 – 95/5	-5.13	-3.21	1.92
P4 – 90/10	-5.17	-3.28	1.89
P4 – 85/15	-5.11	-3.22	1.89

$$^a E_{\text{LUMO}} = E_{\text{HOMO}} + E_{\text{g}}^{(\text{opt})}$$

2.7.2 Photovoltaic device optimization

Table S2: Optimized solar cell efficiencies for BHJ blends based on P3HT or copolymers **P1–P4**.

Donor material	V _{oc}	J _{sc}	FF	η
P3HT	0.52	11.86	0.56	3.48
P1 – 95/5	0.54	7.97	0.62	2.67
P1 – 90/10	0.52	8.39	0.60	2.61
P1 – 85/15	0.52	5.70	0.58	1.68
P2 – 95/5	0.58	10.20	0.62	3.69
P2 – 90/10	0.54	9.26	0.58	2.88
P2 – 85/15	0.58	9.18	0.57	3.04
P3 – 95/5	0.56	9.33	0.64	3.34
P3 – 90/10	0.60	6.39	0.57	2.19
P3 – 85/15	0.64	6.11	0.61	2.39
P4 – 95/5	0.56	8.72	0.63	3.07
P4 – 90/10	0.60	6.71	0.60	2.43
P4 – 85/15	0.60	6.61	0.65	2.58

2.7.3 UV-Vis spectra

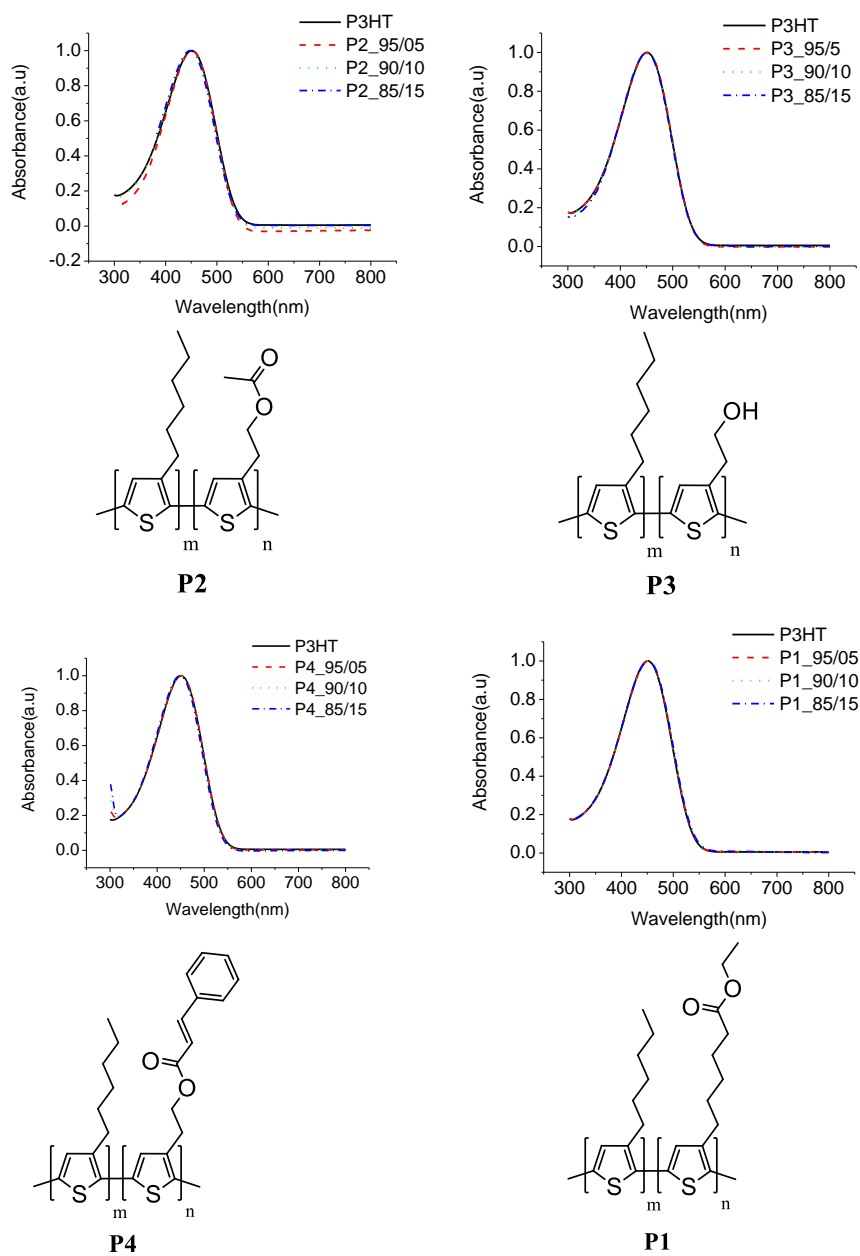


Figure S1: UV-Vis characteristics of the copolymers in chloroform solution.

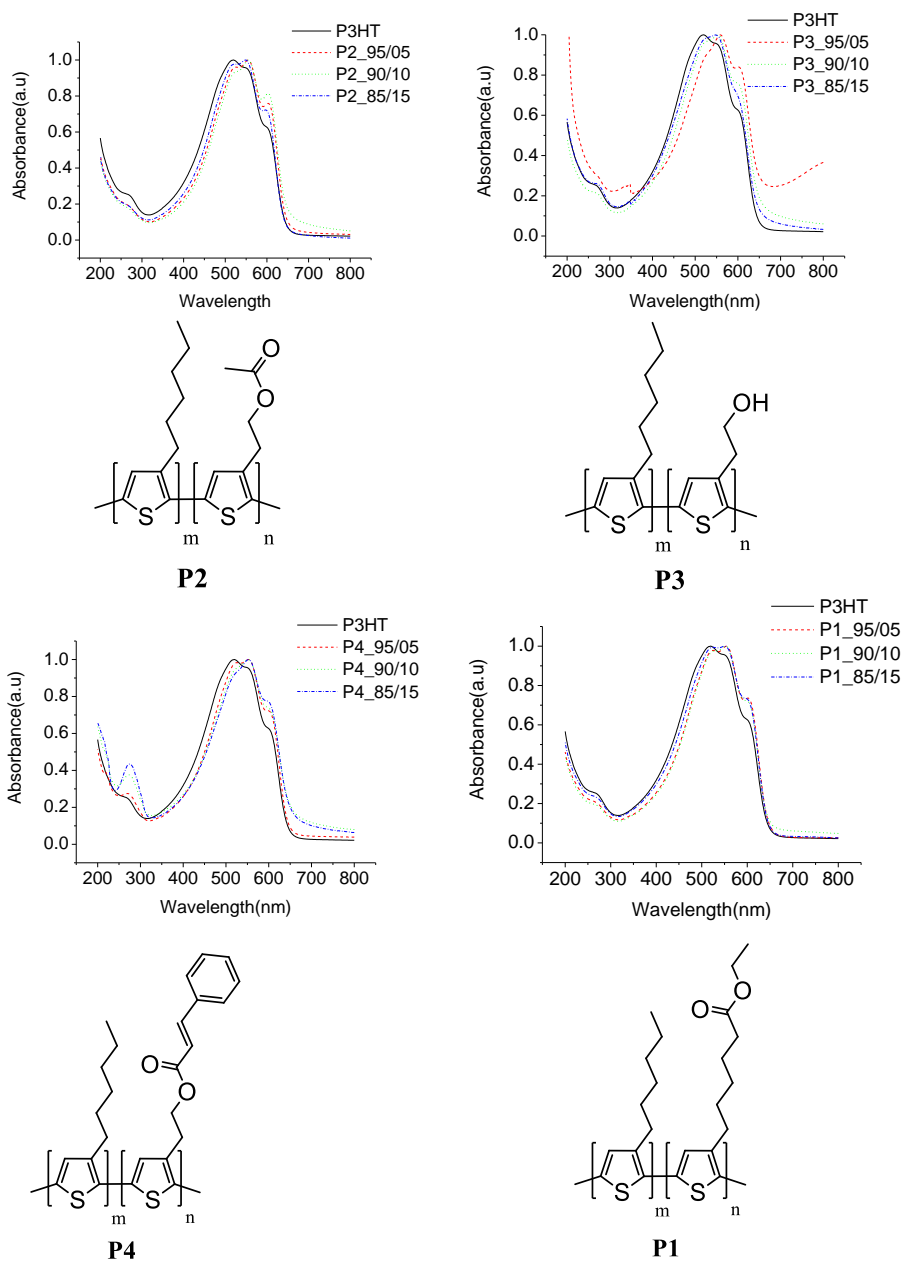


Figure S2: UV-Vis characteristics of the copolymers in thin film.

2.7.4 FT-IR spectra

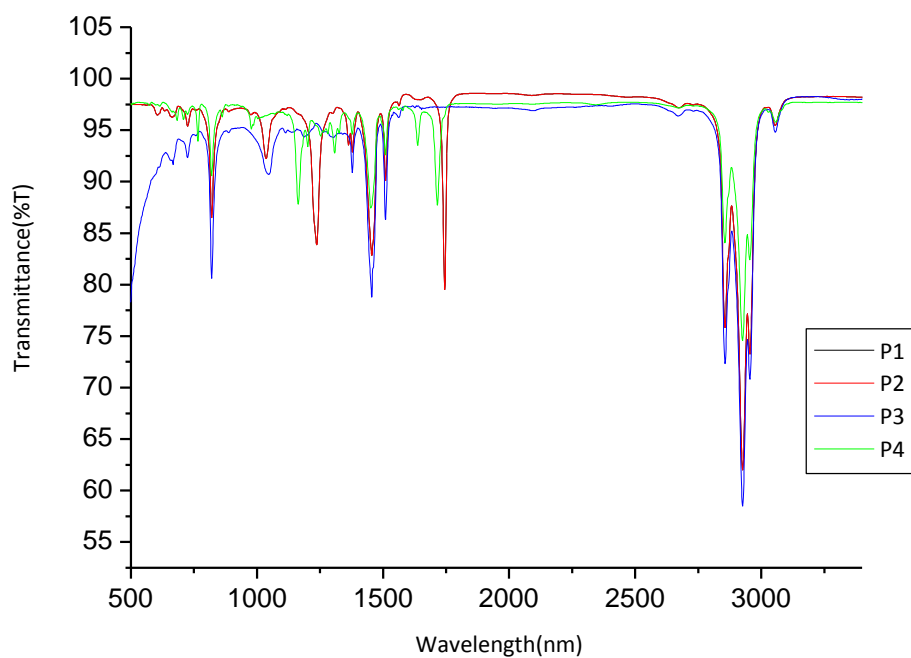


Figure S3: FT-IR spectra of copolymers **P1–P4–85/15**.

2.7.5 Photovoltaic degradation measurements

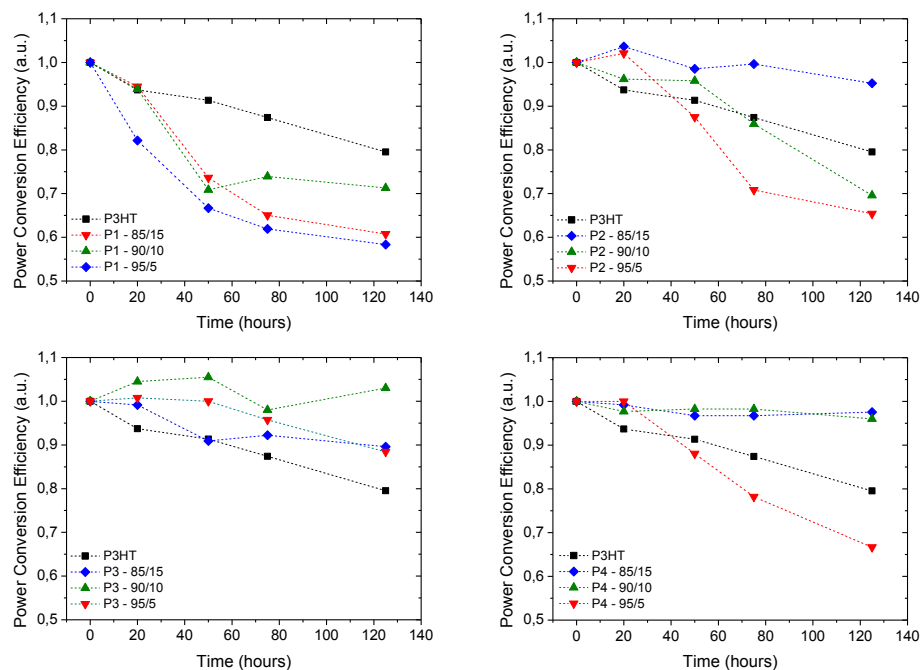


Figure S4: Output characteristics for the 'basic' thermal degradation study at 100 °C (for 140 h) for devices based on **P1–P4**:PC₆₁BM active layers. Dashed lines serve as a guide to the eye only.

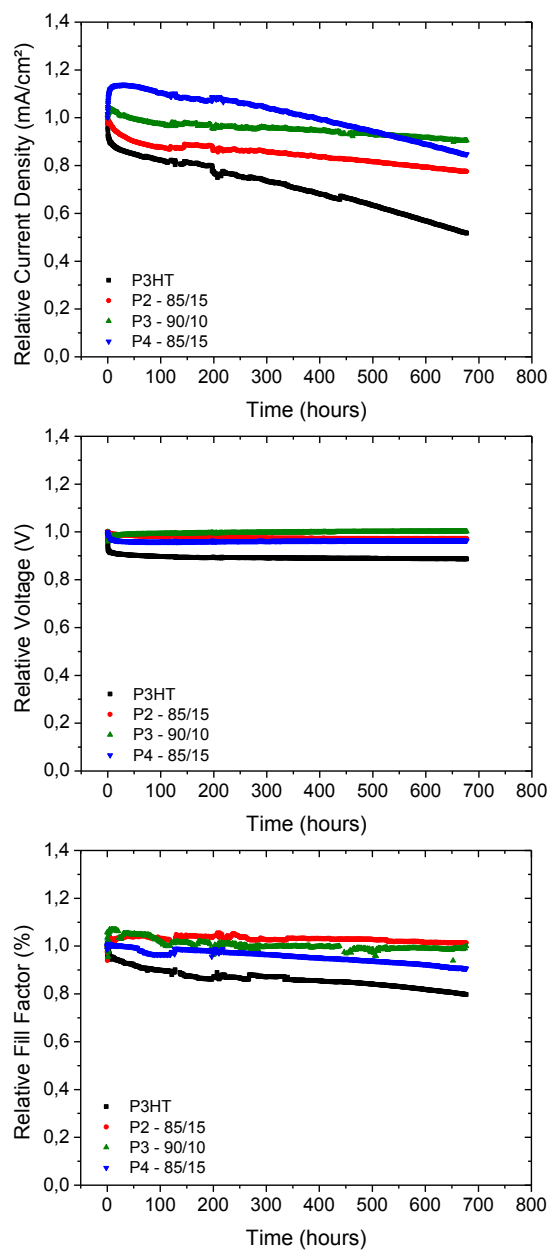
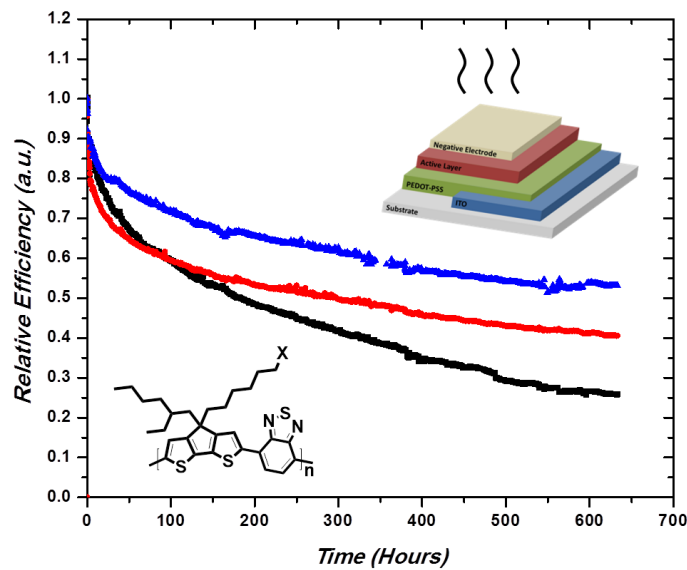


Figure S5: Degradation curves (V_{oc} , J_{sc} and FF) for BHJ organic solar cells based on P3HT and the best-performing P3AT (**P2–P4**) copolymers (700 h at 85 °C). The curves were normalized to the first measurement point at 85 °C.

Chapter 3

Enhanced Organic Solar Cell Stability by Polymer (PCPDTBT) Side Chain Functionalization



J. Kesters, P. Verstappen, J. Raymakers, W. Vanormelingen, J. Drijkoningen, J. D'Haen, J. Manca, L. Lutsen, D. Vanderzande, W. Maes, manuscript submitted.

ABSTRACT

Organic photovoltaics represent a promising thin-film solar cell technology with appealing mechanical, aesthetical and cost features. In recent years, a strong growth in power conversion efficiency (to over 10%) has been realized for organic solar cells through extensive material and device research. To be competitive in the renewable energy market, further improvements are mandatory though, both with respect to efficiency and lifetime. High intrinsic stability of the photoactive layer is obviously a crucial requirement for long lifetimes, but the generally applied bulk heterojunction blends and their components are prone to light-induced and thermal degradation processes. In the present contribution, the high- T_g polymer strategy is combined with specific side chain functionalization to address the thermal stability of polymer solar cells. These two design concepts are applied to a prototype low bandgap copolymer, PCPDTBT. Accelerated aging tests (at 85 °C) indicate an improved thermal durability of the PCPDTBT:PC₇₁BM blends and the resulting devices by the insertion of ester or alcohol moieties on the polymer side chains. The different stages in the efficiency decay profiles are addressed by dedicated experiments to elucidate the (simultaneously occurring) degradation mechanisms.

3.1 INTRODUCTION

Over the past two decades, organic photovoltaics (OPV) have evolved into an attractive solar energy technology.^[1] Besides the general advantages of thin-film photovoltaics – reduced weight, flexibility and (semi-)transparency – organic solar cells show additional interesting features such as improved low-light performance, narrow band widths, design freedom (color and uniformity), and compatibility to large scale (roll-to-roll) printing techniques, further decreasing production costs. At present, power conversion efficiencies (PCE's) in the range of 10% have been achieved for single junction solution-processed OPV devices through simultaneous photoactive material, interlayer and device optimization.^[2] However, for OPV to become an economically viable technology, with projected integration in (energy neutral) buildings, vehicles and specific fast-deployable consumer goods, further leaps forward are required with respect to both efficiency and stability. Improving the lifetime of organic solar cells has for a long time been underexposed compared to the chase for enhanced efficiencies, but the field has recently caught up with a number of encouraging results in terms of durability.^[3] A first important step was taken by the concept of inverted solar cells, procuring P3HT:PC₆₁BM devices retaining 90% of their initial performance for over 1.5 years under exposure to direct sunlight.^[4] Optimization of the charge transport layers was also performed to increase device stability. Doping PEDOT:PSS with WO_x was shown to provide more efficient and durable devices, with only 5% reduced performance over 5000 hours in ambient conditions.^[5] On the opposite side of the (standard) organic solar cell stack, Ca, which is sensitive to oxidation,^[6] was replaced by an n-type TiO_x buffer layer, affording devices which are more resistant to the intrusion of oxygen and

moisture.^[7] The bulk heterojunction (BHJ) photoactive layer at the heart of an organic solar cell is one of the most challenging components to optimize for improved device lifetime. Even when properly encapsulated, keeping oxygen and moisture out of the device as much as possible, intrinsic active layer degradation can be induced by light or by the elevated temperatures imposed by continued exposure to sunlight.^[8] Photochemical (oxidative) degradation of the active layer (polymer) materials and blends is examined extensively within the group of Gardette and Rivaton, suggesting rearrangements of the chemical structures, the formation of oxidation products, crosslinking and chain scissions as the main malefactors.^[9]

In this work, the main focus lies on the thermal degradation of the active layer donor:acceptor blend in polymer:fullerene BHJ solar cells. Under the influence of elevated temperatures, reorganization of the active layer components may occur, depending on the glass transition temperature (T_g) of the blend (components). The peak-performing active layer nanomorphology, a finely intermixed interpenetrating network of the electron donor and acceptor compounds, gradually changes during device operation, whether it be through diffusion and demixing (depending on the T_g), degradation of the bulk materials or interface-related processes. For the workhorse P3HT:PC₆₁BM combination, operating at an optimal polymer:fullerene ratio of 1:0.8, it has been observed that the fullerene material diffuses into microcrystals upon heating the blend (well) above 60 °C (i.e. above the T_g of the P3HT:PC₆₁BM blend^[10]), leading to a near-to-complete phase separation and strongly reduced device efficiency.^[11] Important insights on the thermal stabilization of OPV materials and devices were obtained within the McGehee group at Stanford.^[12] They emphasized the importance of material purity when aiming for long-term stability of polymer

solar cells.^[12c] Additionally, through the investigation of polymer:fullerene blends at temperatures above the T_g of the polymer, it was found that a thin polymer layer is formed at the interface between the active layer and the top electrode, thereby lowering the device performance over time.^[12d] To alleviate (or at least slow down) polymer solar cell degradation under thermal stress, various approaches to 'freeze in' the top-performing BHJ blend (nano)morphology have been explored in the past years, including, amongst others, thermocleavage of the solubilizing side chains,^[13] the use of non-crystalline fullerene additives,^[14] compatibilizers^[15] or the addition of nucleating agents^[16]. Another acknowledged pathway involves the synthesis of polymer materials with a higher T_g , resulting in more rigid polymer:fullerene blends, hindering fullerene diffusion and crystallization and hence procuring OPV devices with longer lifetimes.^[11b,17] Thermal stabilization of the photoactive blend has also been achieved through the application of (photo)crosslinkable polymer and/or fullerene derivatives.^[18]

In previous work, we have noted a remarkable improvement of the intrinsic stability of the OPV active layer blend morphology by the incorporation of functional moieties (ester, alcohol or cinnamoyl) on the side chains of P3HT-based copolymers, even for fairly low built-in ratios (5–15%) and without crosslinking to covalently anchor the polymer and/or fullerene molecules.^[19] Moreover, these alterations did not influence the initial PCE to a large extent. As such, this approach can be regarded as an attractive paradigm for OPV active layer stability. In this manuscript, this concept is extended to a proof-of-concept low bandgap copolymer, PCPDTBT, simultaneously targeting high efficiency and improved (thermal) stability by combining the high- T_g and side chain functionalization strategies. PCPDTBT (poly{4,4-dialkyl-4*H*-cyclopenta[2,1-

b;3,4-b']dithiophene-2,6-diyl-*alt*-2,1,3-benzothiadiazole-4,7-diyl}) has attracted quite some interest from the OPV community as it was the first push-pull low bandgap copolymer, with an extended absorption beyond 800 nm, affording a PCE above 5% in polymer solar cells.^[20,21] Despite the high initial PCE, the applicability of PCPDTBT in OPV is hampered by its rapidly decreasing performance under thermal stress (during operation or annealing), and only preliminary efforts were made to improve the device lifetime.^[22] PCPDTBT copolymers containing crosslinkable functional groups at the end of the alkyl side chains were synthesized and the resulting polymer solar cells displayed an enhanced stability under ambient conditions^[22a] or during light-soaking aging^[22b] experiments. Based on the reasonable efficiency of PCPDTBT-based solar cells, the limited intrinsic stability of these devices and our previously established synthetic procedures toward smooth CPDT side chain variation (*vide infra*), PCPDTBT was regarded as an ideal test case for our hypothesis of combined high efficiency and improved lifetime by polymer side chain modification.

3.2 RESULTS AND DISCUSSION

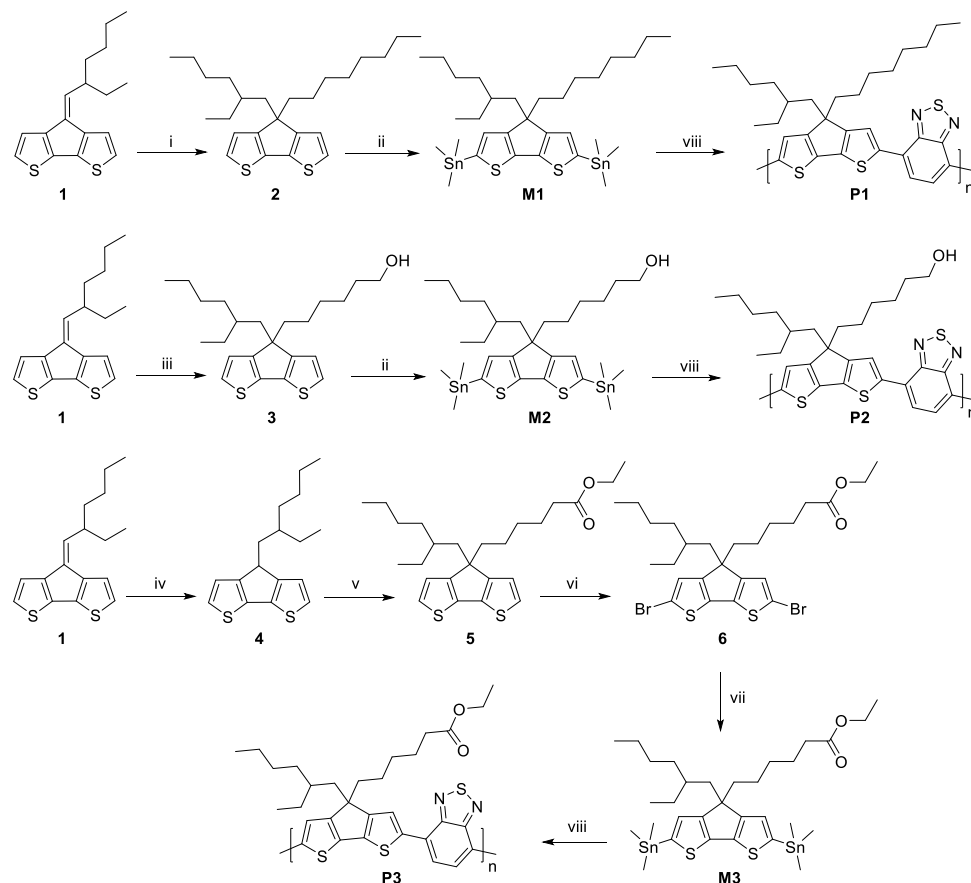
3.2.1 Synthesis and characterization

Functionalization of the alkyl side chains on 4,4-dialkyl-4*H*-cyclopenta[2,1-*b;3,4-b'*]dithiophene (CPDT) derivatives has been performed by several research groups for specific purposes.^[22-25] Bazan and co-workers introduced ionic groups to achieve conjugated poly- and oligoelectrolytes.^[23] The introduction of functional groups has also been prevailed as a tool to alter the solubility of the resulting conjugated polymers, enabling processing from more benign solvents.^[24] The Müllen group introduced double bonds in the alkyl side

chains of PCPDTBT to tune the packing and solubility of this material.^[25] In all of the examples mentioned above, symmetrically functionalized CPDT moieties were obtained through application of the rather tedious classical CPDT synthesis route.^[26] Our group previously developed two shortened, convenient synthetic protocols, which additionally allow smooth asymmetric alkyl side chain substitution. In 2010, a three-step synthetic strategy – (i) synthesis of 3-bromo-2,2'-bithiophene by a Kumada coupling, (ii) lithiation and subsequent reaction with a ketone to afford a dialkylated tertiary alcohol derivative, and (iii) Friedel-Crafts dehydration cyclization – toward 4,4-dialkyl-CPDT building blocks was reported.^[27] Although this procedure provides straightforward access to asymmetrically dialkylated (functionalized) CPDT's, it suffers from relatively low yields for more bulky side chain patterns. Therefore, an alternative synthesis protocol was developed.^[28] In this approach, the first side chain is introduced by a Wittig-type carbonyl olefination reaction between 4*H*-cyclopenta[2,1-*b*:3,4-*b'*]dithiophen-4-one and an alkylidene triphenylphosphorane, yielding a 4-alkylidene-4*H*-cyclopenta[2,1-*b*:3,4-*b'*]dithiophene (e.g. compound **1** in Scheme 1). Subsequently, the second side chain is introduced via regioselective reductive alkylation of the exocyclic double bond. In this way, asymmetric substitution is easily achieved and for both steps the products can be isolated in reasonably high yields (>70%), hence favoring the Wittig route as the most versatile procedure for asymmetric CPDT side chain functionalization.

Based on the previously employed series of side chain functionalized poly(3-alkylthiophene)s,^[19c] it was envisaged to introduce ester and alcohol groups at the end of one of the CPDT alkyl side chains, and an asymmetrically dialkylated CPDT derivative was synthesized as a reference compound. Both the alcohol and ester moieties enable further side chain variation by different pre- or post-

polymerization functional group interconversions. The synthetic strategy affording the monomers and final polymers is depicted in Scheme 1.



Scheme 1: Synthesis of the different CPDT monomers and PCPDTBT polymers: i)

LiAlH₄, *n*-octylbromide, THF; ii) *n*-BuLi, Me₃SnCl, THF; iii) A: LiAlH₄, (6-bromohexyloxy)triisopropylsilane, THF; B: TBAF, THF; iv) LiAlH₄, THF; v) A: *t*-BuOK, 6-bromohexanoic acid, KI, DMSO; B: EtOH, H₂SO₄; vi) NBS, CHCl₃; vii) hexamethylditin, LiCl, Pd(PPh₃)₄, toluene; viii) 4,7-dibromo-2,1,3-benzothiadiazole, Pd₂(dba)₃, P(*o*-tol)₃, toluene/DMF 4/1, 110 °C, 15 h.

In a first step, 4-(2'-ethylhexylidene)-4*H*-cyclopenta[2,1-*b*:3,4-*b'*]dithiophene (**1**) was reductively alkylated to obtain the asymmetrically dialkylated CPDT's **2** and **3**.^[28] For compound **3**, the alcohol functional group had to be protected (as a silyl ether) during this step. Next, both building blocks were stannylated via lithiation and reaction with trimethyltin chloride, affording the required CPDT monomers **M1** and **M2**. For the ester-functionalized monomer **M3**, a slightly adapted procedure had to be followed. Attempts to protect the ester functional group as an ortho-ester or 2-alkyl-1,3-oxazoline failed. On the other hand, milder reducing agents such as NaBH₄ and DIBAL were not capable of reducing the exocyclic double bond. Therefore, the double bond was first reduced with LiAlH₄ in a separate step. Alkylation was then performed with 6-bromohexanoate instead of ethyl 6-bromohexanoate to avoid competition between the bromide and the ester groups in the nucleophilic substitution reaction. After the alkylation reaction, the obtained carboxylic acid functionalized CPDT was immediately transformed to the ethyl ester analogue **5** via an acid-catalyzed esterification in ethanol. The ester-functionalized CPDT was also synthesized via the older three-step route,^[27a] but purification was less straightforward in this case. Ester-CPDT **5** was dibrominated and further converted to monomer **M3** via stannylation with hexamethylditin in the presence of Pd(PPh₃)₄.

Since monomer purity is crucial to obtain high molar mass species in polycondensation-type polymerization reactions, all three CPDT monomers were further purified by preparative recycling size exclusion chromatography (prep-SEC). After Stille polymerization with 4,7-dibromo-2,1,3-benzothiadiazole (BT), the PCPDTBT copolymers were purified by soxhlet extractions with methanol, acetone, *n*-hexane and chloroform, respectively. All three polymers were collected with chloroform and the low molar mass fractions of polymers **P1** and

P3 were removed via prep-SEC. Due to its limited solubility in chloroform, alcohol-functionalized PCPDTBT copolymer **P2** could not be subjected to prep-SEC. The number average molar masses (M_n) and polydispersity indices (PDI) of the polymers are gathered in Table 1. While the molar masses of **P1** and **P3** were reasonably high, a relatively low value was obtained for **P2**.

Table 1: Molar mass, thermal and electrochemical data for PCPDTBT copolymers **P1–P3**.

Polymer	$M_n^{a)}$ [kDa]	PDI ^{a)}	$T_g^{b)}$ [°C]	HOMO ^{c)} [eV]	LUMO ^{c)} [eV]	$E_g^{OPd)}$ [eV]
P1	26	3.2	174	-5.09	-3.34	1.40
P2	13	2.5	198	-4.95	-3.36	1.40
P3	46	1.7	161	-4.95	-3.41	1.37

^{a)} Determined by analytical SEC using polystyrene standards in THF at 40 °C. ^{b)} Determined by RHC. ^{c)} Determined by CV from the onset of oxidation/reduction. ^{d)} Optical bandgap, as determined by the onset of the solid-state UV-Vis spectra.

The thermal transitions of the three novel copolymers were investigated via rapid heat-cool calorimetry (RHC),^[29] preferred above regular differential scanning calorimetry (DSC) because of its increased sensitivity to thermal transitions (as a result of the fast scanning rates) and the low sample amounts required. The glass transition temperatures were determined to be 174, 198 and 161 °C for **P1–P3**, respectively (Figure S1), and no melting transitions could be observed, suggesting a highly amorphous polymer nature. The (very) high T_g values for the three copolymers, well above the ISOS-3 temperature of 85 °C employed for standard aging tests,^[30] suggest a minor influence of T_g during OPV device stability tests. In this respect, it has to be mentioned that, despite

its huge importance for device stability, there is a noteworthy lack of (accurate) T_g values for (OPV) low bandgap copolymers in literature.

The HOMO and LUMO energy levels of the PCPDTBT alternating copolymers were estimated via cyclic voltammetry (CV) from the onset of the oxidation and reduction peaks, respectively. The frontier molecular orbital energy levels of the functionalized copolymers **P2** and **P3** show comparable values to the reference polymer **P1**. Normalized UV-Vis absorption spectra in solution and thin film for the three copolymers are shown in Figure 1. In all cases, the absorption extends to the near-IR region of the solar spectrum and the profiles are very similar, even more so in thin film. Therefore, it can be concluded that modification of the side chains does not influence the opto-electronic solid-state properties of the PCPDTBT copolymers to a large extent. The functional groups do seem to influence (i.e. to reduce) the aggregation tendency of the polymers in solution, as the long-wavelength shoulder is affected by the presence and the nature of the functional groups.

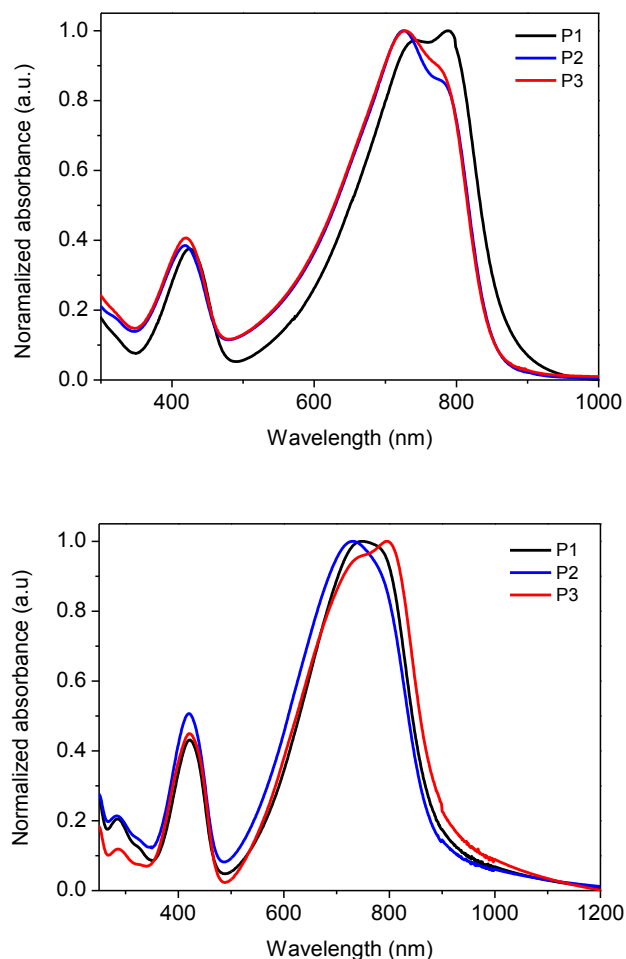


Figure 1: Normalized UV-Vis absorption spectra for the three PCPDTBT copolymers in chloroform solution (top) and thin film (bottom).

3.2.2 Polymer solar cells

To evaluate the influence of the side chain modification on photovoltaic performance, polymer solar cells were prepared using the standard architecture glass/ITO/PEDOT:PSS/active layer/Ca/Al. For the photoactive layers, blend solutions were prepared in a 1:3 ratio with PC₇₁BM. Whereas **P1** and **P3** could

readily be dissolved in chloroform (CF), polymer **P2** required a mixture of *ortho*-dichlorobenzene (oDCB) and 4% of *N*-methylpyrrolidone (NMP) due to its higher aggregation tendency. Nonetheless, as evidenced by the *I-V* parameters summarized in Table 2 and Figure 2, the incorporation of the functional moieties on the PCPDTBT side chains hardly affected the average PCE's. The slightly lower performance for **P2** might be attributed to the lower M_n for this material and/or the addition of NMP to the blend solution, affecting mainly the short-circuit current density (J_{sc}) and resulting in a slightly lower average PCE of 2.05% (in comparison to 2.46% for the reference device). The solar cells based on ester-functionalized copolymer **P3** showed an enhanced fill factor (FF) (from 43–44% to 49%), combined with a slightly reduced open-circuit voltage (V_{oc}) (from 0.59 to 0.56 V). In literature, optimized device efficiencies up to 5.5% were obtained for PCPDTBT:PC₇₁BM through the addition of 1,8-octanedithiol (ODT) as an additive to the active layer blend solution.^[20] Recent work indicated, however, that even though the initial performance can be enhanced significantly by inclusion of the additive, the lifetime of these solar cells decreased more rapidly under light-soaking conditions.^[22c] To avoid complications due to the effect of (different optimal) additives and to isolate the influence of the side chain moieties, the use of additives was omitted during these studies.

Table 2: Photovoltaic parameters for the pristine solar cell devices based on PCPDTBT copolymers **P1–P3**.

Material	Processing solvent	Voc [V]	Jsc [mA cm ⁻²]	FF	Best PCE [%]	Average PCE ^{a)} [%]
P1	CF	0.59	9.49	0.44	2.76	2.46
P2	oDCB + 4% NMP	0.59	7.94	0.43	2.43	2.05
P3	CF	0.56	9.12	0.49	3.21	2.50

^{a)}Averages were taken across 16–20 devices, with an active area of 3 mm².

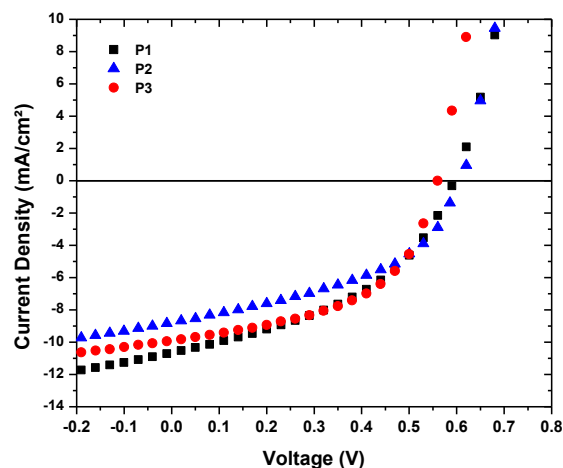


Figure 2: J - V curves for the best solar cell devices produced from the **P1–P3**:PC₇₁BM (1:3) blends.

In the external quantum efficiency (EQE) spectra, photocurrent generation over a broad wavelength range, up to 900 nm, was observed (Figure 3). The **P2**:PC₇₁BM device showed lower EQE values, in line with the lower J_{sc} observed in the I - V measurements, in particular in the spectral range where the polymer contribution is seen. The integrated current densities (J_{EQE} 's) correspond rather well with the measured J_{sc} 's, in line with standard measurement deviations.

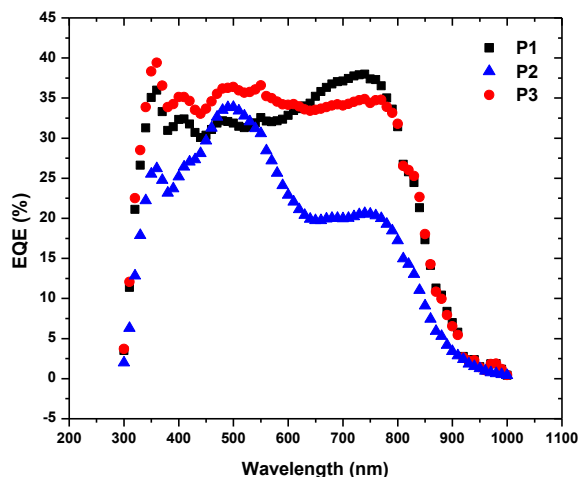


Figure 3: EQE spectra for the solar cell devices based on **P1–P3** (measured J_{sc} 's: 10.01, 7.81 and 11.08 mA cm^{-2} ; J_{EQE} 's: 10.49, 7.33 and 10.67 mA cm^{-2} for **P1**, **P2** and **P3**, respectively).

3.2.3 Photovoltaic behavior under prolonged thermal stress

In a next step, the solar cells were mounted in an automated degradation chamber and subjected to a precisely controlled temperature of 85 °C for 650 hours, with I - V measurements at predetermined intervals to investigate the progression of the photovoltaic parameters over time. The temperature chosen for this accelerated aging test was instigated by the ISOS-3 standards and the desire to stay well below the T_g of all materials.^[30] All three PCPDTBT:PC₇₁BM polymer solar cells showed a strong initial drop in efficiency (within the first 50 hours), followed by a more 'linear' degradation regime for the remainder of the lifetime experiment (Figure 4; separate J_{sc} , V_{oc} and FF profiles in Figure S2). After 150 hours of exposure to 85 °C, more indicative differences in relative PCE's are revealed. The **P1**:PC₇₁BM reference device still exhibits a rather steep slope, resulting in a final PCE diminished to 26% of its initial value after 650

hours. In contrast, the relative efficiencies of the polymer solar cells based on side chain functionalized PCPDTBT copolymers **P2** and **P3** remain more stable after the initial 'burn-in' phase (vide infra), with values of 53 and 40% of the starting performance after 650 hours, respectively.

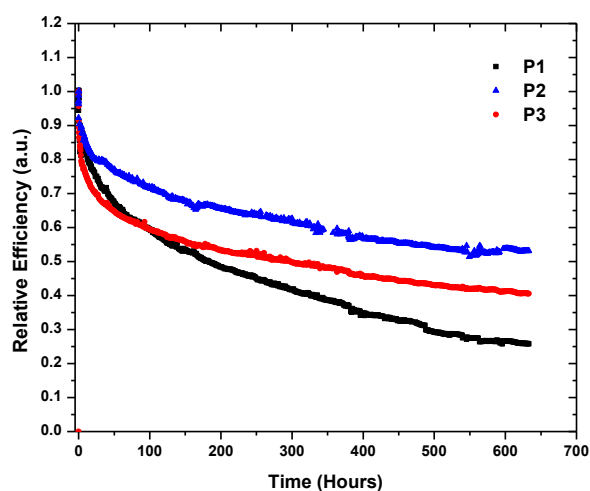


Figure 4: Relative efficiency decay profiles for the three PCPDTBT:PC₇₁BM polymer solar cells upon exposure to a temperature of 85 °C for 650 h. The curves are normalized to the first measurement point at 85 °C.

For P3HT:PC₆₁BM BHJ OPV devices, a similar thermal stress results in the appearance of a multitude of crystalline structures in the photoactive layer, indicative of diffusion and phase separation of the polymer donor and fullerene acceptor.^[11] Polythiophene side chain functionalization (by ester and in particular alcohol moieties) was shown to reduce this crystallization and demixing tendency considerably, thereby diminishing the efficiency drop.^[19b,c] To analyze the BHJ blend nanomorphology of the PCPDTBT:PC₇₁BM polymer solar cells and its evolution over time, transmission electron microscopy (TEM) and atomic force microscopy (AFM) imaging was performed (Figure 5 and 6). For the

pristine solar cells from ester-PCPDTBT **P3**, a slightly different bulk morphology and topography (increased peak to peak distance and somewhat higher roughness, Table S1) was observed, possibly corroborating with the slightly reduced V_{oc} and higher FF (Table 2). After exposure of the devices to a temperature of 85 °C for 650 hours, no crystallization or large demixing was observed (Figure 5 and 6), which can be linked to the high T_g 's of all copolymers and, as a result, the high T_g 's of the polymer:fullerene active layer blends. The T_g 's of the blends were also determined by RHC and they were found at 143, 158 and 148 °C for the **P1–P3**:PC₇₁BM (1:3) blends, respectively (Figure S1). These values are all below the T_g 's of the separate blend components (174, 198 and 161 °C for **P1–P3**, respectively, and 170 °C for PC₇₁BM). The TEM-selected area electron diffraction (SAED) patterns show no formation of crystalline structures in the films, not even after 650 hours of aging (Figure 5). For completeness, TEM was also performed on similarly prepared films exposed for 3 hours to a temperature of 220 °C on a hotplate in the dark, i.e. above the T_g of all individual polymers and polymer:PC₇₁BM blends (Figure 5 and S3). Obviously, the PEDOT:PSS layer and the top electrode are not resistant to such elevated temperatures, and device characterization is not representative. Nevertheless, crystallization and extensive phase separation did occur at this temperature, although not in equal amounts for the three different blends. The most deteriorated active layer morphology was found for the **P1**:PC₇₁BM reference system, followed by **P3**:PC₇₁BM and finally **P2**:PC₇₁BM, in line with the relative efficiency decay profiles as observed at 85 °C (Figure 4). Additionally, SAED for the **P1**:PC₇₁BM blend revealed the presence of microcrystals in the center of the 'aggregated' domains (as illustrated in more detail in Figure S3). Noteworthy, the amount of phase separation varies quite strongly, even though the T_g 's of

the blends are similar, indicating that the incorporation of the functional moieties enhances the resistivity of the blends toward diffusion and crystallization (of PC₇₁BM).

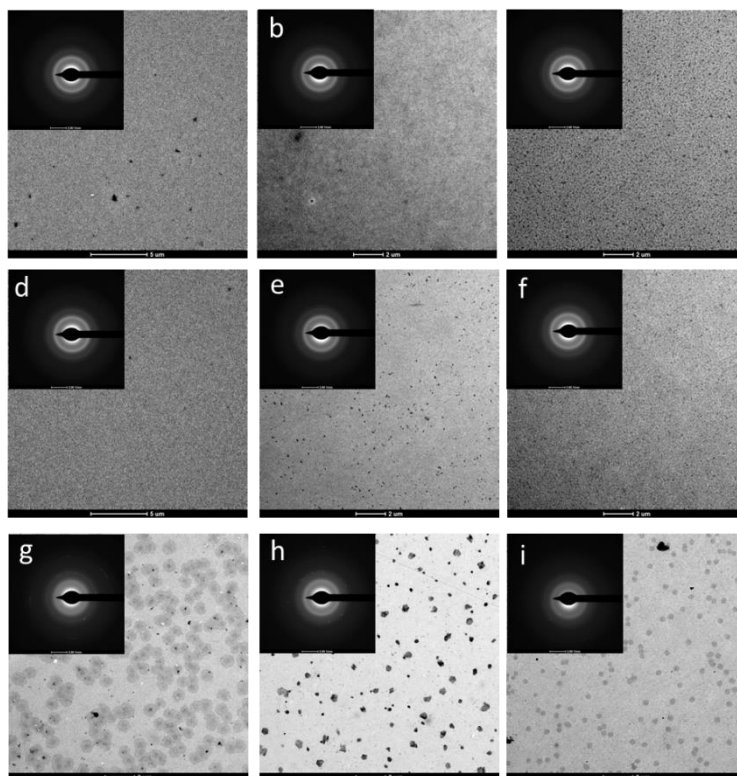


Figure 5: TEM images for **P1**:PC₇₁BM (a, d, g), **P2**:PC₇₁BM (b, e, h) and **P3**:PC₇₁BM (c, f, i) BHJ blends annealed at 85 °C for 0 h (top row), 85 °C for 650 h (middle row) and 220 °C for 3 h (bottom row).

Enhanced Solar Cell Stability by Polymer (PCPDTBT) Side Chain Functionalization

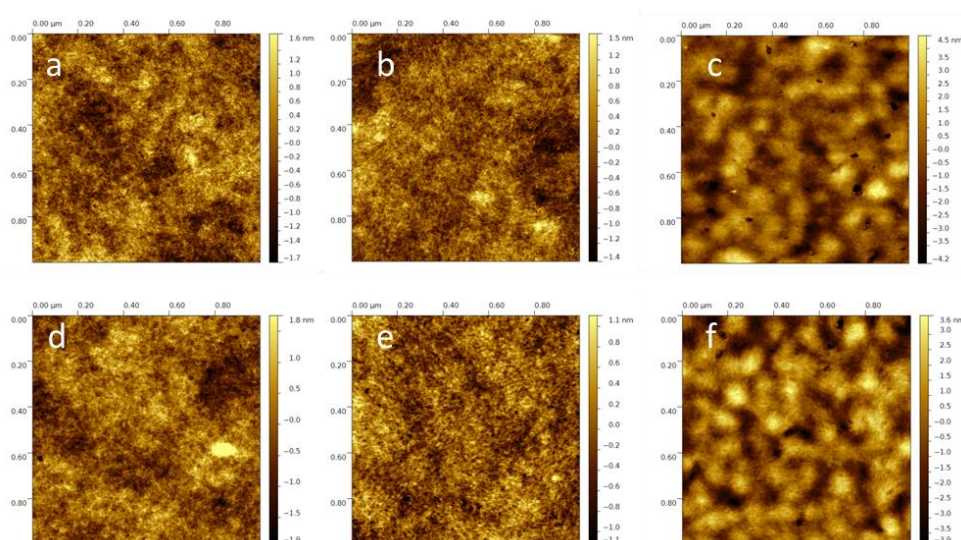


Figure 6: AFM images for **P1**:PC₇₁BM (a, d), **P2**:PC₇₁BM (b, e,) and **P3**:PC₇₁BM (c, f) polymer solar cells before (top row) and after (bottom row) thermal aging for 650 h at 85 °C.

Last year, the groups of Durrant and Manca independently reported on the light-induced dimerization of fullerenes, hindering phase separation in polymer:fullerene systems.^[31] As our aging experiments require frequent exposure to light (measurement intervals of 5 minutes for the initial phase, with a total sweep time of approximately 4 minutes over 16 devices, followed by intervals up to 1 hour at later stages), light and thermally-induced effects might intermix, especially in the initial phase of the degradation experiment. To address this concern, a new set of solar cell samples was prepared which were continuously annealed at 85 °C in the dark (on a hotplate) prior to the *I-V* measurements. After 150 hours, the non-illuminated samples still did not show any crystallites, as confirmed by TEM (Figure S4), suggesting that the specific

nature of the thermal stabilization effect originates from a different (i.e. non-light-induced) mechanism.

More detailed investigation of the degradation profiles allows for a further deconvolution of the degradation process(es) occurring in the thermally stressed PCPDTBT:PC₇₁BM photovoltaic devices. The exponential efficiency decay within the first 100 hours of the aging experiment can be attributed to the combination of a rapid decay in the *V*_{oc} (reducing by 20%) and a more drawn-out decrease in *J*_{sc}, resulting in an overall strong reduction of the PCE (by 30% for **P2** and up to 40% for **P1** and **P3**). The strong initial loss in *V*_{oc} is higher for **P3** than for **P1** and **P2**, explaining the stronger initial PCE decay for the device based on the ester-functionalized copolymer (Figure 4). This initial strong efficiency drop has been referred to as the 'burn-in' phase.^[12] The McGehee group has recently provided more thorough understandings of the initial *V*_{oc} loss and the burn-in stage through light-induced aging of several polymer:fullerene systems, including both crystalline and amorphous polymers.^[12e] The fast initial loss in *V*_{oc} was found to be characteristic for amorphous systems (such as the PCPDTBT polymer under investigation here), whereas light-induced traps, as revealed by transient photocurrent measurements, were observed for both material types upon aging. Related work by Voroshazi et al. on the light soaking of PCDTBT:PC₇₁BM devices revealed that the initial *V*_{oc} could almost completely be recovered through re-deposition of the top electrode after the aging experiment, supporting the hypothesis of light-induced traps.^[32] Consequently, as the initial phase of our aging experiment is characterized by frequent exposure to light, additional mechanisms (i.e. light soaking) other than those induced by pure thermal stress are likely to affect the overall degradation process. To shed more light on this, a set of PCPDTBT:PC₇₁BM samples was

exposed to 85 °C in a dark environment. This control experiment revealed that the initial reduction in V_{oc} was almost non-existent in comparison with the results obtained from the automated degradation chamber (PCE drop <5% vs 20%) (Table S2), confirming the attribution of the burn-in phase to a light-induced (V_{oc} loss) effect. Exclusion of the light-induced effects does, however, not clarify the continuous reduction in J_{sc} , with observable differences for the **P1–P3** copolymers, indicating other mechanisms must be present.

It is generally known that the quality of the interface between the active layer and the top electrode is worsening when applying external stress factors, thereby leading to a reduced charge extraction. Plausible causes reported in literature include the delamination of the top electrode and the creation of voids or electrically insulating patches at the interface.^[33] To investigate the active layer-top electrode interface, the three different PCPDTBT:PC₇₁BM films were exposed to 85 °C for 85 hours in the dark prior to electrode deposition (since the standard solar cell architecture employed in this work did not allow for smooth peeling off of the top electrode). Simultaneously, 12 operational devices were processed from the same batch solutions to grant I - V results comparable with the pristine solar cells. As summarized in Table 3, comparison of the average J_{sc} 's of the blend films degraded with and without Ca/Al top electrodes revealed a less pronounced decay for the latter. After 85 hours at 85 °C in the dark, no reduction in V_{oc} was observed, supporting the previous findings. Moreover, the J_{sc} showed a relatively small decay, to approximately 92% of the initial J_{sc} for all three copolymers (in comparison to the average J_{sc} of the 12 pristine devices). The resulting PCE's remained at 90, 92 and 85% of their starting values, demonstrating the strong influence of the thermal treatment on the quality of the interface between the active layer and the top electrode. The

slightly lower performance of the device based on ester-PCPDTBT **P3** could be ascribed to the (stronger) loss in FF. Combination of all gathered data suggests that the relative difference in performance stability within the **P1–P3** copolymer series as observed in the initial degradation experiment can possibly be ascribed to a higher resistance of **P2**, and to a lesser extent **P3**, to diminishing active layer-top electrode interface quality upon thermal stress.

Table 3: Comparison of the pristine photovoltaic devices based on copolymers **P1–P3** with devices containing a post-evaporated (Ca/Al) top electrode after exposure to 85 °C for 85 h in the dark.

Polymer	Treatment	Voc [V]	Jsc [mA cm ⁻²]	FF	Average PCE ^{a)} [%]
P1	pristine	0.59	9.26	0.44	2.38
P1	85h at 85 °C + post-evap	0.59	8.64	0.42	2.15
P2	pristine	0.59	7.83	0.43	1.98
P2	85h at 85 °C + post-evap	0.59	7.23	0.43	1.82
P3	pristine	0.56	8.98	0.47	2.38
P3	85h at 85 °C + post-evap	0.56	8.50	0.42	2.02

^{a)}Averages were taken across 4–8 devices, with an active area of 3 mm².

3.3 CONCLUSIONS

A small series of side chain functionalized PCPDTBT low bandgap copolymers was efficiently prepared with the general aim to improve the intrinsic thermal stability of the photovoltaic devices based on these donor materials, while maintaining the power conversion efficiency for standard PCPDTBT:PC₇₁BM polymer solar cells. Accelerated aging tests at a temperature of 85 °C showed that the stability of the photovoltaic cells under prolonged thermal stress was enhanced by the insertion of ester or alcohol moieties on the CPDT side chains,

with the best results being obtained for the alcohol-functionalized PCPDTBT derivative. A relative efficiency up to 55% of its starting value could be maintained after 650 hours at 85 °C, whereas the reference device exhibited a relative performance of only 26%. TEM and AFM imaging revealed the absence of (extensive) phase separation and crystallization after the aging experiment at 85 °C, which can be attributed to the high T_g 's of the PCPDTBT-type copolymers and the corresponding photoactive layer blends, obviating crosslinking approaches. Stepwise examination of some of the various possible degradation pathways revealed that the decay in photovoltaic performance can be attributed to a combination of light-induced and thermal processes, resulting (amongst others) in a decrease of the active layer-top electrode interface quality. Further efforts in our group will be directed toward the extension of the presented functionalized side chain method to alternative high(er) performance low bandgap copolymers. Additionally, the degradation behavior of encapsulated devices in climate chamber conditions will be addressed, in combination with an in-depth analysis of the mechanism(s) governing the deteriorating interface quality upon continued thermal stress. On the other hand, the observed differences in light-induced burn-in (stronger for the ester-functionalized PCPDTBT) are worth a closer look as well.

The presented work emphasizes the importance of polymer (side chain) engineering as a powerful tool to improve the lifetime of polymer solar cells. Long-term stability will be a *conditio sine qua non* for OPV to survive in the harsh battle for market share with alternative PV technologies. In this respect, the booming field of perovskite-based hybrid solar cells can be considered a serious competitor, albeit also struggling with durability issues.^[34] Improved

thermal stability is also mandatory if OPV is to take benefit from its positive temperature coefficient, attractive for energy harvesting under extreme (e.g. aerospace) conditions.

3.4 EXPERIMENTAL SECTION

Material Characterization: Preparative (recycling) size exclusion chromatography (prep-SEC) was performed on a JAI LC-9110 NEXT system equipped with JAIGEL 1H, 2H and 3H columns (eluent CHCl₃, flow rate 3.5 mL min⁻¹). NMR chemical shifts (δ , in ppm) were determined relative to the residual CHCl₃ (7.26 ppm) absorption or the ¹³C resonance shift of CDCl₃ (77.16 ppm). High resolution electrospray ionization mass spectrometry (ESI-MS) was performed using an LTQ Orbitrap Velos Pro mass spectrometer equipped with an atmospheric pressure ionization source operating in the nebulizer assisted electrospray mode. The instrument was calibrated in the *m/z* range 220–2000 using a standard solution containing caffeine, MRFA and Ultramark 1621. MALDI-TOF spectra were recorded on a Bruker Daltonics Ultraflex II ToF/ToF. 1 μ L of the matrix solution (4 mg mL⁻¹ DTCB (*trans*-2-[3-(4-*tert*-butylphenyl)-2-methyl-2-propenylidene]malononitrile) in CHCl₃) was spotted onto an MTP Anchorchip 600/384 MALDI plate. The spot was allowed to dry and 1 μ L of the analyte solution (0.5 mg mL⁻¹ in CHCl₃) was spotted on top of the matrix. Reported masses are the 100% intensity peaks of the isotopic distributions. UV-Vis measurements were performed on a VARIAN Cary 500 UV-Vis-NIR spectrophotometer at a scan rate of 600 nm/min. The films for the UV-Vis measurements were prepared by drop casting a solution of the polymer in chloroform on a quartz substrate. The solid-state UV-Vis spectra were used to

estimate the optical band gaps (from the wavelength at the intersection of the tangent line drawn at the low energy side of the absorption spectrum with the x-axis: E_g (eV) = 1240/(wavelength in nm)). Analysis of the molar masses and molar mass distributions of the polymers was performed on a Tosoh EcoSEC System, comprising of an autosampler, a PSS guard column SDV (50 x 7.5 mm), followed by three PSS SDV analytical linear XL columns (5 μ m, 300 x 7.5 mm), and a UV detector using THF as the eluent at 40 °C with a flow rate of 1.0 mL/min. The SEC system was calibrated using linear narrow polystyrene standards ranging from 474 to 7.5×10^6 g mol⁻¹ ($K = 14.1 \times 10^{-5}$ dL g⁻¹ and $\alpha = 0.70$). Rapid heat-cool calorimetry (RHC) experiments were performed on a prototype RHC of TA Instruments, equipped with liquid nitrogen cooling and specifically designed for operation at high scanning rates.^[29,35] RHC measurements were performed at 500 K min⁻¹ in aluminum crucibles, using helium (10 mL min⁻¹) as a purge gas. Electrochemical measurements (cyclic voltammetry) were performed with an Eco Chemie Autolab PGSTAT 30 potentiostat/galvanostat using a three-electrode microcell with a platinum working electrode, a platinum counter electrode and a Ag/AgNO₃ reference electrode (silver wire dipped in a solution of 0.01 M AgNO₃ and 0.1 M NBu₄PF₆ in anhydrous acetonitrile). The reference electrode was calibrated against ferrocene/ferrocenium as an external standard. Samples were prepared by dip coating the platinum working electrode in the respective polymer solutions (also used for the solid-state UV-Vis measurements). The CV measurements were done on the resulting films with 0.1 M NBu₄PF₆ in anhydrous acetonitrile as electrolyte solution. To prevent air from entering the system, the experiments were carried out under a curtain of argon. Cyclic voltammograms were recorded at a scan rate of 100 mV s⁻¹. For the conversion of V to eV, the onset potentials

of the first oxidation/reduction peaks were used and referenced to ferrocene/ferrocenium, which has an ionization potential of -4.98 eV vs. vacuum. This correction factor is based on a value of 0.31 eV for Fc/Fc⁺ vs. SCE^[36a] and a value of 4.68 eV for SCE vs. vacuum^[36b]: $E_{\text{HOMO/LUMO}} \text{ (eV)} = -4.98 - E_{\text{onset ox/red}}^{\text{Ag/AgNO}_3} \text{ (V)} + E_{\text{onset Fc/Fc}^+}^{\text{Ag/AgNO}_3} \text{ (V)}$.

Device Fabrication: Bulk heterojunction polymer solar cells were prepared using the standard architecture substrate/ITO/PEDOT:PSS/polymer:PC₇₁BM/Ca/Al. Prior to device processing, the ITO-coated substrates (100 nm, Kintec, Sheet resistivity 20 Ω/sq) were subjected to a standard cleaning procedure using soap, demineralized water, acetone and isopropanol, followed by a UV/O₃ treatment for 15 min. Subsequently, PEDOT:PSS was deposited via spin-coating with a thickness of approximately 30 nm. Afterwards, the samples were transferred to a glove box containing a nitrogen atmosphere and an annealing step was performed at 130 °C for 15 min to remove any residual water. In a next step, the PCPDTBT:PC₇₁BM (Solenne) layers were deposited through spin-coating. The blend solutions were prepared in a 1:3 ratio polymer:PC₇₁BM, with total concentrations of 12, 16 and 32 mg mL⁻¹ for **P1**, **P2** and **P3**, respectively. Whereas **P1** and **P2** could readily be dissolved in pure chloroform, **P3** required a mixture of *o*-dichlorobenzene and NMP (4 v/v%). Finally, the devices were finished by evaporation of the top electrodes Ca and Al, with layer thicknesses of ~30 and 80 nm, respectively, at a pressure of 2 × 10⁻⁶ mbar. In this way, devices with an active area of 3 mm² were obtained. Initial device performance measurements were done using a Newport class A solar simulator (model 91195A), calibrated with a silicon solar cell to give an AM 1.5G spectrum. EQE measurements were performed with a Newport Apex illuminator (100 W xenon

lamp, 6257) as a light source, a Newport Cornerstone 130° monochromator, and a Stanford SR830 lock-in amplifier for the current measurements. A silicon FDS100-CAL photodiode was employed as a reference cell.

Degradation Measurements: To investigate the thermal degradation behavior, the solar cells were positioned in an automated degradation chamber in nitrogen atmosphere (glove box) with a constant temperature of 85 °C. The *I-V* characteristics were measured at regular time intervals (initially every 5 min, later on every hour) using a White 5500 K LED (Lamina). Duplo experiments on identically processed samples were performed to confirm the findings. Dedicated degradation experiments focusing either on the absence of light or aging without the presence of top electrodes were performed using a hotplate (280 x 200 mm, type PZ28-2ET, Harry Gestigkeit GmbH, with a PR5 programmer controller).

TEM and AFM Measurements: TEM measurements were performed on a FEI Tecnai Spirit using an accelerating voltage of 120 kV. TEM samples were prepared from devices placed in the dark utilizing a hotplate to initiate thermal degradation or, in the case of the accelerated aging test over 650 hours, from the devices utilized in the automated degradation chamber. By washing away the PEDOT:PSS layer with water, freestanding films were obtained. For AFM imaging, a Bruker Multimode 8 AFM was used in PeakForce tapping mode, employing ScanAsyst. The images were produced with a silicon tip on a nitride lever with a spring constant of 4 N m⁻¹.

3.5 REFERENCES

- [1] a) B. Kippelen, J.-L. Brédas, *Energy Environ. Sci.* **2009**, *2*, 251; b) Y. Su, S. Lan, K. Wei, *Mater. Today* **2012**, *15*, 554; c) L. Dou, J. You, Z. Hong, Z. Xu, G. Li, R. A. Street, Y. Yang, *Adv. Mater.* **2013**, *25*, 6642; d) S. Lizin, S. Van Passel, E. De Schepper, W. Maes, L. Lutsen, J. Manca, D. Vanderzande, *Energy Environ. Sci.* **2013**, *6*, 3136.
- [2] a) Z. C. He, C. M. Zhong, S. J. Su, M Xu, H. B. Wu, Y. Cao, *Nat. Photonics* **2012**, *6*, 591; b) A. K. K. Kyaw, D. H. Wang, D. Wynands, J. Zhang, T. -Q. Nguyen, G. C. Bazan, A. J. Heeger, *Nano Lett.* **2013**, *13*, 3796; c) K. H. Hendriks, G. H. L. Heintges, S. Gevaerts, M. M. Wienk, R. A. J. Janssen, *Angew. Chem.* **2013**, *125*, 8499; *Angew. Chem. Int. Ed.* **2013**, *52*, 8341; d) C. Cabanetos, A. E. Labban, J. A. Bartelt, J. D. Douglas, W. M. Mateker, J. M. Fréchet, M. D. McGehee, P. M. Beaujuge, *J. Am. Chem. Soc.* **2013**, *135*, 4556; e) Y. Liu, Y. Yang, C.-C. Chen, Q. Chen, L. Dou, Z. Hong, G. Li, Y. Yang, *Adv. Mater.* **2013**, *25*, 4657; f) W. Zhang, Y. Wu, Q. Bao, F. Gao, J. Fang, *Adv. Energy Mater.* **2014**, *4*, 1400359; g) B. Kan, Q. Zhang, M. Li, X. Wan, W. Ni, G. Long, Y. Wang, X. Yang, H. Feng, Y. Chen, *J. Am. Chem. Soc.* **2014**, *136*, 15529; h) Y. Liu, J. Zhao, Z. Li, C. Mu, W. Ma, H. Hu, K. Jiang, H. Lin, H. Ade, H. Yan, *Nat. Commun.*, **2014**, *5*, 5293.
- [3] a) N Grossiord, J. M. Kroon, R. Andriessen, P. W. M. Blom, *Org. Electron.* **2012**, *13*, 432; b) M. Jorgensen, K. Norrman, S. A. Gevorgyan, T. Tromholt, B. Andreasen, F. C. Krebs, *Adv. Mater.* **2012**, *24*, 580; c) M. Manceau, A. Rivaton, J.-L. Gardette, *Photochemical stability of materials for OPV*, in *Stability and Degradation of Organic and Polymer Solar Cells* (Ed: F. C. Krebs), Wiley, **2012**, 71; d) S. K. Gupta, K. Dharmalingam, L. S. Pali, S. Rastogi, A. Singh, A. Garg,

Nanomater. Energy **2013**, *2*, 42; e) R. Roesch, K.-R. Eberhardt, S. Engmann, G. Gobsch, H. Hoppe, *Sol. Energy Mater. Sol. Cells* **2013**, *117*, 59; f) H. Cao, W. He, Y. Mao, X. Lin, K. Ishikawa, J. H. Dickerson, W. P. Hess, *J. Power Sources* **2014**, *264*, 168; g) D. Angmo, P. M. Sommeling, R. Gupta, M. Hösel, S. A. Gevorgyan, J. M. Kroon, G. U. Kulkarni, F. C. Krebs, *Adv. Eng. Mater.* **2014**, *16*, 8.

[4] a) F. C. Krebs, *Sol. Energy Mater. Sol. Cells* **2008**, *92*, 715; b) B. Zimmermann, U. Würfel, M. Niggemann, *Sol. Energy Mater. Sol. Cells* **2009**, *93*, 491.

[5] A. Kanwat, J. Jang, *J. Mater. Chem. C* **2014**, *2*, 901.

[6] a) S. Gevorgyan, M. Jørgensen, F. C. Krebs, K.O. Sylvester-Hvid, *Sol. Energy Mater. Sol. Cells* **2011**, *95*, 1389; b) R. Rösch, D. M. Tanenbaum, M. Jørgensen, M. Sealand, M. Barenklau, M. Hermenau, E. Voroshazi, M. T. Lloyd, Y. Galagan, B. Zimmermann, U. Würfel, M. Hösel, H. F. Dam, S. Gevorgyan, S. Kudret, W. Maes, L. Lutsen, D. Vanderzande, R. Andriessen, M. Teran-Escobar, M. Lira-Cantu, A. Rivaton, G. Y. Uzunoglu, D. Germack, B. Andreasen, M. V. Madsen, K. Norrman, H. Hoppe, F. C. Krebs, *Energy Environ. Sci.* **2012**, *5*, 6521.

[7] K. Lee, J. Y. Kim, S. H. Park, S. H. Kim, S. Cho, A. J. Heeger, *Adv. Mater.* **2007**, *19*, 2445.

[8] I. Cardinaletti, J. Kesters, S. Bertho, B. Conings, F. Piersimoni, J. D'Haen, L. Lutsen, M. Nesladek, B. Van Mele, G. Van Assche, K. Vandewal, A. Salleo, D. Vanderzande, W. Maes, J. V. Manca, *J. Photon. Energy* **2014**, *4*, 040997.

[9] a) J.-L. Gardette, *Fundamental and technical aspects of the photooxidation of polymers*, in *Handbook of Polymer Degradation*, 2nd Edn., Vol.

1 (Ed: S. H. Hamid), Marcel Dekker, New York, **2000**, 671; b) A. Tournebize, P.-O. Bussière, A. Rivaton, J.-L. Gardette, H. Medlej, R. C. Hiorns, C. Dagron-Lartigau, F. C. Krebs, K. Norrman, *Chem. Mater.* **2013**, *25*, 4522; c) A. Tournebize, P.-O. Bussière, P. Wong-Wah-Chung, S. Thérias, A. Rivaton, J.-L. Gardette, S. Beaupré, M. Leclerc, *Adv. Energy Mater.* **2013**, *3*, 478; d) A. Rivaton, A. Tournebize, J. Gaume, P.-O. Bussière, J.-L. Gardette, S. Thérias, *Polym. Int.* **2014**, *63*, 1335.

[10] a) J. Zhao, A. Swinnen, G. Van Assche, J. Manca, D. Vanderzande, B. Van Mele, *J. Phys. Chem. B* **2009**, *113*, 1587; b) F. Demir, N. Van den Brande, B. Van Mele, S. Bertho, D. Vanderzande, J. Manca, G. Van Assche, *J. Therm. Anal. Calorim.* **2011**, *105*, 845.

[11] a) M. Jorgensen, K. Norrman, F. C. Krebs, *Sol. Energy Mater. Sol. Cells* **2008**, *92*, 686; b) S. Bertho, G. Janssen, T. J. Cleij, B. Conings, W. Moons, A. Gadisa, J. D'Haen, E. Goovaerts, L. Lutsen, J. Manca, D. Vanderzande, *Sol. Energy Mater. Sol. Cells* **2008**, *92*, 753; c) J. U. Lee, J. W. Jung, J. W. Jo, W. H. Jo, *J. Mater. Chem.* **2012**, *22*, 24265; d) E. Bundgaard, M. Helgesen, J. E. Carlé, F. C. Krebs, M. Jorgensen, *Macromol. Chem. Phys.* **2013**, *214*, 1546.

[12] a) C. H. Peters, I. T. Sachs-Quintana, J. P. Kastrop, S. Beaupré, M. Leclerc, M. D. McGehee, *Adv. Energy Mater.* **2011**, *1*, 491; b) C. H. Peters, I. T. Sachs-Quintana, W. R. Mateker, T. Heumueller, J. Rivnay, R. Noriega, Z. M. Beiley, E. T. Hoke, A. Salleo, M. D. McGehee, *Adv. Mater.* **2012**, *24*, 663; c) W. R. Mateker, J. D. Douglas, C. Cabanetos, I. T. Sachs-Quintana, J. A. Bartelt, E. T. Hoke, A. E. Labban, P. M. Beaujuge, J. M. J. Fréchet, M. D. McGehee, *Energy Environ. Sci.* **2013**, *6*, 2529; d) I. T. Sachs-Quintana, T. Heumueller, W. R. Mateker, D. E. Orozco, R. Cheacharoen, S. Sweetnam, C. J. Brabec, M. D. McGehee, *Adv. Funct. Mater.* **2014**, *24*, 3978; e) T. Heumueller, W. R. Mateker,

- I. T. Sachs-Quintana, K. Vandewal, J. A. Bartelt, T. M. Burke, T. Ameri, C. J. Brabec, M. D. McGehee, *Energy Environ. Sci.* **2014**, *7*, 2974.
- [13] a) F. C. Krebs, H. Spanggaard, *Chem. Mater.* **2005**, *17*, 5235; b) M. H. Petersen, S. A. Gevorgyan, F. C. Krebs, *Macromolecules* **2008**, *41*, 8986.
- [14] H. W. Liu, D. Y. Chang, W. Y. S. P. Chiu Rwei, L. Wang, *J. Mater. Chem.* **2012**, *22*, 15586.
- [15] a) K. Sivula, Z. T. Ball, N. Watanabe, J. M. J. Fréchet, *Adv. Mater.* **2006**, *18*, 206; b) J. U. Lee, J. W. Jung, T. Emrick, T. P. Russell, W. H. Jo, *Nanotechnology* **2010**, *21*, 105201; c) J. U. Lee, J. W. Jung, T. Emrick, T. P. Russell, W. H. Jo, *J. Mater. Chem.* **2010**, *20*, 3287.
- [16] C. Lindqvist, J. Bergqvist, C.-C. Feng, S. Gustafsson, O. Bäcke, N. D. Treat, C. Bounioux, P. Henriksson, R. Kroon, E. Wang, A. Sanz-Velasco, P. M. Kristiansen, N. Stingelin, E. Olsson, O. Inganäs, M. R. Andersson, C. Müller, *Adv. Energy Mater.* **2014**, *4*, 1301437.
- [17] a) D. M. Johansson, G. Srdanov, G. Yu, M. Theander, O. Inganas, R. M. Andersson, *Macromolecules* **2000**, *33*, 2525; b) V. Deimede, J. K. Kallitsis, T. Pakula, *J. Polym. Sci. A: Polym. Chem.* **2001**, *39*, 3168; c) J. Vandenberg, B. Conings, S. Bertho, J. Kesters, D. Spoltore, S. Esiner, J. Zhao, G. Van Assche, M. M. Wienk, W. Maes, L. Lutsen, B. Van Mele, R. A. J. Janssen, J. Manca, D. J. M. Vanderzande, *Macromolecules* **2011**, *44*, 8470.
- [18] a) S. Miyanishi, K. Tajima, H. Kazuhito, *Macromolecules* **2009**, *42*, 1610; b) B. J. Kim, Y. Miyamoto, B. Ma, J. M. J. Fréchet, *Adv. Funct. Mater.* **2009**, *19*, 2273; c) C.-H. Hsieh, Y.-J. Cheng, P.-J. Li, C.-H. Chen, M. Dubosc, R.-M. Liang, C.-S. Hsu, *J. Am. Chem. Soc.* **2010**, *132*, 4887; d) G. Griffini, J. D. Douglas, C. Piliago, T. W. Holcombe, S. Turri, J. M. J. Fréchet, J. L. Mynar, *Adv. Mater.* **2011**, *23*, 1660; e) H. J. Kim, A.-R. Han, C.-H. Cho, H. Kang, H.-H. Cho,

M. Y. Lee, J. M. J. Fréchet, J. H. Oh, B. J. Kim, *Chem. Mater.* **2012**, *24*, 215; f) C.-Y. Nam, Y. Qin, Y. S. Park, H. Hlaing, X. Lu, B. M. Ocko, C. T. Black, R. B. Grubbs, *Macromolecules* **2012**, *45*, 2338; g) F. Ouhib, M. Tomassetti, J. Manca, F. Piersimoni, D. Spoltore, S. Bertho, H. Moons, R. Lazzaroni, S. Desbief, C. Jérôme, C. Detrembleur, *Macromolecules* **2013**, *46*, 785; h) G. Brotas, J. Farinhas, Q. Ferreira, R. Rodrigues, I. L. Martins, J. Morgado, A. Charas, *J. Polym. Sci. A: Polym. Chem.* **2014**, *52*, 652; i) L. Derue, O. Dautel, A. Tournebize, M. Drees, H. Pan, S. Berthumeyrie, B. Pavageau, E. Cloutet, S. Chambon, L. Hirsch, A. Rivaton, P. Hudhomme, A. Facchetti, G. Wantz, *Adv. Mater.* **2014**, *26*, 5831.

[19] a) D. M. Tanenbaum, M. Hermenau, E. Voroshazi, M. T. Lloyd, Y. Galagan, B. Zimmermann, M. Hösel, H. F. Dam, M. Jørgensen, S. A. Gevorgyan, S. Kudret, W. Maes, L. Lutsen, D. Vanderzande, U. Würfel, R. Andriessen, R. Rösch, H. Hoppe, M. Lira-Cantu, A. Rivaton, G. Y. Uzunoğlu, D. Germack, B. Andreasen, M. V. Madsen, K. Norrman, F. C. Krebs, *RSC Adv.* **2012**, *2*, 882; b) S. Bertho, B. Campo, F. Piersimoni, D. Spoltore, J. D'Haen, L. Lutsen, W. Maes, D. Vanderzande, J. Manca, *Sol. Energy Mater. Sol. Cells* **2013**, *110*, 69; c) J. Kesters, S. Kudret, S. Bertho, N. Van den Brande, M. Defour, B. Van Mele, H. Penxten, L. Lutsen, J. Manca, D. J. M. Vanderzande, W. Maes, *Org. Electron.* **2014**, *15*, 549.

[20] a) D. Mühlbacher, M. Scharber, M. Morana, Z. Zhu, D. Waller, R. Gaudiana, C. Brabec, *Adv. Mater.* **2006**, *18*, 2884; b) J. Peet, J. Y. Kim, N. E. Coates, W. L. Ma, D. Moses, A. J. Heeger, G. C. Bazan, *Nat. Mater.* **2007**, *6*, 497; c) J. K. Lee, W. L. Ma, C. J. Brabec, J. Yuen, J. S. Moon, J. Y. Kim, K. Lee, G. C. Bazan, A. J. Heeger, *J. Am. Chem. Soc.* **2008**, *130*, 3619.

- [21] a) C. I. Soci, W. Hwang, D. Moses, Z. Zhu, D. Waller, R. Gaudiana, C. J. Brabec, A. J. Heeger, *Adv. Funct. Mater.* **2007**, *17*, 632; b) M. Zhang, H. N. Tsao, W. Pisula, C. Yang, A. K. Mishra, K. Müllen, *J. Am. Chem. Soc.* **2007**, *129*, 3472; c) A. P. Zoombelt, S. G. J. Mathijssen, M. G. R. Turbiez, M. M. Wienk, R. A. J. Janssen, *J. Mater. Chem.* **2010**, *20*, 2240; d) J. Kettle, M. Horie, L. A. Majewski, B. R. Saunders, S. Tuladhar, J. Nelson, M. I. Turner, *Sol. Energy Mater. Sol. Cells* **2011**, *95*, 2186; e) A. V. Tunc, A. De Sio, D. Riedel, F. Deschler, E. Da Como, J. Parisi, E. von Hauff, *Org. Electron.* **2012**, *13*, 290; f) S. Albrecht, S. Janietz, W. Schindler, J. Frisch, J. Kurpiers, J. Kniepert, S. Inal, P. Pingel, K. Fostiropoulos, N. Koch, D. J. Neher, *J. Am. Chem. Soc.* **2012**, *134*, 14932; g) L. Marin, H. Penxten, S. Van Mierloo, R. Carleer, L. Lutsen, D. Vanderzande, W. Maes, *J. Polym. Sci. A: Polym. Chem.* **2013**, *51*, 4912.
- [22] a) U. R. Lee, T. W. Lee, M. H. Hoang, N. S. Kang, J. W. Yu, K. H. Kim, K.-G. Lim, T.-W. Lee, J.-I. Jin, D. H. Choi, *Org. Electron.* **2011**, *12*, 269; b) H. Waters, J. Kettle, S.-W. Chang, C.-J. Su, W.-R. Wu, U.-S. Jeng, Y.-C. Tsai, M. Horie, *J. Mater. Chem. A* **2013**, *1*, 7370; c) H. Waters, N. Bristow, O. Moudam, S.-W. Chang, C.-J. Sun, W.-R. Wu, U.-S. Jeng, M. Horie, J. Kettle, *Org. Electron.* **2014**, *15*, 2433.
- [23] a) C.-K. Mai, H. Zhou, Y. Zhang, Z. B. Henson, T.-Q. Nguyen, A. J. Heeger, G. C. Bazan, *Angew. Chem.* **2013**, *125*, 13112; *Angew. Chem. Int. Ed.* **2013**, *52*, 12874; b) A. W. Thomas, Z. B. Henson, J. Du, C. A. Vandenberg, G. C. Bazan, *J. Am. Chem. Soc.* **2014**, *136*, 3736; c) H. Zhou, Y. Zhang, C.-K. Mai, S. D. Collins, T.-Q. Nguyen, G. C. Bazan, A. J. Heeger, *Adv. Mater.* **2014**, *26*, 780.
- [24] Z. B. Henson, P. Zalar, X. Chen, G. C. Welch, T.-Q. Nguyen, G. C. Bazan, *J. Mater. Chem. A* **2013**, *1*, 11117.

- [25] F. Hinkel, T. Marszalek, W. Zajaczkowski, S. R. Puniredd, M. Baumgarten, W. Pisula, K. Müllen, *Chem. Mater.* **2014**, *26*, 4844.
- [26] a) A. Kraak, A. K. Wiersema, P. Jordens, H. Wynberg, *Tetrahedron* **1968**, *24*, 3381; b) J. R. Reynolds, J. Z. Brzezinski, *Synthesis* **2002**, 1053; c) P. Coppo, D. C. Cupertino, S. C. Yeates, M. L. Turner, *J. Mater. Chem.* **2002**, *12*, 2597; d) P. Coppo, D. C. Cupertino, S. C. Yeates, M. L. Turner, *Macromolecules* **2003**, *36*, 2705; e) J. H. Park, B. Y. Lee, *Bull. Korean Chem. Soc.* **2010**, *31*, 1064.
- [27] a) S. Van Mierloo, P. J. Adriaensens, W. Maes, L. Lutsen, T. J. Cleij, E. Botek, B. Champagne, D. J. Vanderzande, *J. Org. Chem.* **2010**, *75*, 7202; b) S. Van Mierloo, A. Hadipour, M.-J. Spijkman, N. Van den Brande, B. Ruttens, J. Kesters, J. D'Haen, G. Van Assche, D. M. de Leeuw, T. Aernouts, J. Manca, L. Lutsen, D. Vanderzande, W. Maes, *Chem. Mater.* **2012**, *24*, 587.
- [28] W. Vanormelingen, P. Verstappen, V. Maes, D. Bevk, L. Lutsen, D. Vanderzande, W. Maes, *Synlett* **2013**, *24*, 2389.
- [29] a) R. L. Danley, P. A. Caulfield, S. R. Aubuchon, *Am. Lab.* **2008**, *40*, 9; b) T. Ghoo, N. Van den Brande, M. Defour, J. Brassinne, C.-A. Fustin, J.-F. Gohy, S. Hoepfener, U. S. Schubert, W. Vanormelingen, L. Lutsen, D. J. Vanderzande, B. Van Mele, W. Maes, *Eur. Polym. J.* **2014**, *53*, 206.
- [30] M. O. Reese, S. A. Gevorgyan, M. Jørgensen, E. Bundgaard, S. R. Kurtz, D. S. Ginley, D. C. Olson, M. R. Lloyd, P. Morvillo, E. A. Katz, A. Elschner, O. Haillant, T. R. Currier, V. Shrotriya, M. Hermenau, M. Riede, K. R. Kirov, G. Trimmel, T. Rath, O. Inganäs, F. Zhang, M. Andersson, K. Tvingstedt, M. Lira-Cantu, D. Laird, C. McGuinness, S. J. Gowrisanker, M. Pannone, M. Xiao, J. Hauch, R. Steim, D. M. DeLongchamp, R. Rösch, H. Hoppe, N. Espinosa, A.

- Urbina, G. Yaman-Uzunoglu, J. -B. Bonekamp, A. J. J. M. van Breemen, C. Girotto, E. Voroshazi, F. C. Krebs, *Sol. Energy Mater. Sol. Cells* **2011**, *95*, 1253.
- [31] a) Z. Li, H. C. Wong, Z. Huang, H. Zhong, C. H. Tan, W. C. Tsoi, J. S. Kim, J. R. Durrant, J. T. Cabral, *Nat. Commun.* **2013**, *4*, 2227; b) F. Piersimoni, G. Degutis, S. Bertho, K. Vandewal, D. Spoltore, T. Vangerven, J. Drijkoningen, M. K. Van Bael, A. Hardy, J. D'Haen, W. Maes, D. Vanderzande, M. Nesladek, J. Manca, *J. Polym. Sci. B: Polym. Phys.* **2013**, *51*, 1209.
- [32] E. Voroshazi, I. Cardinaletti, T. Conard, B. P. Rand, *Adv. Energy Mater.* **2014**, DOI:10.1002/aenm.201400848.
- [33] a) M. O. Reese, M. S. White, G. Rumbles, D. S. Ginley, S. E. Shaheen, *Appl. Phys. Lett.* **2008**, *92*, 053307; b) M. T. Lloyd, D. C. Olson, P. Lu, E. Fang, D. L. Moore, M. S. White, M. O. Reese, D. S. Ginley, J. W. P. Hsu, *J. Mater. Chem.* **2009**, *19*, 7638.
- [34] a) M. M. Lee, J. Teuscher, T. Miyasaka, T. N. Murakami, H. J. Snaith, *Science* **2012**, *338*, 643; b) S. Kazim, M. K. Nazeeruddin, M. Grätzel, S. Ahmad, *Angew. Chem.* **2014**, *126*, 2854; *Angew. Chem. Int. Ed.* **2014**, *53*, 2812; c) H. Zhou, Q. Chen, G. Li, S. Luo, T.-B. Song, H.-S. Duan, Z. Hong, J. You, Y. Liu, Y. Yang, *Science* **2014**, *345*, 542.
- [35] S. Wouters, F. Demir, L. Beenaerts, G. Van Assche, *Thermochim. Acta* **2012**, *530*, 64.
- [36] a) J. Bard, L. R. Faulkner, *Electrochemical methods: fundamentals and applications*, 2nd Ed., Wiley, **2001**; b) S. Trasatti, *Pure Appl. Chem.* **1986**, *58*, 955.

3.6 ACKNOWLEDGEMENTS

This work was supported by the project ORGANEXT (EMR INT4-1.2-2009-04/054), selected in the frame of the operational program INTERREG IV-A Euregio Maas-Rijn, and the IAP 7/05 project FS2 (Functional Supramolecular Systems), granted by the Science Policy Office of the Belgian Federal Government (BELSPO). We are also grateful for financial support by the Research Programme of the Research Foundation – Flanders (FWO) (project G.0415.14N and M.ERA-NET project RADESOL). J. Kesters and J. Drijkoningen thank Hasselt University for their PhD scholarships. P. Verstappen acknowledges the Agency for Innovation by Science and Technology in Flanders (IWT) for his PhD grant. J. Kesters and P. Verstappen contributed equally to this work. The authors are also grateful to B. Van Mele, N. Van den Brande and M. Defour for the thermal analysis, and H. Penxten for the CV measurements. We further acknowledge Hercules for providing the funding for the LTQ Orbitrap Velos Pro mass spectrometer. Hasselt University and IMO-IMOMEC are partners within the Solliance network, the strategic alliance for research and development in the field of thin-film PV energy in the Eindhoven-Leuven-Aachen region.

3.7 SUPPORTING INFORMATION

3.7.1 Monomer and polymer synthesis

Unless stated otherwise, all reagents and chemicals were obtained from commercial sources and used without further purification. Solvents were dried by a solvent purification system (MBraun, MB-SPS-800) equipped with alumina columns. 4-(2'-Ethylhexylidene)-4*H*-cyclopenta[2,1-*b*:3,4-*b'*]dithiophene (**1**),^[1] 4-(2'-ethylhexyl)-4-octyl-4*H*-cyclopenta[2,1-*b*:3,4-*b'*]dithiophene (**2**)^[1], 4-(2'-ethylhexyl)-4-(6'-hydroxyhexyl)-4*H*-cyclopenta[2,1-*b*:3,4-*b'*]dithiophene (**3**),^[1] and 4,7-dibromo-2,1,3-benzothiadiazole^[2] were prepared according to literature procedures.

2,6-Bis(trimethylstannyl)-4-(2'-ethylhexyl)-4-octyl-4*H*-cyclopenta[2,1-*b*:3,4-*b'*]dithiophene (M1)

4-(2'-Ethylhexyl)-4-octyl-4*H*-cyclopenta[2,1-*b*:3,4-*b'*]dithiophene (**2**) (2.93 g, 7.28 mmol) was dissolved in dry THF (60 mL) and the solution was cooled down to -78 °C before a solution of *n*-BuLi in *n*-hexane (2.5 M; 11.6 mL, 29.1 mmol) was added dropwise. After stirring an additional hour at -78 °C, a solution of trimethyltin chloride (1 M in THF; 32.8 mL) was added. The resulting solution was allowed to warm gently to room temperature (overnight). Water was added and the mixture was extracted with diethyl ether. The organic phase was washed with brine, dried with MgSO₄, filtered and evaporated to dryness. The crude product was purified via preparative recycling SEC to yield the pure monomer as a pale yellow oil (3.29 g, 62%). ¹H NMR (400 MHz, CDCl₃, δ): 6.94 (s, 1H), 6.93 (s, 1H), 1.95–1.70 (m, 4H), 1.30–1.05 (m, 10H), 1.05–0.80 (m, 13H), 0.73 (t, *J* = 7.0 Hz, 3H), 0.65–0.55 (m, 4H), 0.36 (s, 18H).

2,6-Bis(trimethylstannyl)-4-(2'-ethylhexyl)-4-(6'-hydroxyhexyl)-4H-cyclopenta[2,1-b:3,4-b']dithiophene (M2)

To a solution of 4-(2'-ethylhexyl)-4-(6'-hydroxyhexyl)-4H-cyclopenta[2,1-b:3,4-b']dithiophene (**3**) (0.404 g, 1.03 mmol) in dry THF (18 mL), *n*-BuLi (2.5 M in *n*-hexane; 1.36 mL, 3.40 mmol) was added dropwise at -15 °C under a N₂ atmosphere. The resulting mixture was stirred for 20 min at -15 °C and a solution of trimethyltin chloride (1 M in THF; 3.71 mL) was added. The solution was allowed to warm gently to room temperature (overnight) and water was added. After extraction with diethyl ether, the organic phase was washed with brine, dried with Na₂SO₄, filtered and evaporated to dryness. The crude product was purified via preparative recycling SEC to yield the pure monomer as a pale yellow oil (0.393 g, 53%). ¹H NMR (300 MHz, CDCl₃, δ): 6.93 (s, 1H), 6.92 (s, 1H), 3.57 (td, *J* = 6.6, 5.4 Hz, 2H), 1.93–1.70 (m, 4H), 1.45 (q, *J* = 6.7 Hz, 2H), 1.32–1.08 (m, 5H), 1.07–0.79 (m, 10H), 0.78–0.68 (t, *J* = 6.9 Hz, 3H), 0.64–0.53 (m, 4H), 0.36 (s, 18H).

4-(2'-Ethylhexyl)-4H-cyclopenta[2,1-b:3,4-b']dithiophene (4)

A solution of 4-(2'-ethylhexylidene)-4H-cyclopenta[2,1-b:3,4-b']dithiophene (**1**) (930 mg, 3.23 mmol) in dry THF (30 mL) was added dropwise to a suspension of LiAlH₄ (264 mg, 6.96 mmol) in THF (30 mL). The resulting mixture was stirred for 2 h at room temperature, cooled down to 0 °C and water was carefully added. After extraction with diethyl ether, the organic layer was dried with MgSO₄, filtered and the solvent was removed under vacuum. Purification of the crude product by column chromatography (silica, eluent petroleum ether) yielded the pure product as a colorless oil (730 mg, 78%). ¹H NMR (400 MHz, CDCl₃, δ): 7.16 (d, *J* = 4.9 Hz, 2H), 7.06 (d, *J* = 4.9 Hz, 1H), 7.05 (d, *J* = 4.9

Hz, 1H), 3.70 (t, $J = 7.7$ Hz, 1H), 1.73–1.54 (m, 3H), 1.53–1.35 (m, 4H), 1.35–1.20 (m, 4H), 0.93–0.83 (m, 6H); ^{13}C NMR (75 MHz, CDCl_3 , δ): 154.9, 154.8, 137.5, 124.4, 122.8, 42.4, 37.4, 36.1, 32.8, 28.7, 25.9, 23.2, 14.3, 10.6; MS (MALDI-TOF) m/z : 289.8 ($[\text{M}]^+$).

Ethyl 6-{4'-(2''-ethylhexyl)-4H-cyclopenta[2,1-b:3,4-b']dithiophen-4'-yl}hexanoate (5)

4-(2'-Ethylhexyl)-4H-cyclopenta[2,1-b:3,4-b']dithiophene (**4**) (630 mg, 2.18 mmol), 6-bromohexanoic acid (468 mg, 2.40 mmol) and KI (30 mg, 0.18 mmol) were dissolved in DMSO (16 mL) and *t*-BuOK (612 mg, 5.45 mmol) was added. After stirring at room temperature for 15 h, an aqueous HCl (1 M) solution was added and the mixture was extracted with hexanes. After drying the organic phase with MgSO_4 , filtration and solvent removal under vacuum, the obtained product was dissolved in EtOH (15 mL) and H_2SO_4 (0.5 mL) was added. After reaction for 1 h at room temperature, ice water was added and the mixture was extracted with diethyl ether. The collected organic layers were washed with a saturated NaHCO_3 solution, dried with MgSO_4 , filtered and the solvent was removed under vacuum. After column chromatographic purification (silica, eluent petroleum ether:diethyl ether, 97:3), the pure product was obtained as a colorless oil (785 mg, 83%). ^1H NMR (300 MHz, CDCl_3 , δ): 7.13 (d, $J = 4.9$ Hz, 2H), 6.91 (d, $J = 4.9$ Hz, 1H), 6.90 (d, $J = 4.9$ Hz, 1H), 4.08 (q, $J = 7.1$ Hz, 2H), 2.15 (t, $J = 7.5$ Hz, 2H), 1.95–1.75 (m, 4H), 1.55–1.40 (m, 2H), 1.30–1.15 (m, 5H), 1.15–0.80 (m, 10H), 0.75 (t, $J = 6.9$ Hz, 3H), 0.70–0.55 (m, 4H); ^{13}C NMR (100 MHz, CDCl_3 , δ): 173.8, 157.7, 157.6, 136.7, 124.4, 121.9, 60.2, 53.2, 41.7, 39.3, 35.2, 34.3, 34.1, 29.4, 28.6, 27.2, 24.7, 23.9, 22.8, 14.3,

14.1, 10.7; HRMS (ESI) m/z : $[M+Na]^+$ calcd. for $C_{25}H_{36}O_2S_2Na$, 455.2049; found, 455.2038.

Ethyl 6-{2',6'-dibromo-4'-(2''-ethylhexyl)-4H-cyclopenta[2,1-b:3,4-b']-dithiophen-4'-yl}hexanoate (6)

Ethyl 6-{4'-(2''-ethylhexyl)-4H-cyclopenta[2,1-b:3,4-b']dithiophen-4'-yl}hexanoate (**5**) (785 mg, 1.81 mmol) was dissolved in $CHCl_3$ (15 mL) and the solution was cooled down to 0 °C. NBS (678 mg, 3.81 mmol) was added and the resulting solution was stirred for 2 h at room temperature. Water was added and the mixture was extracted with diethyl ether. After drying with $MgSO_4$, filtration, solvent evaporation in vacuo and purification via column chromatography (silica, eluent petroleum ether:diethyl ether, 97:3), the pure product was obtained as a colorless oil (931 mg, 87%). 1H NMR (400 MHz, $CDCl_3$, δ): 6.92 (s, 1H), 6.91 (s, 1H), 4.09 (q, $J = 7.1$ Hz, 2H), 2.18 (t, $J = 7.5$ Hz, 2H), 1.88–1.70 (m, 4H), 1.52–1.42 (m, 2H), 1.23 (t, $J = 7.1$ Hz, 3H), 1.19–1.09 (m, 2H), 1.07–0.81 (m, 10H), 0.78 (t, $J = 7.0$ Hz, 3H), 0.68–0.57 (m, 4H); ^{13}C NMR (100 MHz, $CDCl_3$, δ): 173.8, 155.7, 155.6, 136.6, 124.9, 124.8, 111.2, 111.1, 60.3, 55.0, 41.7, 39.2, 35.4, 34.4, 34.0, 29.5, 28.6, 27.4, 24.8, 24.0, 22.9, 14.4, 14.2, 10.8; HRMS (ESI) m/z : $[M+Na]^+$ calcd. for $C_{25}H_{34}Br_2O_2S_2Na$, 613.0239; found, 613.0204.

Ethyl 6-{4'-(2''-ethylhexyl)-2',6'-bis(trimethylstannyl)-4H-cyclopenta[2,1-b:3,4-b']dithiophen-4'-yl}hexanoate (M3)

Ethyl 6-{2',6'-dibromo-4'-(2''-ethylhexyl)-4H-cyclopenta[2,1-b:3,4-b']dithiophen-4'-yl}hexanoate (**6**) (931 mg, 1.58 mmol), hexamethylditin (2.00 g, 6.10 mmol), LiCl (234 mg, 5.53 mmol) and $Pd(PPh_3)_4$ (92 mg, 0.079 mmol) were dissolved in dry degassed toluene (10 mL) under N_2 atmosphere and heated at

105 °C for 1 h. The mixture was cooled down to room temperature and water was added. After extraction with diethyl ether, the organic phase was washed with water, dried over MgSO₄, filtered and evaporated to dryness. The crude product was passed through a silica plug and purification with preparative recycling SEC yielded the pure product as a pale yellow oil (694 mg, 58%). ¹H NMR (400 MHz, CDCl₃, δ): 6.93 (s, 1H), 6.92 (s, 1H), 4.08 (q, *J* = 7.1 Hz, 2H), 2.17 (t, *J* = 7.6 Hz, 2H), 1.91–1.75 (m, 4H), 1.54–1.45 (m, 2H), 1.22 (t, *J* = 7.1 Hz, 3H), 1.20–1.11 (m, 2H), 1.03–0.80 (m, 10H), 0.73 (t, *J* = 7.0 Hz, 3H), 0.63–0.55 (m, 4H), 0.36 (s, 18H).

Poly{4-(2'-ethylhexyl)-4-octyl-4H-cyclopenta[2,1-b:3,4-b']dithiophene-2,6-diyl-alt-2,1,3-benzothiadiazole-4,7-diyl} (P1)

A solution of 2,6-bis(trimethylstannyl)-4-(2'-ethylhexyl)-4-octyl-4H-cyclopenta[2,1-*b*:3,4-*b'*]dithiophene (**M1**) (102 mg, 0.140 mmol) in dry toluene (3.2 mL) was added to a mixture of 4,7-dibromo-2,1,3-benzothiadiazole (41.2 mg, 0.140 mmol), Pd₂(dba)₃ (3.2 mg, 0.0035 mmol) and P(*o*-tol)₃ (4.3 mg, 0.014 mmol) in dry DMF (0.8 mL) under a N₂ atmosphere. After purging with N₂ for 30 min, the mixture was heated to 110 °C for 15 h. The green-black solution was added dropwise to MeOH and the resulting precipitate was filtered in a Soxhlet timble. The crude polymer was purified by subsequent Soxhlet extractions with methanol, acetone, hexanes and chloroform. The chloroform fraction was further purified by preparative SEC and finally precipitated in MeOH to yield a greenish black solid (43.7 mg, 57%). ¹H NMR (400 MHz, CDCl₃, δ): 9.1–7.5 (br, 2H), 7.5–6.1 (br, 2H), 3.0–0.2 (br, 34H); SEC (THF, 40 °C, PS standards): before prep-SEC: *M_n* 20 kDa, PDI 2.4; after prep-SEC: *M_n* 26 kDa, PDI 3.2.

Poly{4-(2'-ethylhexyl)-4-(6'-hydroxyhexyl)-4H-cyclopenta[2,1-b:3,4-b']dithiophene-2,6-diyl-alt-2,1,3-benzothiadiazole-4,7-diyl} (P2)

P2 was prepared similar to **P1**. CPDT monomer **M2** (0.393 g, 0.548 mmol), 4,7-dibromo-2,1,3-benzothiadiazole (0.161 g, 0.548 mmol), Pd₂(dba)₃ (12.5 mg, 13.7 μmol) and P(*o*-tol)₃ (16.7 mg, 54.8 μmol) were dissolved in 9.0 mL of dry toluene and 2.3 mL of dry DMF. Soxhlet extractions were subsequently performed with hexanes, acetone and CHCl₃. Due to the rather limited solubility of the polymer in CHCl₃, purification by preparative SEC was not performed on this material. The final polymer was obtained as a greenish black solid (223 mg, 77%). ¹H NMR (400 MHz, CDCl₃, δ): 8.6–7.6 (br, 2H), 7.6–6.8 (br, 2H), 4.0–3.3 (br, 2H), 3.0–0.2 (br, 28H); SEC (THF, 40 °C, PS standards): *M_n* 13 kDa, PDI 2.5.

Poly{4-(2'-ethylhexyl)-4-(6'-ethoxy-6'-oxohexyl)-4H-cyclopenta[2,1-b:3,4-b']dithiophene-2,6-diyl-alt-2,1,3-benzothiadiazole-4,7-diyl} (P3)

P3 was prepared similar to **P1**. CPDT monomer **M3** (0.162 g, 0.214 mmol), 4,7-dibromo-2,1,3-benzothiadiazole (0.063 g, 0.214 mmol), Pd₂(dba)₃ (4.9 mg, 5.3 μmol) and P(*o*-tol)₃ (6.5 mg, 21.4 μmol) were dissolved in 5.0 mL of dry toluene and 1.2 mL of dry DMF. The final polymer was obtained as a greenish black solid (66 mg, 55%). ¹H NMR (400 MHz, CDCl₃, δ): 8.3–7.6 (br, 2H), 7.6–6.7 (br, 2H), 4.4–3.8 (br, 2H), 3.0–0.3 (br, 30H); SEC (THF, 40 °C, PS standards): before prep-SEC: *M_n* 39 kDa, PDI 3.0; after prep-SEC: *M_n* 46 kDa, PDI 1.7.

3.7.2 Thermal analysis

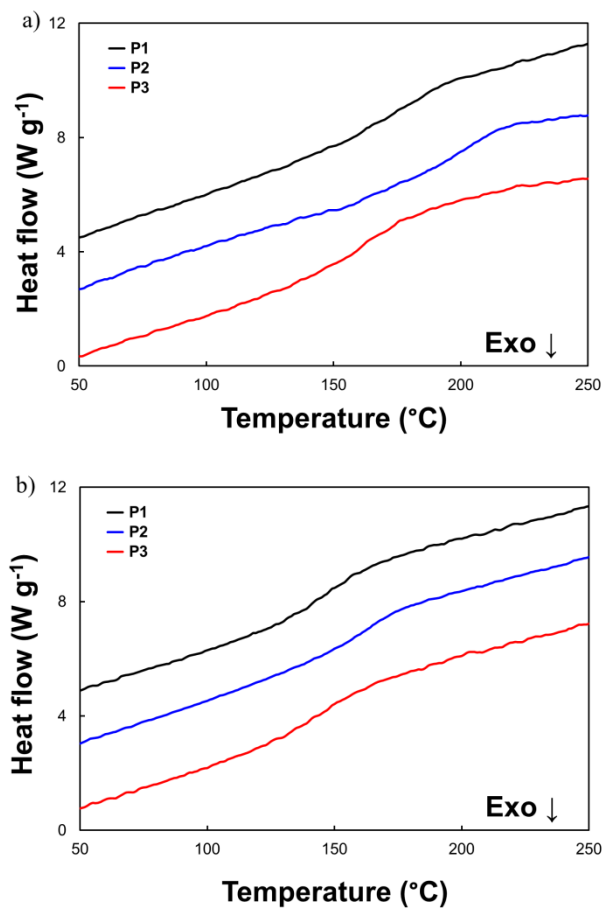


Figure S1: RHC profiles for a) the three PCPDTBT copolymers, and b) the **P1–P3**:PC₇₁BM(1:3) blends (curves shifted vertically for clarity).

3.7.3 Additional solar cell degradation data and TEM figures

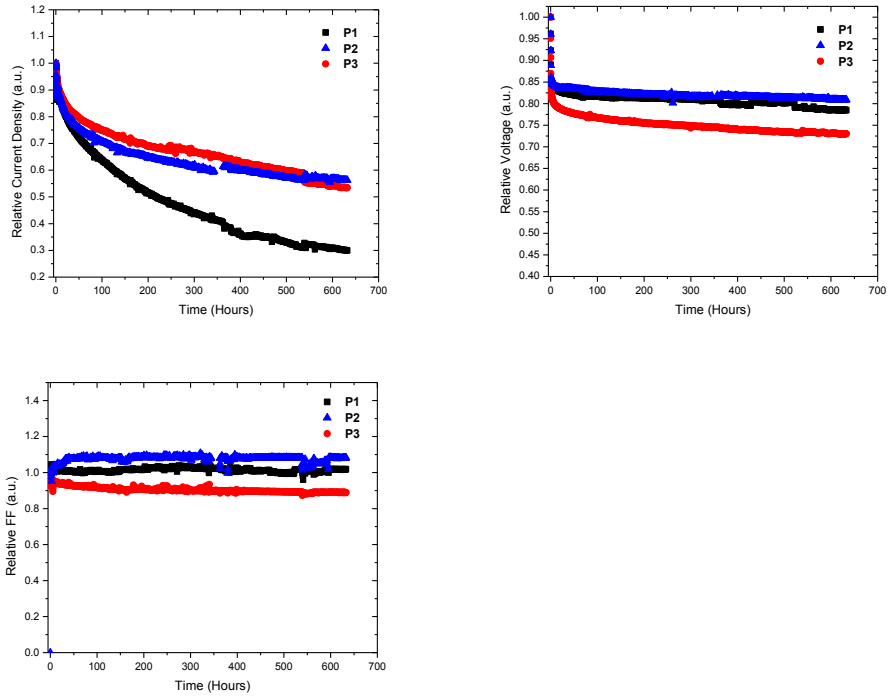


Figure S2: Degradation curves (V_{oc} , J_{sc} and FF) for the polymer solar cells based on **P1–P3** (650 h at 85 °C). The curves are normalized to the first measurement point at 85 °C.

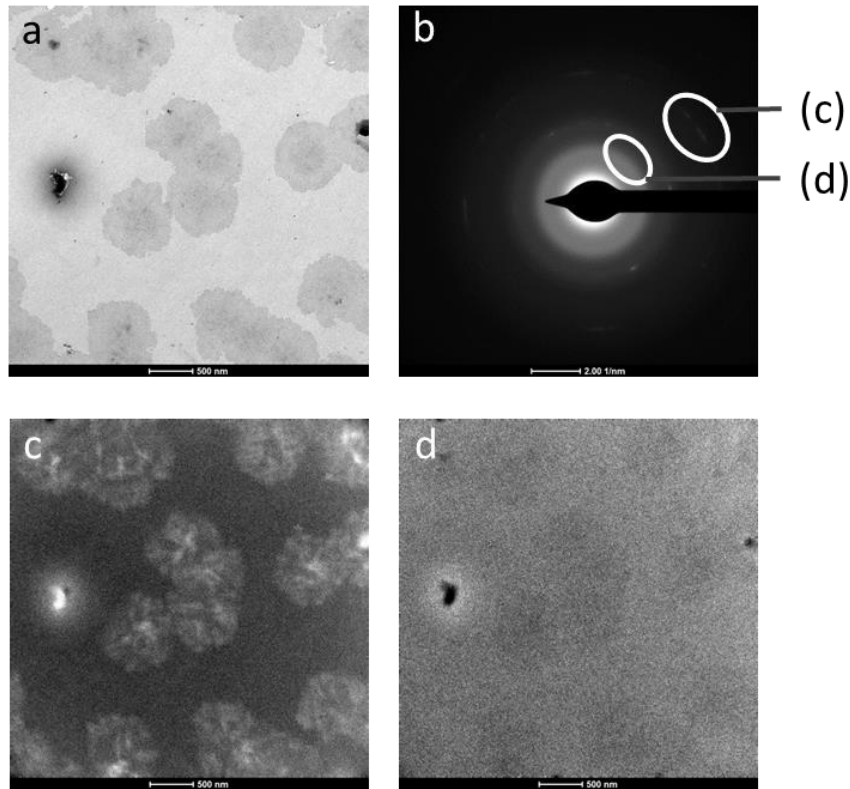


Figure S3: (a) TEM bright field image of a **P1**:PC₇₁BM blend film annealed at 220 °C for 3 h, showing the formation of microcrystals and phase separation. (b) SAED image procured from aggregated domains in the bright field image, illustrating the formation of crystalline regions, most likely to be ascribed to PC₇₁BM. (c) Circular dark field image made by electrons scattered into the sharp diffraction ring. (d) Circular dark field image made by electrons scattered into the diffuse diffraction ring, indicating the more amorphous matrix in the polymer:PC₇₁BM blend.

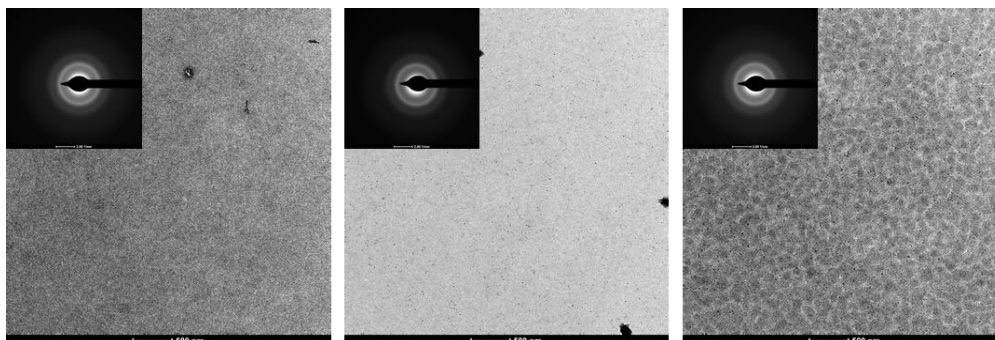


Figure S4: TEM images of **P1–P3**:PC₇₁BM (left to right) BHJ blends exposed to 85 °C for 150 h in the dark.

Table S1: Roughness and peak to peak (P2P) distance data procured from AFM measurements and polymer solar cell devices.

Polymer	Treatment	R_a	R_q	P2P
P1	0 h at 85 °C	0.61	1.11	37.62
P1	650 h at 85 °C	0.56	0.98	43.94
P2	0 h at 85 °C	0.43	0.55	9.02
P2	650 h at 85 °C	0.36	0.46	5.55
P3	0 h at 85 °C	1.09	1.38	19.56
P3	650 h at 85 °C	1.09	1.37	13.96

Enhanced Solar Cell Stability by Polymer (PCPDTBT) Side Chain Functionalization

Table S2: *I-V* characteristics of the polymer solar cells based on **P1–P3** after aging in the dark at 85 °C for 0, 6 and 25 h.

Polymer	Treatment	Voc	Jsc	FF	Best PCE	Average PCE ^{a)}
		[V]	[mA cm ⁻²]		[%]	[%]
P1	pristine	0.59	9.57	0.44	2.57	2.49
P1	dark + 6 h at 85 °C	0.59	7.04	0.43	1.90	1.78
P1	dark + 25 h at 85 °C	0.59	6.58	0.43	1.71	1.67
P2	pristine	0.59	7.54	0.44	1.99	1.94
P2	dark + 6 h at 85 °C	0.59	6.58	0.45	1.80	1.76
P2	dark + 25 h at 85 °C	0.59	6.17	0.45	1.67	1.64
P3	pristine	0.56	9.58	0.51	3.21	2.72
P3	dark + 6 h at 85 °C	0.54	7.45	0.47	2.18	1.78
P3	dark + 25 h at 85 °C	0.55	6.58	0.46	1.70	1.64

^{a)}Averages were taken across 4–8 devices, with an active area of 3 mm².

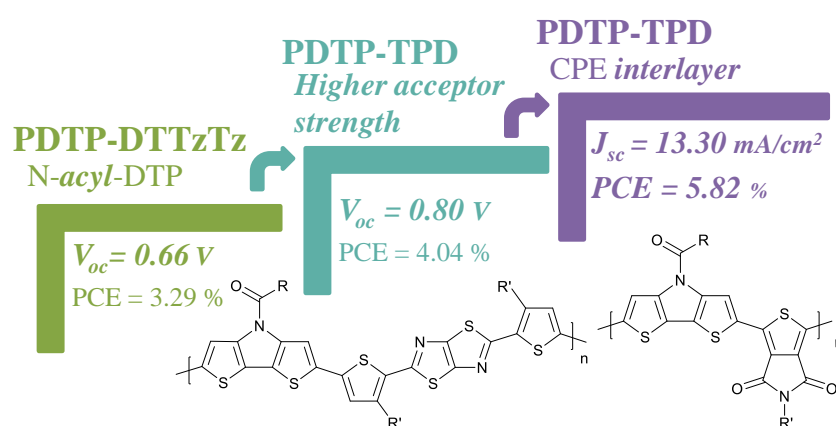
3.7.4 References

[1] Vanormelingen, W.; Verstappen, P.; Maes, V.; Bevk, D.; Lutsen, L.; Vanderzande, D.; Maes, W. *Synlett* **2013**, *24*, 2389.

[2] Karsten, B. P.; Bijleveld, J. C.; Viani, L.; Cornil, J.; Gierschner, J.; Janssen, R. A. J. *J. Mater. Chem.* **2009**, *19*, 5343.

Chapter 4

Enhanced Open-Circuit Voltage in Polymer Solar Cells by Dithieno[3,2-*b*:2',3'-*d*]pyrrole N-Acylation



W. Vanormelingen, J. Kesters, P. Verstappen, J. Drijkoningen, J. Kudrjasova, S. Koudjina, V. Liégeois, B. Champagne, J. Manca, L. Lutsen, D. Vanderzande, W. Maes, *J. Mater. Chem. A*, **2014**, 2, 7535.

ABSTRACT

A series of low bandgap copolymers composed of N-acyl-substituted dithieno[3,2-*b*:2',3'-*d*]pyrroles (DTP's) as the electron rich donor constituents (with various alkyl side chain patterns) combined with different electron deficient acceptor building blocks are developed for polymer solar cell applications. Due to the introduction of the N-acyl substituents, the HOMO energy levels of the push-pull copolymers decrease as compared to the N-alkyl-DTP analogues, resulting in an increased open-circuit voltage (V_{oc}) and hence solar cell performance. For an N-acyl-DTP-*alt*-thieno[3,4-*c*]pyrrole-4,6-dione (PDTP-TPD) copolymer a bulk heterojunction device with a V_{oc} up to 0.80 V and a power conversion efficiency of 4.0% is obtained, the highest value for DTP-based polymer materials to date. Moreover, by implementation of a conjugated polyelectrolyte cathode interlayer the short-circuit current noticeably increases, enhancing the solar cell efficiency to 5.8%.

4.1 INTRODUCTION

Polymer solar cells (PSC's) are studied extensively since they offer the potential of low-cost solution processing and manufacturing of large areas via (roll-to-roll) printing technologies.¹ Furthermore, they can be produced with tuneable colour and transparency on flexible substrates and they are light-weight, attractive features that allow to target photovoltaic (PV) applications and products beyond traditional Si-based PV. Through careful molecular and device engineering the power conversion efficiencies (PCE's) of bulk heterojunction (BHJ) PSC's have steadily increased to over 9%.^{1,2} The photoactive layer of high performance BHJ PSC devices consists of an intimate blend of a low bandgap electron donor polymer and a fullerene acceptor (most often [6,6]-phenyl-C₇₁-butyric acid methyl ester or PC₇₁BM). The state of the art low bandgap copolymers are composed of alternating electron rich (donor) and electron poor (acceptor) heterocyclic moieties, affording intramolecular charge transfer and thereby broadening the absorption window. Conjugated polymer engineering mostly focuses on the design and variation of the donor and acceptor subunits. As such, the performance of PSC's based upon a wide variety of different push-pull copolymers has been reported and the fundamental understanding of molecular structure-device efficiency relations has strongly increased.¹ Prerequisites for high performance solar cells in terms of the electron donor copolymers are a high extinction coefficient throughout the whole solar emission range and a low-lying HOMO (highest occupied molecular orbital) level. While photon absorption is a determining parameter for the short-circuit current density (J_{sc}), the difference between the HOMO of the electron donor polymer and the LUMO (lowest unoccupied molecular orbital) of the electron acceptor component has

been shown to be proportional to the open-circuit voltage (V_{oc}). A sufficiently large LUMO offset is required to provide enough driving force for electron transfer.¹ On the other hand, an increase in the bandgap of the donor copolymer reduces the absorption width. In this respect, there is always a trade-off between V_{oc} and J_{sc} , and fine-tuning of the HOMO/LUMO levels of the push-pull copolymers is imperative to achieve optimal solar cell efficiencies. An attractive approach to optimize the energy levels involves the introduction of electron withdrawing substituents on the conjugated polymer backbone. Fluorination has become a quite general and effective strategy, either on the donor or acceptor building block,^{2,3} resulting in a lowering of both the HOMO and LUMO levels. Combinations of several electron withdrawing groups have also been investigated.⁴

Copolymers composed of alternating N-alkyl-substituted dithieno[3,2-*b*:2',3'-*d*]pyrroles (DTP's) and various electron poor building blocks have been applied in PSC's with limited success,^{5,6} mainly due to the high HOMO levels, majorly determined by the electron rich DTP units. These high HOMO levels give rise to rather low V_{oc} 's and consequently, although J_{sc} 's as high as 14.9 mA cm^{-2} have been observed for DTP-alt-DPP copolymers,^{6b} the highest PCE to be reported was only 2.8%.^{6a,h} On the other hand, the DTP fused heterocyclic system also has a few important strengths. It is readily accessible and copolymers with thiophene have shown high charge carrier mobilities in field-effect transistors (FET's), despite being amorphous.⁷ Dye-sensitized solar cells based on DTP materials have shown excellent performances as well,⁸ and recently small molecule organic solar cells based on N-alkyl-DTP have afforded up to 4.8% efficiency.^{7,9}

In 2010, Rasmussen and co-workers reported the synthesis of N-acyl-substituted DTP's,¹⁰ offering a novel pathway to lower the HOMO levels. In the presented work we have employed this strategy towards the synthesis of alternating low bandgap copolymers, combining N-acyl-DTP's with variable side chain patterns with a number of different acceptor derivatives. For the solar cells based on these copolymers (in combination with PC₇₁BM) the Voc was effectively enhanced (up to 0.80 V), enabling to obtain a record solar cell efficiency of 4.0% for DTP-based copolymers. By spin-coating an additional very thin conjugated polyelectrolyte (CPE) layer on top of the active layer,¹¹ the short-circuit current density was further increased, leading to a maximum PCE of 5.8%.

4.2 RESULTS AND DISCUSSION

4.2.1 Synthesis and characterization

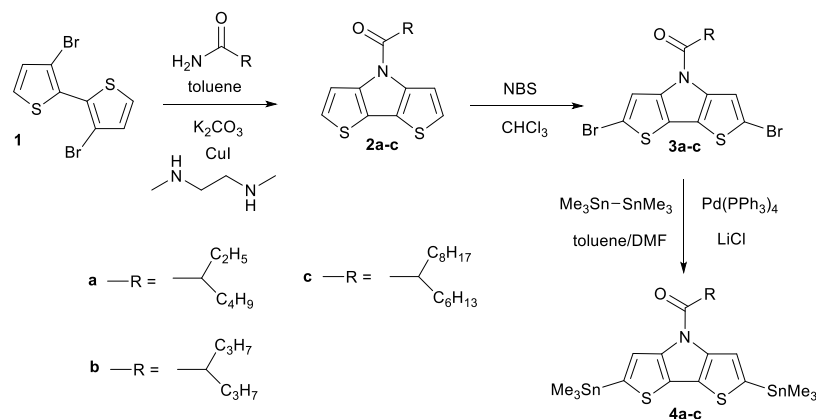
For the construction of the low bandgap copolymers, the Stille polycondensation reaction was chosen, combining distannylated N-acyl-substituted DTP's and several dibrominated acceptor derivatives. The required bis(trimethylstannyl)-N-acyl-DTP's **4a–c** were synthesized by Stille cross-coupling of hexamethylditin and dibrominated DTP precursors **3a–c** (Scheme 1), prepared by a literature procedure.^{10,12} This protocol consists of a copper catalyzed tandem reaction¹³ of an alkyl amide and 3,3'-dibromo-2,2'-bithiophene (**1**)¹⁴ to obtain DTP's **2a–c**, followed by dibromination with *N*-bromosuccinimide (NBS). Three different alkyl side chain patterns were introduced to optimize polymer solubility, taking into account the side chain decoration of the acceptor building blocks, and final active layer blend morphology. Synthesis of 2-ethylhexanamide¹⁵ and 2-propylpentanamide¹⁶ was done according to literature and 2-hexyldecanamide

was synthesized via a similar approach. As the purity of the bisstannyl-DTP monomers is of crucial importance for the correct stoichiometric balance in the polycondensation reactions to enable the formation of high molar mass materials, and the monomers (oily substances) cannot be crystallized, recycling (preparative) size exclusion chromatography (SEC) was applied for monomer purification. In this way, residual amounts of monostannylated DTP and DTP oligomers were readily removed. Due to side reactions and the aim for high purity, the yields for the final stannylation step were moderate (39–55 %).

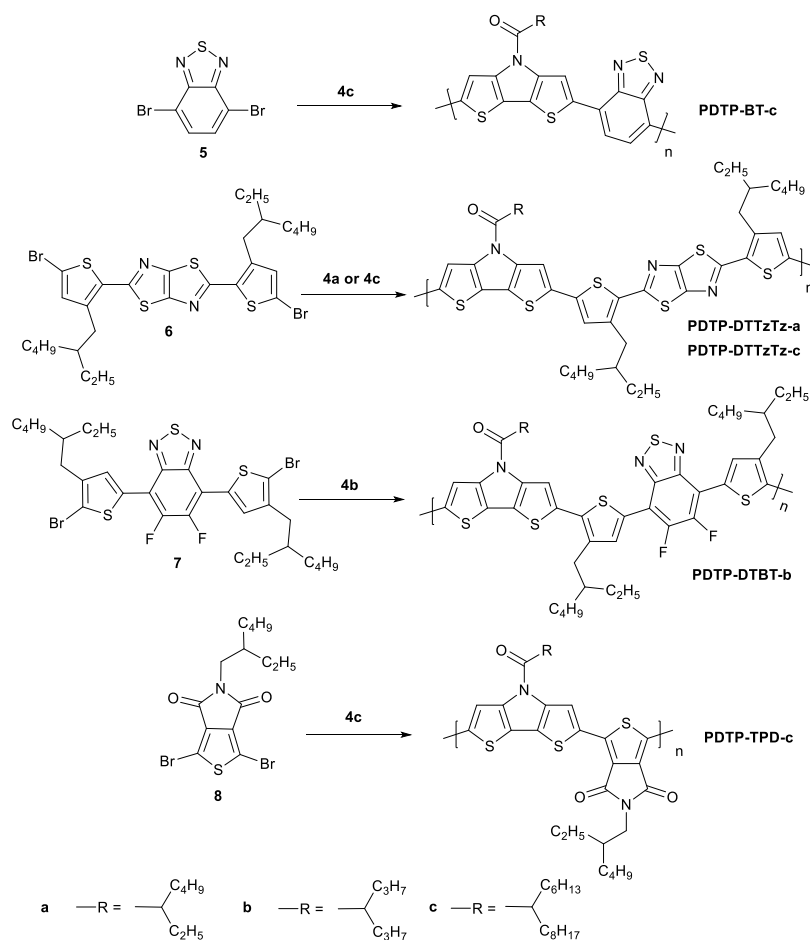
Dibrominated acceptors 4,7-dibromo-2,1,3-benzothiadiazole (**BT 5**),¹⁷ 2,5-bis-[5'-bromo-3'-(2''-ethylhexyl)thiophen-2'-yl]thiazolo[5,4-*d*]thiazole (DTTzTz **6**),¹⁸ and 4,7-bis[5'-bromo-4'-(2''-ethylhexyl)thiophen-2'-yl]-5,6-difluoro-2,1,3-benzothiadiazole (DTBT **7**)¹⁹ were synthesized according to literature procedures, whereas 1,3-dibromo-5-(2'-ethylhexyl)-4*H*-thieno[3,4-*c*]pyrrole-4,6(5*H*)-dione (TPD **8**) was purchased from Sigma-Aldrich and purified by preparative SEC prior to use. The Stille polycondensation reactions were performed under standard conditions (2.5 mol% Pd₂dba₃, 10 mol% P(*o*-tolyl)₃, toluene/DMF, 105 °C, 1 h; Scheme 2) and the crude polymer materials were isolated upon precipitation in ice-cold methanol. No end-capping procedures were applied. The low molar mass fractions were removed by sequential Soxhlet extractions. The copolymers **PDTP-DTTzTz-c** and **PDTP-TPD-c** were readily soluble in chloroform. For **PDTP-BT-c** a fraction soluble in (hot) chlorobenzene was isolated by Soxhlet extraction. However, a large insoluble fraction remained in the Soxhlet timble. **PDTP-DTBT-b** dissolved in (hot) *o*-dichlorobenzene only and for **PDTP-DTTzTz-a** no suitable solvent was found. In general, the solubility of the synthesized copolymers is lower as compared to the *N*-alkyl-DTP analogues (for example, the copolymer *N*-1-pentylhexyl-DTP-*alt*-BT was

reported to be readily soluble in common organic solvents,^{6a} whereas **PDTP-BT-c** has a very low solubility).

The apparent molar masses of the polymers were determined by SEC relative to polystyrene standards (Table 1). As expected, the M_n of the soluble fraction of **PDTP-BT-c** was rather low (7.6 kg mol^{-1}), but for the **PDTP-DTTzTz-c** and **PDTP-TPD-c** materials bearing long branched alkyl side chains reasonably high molar masses were obtained (28 and 29 kg mol^{-1} , respectively). Since polymer chain length and purity are important factors determining solar cell performance,^{1,20} the low and high molar mass fractions of **PDTP-TPD-c** were separated by preparative SEC to yield a **PDTP-TPD-c-H** fraction with an M_n of 69 kg mol^{-1} (see Fig. S1 for chromatograms prior and after preparative SEC). Fractionation of **PDTP-DTTzTz-c** was hindered by its strong aggregation in chloroform and *o*-dichlorobenzene.



Scheme 1: Synthesis of distannylated N-acyl-DTP monomers **4a-c**.



Scheme 2: Polymerization of N-acyl-DTP monomers **4a–c** with various acceptors by Stille cross-coupling (similar reaction conditions for all polymerizations: 2.5 mol% Pd_2dba_3 , 10 mol% $\text{P}(o\text{-tolyl})_3$, toluene/DMF, 105 °C, 1 h; a,b and c denote the alkyl side chain patterns).

4.2.2 Photophysical and electrochemical properties

UV-Vis absorption spectra in solution and thin film were recorded for all copolymers (Fig. 1). All polymers have a broad absorption in the visible region and PDTP-BT-c and PDTP-DTBT-b also absorb in the UV range. Upon transition

from solution to film, a broad shoulder around 760 nm appears in the spectrum of PDTP-BT-c, and the absorption maximum shifts from 632 to 651 nm. The PDTP-DTTzTz-c material shows a larger optical bandgap, in accordance with the electrochemical data (*vide infra*, Table 1). The wavelength at maximum absorption for PDTP-DTTzTz-c shows only a slight red shift from 572 nm to 580 nm upon transition to film, probably because the polymer is already strongly aggregated in chloroform solution. A similar behaviour was previously observed for a 4*H*-cyclopenta[2,1-*b*:3,4-*b'*]dithiophene-*alt*-dithienylthiazolo[5,4-*d*]thiazole (PCPDT-DTTzTz) copolymer.^{20a} This is consistent with the observation that filtration over a 0.45 μm filter renders a colourless filtrate. PDTP-DTBT-b behaves similar since no substantial red shift is observed between the spectra in solution and film. Finally, PDTP-TPD-c does show a significant red shift of the absorption maxima in thin film (from 610 and 666 nm to 644 and 685 nm, respectively). The relative intensity of the absorption band at higher wavelength slightly increases as well.

The electrochemical properties of the polymers were investigated by cyclic voltammetry (CV) and HOMO and LUMO energy levels were determined from the onset of the first oxidation and reduction peaks, respectively (see Table 1). The HOMO levels of all polymers are comparable, except for PDTP-TPD-c, which has a substantially deeper HOMO. If one compares these values to the previously reported HOMO energies for analogous N-alkyl-substituted DTP copolymers 'alkyl-PDTP-BT'^{6a} and 'alkyl-PDTP-TPD'^{6c-e} (Table 1 and Fig. S2), it is clear that the HOMO's of PDTP-BT-c and PDTP-TPD-c are lowered substantially (by 0.46 and 0.30 eV, respectively) due to the introduction of the N-acyl groups.

Table 1: SEC, UV-Vis and CV data of the DTP-*alt*-acceptor copolymers and a comparison between their experimental and DFT-calculated frontier orbital energies

Polymer	Experimental				Calculated ^g				
	M_n^a (kg mol ⁻¹)	D^a	$E_{g,opt}$ (eV)	HOMO ^b (eV)	LUMO ^b (eV)	Structure	HOMO (eV)	LUMO (eV)	Torsion angle ^h
PDTP-BT-c	7.6 ^c	1.1	1.36	-5.27	-3.38	DA (DADA)	-5.82 (-5.44)	-2.53 (-2.77)	8.9
PDTP-DTTzTz-a	\ ^d	\ ^d	\ ^d	\ ^d	\ ^d	DA (DADA)	-5.58 (-5.36)	-2.26 (-2.50)	19.0, 2.0
PDTP-DTTzTz-c	28	2.4	1.81	-5.27	-3.08	DA (DADA)	-5.60 (-5.41)	-2.66 (-2.77)	37.0, 14.2
PDTP-DTBT-b	\ ^d	\ ^d	1.48	-5.21	-3.31	DA (DADA)	-5.93 (-5.63)	-2.26 (-2.64)	3.1
PDTP-TPD-c	29	2.1	1.62	-5.39	-3.31	DA (DADA)	-5.93 (-5.63)	-2.26 (-2.64)	3.1
PDTP-TPD-c-H^e	69	1.9	\	\	\	DA	-5.69	-2.04	\
Alkyl-PDTP-TPD (Lit.)	\	\	\	-5.09 ^f	-3.42 ^f	DA	-5.69	-2.04	\

^a Determined by SEC in THF at 40 °C, ^b Determined by CV, ^c Determined by SEC in chlorobenzene at 60 °C, ^d Not measured due to low solubility, ^e High molar mass fraction isolated by preparative SEC. ^f Experimental values from literature (ref. 6c-e). ^g For the calculations, the alkyl side chains were replaced by methyl groups. ^h The values correspond to the deviation with respect to planarity; the first value is the average inter-DA torsion angle of the DADA structures, whereas the second (if given) is the average intra-acceptor torsion angle

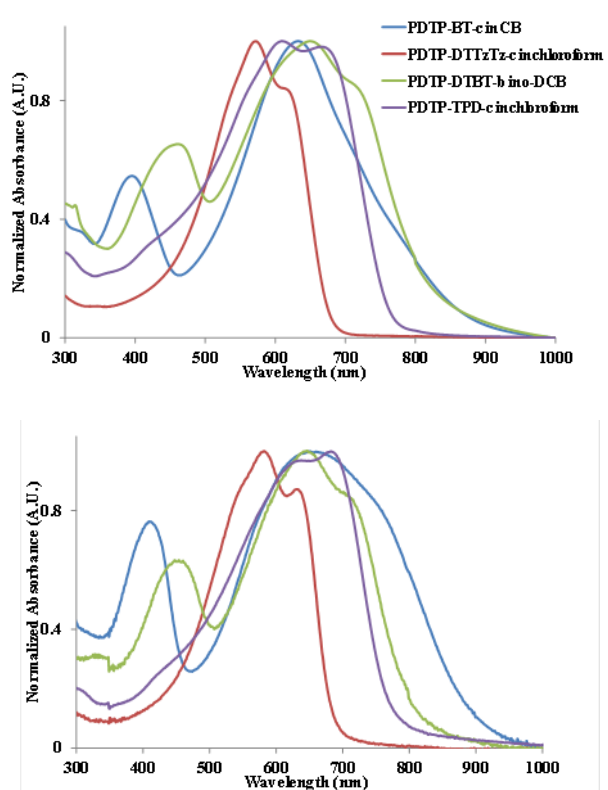


Figure 1: UV-Vis absorption spectra for all soluble DTP-based copolymers in solution (top) and thin film (bottom; same colour code)

4.2.3 DFT calculations

To analyze the interactions between the donor and acceptor moieties of the polymers and their impact on the positions of the HOMO and LUMO levels, density functional theory (DFT) calculations were performed using the M05²¹ exchange-correlation functional and the 6-311G(d) basis set. The effects of the solvent (THF) were taken into account within the integral equation formalism of the polarizable continuum model (IEF-PCM).²² All calculations were carried out using Gaussian09.²³ First, the ground state geometries were fully optimized for the individual donor and acceptor moieties as well as for the donor-acceptor

combinations (DA). Several conformations differing by the torsion angle between the donor and acceptor units have been considered and the most stable ones were selected to perform calculations on the dimers of donor-acceptor units (DADA). In the calculations, the large alkyl chains were substituted by methyl groups, which accelerates the calculations without impacting the results. Using the optimized geometries, the energies and the topologies of HOMO and LUMO were determined (Table 1). The experimental trends are confirmed by the calculations, i.e. i) **PDTP-TPD** has the lowest-energy HOMO, whereas the other N-acyl-DTP-based materials exhibit similar HOMO energies (most clear for the DADA systems), ii) **PDTP-DTTzTz** has the highest LUMO, and iii) replacing the alkyl by an acyl substituent stabilizes the HOMO by about 0.3 eV. The lowest HOMO of **PDTP-TPD** can be explained by referring to two effects: i) the larger the difference between the HOMO's of the donor and acceptor moieties, the smaller the splitting of the HOMO levels and therefore the lower the HOMO of the DA and DADA oligomers, and ii) in case of similar energy levels, larger torsion angles - between the donor and acceptor pairs or, for **PDTP-DTTzTz** and **PDTP-DTBT**, inside the acceptor - lead to smaller splitting and lower HOMO. So, the HOMO of the TPD acceptor (-7.67 eV) of **PDTP-TPD** is much lower than the HOMO of the N-acyl-DTP moiety (-6.01 eV), which gives a HOMO for the DA unit of -5.93 eV (i.e. close to the DTP donor unit). On the contrary, the splitting of the HOMO levels in **PDTP-DTTzTz** is larger since the HOMO of the DTTzTz acceptor is located at -5.87 eV (closer to the HOMO of the N-acyl-DTP moiety). Consequently, the HOMO of the DA unit goes up to -5.58 eV. Moreover, when going from the N-alkyl to the N-acyl derivatives, the stabilization of the HOMO of the oligomers results from a stabilization of the HOMO of the donor by 0.30 eV. Finally, as shown in Fig. 2, the delocalization of the HOMO over the whole

system, and therefore the size of the units and the amplitude of the torsion angles, plays also a role on the evolution of the frontier orbital levels as a function of system size, going from DA to DADA.

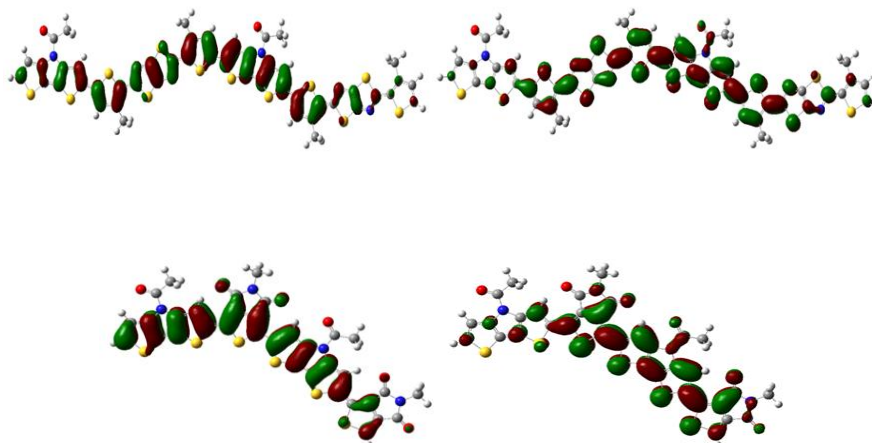


Figure 2: Sketch of the HOMO (left) and LUMO (right) of **PDTP-DTTzTz** (top) and **PDTP-TPD** (bottom) for the most stable conformer (isosurfaces of 0.02 a.u.; DADA oligomers).

4.2.4 Photovoltaic properties

To evaluate their photovoltaic properties, the N-acyl-DTP-based copolymers were blended with PC₇₁BM and applied as photoactive layers in BHJ organic solar cells with a standard configuration (glass:ITO:PEDOT-PSS:active layer:Ca:Al, Table 2 and Fig. 3). The low solubility of **PDTP-BT-c** and **PDTP-DTBT-b** impeded smooth processing and lead to poor active layer film quality and very low PCE's. For the devices with **PDTP-DTTzTz-c**:PC₇₁BM (1:3 optimized ratio) active layer blends spin-coated from chlorobenzene (CB), a Voc of 0.64 V was obtained (PCE 2.47%), which is rather high when compared to most N-alkyl-DTP based copolymers.^{5,6} This is consistent with both the experimentally and theoretically derived deepened HOMO levels due to the introduction of the N-

acyl groups. By using 1-chloronaphthalene (CN) as a processing additive, the J_{sc} and fill factor (FF) were increased by approximately 10% and a PCE of 3.29% was obtained (Fig. 3, Table 2).

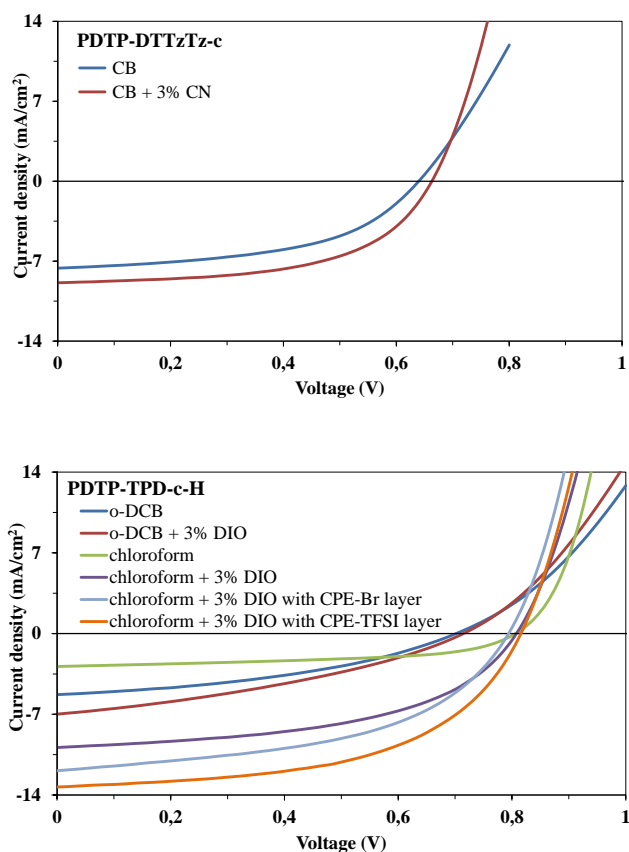


Figure 3: J - V curves of PSC's with **PDTP-DTTzTz-c**:PC₇₁BM (top) or **PDTP-TPD-c-H**:PC₇₁BM (bottom) photoactive layers processed from different solvents

The combination of TPD with various donor units has already been reported to lead to excellent solar cell performances and improved V_{oc} 's.^{6c-e,24} As the **PDTP-TPD** copolymer showed the lowest HOMO value amongst the series, this material was thought to have the most promising characteristics to afford high solar cell efficiencies. TPD was combined with N-acyl-DTP **4c** decorated with the

longest branched alkyl side chain to ensure good solubility. Furthermore, the obtained crude polymer (after Soxhlet extractions) was further purified and fractionated by preparative SEC, which was previously shown to be an effective means to enhance solar cell performance (by improving material purity and increasing M_n).²⁰ Processing **PDTP-TPD-c-H**:PC₇₁BM (1:3 optimized ratio) blends from *o*-dichlorobenzene (*o*-DCB) resulted in devices with an open-circuit voltage of 0.70 V and blends in chloroform afforded an even higher Voc of 0.80 V, the highest value reported for DTP-based copolymers to date. Addition of a processing additive (1,8-diiodooctane or DIO) again resulted in an increase in J_{sc} , which was most pronounced for chloroform as a solvent. In this case, the J_{sc} increased quite drastically (by a factor 3.5 up to 9.88 mA cm⁻²), without affecting the FF and Voc, giving rise to a PCE of 4.04% (Fig. 3, Table 2). The external quantum efficiency (EQE) was determined for the best performing devices (Fig. 4), showing the PC₇₁BM contribution at shorter wavelengths and a polymer contribution up to ~650 or 750 nm for **PDTP-DTTzTz-c** and **PDTP-TPD-c-H**, respectively, in accordance with the UV-Vis absorption spectra.

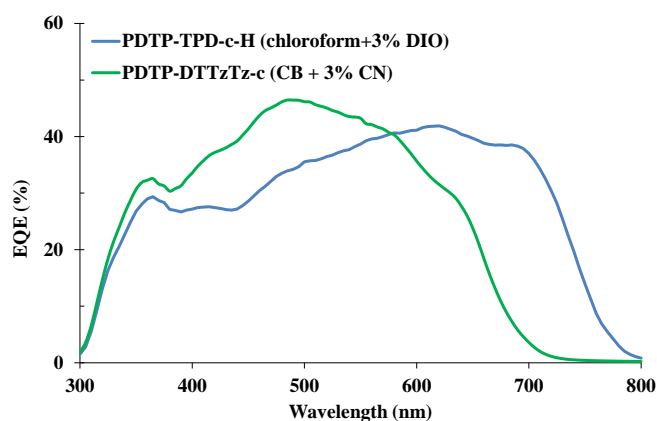


Figure 4: EQE spectra for the best performing PSC devices.

The influence of the processing additives can be related to an optimized BHJ blend morphology, as clearly evidenced by AFM imaging.^{1f,6g} The thin film topography of the active layers as investigated by PeakForce AFM showed (similar) large scale phase segregation if no processing additive was employed (Fig. 5). From these images, characteristic spherical structures can be observed, for which the calculated surface coverage was found to be $\sim 70\text{--}75\%$. Additionally, the obtained layers were subjected to conductive AFM (C-AFM) under positive and negative sample bias (Fig. S3). When applying a positive bias, the spherical shapes showed conductivity, which was absent under negative bias. The opposite holds true for the space around the spherical shapes.²⁵ This confirms the idea that these spherical structures consist mainly of PC₇₁BM, and that the polymer rather forms the surrounding matrix. A similar topography has been described for other DTP-based materials.^{6f-g} The observed large phase segregation is unfavourable for solar cell performance since it leads to a reduced interfacial area between PC₇₁BM and copolymer, necessary for efficient charge separation. It is well known that processing additives can greatly suppress the size of these phase-segregated domains.^{1f} Through the addition of a small amount of CN (for **PDTP-DTTzTz-c**) or DIO (for **PDTP-TPD-c-H**), a strong improvement in blend (nano)morphology could be obtained (Fig. 5). This phenomenon was confirmed by C-AFM images under positive and negative bias showing a uniform conductance (Fig. S3).

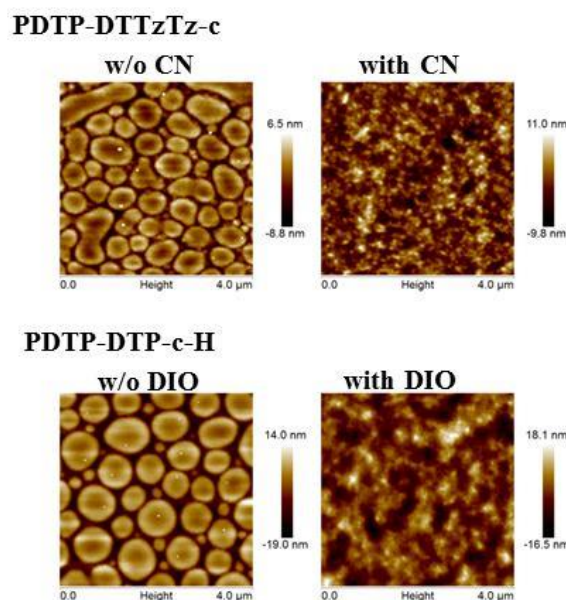


Figure 5: Topographic PeakForce tapping mode AFM images of spin-coated films of **PDTP-X** and PC₇₁BM (measurements on solar cell devices).

Finally, to enhance the PCE of the **PDTP-TPD-c-H**:PC₇₁BM PSC's even further, an additional CPE interlayer^{26,27} was spin-coated between the active layer and the Al top electrode (replacing the oxidatively labile Ca layer). In previous work, we have introduced imidazolium-substituted ionic polythiophenes as effective cathode interlayer materials pushing up the efficiencies of polymer solar cells, mainly by increasing the short-circuit current.^{11,28} The addition of a thin cathode interlayer is generally believed to induce an aligned interphase dipole, reducing resistance and affording more efficient charge extraction from the active layer to the top electrode. Two different CPE's, differing by their composition (homo- vs copolymer), side chain patterns and counter ions (Br and TFSI,²⁸ see Fig. S4), were applied on top of **PDTP-TPD-c**:PC₇₁BM active layers to investigate their influence on the I-V characteristics. As shown in Table 2 and Fig. 3 (EQE's in Fig.

S5), this resulted in a substantial increase of the J_{sc} for both cases (with smaller effects on V_{oc} and FF). The effect was most pronounced for the **CPE-TFSI** interlayer, with a noticeable increase in J_{sc} of $\sim 35\%$ (up to 13.3 mA cm^{-2}), leading to a final PCE of 5.82%.

Table 2: Photovoltaic performances of N-acyl-DTP-based BHJ polymer solar cell devices.

Material ^a	Processing solvent	V_{oc} (V)	J_{sc} (mA cm^{-2})	FF	Best PCE (%)	Average PCE ^b (%)
PDTP-DTTzTz-c :PC ₇₁ BM	CB	0.64	7.61	0.51	2.47	2.31
PDTP-DTTzTz-c :PC ₇₁ BM	CB + 3% (v/v) CN	0.66	8.89	0.56	3.29	3.09
PDTP-TPD-c-H :PC ₇₁ BM	<i>o</i> -DCB	0.70	5.30	0.39	1.46	1.17
PDTP-TPD-c-H :PC ₇₁ BM	<i>o</i> -DCB + 3% (v/v) DIO	0.72	6.99	0.35	1.74	1.65
PDTP-TPD-c-H :PC ₇₁ BM	CHCl ₃	0.80	2.85	0.52	1.20	1.15
PDTP-TPD-c-H :PC ₇₁ BM	CHCl ₃ + 3% (v/v) DIO	0.80	9.88	0.51	4.04	3.74
PDTP-TPD-c-H :PC ₇₁ BM /CPE-Br/Al	CHCl ₃ + 3% (v/v) DIO	0.82	12.35	0.50	5.40	5.01
PDTP-TPD-c-H :PC ₇₁ BM /CPE-TFSI/Al	CHCl ₃ + 3% (v/v) DIO	0.82	13.30	0.53	5.82	5.42

^a 1:3 polymer:fullerene ratio. ^b Averages over 4–8 devices

4.3 CONCLUSIONS

In summary, N-acyl-DTP's have been identified as attractive building blocks for light-harvesting low bandgap copolymers for organic photovoltaics. The open-circuit voltage of polymer solar cells derived from N-acyl-substituted DTP-*alt*-acceptor copolymers is notably higher than previously observed for the N-alkyl-DTP analogues, with **PDTP-TPD** showing the highest V_{oc} (0.80 V) among the series. Consequently, the solar cell efficiencies are significantly higher than for

the best performing N-alkyl-substituted DTP-based polymer donor material reported so far (PCE of 2.8%).^{6a,h} N-acyl-substitution of DTP is hence an effective approach to an increased Voc for polymer solar cells. Moreover, the solar cell efficiencies were further enhanced by the addition of a conjugated polyelectrolyte cathode interlayer, mainly by an increase in short-circuit current, up to a PCE of 5.82%. Further improvements are currently pursued by continued energy level tailoring, variation of the (N-acyl-DTP) side chain pattern and device optimization.²⁹

4.4 EXPERIMENTAL SECTION

4.4.1 Materials and instruments

Unless stated otherwise, all reagents and chemicals were obtained from commercial sources and used without further purification. 1,3-Dibromo-5-(2'-ethylhexyl)-4*H*-thieno[3,4-*c*]pyrrole-4,6(5*H*)-dione (TPD **8**) (Sigma-Aldrich, 97 %) was purified by preparative SEC prior to use. Preparative (recycling) SEC was performed on JAIGEL 1H and 2H columns attached to an LC system equipped with a UV detector (path 0.5 mm) and a switch for recycling and collecting the eluent (CHCl₃; flow rate 3.5 mL min⁻¹, injection volume 3.0 mL). Solvents were dried by a solvent purification system (MBraun, MB-SPS-800) equipped with alumina columns. NMR chemical shifts (δ , in ppm) were determined relative to the residual CHCl₃ (7.26 ppm) or CDHCl₂ (5.32 ppm) signals or the ¹³C resonance shift of CDCl₃ (77.16 ppm). For the N-acyl-substituted DTP's quantitative ¹³C NMR measurements were obtained with chromium(III) acetylacetonate as a relaxation agent. High resolution electrospray ionization-mass spectrometry (ESI-MS) was performed using an

LTQ Orbitrap Velos Pro mass spectrometer equipped with an atmospheric pressure ionization source operating in the nebulizer assisted electrospray mode. The instrument was calibrated in the m/z range 220–2000 using a standard solution containing caffeine, MRFA and Ultramark 1621. UV-Vis measurements were performed on a VARIAN Cary 5000 UV-Vis-NIR spectrophotometer with a scan rate of 600 nm min^{-1} . The films for the UV-Vis measurements were prepared by drop-casting the polymer solutions (**PDTP-BT-c** in chlorobenzene, **PDTP-DTBT-b** in (warm) *o*-dichlorobenzene, and **PDTP-DTTzTz-c** and **PDTP-TPD-c** in chloroform) on a quartz substrate. The solid-state UV-Vis spectra were used to estimate the optical band gaps (from the wavelength at the intersection of the tangent drawn at the low energy side of the absorption spectrum with the x-axis; $E_g \text{ (eV)} = 1240/(\text{wavelength in nm})$). FT-IR spectra of 2-hexyldecanamide and dibrominated DTP's **3a-c** were recorded as thin films on a NaCl disk with a Bruker Tensor 27 from 1000 to 4000 cm^{-1} . Analysis of the molar masses and molar mass distributions of the polymers was performed on a Tosoh EcoSEC System comprising of an autosampler, a PSS guard column SDV ($50 \times 7.5 \text{ mm}$), followed by three PSS SDV analytical linear XL columns ($5 \mu\text{m}$, $300 \times 7.5 \text{ mm}$), a differential refractive index detector (Tosoh EcoSEC RI) and a UV-detector (254 nm) using THF as the eluent at $40 \text{ }^\circ\text{C}$ with a flow rate of 1.0 mL min^{-1} . In particular cases (due to solubility issues) a Spectra Series P100 (Spectra Physics) pump equipped with two mixed-B columns ($10 \mu\text{m}$, $2 \times 30 \text{ cm}$, Polymer Laboratories) and an Agilent 1100 DAD UV detector (600 nm) was applied with chlorobenzene as an eluent at $60 \text{ }^\circ\text{C}$ and a flow rate of 1.0 mL min^{-1} . Both systems were calibrated using linear narrow polystyrene standards. Electrochemical measurements (cyclic voltammetry) were performed with an Eco Chemie Autolab PGSTAT 30 potentiostat/galvanostat using a three-electrode

microcell with a Pt working electrode, a Pt counter electrode and a Ag/AgNO₃ reference electrode (Ag wire dipped in a solution of 0.01 M AgNO₃ and 0.1 M NBu₄PF₆ in anhydrous acetonitrile). The reference electrode was calibrated against ferrocene/ferrocenium as an external standard. Samples were prepared by dip-coating the Pt working electrode in the respective polymer solutions (also used for the film preparation for solid-state UV-Vis). The CV measurements were done on the resulting films with 0.1 M NBu₄PF₆ in anhydrous acetonitrile as the electrolyte solution. To prevent air from entering the system, the experiments were conducted under a curtain of Ar. Cyclic voltammograms were recorded at a scan rate of 100 mV s⁻¹. The HOMO-LUMO frontier energy levels were determined using the onset potentials for oxidation and reduction, referenced to ferrocene/ferrocenium, which is estimated to have an oxidation potential of -4.98 eV vs. vacuum.

4.4.2 Monomer synthesis

2-Hexyldecanamide

A mixture of 2-hexyldecanoic acid (8.28 g, 32.3 mmol) and SOCl₂ (2.93 mL, 40.4 mmol) was refluxed for 30 min and subsequently added drop wise to an ice-cold ammonia solution (32% in H₂O; 25.8 mL). The resulting precipitate was filtered off, washed with H₂O and recrystallized from MeOH, yielding a white solid (6.13 g, 74 %). δ_{H} (400 MHz, CDCl₃): 5.82 (br, 1H), 5.70 (br, 1H), 2.16–2.06 (m, 1H), 1.64–1.51 (m, 2H), 1.48–1.37 (m, 2H), 1.36–1.18 (m, 20H), 0.90–0.84 (m, 6H), δ_{C} (100 MHz, CDCl₃): 179.2 (CO), 47.4, 33.2, 32.0, 31.8, 29.8, 29.6, 29.5, 29.4, 27.7, 22.7, 14.3, HRMS: Calcd. for C₁₆H₃₄NO [M+H]⁺: 256.2562, found: 256.2651, FT-IR: ν_{max} /cm⁻¹ 3370, 3181, 2952, 2920, 2851, 1655, 1465, 1423, 1319, 1284, 1147, 1134.

N-acyl-substituted DTP's **3a-c** were prepared according to literature procedures.^{10,12}

***N*-(2-Ethylhexanoyl)dithieno[3,2-*b*:2',3'-*d*]pyrrole (2a)**

Green solid (1.642 g, 44%), δ_{H} (400 MHz, CD₂Cl₂): 8.10–7.00 (br, 2H), 7.28 (d, $J = 5.3$ Hz, 2H), 3.40–3.28 (m, 1H), 1.98–1.84 (m, 2H), 1.80–1.62 (m, 2H), 1.42–1.25 (m, 4H), 0.97 (t, $J = 7.4$ Hz, 3H), 0.87 (t, $J = 7.1$ Hz, 3H), δ_{C} (100 MHz, CDCl₃): 173.0 (1C), 143.3 (1C), 140.5 (1C), 124.3 (2C), 121.4 (2C), 118.0 (1C), 115.5 (1C), 46.0 (1C), 31.1 (1C), 29.4 (1C), 24.9 (1C), 22.9 (1C), 14.0 (1C), 11.6 (1C), HRMS: Calcd. for C₁₆H₂₀NOS₂ [M+H]⁺: 306.0908, found: 306.0991.

2,6-Dibromo-*N*-(2-ethylhexanoyl)dithieno[3,2-*b*:2',3'-*d*]pyrrole (3a)

White solid (1.708 g, 71%), δ_{H} (400 MHz, CD₂Cl₂): 7.60 (br, 2H), 3.20–3.11 (m, 1H), 1.95–1.81 (m, 2H), 1.78–1.60 (m, 2H), 1.38–1.23 (m, 4H), 0.95 (t, $J = 7.4$ Hz, 3H), 0.90–0.84 (m, 3H), δ_{C} (100 MHz, CDCl₃): 172.6 (1C), 139.7 (1C), 137.5 (1C), 121.0 (3C), 118.7 (1C), 111.6 (2C), 46.0 (1C), 30.9 (1C), 29.3 (1C), 24.9 (1C), 22.9 (1C), 13.9 (1C), 11.4 (1C), HRMS: Calcd for C₁₆H₁₇Br₂NOS₂ [M]⁺: 462.9098, found: 462.9114, FT-IR: ν_{max} /cm⁻¹ 3126, 2959, 2930, 2871, 1709, 1491, 1458, 1383, 1267, 1233, 1169, 1092, 1033.

2,6-Bis(trimethylstannyl)-*N*-(2-ethylhexanoyl)dithieno[3,2-*b*:2',3'-*d*]pyrrole (4a)

A solution of dibromo-DTP **3a** (0.450 g, 0.971 mmol) in dry toluene (2 mL) was added to a mixture of hexamethylditin (1.34 g, 4.08 mmol), LiCl (0.247 g, 5.83 mmol) and Pd(PPh₃)₄ (56 mg, 0.049 mmol) in dry toluene (4 mL). The resulting mixture was purged with N₂ for 10 min and subsequently heated to 105 °C.

After 1 h the mixture was allowed to cool down to room temperature and diethyl ether and water were added. The organic layer was washed with water and dried over Na₂SO₄. Purification of the crude product by preparative SEC yielded a pale yellow oil (0.338 g, 55%). δ_{H} (300 MHz, CD₂Cl₂): 7.76 (br, 1H), 7.28 (br, 1H), 3.31 (quint, $J = 6.0$ Hz, 1H), 1.95–1.80 (m, 2H), 1.78–1.57 (m, 2H), 1.40–1.21 (m, 4H), 0.95 (t, $J = 7.4$ Hz, 3H), 0.86 (t, $J = 7.1$ Hz, 3H), 0.40 (s, 18H).

***N*-(2-Propylpentanoyl)dithieno[3,2-*b*:2',3'-*d*]pyrrole (2b)**

Viscous colorless oil (0.958 g, 27%), δ_{H} (400 MHz, CD₂Cl₂): 7.90–7.10 (br, 2H), 7.26 (d, $J = 5.3$ Hz, 2H), 3.43–3.34 (m, 1H), 1.92–1.77 (m, 2H), 1.70–1.57 (m, 2H), 1.42–1.30 (m, 4H), 0.88 (t, $J = 7.3$ Hz, 6H), δ_{C} (100 MHz, CDCl₃): 173.1 (1C), 143.4 (1C), 140.4 (1C), 124.3 (2C), 121.5 (2C), 117.9 (1C), 115.4 (1C), 44.3 (1C), 34.1 (2C), 20.4 (2C), 14.2 (2C), HRMS: Calcd. for C₁₆H₁₉NOS₂Na [M+Na]⁺: 328.0800, found: 328.0812.

2,6-Dibromo-*N*-(2-propylpentanoyl)dithieno[3,2-*b*:2',3'-*d*]pyrrole (3b)

White solid (0.993 g, 91%), δ_{H} (300 MHz, CD₂Cl₂): 7.56 (br, 2H), 3.28–3.17 (m, 1H), 1.92–1.75 (m, 2H), 1.71–1.52 (m, 2H), 1.45–1.22 (m, 4H), 0.88 (t, $J = 7.3$ Hz, 6H), δ_{C} (100 MHz, CDCl₃): 172.8 (1C), 140.0 (1C), 137.2 (1C), 121.0 (3C), 118.4 (1C), 111.6 (2C), 44.4 (1C), 34.0 (2C), 20.3 (2C), 14.2 (2C), HRMS: Calcd. for C₁₆H₁₇Br₂NOS₂ [M]⁺: 462.9098, found: 462.9116, FT-IR: $\nu_{\text{max}}/\text{cm}^{-1}$ 3126, 2958, 2930, 2871, 1709, 1491, 1463, 1384, 1357, 1257, 1219, 1169, 1092, 1035.

2,6-Bis(trimethylstannyl)-*N*-(2-propylpentanoyl)dithieno[3,2-*b*:2',3'-*d*]pyrrole (4b)

According to the procedure as outlined for **4a**: pale yellow oil (0.263 g 39%), δ_{H} (400 MHz, CD_2Cl_2): 7.81 (br, 1H), 7.27 (br, 1H), 3.46–3.38 (m, 1H), 1.92–1.80 (m, 2H), 1.67–1.58 (m, 2H), 1.46–1.33 (m, 4H), 0.91 (t, $J = 7.3$ Hz, 6H), 0.42 (s, 18H).

***N*-(2-Hexyldecanoyl)dithieno[3,2-*b*:2',3'-*d*]pyrrole (2c)**

Beige solid (3.62 g, 58%), δ_{H} (400 MHz, CD_2Cl_2): 7.95–7.15 (br, 2H), 7.28 (d, $J = 5.3$ Hz, 2H), 3.40–3.31 (m, 1H), 1.93–1.81 (m, 2H), 1.72–1.60 (m, 2H), 1.41–1.15 (m, 20H), 0.87–0.81 (m, 6H), δ_{C} (100 MHz, CDCl_3): 173.1 (1C), 143.6 (1C), 140.3 (1C), 124.3 (2C), 121.8 (1C), 121.1 (1C), 118.0 (1C), 115.4 (1C), 44.7 (1C), 31.9 (2C), 31.8 (1C), 31.6 (1C), 29.8 (1C), 29.5 (1C), 29.4 (1C), 29.2 (1C), 27.2 (2C), 22.64 (1C), 22.59 (1C), 14.12 (1C), 14.05 (1C), HRMS: Calcd. for $\text{C}_{24}\text{H}_{35}\text{NOS}_2\text{Na}$ $[\text{M}+\text{Na}]^+$: 440.2052, found: 440.2078.

2,6-Dibromo-*N*-(2-hexyldecanoyl)dithieno[3,2-*b*:2',3'-*d*]pyrrole (3c)

White solid (4.11 g, 92%), δ_{H} (400 MHz, CD_2Cl_2): 7.79 (br, 1H), 7.37 (br, 1H), 3.25–3.16 (m, 1H), 1.90–1.79 (m, 2H), 1.70–1.59 (m, 2H), 1.37–1.17 (m, 20H), 0.88–0.82 (m, 6H), δ_{C} (100 MHz, CDCl_3): 172.8 (1C), 140.1 (1C), 137.1 (1C), 121.0 (3C), 118.3 (1C), 111.6 (2C), 44.8 (1C), 31.8 (3C), 31.6 (1C), 29.7 (1C), 29.4 (1C), 29.3 (1C), 29.2 (1C), 27.1 (2C), 22.63 (1C), 22.56 (1C), 14.1 (1C), 14.0 (1C), HRMS: calcd. for $\text{C}_{24}\text{H}_{33}\text{Br}_2\text{NOS}_2\text{Na}$ $[\text{M}+\text{Na}]^+$: 589.0242, found: 589.0257, FT-IR: $\nu_{\text{max}}/\text{cm}^{-1}$ 3127, 2953, 2925, 2854, 1710, 1491, 1464, 1382, 1359, 1240, 1093, 1030.

2,6-Bis(trimethylstannyl)-N-(2-hexyldecanoyl)dithieno[3,2-b:2',3'-d]pyrrole (4c)

According to the procedure as outlined for **4a**: pale yellow oil (0.896 g, 46%), ¹H NMR (400 MHz, CD₂Cl₂): 7.82 (br, 1H), 7.24 (br, 1H), 3.43–3.32 (m, 1H), 1.93–1.78 (m, 2H), 1.72–1.58 (m, 2H), 1.42–1.17 (m, 20H), 0.88–0.82 (m, 6H), 0.42 (s, 18H).

4.4.3 Polymer synthesis**PDTP-BT-c**

A solution of DTP monomer **4c** (255.1 mg, 0.343 mmol) in dry toluene (10 mL) was added drop wise via a syringe to a mixture of 4,7-dibromo-2,1,3-benzothiadiazole (100.9 mg, 342 μmol), Pd₂dba₃ (7.9 mg, 8.6 μmol) and P(*o*-tolyl)₃ (10.5 mg, 34.3 μmol) in dry DMF (2.5 mL) under inert atmosphere. After purging with N₂ for 15 min, the mixture was heated to 105 °C for 1 h. The resulting blue-green solution was added drop wise to ice cold MeOH. The precipitate was filtered off and purified by subsequent Soxhlet extractions with acetone, hexanes, chloroform and chlorobenzene. The chlorobenzene fraction was precipitated in ice-cold MeOH to yield a black solid (28%). ¹H NMR could not be recorded due to the low product solubility. GPC (chlorobenzene, 60 °C, PS standards): $M_n = 7.6 \text{ kg mol}^{-1}$, $D = 1.1$.

PDTP-DTTzTz-a

Similar to the procedure as outlined for **PDTP-BT-c**, but with a solvent mixture DMF:toluene 1:5. After precipitation in MeOH, the polymer could not be redissolved again.

PDTP-DTTzTz-c

Similar to the procedure as outlined for **PDTP-BT-c**. Soxhlet extractions were done with acetone, hexanes and chloroform. The chloroform fraction was precipitated in ice-cold MeOH, yielding a black solid (89%). δ_{H} (400 MHz, CDCl_3) 8.0–5.6 (br, 4H), 3.28 (br, 1H), 2.2–1.0 (br, 46H), 1.0–0.5 (br, 18H), GPC (THF, 40 °C, PS standards): $M_n = 28 \text{ kg mol}^{-1}$, $D = 2.4$.

PDTP-DTBT-b

Similar to the procedure as outlined for **PDTP-BT-c**. Soxhlet extractions were done with acetone, hexanes, chloroform and chlorobenzene. The fraction remaining in the Soxhlet timble was dissolved in *o*-dichlorobenzene under reflux. The resulting solution was concentrated *in vacuo* and added drop wise to ice-cold MeOH, yielding a black solid (62%). Due to the low product solubility, no NMR or GPC could be obtained.

PDTP-TPD-c

Similar to the procedure as outlined for **PDTP-BT-c**. Soxhlet extractions were done with acetone, hexanes and chloroform. The chloroform fraction was precipitated in ice-cold MeOH, yielding a black solid (84%). δ_{H} (400 MHz, CD_2Cl_2): 9.50–8.10 (br, 1H), 8.10–6.30 (br, 1H), 4.10–2.80 (br, 3H), 2.50–0.40 (br, 44H), GPC (THF, 40 °C, PS standards): $M_n = 29 \text{ kg mol}^{-1}$, $D = 2.1$.

4.4.4 PSC processing and characterization

BHJ organic solar cells were produced using the standard glass:ITO:PEDOT-PSS:active layer:Ca:Al architecture. ITO (Kintec, 100 nm, 20 Ohm/sq) covered glass substrates were cleaned thoroughly with soap, demineralized water, acetone and isopropanol prior to a UV/O₃ treatment for 15 min. Afterwards,

PEDOT-PSS [poly(3,4-ethylenedioxythiophene)-poly(styrene-sulfonic acid)] was spin-coated at a thickness of approximately 30 nm. The rest of the processing was performed in an inert atmosphere (glove box), starting with an annealing step of 15 min at 130 °C. Consequently, the active layer, consisting of **PDTP-DTTzTz-c**:PC₇₁BM (40 mg mL⁻¹ total conc.) or **PDTP-TPD-c-H**:PC₇₁BM (20 mg mL⁻¹ total conc.), was spin-coated on top at varying thicknesses. As a final step, Ca and Al were deposited under vacuum as top electrodes with thicknesses of 30 and 80 nm, respectively. In this way, an active device area of 3 mm² was obtained. For the devices containing the CPE materials (see structures in Fig. S4), the cathode interlayers were spin-coated on top of the active layer (from a 0.025 w/v% solution in MeOH) before deposition of the Al top electrode.^{11,27b} I-V characteristics were measured using a Newport class A solar simulator (model 91195A) calibrated with a silicon solar cell to give an AM 1.5g solar spectrum. For AFM imaging, a Bruker Multimode 8 AFM was used. C-AFM images were made using Pt/Ir coated probes with a force constant of ~0.4 N m⁻¹ at bias voltages of +5 or -5 V with a maximum deflection setpoint of 0.6 V. EQE measurements were performed with a Newport Apex illuminator (100 W Xenon lamp, 6257) as the light source, a Newport Cornerstone 130° monochromator, and a Stanford SR830 lock-in amplifier for the current measurements. A silicon FDS100-CAL photodiode was employed as a reference cell.

4.5 REFERENCES

1 Reviews on polymer-based OPV's: (a) M. Jørgensen, K. Norrman, S. A. Gevorgyan, T. Tromholt, B. Andreasen and F. C. Krebs, *Adv. Mater.*, 2012, **24**, 580; (b) H. Zhou, L. Yang and W. You, *Macromolecules*, 2012, **45**, 607; (c) Y. Li, *Acc. Chem. Res.*, 2012, **45**, 723; (d) Y. Su, S. Lan and K. Wei, *Mater. Today*, 2012, **15**, 554; (e) R. A. J. Janssen and J. Nelson, *Adv. Mater.*, 2013, **25**, 1847; (f) H.-C. Liao, C.-C. Ho, C.-Y. Chang, M.-H. Jao, S. B. Darling and W.-F. Su, *Mater. Today*, 2013, **16**, 326; (g) S. Lizin, S. Van Passel, E. De Schepper, W. Maes, L. Lutsen, J. Manca and D. Vanderzande, *Energy Environ. Sci.*, 2013, **6**, 3136.

2 (a) Z. He, C. Zhong, S. Su, M. Xu, H. Wu and Y. Cao, *Nat. Photonics*, 2012, **6**, 591; (b) C. Cabanetos, A. El Labban, J. A. Bartelt, J. D. Douglas, W. M. Mateker, J. M. Fréchet, M. D. McGehee and P. M. Beaujuge, *J. Am. Chem. Soc.*, 2013, **135**, 4556; (c) M. Zhang, X. Guo, S. Zhang and J. Hou, *Adv. Mater.*, 2014, **26**, 1118.

3 (a) Z. Li, J. Lu, S.-C. Tse, J. Zhou, X. Du, Y. Tao and J. J. Ding, *J. Mater. Chem.*, 2011, **21**, 3226; (b) Y. Zhang, S.-C. Chien, K.-S. Chen, H.-L. Yip, Y. Sun, J. A. Davies, F.-C. Chen and A. K.-Y. Jen, *Chem. Commun.*, 2011, **47**, 11026; (c) S. Albrecht, S. Janietz, W. Schindler, J. Frisch, J. Kurpiers, J. Kniepert, S. Inal, P. Pingel, K. Fostiropoulos, N. Koch and D. J. Neher, *J. Am. Chem. Soc.*, 2012, **134**, 14932; (d) H. Chang, C. Tsai, Y. Lai, D. Chiou, S. Hsu, C. Hsu and Y. Cheng, *Macromolecules*, 2012, **45**, 9282; (e) T. Umeyama, Y. Watanabe, E. Douvogianni and H. J. Imahori, *J. Phys. Chem. C*, 2013, **117**, 21148; (f) H. Bronstein, J. M. Frost, A. Hadipour, Y. Kim, C. B. Nielsen, R. S.

Ashraf, B. P. Rand, S. Watkins and I. McCulloch, *Chem. Mater.*, 2013, **25**, 277; (g) A. C. Stuart, J. R. Tumbleston, H. Zhou, W. Li, S. Liu, H. Ade and Y. Wei, *J. Am. Chem. Soc.*, 2013, **135**, 1806; (h) L. Xiao, B. Liu, X. Chen, Y. Li, W. Tang and Y. Zou, *RSC Adv.*, 2013, **3**, 11869; (i) W. Zhuang, H. Zhen, R. Kroon, Z. Tang, S. Hellström, L. Hou, E. Wang, D. Gedefaw, O. Inganäs, F. Zhang and M. R. Andersson, *J. Mater. Chem. A*, 2013, **1**, 13422.

4 (a) H. Chen, J. Hou, S. Zhang, Y. Liang, G. Yang, Y. Yang, L. Yu, Y. Wu and G. Li, *Nat. Photonics*, 2009, **3**, 649; (b) Y. Huang, L. Huo, S. Zhang, X. Guo, C. C. Han, Y. Li and J. Hou, *Chem. Commun.*, 2011, **47**, 8904; (c) L. Huo, Z. Li, X. Guo, Y. Wu, M. Zhang, L. Ye, S. Zhang and J. Hou, *Polym. Chem.*, 2013, **4**, 3047; (d) B.-G. Kim, X. Ma, C. Chen, Y. Ie, E. W. Coir, H. Hashemi, Y. Aso, P. F. Green, J. Kieffer and J. Kim, *Adv. Funct. Mater.*, 2013, **23**, 439.

5 Review on DTP-based materials: S. C. Rasmussen and S. J. Evenson, *Prog. Polym. Sci.*, 2013, **38**, 1773.

6 DTP-based copolymers for PSC's: (a) W. Yue, Y. Zhao, S. Shao, H. Tian, Z. Xie, Y. Geng and F. Wang, *J. Mater. Chem.*, 2009, **19**, 2199; (b) E. Zhou, Q. Wei, S. Yamakawa, Y. Zhang, K. Tajima, C. Yang and K. Hashimoto, *Macromolecules*, 2010, **43**, 821; (c) M. Shi, L. Fu, X. Hu, L. Zuo, D. Deng, J. Chen and H. Chen, *Polym. Bull.*, 2011, **68**, 1867; (d) E. Zhou, J. Cong, L. Tajima, C. Yang and K. Hashimoto, *Macromol. Chem. Phys.*, 2011, **212**, 305; (e) X. Hu, M. Shi, L. Zuo, Y. Nan, Y. Liu, L. Fu and H. Chen, *Polymer*, 2011, **52**, 2559; (f) X. Zhang, J. W. Shim, S. P. Tiwari, Q. Zhang, J. E. Norton, P.-T. Wu, S. Barlow, S. A. Jenekhe, B. Kippelen, J.-L. Brédas and S. R. Marder, *J. Mater. Chem.*, 2011, **21**, 4971; (g) E. Zhou, J. Cong, K. Tajima, C. Yang, K. Hashimoto,

J. Phys. Chem. B, 2012, **116**, 2608; (h) B. Burkhart, P. P. Khlyabich and B. C. Thompson, *J. Photon. Energy* 2012, **2**, 021002.

7 J. Liu, R. Zhang, G. Sauvé, T. Kowalewski and R. D. McCullough, *J. Am. Chem. Soc.*, 2008, **130**, 13167.

8 (a) L. E. Polander, A. Yella, J. Teuscher, R. Humphry-Baker, B. F. E. Curchod, N. A. Astani, P. Gao, J.-E. Moser, I. Tavernelli, U. Rothlisberger, M. Grätzel, Md. K. Nazeeruddin and J. Frey, *Chem. Mater.*, 2013, **25**, 2642; (b) N. Cai, J. Zhang, M. Xu, M. Zhang and P. Wang, *Adv. Funct. Mater.*, 2013, **23**, 3539.

9 M. Weideler, C. D. Wessendorf, J. Hanisch, E. Ahlswede, G. Götz, M. Lindén, G. Schulz, E. Mena-Osteritz, A. Mishra and P. Bäuerle, *Chem. Commun.*, 2013, **48**, 10865.

10 S. J. Evenson and S. C. Rasmussen, *Org. Lett.*, 2010, **12**, 4054.

11 J. Kesters, T. Ghoo, H. Penxten, J. Drijkoningen, T. Vangerven, D. M. Lyons, B. Verreet, T. Aernouts, L. Lutsen, D. Vanderzande, J. Manca and W. Maes, *Adv. Energy Mater.*, 2013, **3**, 1180.

12 S. J. Evenson, T. M. Pappenfus, M. C. R. Delgado, K. R. Radke-Wohlers, J. T. L. Navarrete and S. C. Rasmussen, *Phys. Chem. Chem. Phys.*, 2012, **14**, 6101.

13 R. Martin, C. H. Larsen, A. Cuenca and S. L. Buchwald, *Org. Lett.*, 2007, **9**, 3379.

14 E. Khor, S. C. Nd, H. C. Li and S. Chai, *Heterocycles*, 1991, **32**, 1805.

- 15 D. Kaufmann, M. Bialer, J. A. Shimshoni, M. Devor and B. Yagen, *J. Med. Chem.*, 2009, **52**, 7236.
- 16 G. H. Werstuck, A. J. Kim, T. Brenstrum, S. A. Ohnmacht, E. Panna and A. Capretta, *Bioorg. Med. Chem. Lett.*, 2004, **14**, 5465.
- 17 K. Pilgram, M. Zupan and R. Sikes, *J. Heterocyclic Chem.*, 1970, **7**, 629.
- 18 I. Osaka, G. Sauvé, R. Zhang, T. Kowalewski and R. D. McCullough, *Adv. Mater.*, 2007, **19**, 4160.
- 19 H. Zhou, L. Yang, A. C. Stuart, S. C. Price, S. Liu and W. You, *Angew. Chem., Int. Ed.*, 2011, **50**, 2995.
- 20 (a) S. Van Mierloo, A. Hadipour, M. Spijkman, N. Van den Brande, B. Ruttens, J. Kesters, J. D'Haen, G. Van Assche, D. M. De Leeuw, T. Aernouts, J. Manca, L. Lutsen, D. J. Vanderzande and W. Maes, *Chem. Mater.*, 2012, **24**, 587; (b) T.-Y. Chu, J. Lu, S. Beaupré, Y. Zhang, J.-R. Pouliot, J. Zhou, A. Najari, M. Leclerc and Y. Tao, *Adv. Funct. Mater.*, 2012, **22**, 2345; (c) R. S. Ashraf, B. C. Schroeder, H. A. Bronstein, Z. Huang, S. Thomas, R. J. Kline, C. J. Brabec, P. Rannou, T. D. Anthopoulos, J. R. Durrant and I. McCulloch, *Adv. Mater.*, 2013, **25**, 2029.
- 21 Y. Zhao, N. E. Schultz and D. G. Truhlar, *J. Chem. Phys.*, 2005, **123**, 161103.
- 22 J. Tomasi and M. Persico, *Chem. Rev.*, 1994, **94**, 2027; (b) J. Tomasi, B. Mennucci and R. Cammi, *Chem. Rev.*, 2005, **105**, 299.

23 M. J. Frisch, G. W. Trucks, H. B. Schlegel, G. E. Scuseria, M. A. Robb, J. R. Cheeseman, G. Scalmani, V. Barone, B. Mennucci, G. A. Petersson, H. Nakatsuji, M. Caricato, X. Li, H. P. Hratchian, A. F. Izmaylov, J. Bloino, G. Zheng, J. L. Sonnenberg, M. Hada, M. Ehara, K. Toyota, R. Fukuda, J. Hasegawa, M. Ishida, T. Nakajima, Y. Honda, O. Kitao, H. Nakai, T. Vreven, J. A. Montgomery Jr., J. E. Peralta Jr., F. Ogliaro, M. Bearpark, J. J. Heyd, E. Brothers, K. N. Kudin, V. N. Staroverov, R. Kobayashi, J. Normand, K. Raghavachari, A. Rendell, J. C. Burant, S. S. Iyengar, J. Tomasi, M. Cossi, N. Rega, J. M. Millam, M. Klene, J. E. Knox, J. B. Cross, V. Bakken, C. Adamo, J. Jaramillo, R. Gomperts, R. E. Stratmann, O. Yazyev, A. J. Austin, R. Cammi, C. Pomelli, J. W. Ochterski, R. L. Martin, K. Morokuma, V. G. Zakrzewski, G. A. Voth, P. Salvador, J. J. Dannenberg, S. Dapprich, A. D. Daniels, Ö. Farkas, J. B. Foresman, J. V. Ortiz, J. Cioslowski and D. J. Fox, Gaussian 09, Revision A.1, Gaussian, Inc., Wallingford CT, 2009.

24 (a) Y. Zou, A. Najari, P. Berrouard and S. Beaupré, *J. Am. Chem. Soc.*, 2010, **132**, 5330; (b) Y. Zhang, S. K. Hau, H.-L. Yip, Y. Sun, O. Acton and A. K.-Y. Jen, *Chem. Mater.*, 2010, **22**, 2696; (c) C. Piliego, T. W. Holcombe, J. D. Douglas, C. H. Woo, P. M. Beaujuge and J. M. Fréchet, *J. Am. Chem. Soc.*, 2010, **132**, 7595; (d) M.-C. Yuan, M.-Y. Chiu, S.-P. Liu, C.-M. Chen and K.-H. Wei, *Macromolecules*, 2010, **43**, 6936; (e) Y.-R. Hong, H.-K. Wong, L. C. H. Moh, H.-S. Tan and Z.-K. Chen, *Chem. Commun.*, 2011, **47**, 4920; (f) J. Jo, A. Pron, P. Berrouard, W. L. Leong, J. D. Yuen, J. S. Moon, M. Leclerc and A. J. Heeger, *Adv. Energy Mater.*, 2012, **2**, 1397; (g) Y.-L. Chen, C.-Y. Chang, Y.-J. Cheng and C.-S. Hsu, *Chem. Mater.*, 2012, **24**, 3964; (h) J. Yuan, Z. Zhai, H. Dong, J. Li, Z. Jiang, Y. Li and W. Ma, *Adv. Funct. Mater.*, 2013, **23**, 885; (i) S. Shi, P.

Jiang, S. Yu, L. Wang, X. Wang, M. Wang, H. Wang, Y. Li and X. Li, *J. Mater. Chem. A.*, 2013, **1**, 1540; (j) H. Zhong, Z. Li, F. Deledalle, E. C. Fregoso, M. Shahid, Z. Fei, C. B. Nielsen, N. Yaacobi-Gross, S. Rossbauer, T. D. Anthopoulos, J. R. Durrant and M. Heeney, *J. Am. Chem. Soc.*, 2013, **135**, 2040.

25 O. Douhéret, L. Lutsen, A. Swinnen, M. Bresselge, K. Vandewal, L. Goris and J. Manca, *Appl. Phys. Lett.*, 2006, **89**, 032107.

26 Reviews on CPE's for optoelectronic applications: (a) F. Huang, H. Wu and Y. Cao, *Chem. Soc. Rev.*, 2010, **39**, 2500; (b) A. Duarte, K.-Y. Pu, B. Liu and G. C. Bazan, *Chem. Mater.*, 2011, **23**, 501; (c) H.-L. Yip and A. K.-J. Jen, *Energy Environ. Sci.*, 2012, **5**, 5994; (d) C. Duan, K. Zhang, C. Zhong, F. Huang and Y. Cao, *Chem. Soc. Rev.*, 2013, **42**, 9071.

27 (a) J. Fang, B. H. Wallikewitz, F. Gao, G. Tu, C. Müller, G. Pace, R. H. Friend and W. T. S. Huck, *J. Am. Chem. Soc.*, 2011, **133**, 683; (b) J. H. Seo, A. Gutacker, Y. Sun, H. Wu, F. Huang, Y. Cao, U. Scherf, A. J. Heeger and G. C. Bazan, *J. Am. Chem. Soc.*, 2011, **133**, 8416; (c) T. Yang, M. Wang, C. Duan, X. Hu, L. Huang, J. Peng, F. Huang and X. Gong, *Energy Environ. Sci.*, 2012, **5**, 8208; (d) Y. Chen, Z. Jiang, M. Gao, S. E. Watkins, P. Lu, H. Wang and X. Chen, *Appl. Phys. Lett.*, 2012, **100**, 203304; (e) C. Duan, W. Cai, B. B. Y. Hsu, C. Zhong, K. Zhang, C. Liu, Z. Hu, F. Huang, G. C. Bazan, A. J. Heeger and Y. Cao, *Energy Environ. Sci.*, 2013, **6**, 3022.

28 (a) T. Ghooos, J. Brassinne, C.-A. Fustin, J.-F. Gohy, M. Defour, N. Van den Brande, B. Van Mele, L. Lutsen, D. J. Vanderzande and W. Maes, *Polymer*,

2013, **54**, 6293; (b) T. Ghooos, O. Malinkiewicz, B. Conings, J. Manca, L. Lutsen, D. Vanderzande, H. J. Bolink and W. Maes, *RSC Adv.*, 2013, **3**, 25197.

29 During final redaction of this manuscript, Chen *et al.* reported on N-acyl-DTP-based PSC's with efficiencies up to 3.95% (employing a diamine-modified fullerene cathode interlayer material): D. Hong, M. Lv, M. Lei, Y. Chen, P. Lu, Y. Wang, J. Zhu, H. Wang, M. Gao, S. E. Watkins and X. Chen, *ACS Appl. Mater. Interfaces*, 2013, **5**, 10995.

4.6 ACKNOWLEDGEMENTS

The authors gratefully acknowledge financial support from Hasselt University and the IWT (Flemish government agency for Innovation by Science and Technology). The authors further thank BELSPO for funding the IAP 7/05 network. The reported activity is partly supported by the project ORGANEXT (EMR. INT4-1.2.-2009-04/054), selected in the frame of the operational program INTERREG IV-A Euregio Maas-Rijn. The FWO (Research Foundation Flanders) and SIM (Strategisch Initiatief Materialen vzw) are acknowledged for the M.ERA-NET project "RADESOL" (GA.013.13N) and the program "Solution based Processing of Photovoltaic Modules" (SoPPoM, GA n°2010-01, including the projects OPvTECH and absCIGS), respectively. V.L. thanks the F.R.S.-FNRS for his Research Associate position. The calculations were performed on the computing facilities of the Consortium des Équipements de Calcul Intensif (CÉCI), in particular those of the Plateforme Technologique de Calcul Intensif (PTCI) installed in the University of Namur, for which the authors acknowledge financial support of the FNRS-FRFC (Conventions No. 2.4.617.07.F and 2.5020.11) and the University of Namur. We also acknowledge Hercules for providing the funding for the LTQ Orbitrap Velos Pro mass spectrometer.

4.7 SUPPORTING INFORMATION

4.7.1 Analytical size exclusion chromatograms

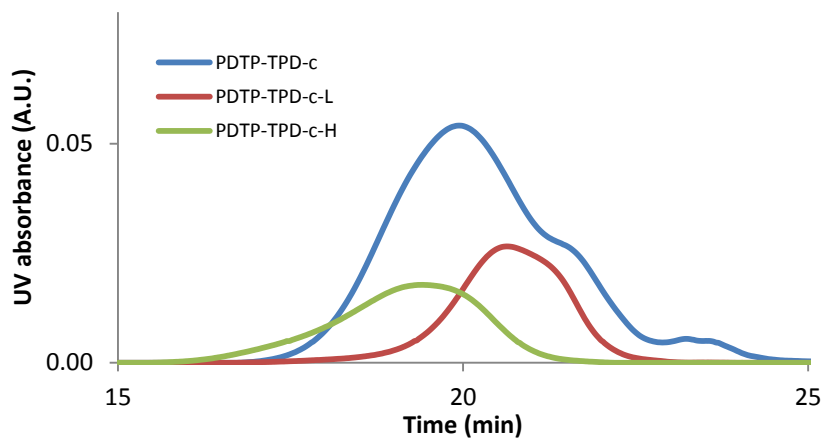


Figure S1: Analytical size exclusion chromatograms (THF, 40 °C, UV detection at 254 nm) of the crude **PDTP-TPD-c** polymer (after Soxhlet extractions) and the low (**PDTP-TPD-c-L**) and high (**PDTP-TPD-c-H**) molar mass fractions obtained after fractionation by preparative SEC.

4.7.2 Visualization of the HOMO-LUMO energy levels for different DTP-based polymers

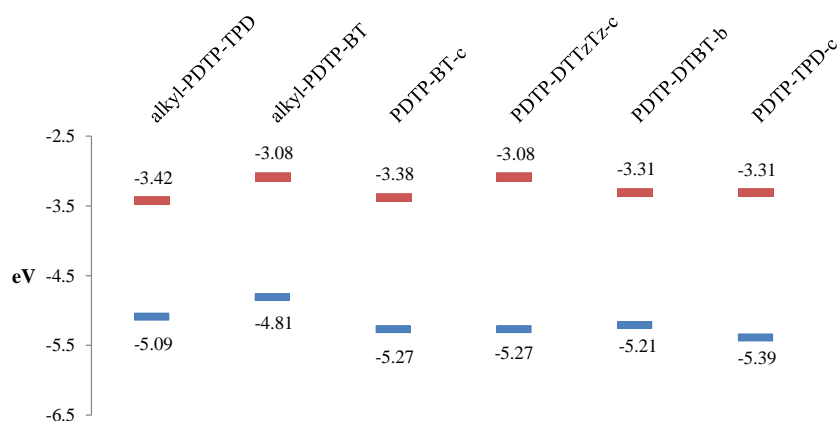


Figure S2: Visualization of the HOMO (blue) and LUMO (red) energy levels for the N-acyl-DTP copolymers (as determined by CV) and previously reported N-alkyl-substituted PDTP-acceptor analogues.^{1,2}

¹ **Alkyl-PDTP-BT**: W. Yue, Y. Zhao, S. Shao, H. Tian, Z. Xie, Y. Geng and F. Wang, *J. Mater. Chem.*, **2009**, *19*, 2199.

² **Alkyl-PDTP-TPD**: a) M. Shi, L. Fu, X. Hu, L. Zuo, D. Deng, J. Chen and H. Chen, *Polym. Bull.*, 2011, **68**, 1867; (b) E. Zhou, J. Cong, L. Tajima, C. Yang and K. Hashimoto, *Macromol. Chem. Phys.*, **2011**, *212*, 305; (c) X. Hu, M. Shi, L. Zuo, Y. Nan, Y. Liu, L. Fu and H. Chen, *Polymer*, **2011**, *52*, 2559.

4.7.3 PeakForce AFM images

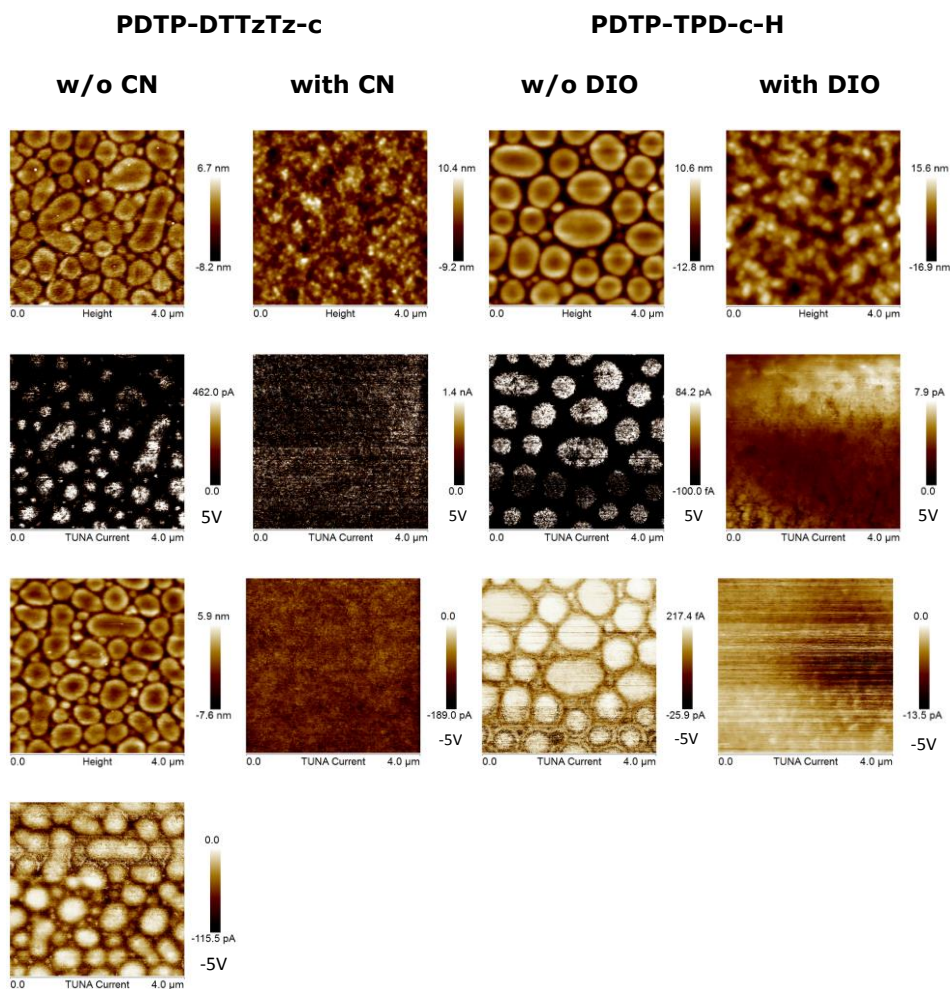


Figure S3: Topographic and corresponding conductive AFM (under negative or positive sample bias of 5 V) images of spin-coated films of **PDTP-X** and PC₇₁BM (measurements done on solar cell devices).

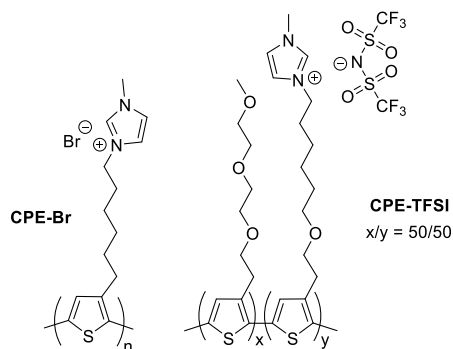
4.7.4 CPE interlayer materials

Figure S4: Structures of the CPE's applied as interlayer materials: imidazolium-functionalized (co)polythiophenes with a bromine or bis(trifluoromethylsulfonyl)-imide (TFSI) counter ion.³

³ (a) T. Ghoos, J. Brassinne, C.-A. Fustin, J.-F. Gohy, M. Defour, N. Van den Brande, B. Van Mele, L. Lutsen, D. J. Vanderzande and W. Maes, *Polymer*, **2013**, *54*, 6293; (b) T. Ghoos, O. Malinkiewicz, B. Conings, J. Manca, L. Lutsen, D. Vanderzande, H. J. Bolink and W. Maes, *RSC Adv.*, **2013**, *3*, 25197; (c) T. Ghoos, N. Van den Brande, M. Defour, J. Brassinne, C.-A. Fustin, J.-F. Gohy, S. Hoeppeener, U. S. Schubert, W. Vanormelingen, L. Lutsen, D. J. Vanderzande, B. Van Mele and W. Maes, *Eur. Polym. J.*, **2014**, *53*, 206.

4.7.5 EQE spectra for PDTP-TPD-c-H with and without cathode interlayers

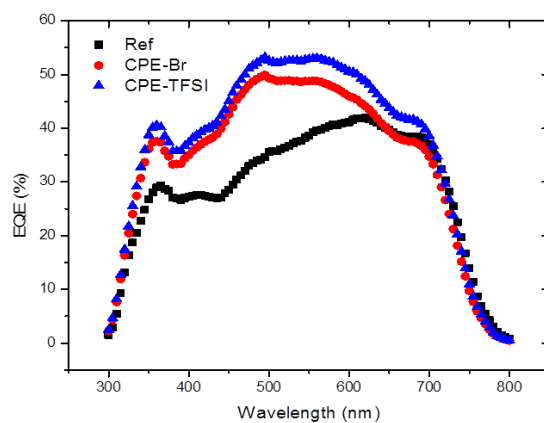
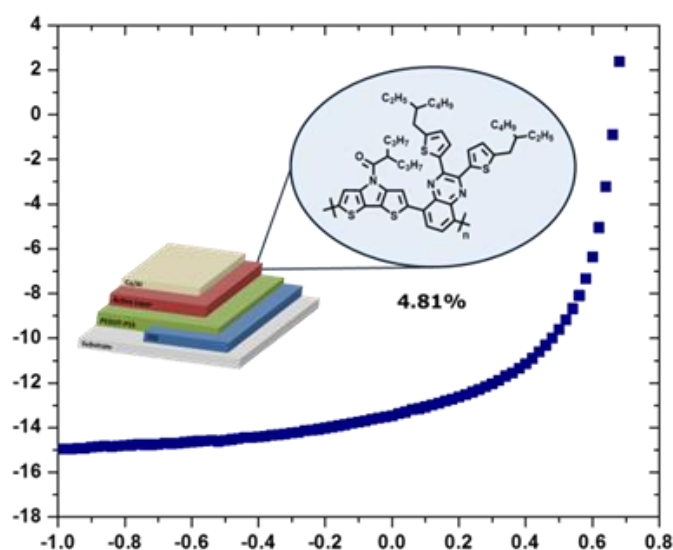


Figure S5: EQE spectra for **PDTP-TPD-c-H** with and without CPE interlayers.

Chapter 5

N-Acyl-Dithieno[3,2-d:2',3'-d]pyrrole- Based Low Bandgap Copolymers Affording Improved Open-Circuit Voltages and Efficiencies in Polymer Solar Cells



J. Kesters, P. Verstappen, W. Vanormelingen, J. Drijkoningen, T. Vangerven, D. Devisscher, L. Marin, B. Champagne, J. Manca, L. Lutsen, D. Vanderzande, W. Maes, *Sol. Energy Mater. Sol. Cells*, **2015**, DOI: 10.1016/j.solmat.2014.12.037.

ABSTRACT

Three distinct low bandgap copolymers are synthesized by the combination of *N*-(2'-propylpentanoyl)dithieno[3,2-*b*:2',3'-*d*]pyrrole (DTP) and (fluorinated) 2,3-bis[5'-(2''-ethylhexyl)thiophen-2'-yl]quinoxaline (Qx) and these PDTPQx derivatives are investigated as electron donor materials in bulk heterojunction polymer solar cells. Due to the DTP *N*-acylation and the introduction of the Qx units, both the open-circuit voltage (V_{oc}) and the short-circuit current density (J_{sc}) increase compared to previous devices based on DTP-type donor polymers. Organic solar cells with an average V_{oc} of 0.67 V, a J_{sc} of 12.57 mA/cm² and a fill factor of 0.54 are obtained, affording a power conversion efficiency of 4.53% (4.81% for the top-performing device), a record value for (*N*-acyl-)DTP-based polymer solar cells devoid of special interlayer materials. Despite further enhancement of the V_{oc} , the solar cell efficiency declines for the fluorinated PDTPQx copolymers because of the inability to achieve a finely intermixed bulk heterojunction blend nanomorphology.

5.1 INTRODUCTION

Organic photovoltaics (OPV) have emerged as a promising alternative thin-film PV technology^[1-9]. In contrast to traditional Si-based devices, organic solar cells are light-weight and can be produced on flexible substrates, in different colors and with various degrees of transparency, and they also show improved diffuse-light performance. Moreover, the possibility to process the organic active layer materials in thin films from solution opens a way to facile and low-cost large-area production by techniques such as roll-to-roll printing^[10]. In recent years, extensive efforts on material synthesis and device engineering have resulted in strong improvements in the power conversion efficiencies (PCE's) of organic solar cells, currently approaching 10% for both small molecule and polymer single junction devices^[11-21]. State of the art bulk heterojunction (BHJ) polymer solar cells contain an active layer consisting of a nanoscale bicontinuous interpenetrating network of a 'push-pull'-type low bandgap electron donor polymer and a (methano)fullerene electron acceptor (usually [6,6]-phenyl-C₇₁-butyric acid methyl ester or PC₇₁BM)^[8]. A large variety of heterocyclic building blocks has already been combined in the light-harvesting donor-acceptor low bandgap copolymers, with the general goal of improving the overall PCE of the resulting polymer solar cells. As the number of material combinations is not unlimited, a lot of effort is recently also devoted to the fine-tuning of the properties of existing materials by tedious side chain optimization and the introduction of specific functional groups^[22-26]. A popular approach is the incorporation of electron withdrawing substituents on the conjugated polymer backbone. As such, fluorination of the acceptor building block was shown to lower both the highest occupied molecular orbital (HOMO) and lowest

unoccupied molecular orbital (LUMO) levels of the final materials. As the open-circuit voltage (V_{oc}) of an organic solar cell is proportional to the energy gap between the HOMO level of the electron donor and the LUMO of the electron accepting material, this can lead to enhanced photovoltaic performance, warranted the other photovoltaic parameters – short-circuit current density (J_{sc}) and fill factor (FF) – remain (at least) the same^[27-31].

Dithieno[3,2-*b*:2',3'-*d*]pyrrole (DTP) is an attractive heterocyclic building block because of its planar electron rich fused structure^[32-35]. Copolymers combining DTP and thiophene derivatives have shown excellent charge carrier mobilities (0.21 cm²/Vs) in organic field-effect transistors^[36-39]. In past efforts, when combined with electron poor moieties, no excelling OPV results were obtained though, mainly because of the intrinsically high HOMO levels imposed by the electron rich DTP unit, affording low V_{oc} 's^[40-52]. Only very recently, a more competitive OPV performance was achieved in the Janssen group, with a PCE up to 4.8% (5.3% through application of a retro-reflective foil)^[53]. Similarly, efficiencies up to 4.8% were obtained for (solution-processed) DTP-based small molecule organic solar cells^[40,54-57].

It has recently been shown that the HOMO levels of DTP derivatives can effectively be decreased by changing the solubilizing N-alkyl substituent to an N-acyl analogue^[58] (a strategy also beneficially applied to thieno[3,4-*c*]pyrrole-4,6-diones or TPDs^[59]). This concept has successfully been translated to organic semiconducting materials, affording N-acyl-DTP-based low bandgap copolymers affording enhanced V_{oc} 's and efficiencies in BHJ OPV devices^[60,61]. In previous work, we have combined various N-acyl-DTP precursors (decorated with different alkyl side chains) with diverse acceptor-type monomers. The best

materials in terms of solar cell efficiency were obtained using thiazolo[5,4-*d*]thiazole (TzTz) or TPD electron deficient units, affording PCE's up to 4.0% in standard BHJ polymer solar cells^[61]. The gain in efficiency could mainly be attributed to an increased *V*_{oc} by N-acylation of the DTP component. In the search for related materials with even better performance, we now report on the combination of N-acylated DTP with (fluorinated) quinoxalines (Qx). Quinoxalines have emerged as a promising class of electron poor moieties for low bandgap copolymers because of their high electron affinity, resulting in deep HOMO energy levels and strong intramolecular charge transfer, broadening the absorption window. Donor-acceptor copolymers combining Qx and thiophene building blocks afforded polymer solar cells with *V*_{oc}'s up to 0.9 V^[62-64]. Moreover, quinoxalines allow for the introduction of two alkyl side chains per monomer unit, providing well-soluble polymer materials. Additionally, the monomer permits the incorporation of up to 2 fluorine atoms. Chou et al. achieved impressive PCE's up to 8.0% upon combining a fluorinated Qx and benzo[1,2-*b*:4,5-*b'*]dithiophene (BDT)^[28]. In the Andersson group, polymer solar cells with *V*_{oc}'s up to 1.01 V were obtained upon Qx difluorination^[65]. On the other hand, it has recently been shown that the absorption spectrum of Qx-based materials can be extended when exchanging the 2,3-phenyl substituents by alkylated thiophenes^[62,66,67]. In this work, we have combined several of the above-mentioned design strategies – DTP N-acylation and Qx fluorination (to enhance the *V*_{oc}), and thienyl substitution of the Qx building block (to enhance the *J*_{sc}) – toward improved efficiencies in PDTPQx-based polymer solar cells.

5.2 EXPERIMENTAL SECTION

5.2.1 Materials and methods

Unless stated otherwise, all reagents and chemicals were obtained from commercial sources and used without further purification. Solvents were dried by a solvent purification system (MBraun, MB-SPS-800) equipped with alumina columns. Precursors 1,2-bis[5'-(2''-ethylhexyl)thiophen-2'-yl]ethane-1,2-dione (**9**)^[66,67], 3,6-dibromo-1,2-phenylenediamine (**8a**)^[66,67], 3,6-dibromo-4-fluoro-1,2-phenylenediamine (**8b**)^[68], 3,6-dibromo-4,5-difluoro-1,2-phenylenediamine (**8c**)^[68], and 2,6-bis(trimethylstannyl)-*N*-(2'-propylpentanoyl)dithieno[3,2-*b*:2',3'-*d*]pyrrole (**5**)^[58,61] were prepared according to literature procedures. Other synthetic procedures can be found in the supplementary materials.

Preparative (recycling) size exclusion chromatography (SEC) was performed on a JAI LC-9110 NEXT system equipped with JAIGEL 1*H*, 2*H* and 3*H* columns (eluent CHCl₃, flow rate 3.5 mL/min). NMR chemical shifts (δ , in ppm) were determined relative to the residual CHCl₃ (7.26 ppm) signal or the ¹³C resonance shift of CDCl₃ (77.16 ppm). High resolution electrospray ionization-mass spectrometry (ESI-MS) was performed using an LTQ Orbitrap Velos Pro mass spectrometer equipped with an atmospheric pressure ionization source operating in the nebulizer assisted electrospray mode. The instrument was calibrated in the *m/z* range 220–2000 using a standard solution containing caffeine, MRFA and Ultramark 1621. Reported masses are the 100% intensity isotope peaks. UV-Vis measurements were performed on a VARIAN Cary 5000 UV-Vis-NIR spectrophotometer with a scan rate of 600 nm/min. The films for the UV-Vis measurements were prepared by drop casting the polymer solutions (in

chloroform) on a glass substrate. The solid-state UV-Vis spectra were used to estimate the optical band gaps (from the wavelength at the intersection of the tangent drawn at the low energy side of the absorption spectrum with the x-axis; E_g (eV) = 1240/(wavelength in nm). Analysis of the molar masses and molar mass distributions of the polymers was performed on a Tosoh EcoSEC System, comprising of an autosampler, a PSS guard column SDV (50 x 7.5 mm), followed by three PSS SDV analytical linear XL columns (5 μ m, 300 x 7.5 mm) and a UV detector (254 nm) using THF as the eluent at 40 °C with a flow rate of 1.0 mL min⁻¹. The SEC system was calibrated using linear narrow polystyrene standards ranging from 474 to 7.5 x 10⁶ g/mol (K = 14.1 x 10⁻⁵ dL/g and α = 0.70). Rapid heat-cool calorimetry (RHC) experiments were performed on a prototype RHC of TA Instruments, equipped with liquid nitrogen cooling and specifically designed for operation at high scanning rates^[69,70]. RHC measurements were performed at 250 or 500 K min⁻¹ in aluminum crucibles, using helium (6 mL min⁻¹) as a purge gas. Electrochemical measurements (cyclic voltammetry) were performed with an Eco Chemie Autolab PGSTAT 30 potentiostat/galvanostat using a three-electrode microcell with a platinum working electrode, a platinum counter electrode and a Ag/AgNO₃ reference electrode (silver wire dipped in a solution of 0.01 M AgNO₃ and 0.1 M NBu₄PF₆ in anhydrous acetonitrile). The reference electrode was calibrated against ferrocene/ferrocenium as an external standard. Samples were prepared by dip coating the platinum working electrode in the respective polymer solutions (also used for the solid-state UV-Vis measurements). The CV measurements were done on the resulting films with 0.1 M NBu₄PF₆ in anhydrous acetonitrile as electrolyte solution. To prevent air from entering the system, the experiments were carried out under a curtain of argon. Cyclic voltammograms were recorded

at a scan rate of 100 mV s^{-1} . For the conversion of V to eV, the onset potentials of the first oxidation/reduction peaks were used and referenced to ferrocene/ferrocenium, which has an ionization potential of -4.98 eV vs. vacuum. This correction factor is based on a value of 0.31 eV for Fc/Fc^+ vs. $\text{SCE}^{[71]}$ and a value of 4.68 eV for SCE vs. vacuum^[72]: $E_{\text{HOMO/LUMO}} (\text{eV}) = -4.98 - E_{\text{onset ox/red}}^{\text{Ag/AgNO}_3} (\text{V}) + E_{\text{onset Fc/Fc}^+}^{\text{Ag/AgNO}_3} (\text{V})$.

5.2.2 OPV device fabrication and characterization

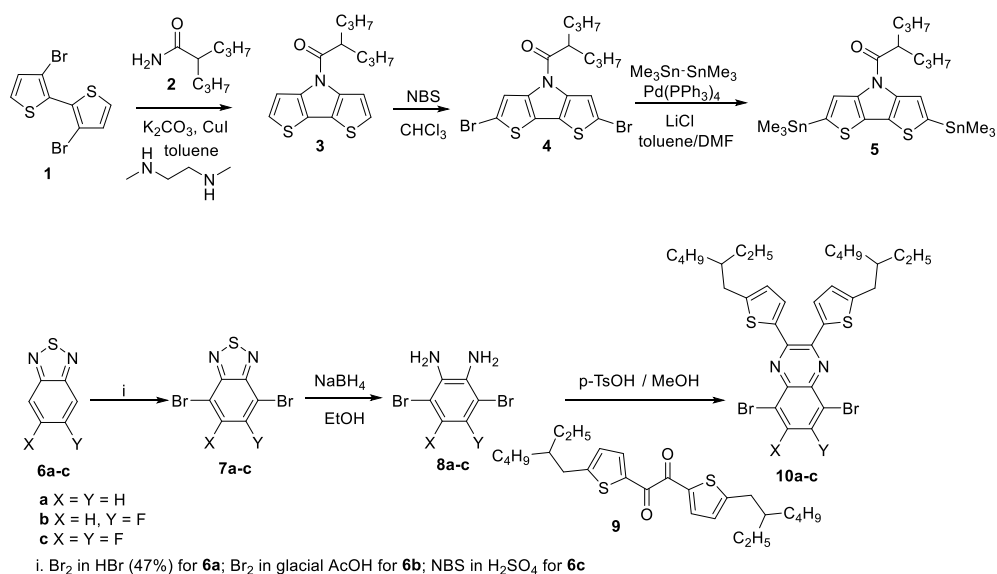
Bulk heterojunction polymer solar cells were constructed using the traditional device architecture glass/ITO/PEDOT-PSS/active layer/Ca/Al. Prior to processing, the indium tin oxide (ITO, Kintec, 100 nm , 20 Ohm/sq) coated substrates were thoroughly cleaned using soap, demineralized water, acetone, isopropanol and a UV/O_3 treatment. PEDOT:PSS [poly(3,4-ethylenedioxythiophene):poly(styrenesulfonic acid), Heraeus Clevios] was deposited by spincoating to obtain a layer of $\sim 30 \text{ nm}$. Afterwards, processing was continued under nitrogen atmosphere in a glove box, starting off with an annealing step at $130 \text{ }^\circ\text{C}$ for 15 min to remove any residual water. Subsequently, all active layer polymer:PC₇₁BM (1:3) (Solenne) solutions were spincoated with optimal thicknesses of $\sim 80\text{--}95 \text{ nm}$, as confirmed by profilometry (DEKTAK). Polymer:fullerene processing concentrations were varied depending on the solvent system: chloroform-based blends were prepared with a polymer concentration of 5 mg/mL , whereas for chlorobenzene-based blends a polymer concentration of 8 mg/mL was applied and for *ortho*-dichlorobenzene-based blends a polymer concentration of 12 mg/mL was used. The devices were finished off with Ca and Al as top electrodes with thicknesses of ~ 20 and 80 nm , respectively, resulting in an active device area of 3 mm^2 . The J - V characteristics

were measured using a Newport class A solar simulator (model 91195A), calibrated with a silicon solar cell to give an AM 1.5G spectrum. EQE measurements were performed with a Newport Apex illuminator (100 W Xenon lamp, 6257) as light source, a Newport Cornerstone 130° monochromator and a Stanford SR830 lock-in amplifier for the current measurements. A silicon FDS100-CAL photodiode was employed as a reference cell. For atomic force microscopy (AFM) imaging, a Bruker Multimode 8 AFM was used in PeakForce tapping mode, employing ScanAsyst. The images were produced with a silicon tip on a nitride lever with a spring constant of 4 N/m. Photo-induced charge extraction by linearly increasing voltage (Photo-CELIV) signals were registered on complete photovoltaic devices utilizing a pulsed laser (Continuum minilite II, 532nm), a Tektronix TDS 620B oscilloscope and a Tektronix AFG3101 function generator. The samples were placed in a sample holder filled with nitrogen to avoid exposure to ambient air.

5.3 RESULTS AND DISCUSSION

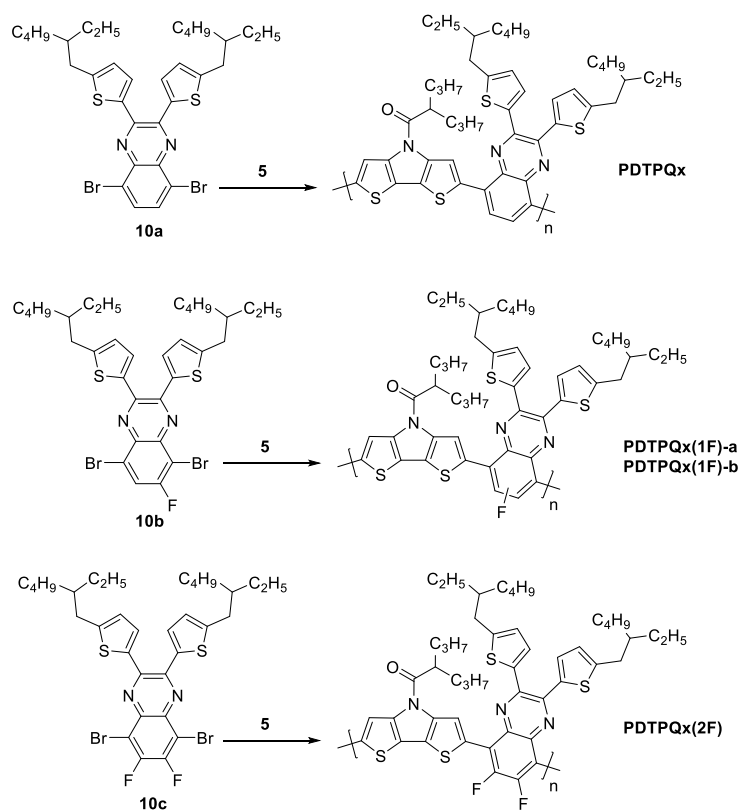
5.3.1 Synthesis and characterization

The N-acyl-DTP-*alt*-Qx copolymers were prepared by Stille polycondensation, combining a distannylated DTP moiety with a dibrominated Qx. The required N-acyl-DTP monomer, 2,6-bis(trimethylstannyl)-*N*-(2'-propylpentanoyl)-dithieno[3,2-*b*:2',3'-*d*]pyrrole (**5**), was prepared by a synthetic sequence involving a copper catalyzed tandem reaction of 3,3'-dibromo-2,2'-bithiophene (**1**) and 2-propylpentanamide (**2**), dibromination with *N*-bromosuccinimide (NBS) and subsequent Stille cross-coupling with hexamethylditin (Scheme 1)^[58,61]. As it was opted to include two solubilizing 2-ethylhexyl substituents on the Qx monomers (*vide infra*), relatively short alkyl side chains were introduced on the N-acyl-DTP part. The non-fluorinated Qx monomer, 5,8-dibromo-2,3-bis[5'-(2''-ethylhexyl)thiophen-2'-yl]quinoxaline (**10a**), was prepared according to a literature procedure^[66,67]. A similar approach was applied for the synthesis of the new monofluorinated (**10b**) and difluorinated (**10c**) quinoxaline monomers. This protocol consists of an acid catalyzed condensation reaction between *o*-phenylenediamines **8a–c** and diketone **9**. The precursors **8a–c** were synthesized from the corresponding benzothiadiazoles **6a–c** (prepared according to literature procedures^[68]) by subsequent bromination and reduction with NaBH₄. Diketone **9** was synthesized from thiophene by a lithiation/alkylation step followed by a Friedel-Crafts acylation reaction with oxalyl chloride^[66-68].



Scheme 1: Synthesis of the DTP and Qx monomers.

The Stille polymerization reactions were performed under standard conditions (2.5 mol% Pd₂(dba)₃, 10 mol% P(*o*-tol)₃, toluene/DMF: 4/1, 105 °C, 1h; Scheme 2). The resulting crude polymer materials were precipitated in methanol. No end-capping procedure was applied and after precipitation the low molar mass fractions were removed by soxhlet extractions. All copolymers were readily soluble in common organic solvents such as chloroform, THF or chlorobenzene. Their apparent molar masses were measured by analytical size exclusion chromatography (SEC) (Table 1). As molar mass and purity have a large influence on final photovoltaic performance, all polymers were additionally purified by preparative (recycling) SEC (prep-SEC), removing the low molar mass fractions (see Fig. S1). For **PDTPQx(1F)**, two batches with slightly different molar mass were prepared (denoted as a and b, *vide infra*).



Scheme 2: Polymerization of N-acyl-substituted DTP monomer **5** with Qx monomers **10a–c** via Stille polycondensation (2.5 mol% $\text{Pd}_2(\text{dba})_3$, 10 mol% $\text{P}(o\text{-tol})_3$, toluene/DMF: 4/1, 105 °C, 1h).

Table 1: Experimental SEC, CV and UV-Vis data for the PDTPQx series and a comparison between their experimental and DFT-calculated frontier orbital energies

Polymer	M_n^a [kg/mol]	D^a	Experimental				Calculated ^e				
			λ_{\max} (nm) solution	λ_{\max} (nm) film	HOMO ^b [eV]	LUMO ^b [eV]	E_g^{EC} [eV]	E_g^{OPd} [eV]	HOMO [eV]	LUMO [eV]	E_g [eV]
PDTPQx(0F)	12 (33)	2.8 (1.5)	684	703	-5.18	-3.34	1.84	1.53	-5.44	-2.44	3.00
PDTPQx(1F)-a	9.9 (18)	2.0 (1.4)	661	666	-5.31	-3.40	1.91	1.60	-5.52	-2.49	3.03
PDTPQx(1F)-b	20 (63)	3.1 (1.9)	/	/	/	/	/	/	/	/	/
PDTPQx(2F)	22 (56)	2.8 (1.8)	646	650	-5.50	-3.45	2.05	1.68	-5.60	-2.51	3.09

^a Determined by analytical SEC in THF at 40 °C. Values for the high molar mass fractions, isolated by prep-SEC, are noted between brackets. ^b Determined by CV from the oxidation/reduction onset. ^c Electrochemical bandgap. ^d Optical bandgap, as determined by the onset of the UV-Vis absorption spectra in film. ^e M05/6-311G(d)/IEFPCM calculations.

Upon analysis by rapid heat-cool calorimetry (RHC), particularly useful because of its increased sensitivity as a result of the fast scanning rates and the low sample amounts required, no visible thermal transitions (glass transition or melting) could be detected for the novel copolymer materials (Fig. S2)^[69,70,73]. UV-Vis measurements revealed that all polymers show a broad absorption in the visible range of the solar spectrum (Fig. 1, Table 1). For **PDTPQx**, the lowest optical bandgap was observed, with a wavelength of maximum absorption (λ_{max}) at 684 nm in solution, shifting to 703 nm in thin film. Upon monofluorination (**PDTPQx(1F)**), a clear blue-shift was observed^[74]. A similar trend, however less pronounced, was seen for the difluorinated copolymer (**PDTPQx(2F)**). The electrochemical properties of the three copolymers were investigated by cyclic voltammetry (CV) and their HOMO and LUMO energy levels were determined by the onset of the first oxidation and reduction peaks, respectively (Table 1). When compared with the values of a previously reported analogous N-alkyl-PDTP-Qx copolymer (HOMO = -4.64 eV, LUMO = -2.61 eV)^[41], it is clear that the HOMO level is lowered substantially by N-acyl substitution of the DTP component, in line with our previously reported results^[61]. Through the introduction of one or two fluorine atoms, the electron withdrawing power of the Qx acceptor increases, leading to a further deepening of the HOMO level. The LUMO levels are affected to a lesser extent, leading to an increased bandgap, as also seen in the UV-Vis spectra (Fig. 1).

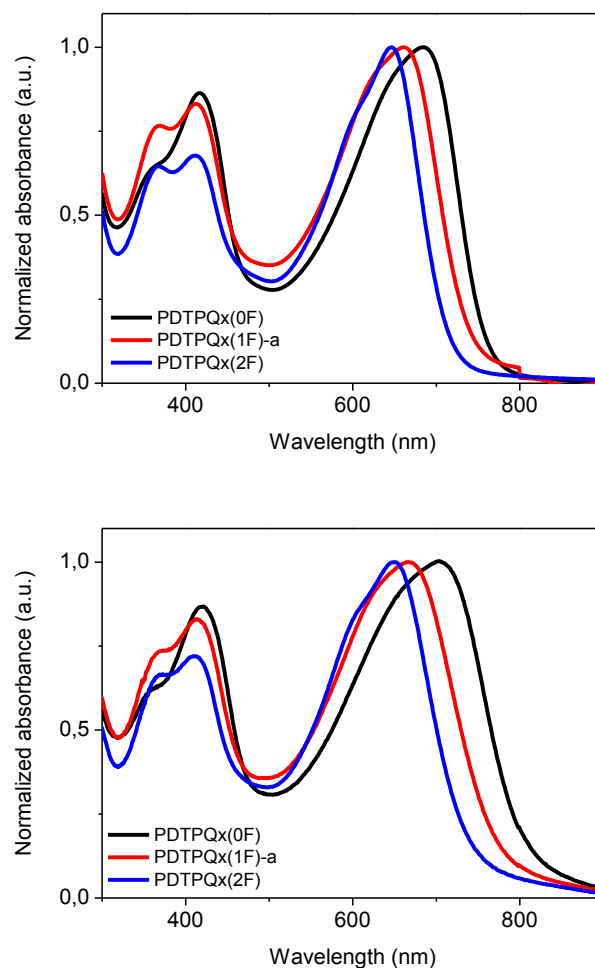


Figure 1: UV-Vis absorption spectra of all DTP-*alt*-Qx copolymers (before fractionation) in chloroform solution (top) and thin film (bottom).

5.3.2 DFT calculations

The impact of the fluorine atoms on the HOMO and LUMO energy levels of the polymers was investigated by density function theory (DFT) calculations using the M05^[75] exchange-correlation functional and the 6-311G(d) basis set. The effects of the solvent (THF) were taken into account by using the polarizable

continuum model^[76], and all calculations were performed using Gaussian09^[77]. Initially, an optimization of the ground state geometries was carried out for the individual donor and acceptor moieties, the donor-acceptor combinations (DA), as well as for dimers of the donor-acceptor units (DADA). The large alkyl chains were replaced by methyl groups to accelerate the calculations without impacting the results. Multiple conformations differing by the torsion angles between the donor and acceptor units have been considered. Table 1 summarizes the energies and the topologies of the HOMO's and LUMO's, as determined from the optimized geometries. Since the energies of the *syn* and *anti* conformers differ little, the reported HOMO and LUMO energies were obtained after performing a Boltzmann averaging ($T = 298.15$ K). The M05 results indicate that upon addition of fluorine atoms onto the Qx moiety, both the HOMO and LUMO levels are stabilized, but due to a stronger impact on the former the HOMO-LUMO gap slightly opens up with increasing number of fluorine atoms. The observed theoretical trends correlate nicely to the experimental results.

5.3.3 Photovoltaic properties

To investigate the photovoltaic features of the novel PDTPQx copolymers, blends were prepared in combination with PC₇₁BM and these were applied as photoactive layers in BHJ polymer solar cells with a standard configuration (glass/ITO/PEDOT:PSS/active layer/Ca/Al). As represented in Fig. 2 and Table 2, the optimized devices (after careful screening of solvent, blend ratio and active layer thickness) based on **PDTPQx**:PC₇₁BM (1:3 ratio in chlorobenzene (CB)) yielded a V_{oc} of 0.67 V, and combined with a J_{sc} of 12.57 mA/cm² and a FF of 0.54, an average power conversion efficiency (PCE) of 4.53% (best device 4.81%) could be obtained (Table 2, Fig. 2). Further optimization by the addition

of processing additives such as 1-chloronaphtalene (CN) or 1,8-diiodooctane (DIO) did not result in further improvements (Table S1). Despite the still modest V_{oc} , a record device efficiency was obtained for N-acyl-DTP-based polymer donor materials, matching the top efficiencies obtained for N-alkyl-DTP-based polymer and small molecule solution-processed BHJ OPV devices^[53,54].

Table 2: Photovoltaic performances of (optimized) PDTPQx:PC₇₁BM(1:3) BHJ polymer solar cells and charge carrier mobilities obtained for these devices^a

Polymer	Processing solvent ^b	V_{oc} [V]	J_{sc} [mA/cm ²]	FF	Average η [%] ^c	Best η [%]	Charge carrier mobility [cm ² /Vs] ^d
PDTPQx	CB	0.67	12.57	0.54	4.53	4.81	6.2 E-4
PDTPQx(1F)-a	CB	0.76	6.66	0.47	2.39	2.78	2.1 E-4
PDTPQx(2F)	CB	0.75	4.25	0.49	1.56	1.74	9.9 E-2
PDTPQx(2F)	CB + 3% DIO	0.64	7.19	0.51	2.34	2.50	/

^a Device structure glass/ITO/PEDOT:PSS/active layer/Ca/Al. The active layer thicknesses for the optimized devices were ~80–95 nm. ^b Total concentration of 32 mg/mL in CB. CB = chlorobenzene, DIO = 1,8-diiodooctane. ^c Average over 4–8 devices. ^d Determined by Photo-CELIV on complete photovoltaic devices.

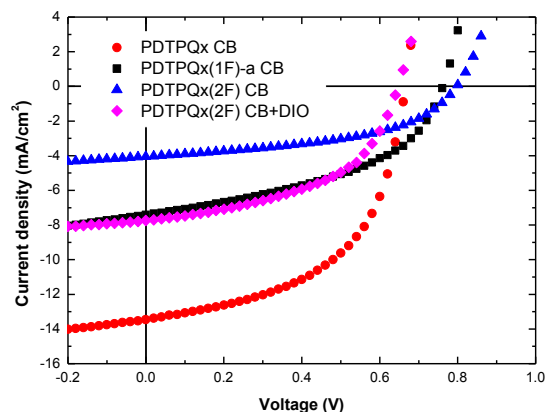


Figure 2: J - V curves under illumination for the best solar cell devices based on the DTP-*alt*-Qx copolymers.

A noticeable increase in V_{oc} (to 0.76 V) was observed when combining the monofluorinated **PDTPQx(1F)** copolymer with PC₇₁BM (Table 2, Fig. 2). However, a simultaneous drop in J_{sc} to an average of 6.66 mA/cm² was observed as well, even after tedious optimization (Table S2). Eventually, the best performing device for the **PDTPQx(1F)**:PC₇₁BM combination showed an efficiency of 2.78%. This decrease in J_{sc} cannot be attributed to reduced charge carrier mobility, as photo-induced charge extraction by linearly increasing voltage (photo-CELIV) measurements indicated that the mobilities (in the appropriate direction of the solar cell mode) are in the same (suitable) range for the three copolymer:PC₇₁BM blends and even increase upon Qx fluorination (Table 2, Fig. S3). To investigate if the reduced J_{sc} could be linked to the active layer nanomorphology, AFM imaging was applied, which revealed the formation of large aggregates in the films, even for the best devices (Fig. 3). Similar previous observations for fluorinated copolymers have been attributed to the fluorophobicity of PC₇₁BM^[74,78]. Therefore, the aggregates can most likely be

ascribed as PC₇₁BM-rich clusters, which is confirmed by the surface ratio (68–75%) matching closely to the polymer:PC₇₁BM 1:3 feed ratio. Aggregation at this large scale (~200 nm) strongly diminishes the donor-acceptor interface available for charge separation. In an attempt to overcome this, a number of processing additives were applied. However, no noticeable improvement in blend nanomorphology (and hence efficiency) could be obtained. It has recently been stated that fluorination of low bandgap copolymers will only lead to enhancements in photovoltaic performance when the polymer molar mass is reasonably high^[27]. As the M_n of **PDTPQx(1F)-a** was rather low (18 kDa after purification by prep-SEC, Table 1) in comparison to the other two copolymers, a new polymer batch (**PDTPQx(1F)-b**) was prepared with a higher M_n (63 kDa after purification by prep-SEC, Table 1) to analyze the influence of molar mass. However, no real differences were observed when comparing both materials (Table S2).

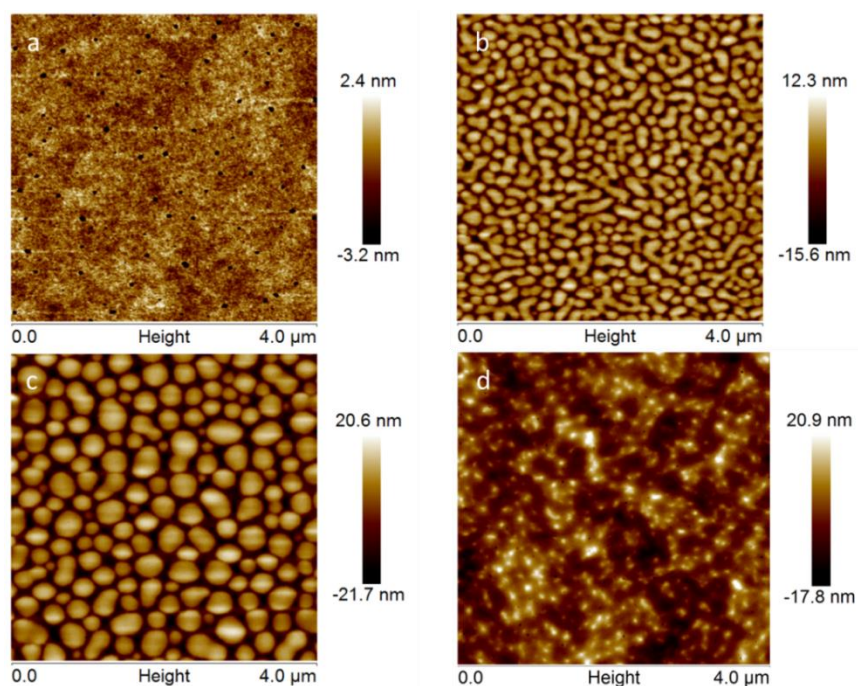


Figure 3: AFM (topography) images ($4.0 \times 4.0 \mu\text{m}^2$) for the optimized BHJ OPV devices based on a) **PDTPQx**, b) **PDTPQx(1F)-a**, c) **PDTPQx(2F)** (in CB), and d) **PDTPQx(2F)** (in CB + 3% DIO).

In a final stage, the difluorinated quinoxaline copolymer **PDTPQx(2F)** was analyzed as well. A further downward trend in J_{sc} was observed (despite the increased mobility), leading to an average value of 4.25 mA/cm^2 when processing the active layer from chlorobenzene (Table 2, Fig. 2). Moreover, no further enhancement in V_{oc} , as expected from the deepened HOMO level (Table 1), was seen. As illustrated by the AFM images (Fig. 3), even larger aggregates were formed during film formation for the **PDTPQx(2F):PC₇₁BM** blend, which suggests that the overall lower photovoltaic performance can be attributed to the far-from-optimal BHJ blend nanomorphology. The addition of 3% DIO to the polymer:fullerene processing solution did provide an enhancement of the blend

nanomorphology, as illustrated in Fig. 3d. Consequently, an improved J_{sc} of 7.19 mA/cm² was achieved for the optimal device, resulting in a PCE of 2.50% (Table 2, Fig. 2). However, the nanomorphology still remained unfavorable as compared to the active layer based on the non-fluorinated copolymer. Although there are no large aggregates any more, a quite rough morphology with spike-shaped structures at the surface is formed. Moreover, the enhancement in V_{oc} due to Qx fluorination was completely lost in this case. For chloroform-based solvent systems, we did observe an enhanced V_{oc} up to 0.82 V. Nonetheless, combined with a lowering of the J_{sc} , poor device properties were still obtained (Table S3). Furthermore, for both the **PDTPQx(1F)-a**:PC₇₁BM and **PDTPQx(2F)**:PC₇₁BM active layer blends, the FF of the optimized devices was never as high as for **PDTPQx**:PC₇₁BM.

From the external quantum efficiency (EQE) spectra the clear difference in performance for the copolymer:fullerene blends can be seen as well (Fig. 4). A maximum EQE of 66% at 500 nm was observed for the **PDTPQx**:PC₇₁BM polymer solar cell. The current densities extracted from the EQE measurements (J_{EQE} = 11.24, 6.50, 3.88 and 7.12 mA/cm² for **PDTPQx**, **PDTPQx(1F)-a**, **PDTPQx(2F)** in CB and **PDTPQx(2F)** in CB+DIO, respectively) correspond rather well to the measured J_{sc} values, in accordance with standard measurement deviations.

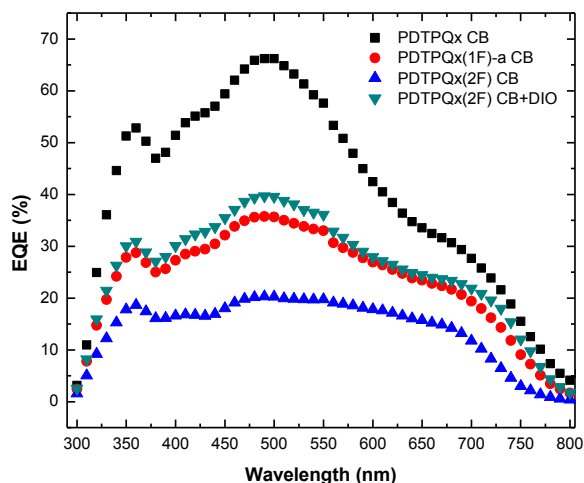


Figure 4: EQE spectra for the optimized solar cell devices based on the DTP-*alt*-Qx copolymers.

5.4 CONCLUSIONS

A novel **PDTPQx** push-pull copolymer based on an N-acyl-DTP donor and a Qx acceptor unit was synthesized and applied in BHJ polymer:fullerene solar cells. The resulting devices showed a rather high J_{sc} , an enhanced V_{oc} and the highest PCE up to date (4.81%) for polymer solar cells (without special cathode interlayers or alternative performance enhancing methods) based on (N-acyl-)DTP copolymers. Nonetheless, comparing with various high-performing donor materials, the V_{oc} remained a limiting factor, and hence fluorination of the Qx building block was applied as an additional tool to improve the V_{oc} . This strategy in the end did not pay off, however, due to the inability to achieve a favorable interpenetrating donor-acceptor network in the photoactive layer, as observed by AFM imaging. The main challenge in our continued studies based on related material systems will hence be to alleviate these morphology issues, possibly

through strategic polymer side chain optimization or implementation of more miscible fullerenes.

5.5 REFERENCES

- [1] C.J. Brabec, S. Gowrisanker, J.J.M. Halls, D. Laird, S. Jia, S.P. Williams, Polymer-fullerene bulk-heterojunction solar cells, *Adv. Mater.* 22 (2010) 3839-3856.
- [2] M. Jørgensen, K. Norrman, S.A. Gevorgyan, T. Tromholt, B. Andreasen, F.C. Krebs, Stability of polymer solar cells, *Adv. Mater.* 24 (2012) 580-612.
- [3] Y. Li, Molecular design of photovoltaic materials for polymer solar cells: toward suitable electronic energy levels and broad absorption, *Acc. Chem. Res.* 45 (2012) 723-733.
- [4] A. Mishra, P. Bäuerle, Small molecule organic semiconductors on the move: promises for future solar energy technology, *Angew. Chem. Int. Ed.* 51 (2012) 2020-2067.
- [5] S. Lizin, S. Van Passel, E. De Schepper, W. Maes, L. Lutsen, J. Manca, D. Vanderzande, Life cycle analyses of organic photovoltaics: a review, *Energy Environ. Sci.* 6 (2013) 3136-3149.
- [6] L. Dou, J. You, Z. Hong, Z. Xu, G. Li, R.A. Street, Y. Yang, 25th Anniversary article: a decade of organic/polymeric photovoltaic research, *Adv. Mater.* 25 (2013) 6642-6671.
- [7] K. Vandewal, S. Himmelberger, A. Salleo, Structural factors that affect the performance of organic bulk heterojunction solar cells, *Macromolecules* 46 (2013) 6379-6387.
- [8] A.J. Heeger, 25th Anniversary article: bulk heterojunction solar cells: understanding the mechanism of operation, *Adv. Mater.* 26 (2014) 10-28.
- [9] Y. Chen, X. Wan, G. Long, High performance photovoltaic applications using solution-processed small molecules, *Acc. Chem. Res.* 46 (2014) 2645-2655.

- [10] R. Søndergaard, M. Hösel, D. Angmo, T.T. Larsen-Olsen, F.C. Krebs, Roll-to-roll fabrication of polymer solar cells, *Mater. Today* 15 (2012) 36-49.
- [11] Z.C. He, C.M. Zhong, S.J. Su, M. Xu, H.B. Wu, Y. Cao, Enhanced power-conversion efficiency in polymer solar cells using an inverted device structure, *Nat. Photonics* 6 (2012) 591-595.
- [12] K.H. Hendriks, G.H.L. Heintges, V.S. Gevaerts, M.M. Wienk, R.A.J. Janssen, High-molecular-weight regular alternating diketopyrrolopyrrole-based terpolymers for efficient organic solar cells, *Angew. Chem. Int. Ed.* 52 (2013) 8341-8344.
- [13] I. Osaka, T. Kakara, N. Takemura, T. Koganezawa, K. Takimiya, Naphthadithiophene-naphthobisthiadiazole copolymers for solar cells: alkylation drives the polymer backbone flat and promotes efficiency, *J. Am. Chem. Soc.* 135 (2013) 8834-8837.
- [14] Y. Deng, J. Liu, J. Wang, L. Liu, W. Li, H. Tian, X. Zhang, Z. Xie, Y. Geng, F. Wang, Dithienocarbazole and isoindigo based amorphous low bandgap conjugated polymers for efficient polymer solar cells, *Adv. Mater.* 26 (2014) 471-476.
- [15] M. Zhang, X. Guo, S. Zhang, J. Hou, Synergistic effect of fluorination on molecular energy level modulation in highly efficient photovoltaic polymers, *Adv. Mater.* 26 (2014) 1118-1123.
- [16] A.K.K. Kyaw, D.H. Wang, D. Wynands, J. Zhang, T.-Q. Nguyen, G.C. Bazan, A.J. Heeger, Improved light harvesting and improved efficiency by insertion of an optical spacer (ZnO) in solution-processed small-molecule solar cells, *Nano Lett.* 13 (2013) 3796-3801.

- [17] Y. Liu, Y. Yang, C-C. Chen, Q. Chen, L. Dou, Z. Hong, G. Li, Y. Yang, Solution-processed small molecules using different electron linkers for high-performance solar cells, *Adv. Mater.* 25 (2013) 4657-4662.
- [18] V.S. Gevaerts, E.M. Herzig, M. Kirkus, K.H. Hendriks, M.M. Wienk, J. Perlich, P. Müller-Buschbaum, R.A.J. Janssen, Influence of the position of the side chain on crystallization and solar cell performance of DPP-based small molecules, *Chem. Mater.* 26 (2014) 916-926.
- [19] D. Liu, M. Xiao, Z. Du, Y. Yan, L. Han, V. A. L. Roy, M. Sun, W. Zhu, C.S. Lee, R. Yang, Solution-processed, indacenodithiophene-based, small-molecule organic field effect transistors and solar cells, *J. Mater. Chem. C* 2 (2014) 7523-7530.
- [20] B. Kan, Q. Zhang, M. Li, X. Wan, W. Ni, G. Long, Y. Wang, X. Yang, H. Feng, Y. Chen, Solution-processed organic solar cells based on dialkylthiol-substituted benzodithiophene unit with efficiency near 10%, *J. Am. Chem. Soc.* 136 (2014) 15529-15532.
- [21] Y. Liu, J. Zhao, Z. Li, C. Mu, W. Ma, H. Hu, K. Jiang, H. Lin, H. Ade, H. Yan, Aggregation and morphology control enables multiple cases of high-efficiency polymer solar cells, *Nat. Commun.*, DOI: 10.1038/ncomms6293.
- [22] G. Ren, P.-T. Wu, S.A. Jenekhe, Enhanced performance of bulk heterojunction solar cells using block copoly(3-alkylthiophene)s, *Chem. Mater.* 22 (2010) 2020-2026.
- [23] G. Ren, P.-T. Wu, S.A. Jenekhe, Solar cells based on block copolymer semiconductor nanowires: effects of nanowire aspect ratio, *ACS Nano* 5 (2011) 376-384.
- [24] C. Cabanetos, A.E. Labban, J.A. Bartelt, J.D. Douglas, W.R. Mateker, J.M.J. Fréchet, M.D. McGehee, P.M. Beaujuge, Linear side chains in benzo[1,2-*b*:4,5-

b]dithiophene-thieno[3,4-*c*]pyrrole-4,6-dione polymers direct self-assembly and solar cell performance, *J. Am. Chem. Soc.* 135 (2013) 4656-4659.

[25] L. Luyao, L. Yu, Understanding low bandgap polymer PTB7 and optimizing polymer solar cells of it, *Adv. Mater.* 26 (2014) 4413-4430.

[26] J. Kesters, S. Kudret, S. Bertho, N. Van den Brande, M. Defour, B. Van Mele, H. Penxten, L. Lutsen, J. Manca, D. Vanderzande, W. Maes, Enhanced intrinsic stability of the bulk heterojunction active layer blend of polymer solar cells by varying the polymer side chain pattern, *Org. Electron.* 15 (2014) 549-562.

[27] X. He, S. Mukherjee, S. Watkins, M. Chen, T. Qin, L. Thomsen, H. Ade, C.R. McNeill, Influence of fluorination and molecular weight on the morphology and performance of PTB7:PC₇₁BM solar cells, *J. Phys. Chem. C.* 118 (2014) 9918-9929.

[28] H.-C. Chen, Y.-H. Chen, C.-C. Liu, Y.-C. Chien, S.-W. Chou, P.-T. Chou, Prominent short-circuit currents of fluorinated quinoxaline-based copolymer solar cells with a power conversion efficiency of 8.0%, *Chem. Mater.* 24 (2012) 4766-4772.

[29] H.-C. Chen, Y.-H. Chen, C.-H. Liu, Y.-H. Hsu, Y.-C. Chien, W.-T. Chuang, C.-Y. Cheng, C.-L. Liu, S.-W. Chou, S.-H. Tung, P.-T. Chou, Fluorinated thienyl-quinoxaline-based D- π -A-type copolymer toward efficient polymer solar cells; synthesis, characterization, and photovoltaic properties, *Polym. Chem.* 4 (2013) 3411.

[30] J.-H. Kim, C.E. Song, H.U. Kim, A.C. Grimsdale, S.-J. Moon, W.S. Shin, S.K. Choi, D.-H. Hwang, High open circuit voltage solution-processed tandem organic photovoltaic cells employing a bottom cell using a new medium band gap semiconducting polymer, *Chem. Mater.* 25 (2013) 2722-2732.

- [31] M. Zhang, X. Guo, S. Zhang, J. Hou, Synergistic effect of fluorination on molecular energy level modulation in highly efficient photovoltaic polymers, *Adv. Mater.* 26 (2013) 1118-1123.
- [32] K. Ogowa, S.C. Rasmussen, A simple and efficient route to N-functionalized dithieno[3,2-*b*:2',3'-*d*]pyrroles: Fused-ring building blocks for new conjugated polymeric systems, *J. Org. Chem.* 68 (2003) 2921-2928.
- [33] G. Koeckelberghs, L. De Cremer, W. Vanormelingen, W. Dehaen, T. Verbiest, A. Persoons, C. Samyn, Improved synthesis of *N*-alkyl substituted dithieno[3,2-*b*:2',3'-*d*]pyrroles, *Tetrahedron* 61 (2005) 687-691.
- [34] K. Ogowa, S.C. Rasmussen, N-functionalized poly(dithieno[3,2-*b*:2',3'-*d*]pyrrole)s: Highly fluorescent materials with reduced band gaps, *Macromolecules* 39 (2006) 1771-1778.
- [35] K.R. Radke, K. Ogowa, S.C. Rasmussen, Highly fluorescent oligothiophenes through the incorporation of central dithieno[3,2-*b*:2',3'-*d*]pyrrole units, *Org. Lett.* 7 (2005) 5253-5256.
- [36] J. Liu, R. Zhang, G. Sauvé, T. Kowalewski, R.D. McCullough, Highly disordered polymer field effect transistors: *N*-alkyl dithieno[3,2-*b*:2',3'-*d*]pyrrole-based copolymers with surprisingly high charge carrier mobilities, *J. Am. Chem. Soc.* 130 (2008) 13167-13176.
- [37] W. Zhang, J. Li, B. Zhang, J. Qin, Z. Lu, Y.F. Poon, M.B. Chan-Park, C.M. Li, Semiconducting polymers containing dithieno[3,2-*b*:2',3'-*d*]pyrrole for organic thin-film transistors, *Macromolecules* 41 (2008) 8953-8955.
- [38] X. Zhan, Z. Tan, E. Zhou, Y. Li, R. Misra, A. Grant, B. Domercq, X.-H. Zhang, Z. An, X. Zhang, S. Barlow, B. Kippelen, S.R. Marder, Copolymers of perylene diimide with dithienothiophene and dithienopyrrole as electron-

transport materials for all-polymer solar cells and field-effect transistors, *J. Mater. Chem.* 19 (2009) 5794-5803.

[39] X. Zhang, T.T. Steckler, R.R. Dasari, S. Ohira, W.J. Potscavage, S.P. Tiwari, S. Coppée, S. Ellinger, S. Barlow, J.-L. Brédas, B. Kippelen, J.R. Reynolds, S.R. Marder, Dithienopyrrole-based donor-acceptor copolymers: low band-gap materials for charge transport, photovoltaics and electrochromism, *J. Mater. Chem.* 20 (2010) 123-134.

[40] S.C. Rasmussen, S.J. Evenson, Dithieno[3,2-*b*:2',3'-*d*]pyrrole-based materials: Synthesis and application to organic electronics, *Prog. Polym. Sci.* 38 (2013) 1773-1804.

[41] K.M. Noone, E. Strein, N. C. Anderson, P.-T. Wu, S.A. Jenekhe, D.S. Ginger, Broadband absorbing bulk heterojunction photovoltaics using low-bandgap solution-processed quantum dots, *Nano Lett.* 10 (2010) 2635-2639.

[42] W. Yue, Y. Zhao, S. Shao, H. Tian, Z. Xie, Y. Geng, F. Wang, Novel NIR-absorbing conjugated polymers for efficient polymer solar cells: effect of alkyl chain length on device performance, *J. Mater. Chem.* 19 (2009) 2199-2206.

[43] E. Zhou, Q. Wei, S. Yamakawa, Y. Zhang, K. Tajima, C. Yang, K. Hashimoto, Diketopyrrolopyrrole-based semiconducting polymer for photovoltaic device with photocurrent response wavelengths up to 1.1 μm , *Macromolecules* 43 (2010) 821-826.

[44] E. Zhou, J. Cong, L. Tajima, C. Yang, K. Hashimoto, Synthesis and photovoltaic properties of donor-acceptor copolymer based on dithienopyrrole and thienopyrroledione, *Macromol. Chem. Phys.* 212 (2011) 305-310.

[45] X. Hu, M. Shi, L. Zuo, Y. Nan, Y. Liu, L. Fu, H. Chen, Synthesis, characterization, and photovoltaic property of a low band gap polymer

alternating dithienopyrrole and thienopyrroledione units, *Polymer* 52 (2011) 2559-2564.

[46] X. Zhang, J.W. Shim, S.P. Tiwari, Q. Zhang, J.E. Norton, P.-T. Wu, S. Barlow, S.A. Jenekhe, B. Kippelen, J.-L. Brédas, S.R. Marder, Dithienopyrrole-quinoxaline/pyridopyrazine donor-acceptor polymers: synthesis and electrochemical, optical, charge-transport, and photovoltaic properties, *J. Mater. Chem.* 21 (2011) 4971-4982.

[47] E. Zhou, J. Cong, K. Tajima, C. Yang, K. Hashimoto, Conjugated polymers based on 1,3-dithien-2-yl-thieno[3,4-c]pyrrole-4,6-dione: Synthesis, characterization, and solvent effects on photovoltaic performance, *J. Phys. Chem. B* 116 (2012) 2608-2614.

[48] B. Burkhart, P.P. Khlyabich, B.C. Thompson, Solar cells based on semi-random P3HT analogues containing dithienopyrrole: influence of incorporating a strong donor, *J. Photon. Energy* 2 (2012) 021002.

[49] Z. Li, D. Zhou, L. Li, Y. Li, Y. He, J. Liu, Q. Peng, Synthesis and characterization of copolymers based on benzotriazoles and different atom-bridged dithiophenes for efficient solar cells, *Polym. Chem.* 4 (2013) 2496-2505.

[50] V. Tamilavan, M. Song, S. Kim, R. Agneeswari, J.-W. Kang, M.H. Hyun, *Polymer* 54 (2013) 3198-3205.

[51] W. Yue, T.T. Larsen-Olsen, X. Hu, M. Shi, H. Chen, M. Hinge, P. Fojan, F.C. Krebs, D. Yu, Synthesis and photovoltaic properties from inverted geometry cells and roll-to-roll coated large area cells from dithienopyrrole-based donor-acceptor polymers, *J. Mater. Chem. A* 1 (2013) 1785-1793.

[52] Y. Geng, J. Cong, K. Tajima, Q. Zeng, E. Zhou, Synthesis and properties of D-A copolymers based on dithienopyrrole and benzothiadiazole with various numbers of thienyl units as spacers, *Polym. Chem.* 5 (2014) 6797-6803.

- [53] K.H. Hendriks, W. Li, M.M. Wienk, R.A.J. Janssen, Small-bandgap semiconducting polymers with high near-infrared photoresponse, *J. Am. Chem. Soc.* 136 (2014) 12130-12136.
- [54] M. Weidelener, C.D. Wessendorf, J. Hanisch, E. Ahlswede, G. Götz, M. Lindén, G. Schulz, E. Mena-Osteritz, A. Mishra, P. Bäuerle, Dithienopyrrole-based oligothiophenes for solution-processed organic solar cells, *Chem. Commun.* 49 (2013) 10865-10867.
- [55] L.G. Mercier, A. Mishra, Y. Ishigaki, F. Henne, G. Schulz, P. Bäuerle, Acceptor-donor-acceptor oligomers containing dithieno[3,2-*b*:2',3'-*d*]pyrrole and thieno[2,3-*c*]pyrrole-4,6-dione units for solution-processed organic solar cells, *Org. Lett.* 16 (2014) 2642-2645.
- [56] H.-I. Lu, C.-W. Lu, Y.-C. Lee, H.-W. Lin, L.-Y. Lin, F. Lin, J.-H. Chang, C.-I. Wu, K.-T. Wong, New molecular donors with dithienopyrrole as electron-donating group for efficient small molecule organic solar cells, *Chem. Mater.* 26 (2014) 4361-4367.
- [57] A.M. Poe, A.M. Della Pelle, A.V. Subrahmanyam, W. White, G. Wantz, S. Thayumanavan, Small molecule BODIPY dyes as non-fullerene acceptors in bulk heterojunction organic photovoltaics, *Chem. Commun.* 50 (2014) 2913-2915.
- [58] S.J. Evenson, S.C. Rasmussen, *N*-acyldithieno[3,2-*b*:2',3'-*d*]pyrroles: Second generation dithieno[3,2-*b*:2',3'-*d*]pyrrole building blocks with stabilized energy levels, *Org. Lett.* 12 (2010) 4054-4057.
- [59] J. Warnan, C. Cabanetos, R. Bude, A. El Labban, L. Li, P.M. Beaujuge, Electron-deficient *N*-alkyloyl derivatives of thieno[3,4-*c*]pyrrole-4,6-dione yield efficient polymer solar cells with open-circuit voltage > 1 V, *Chem. Mater.* 26 (2014) 2829-2835.

- [60] D. Hong, M. Lv, M. Lei, Y. Chen, P. Lu, Y. Wang, J. Zhu, H. Wang, M. Gao, S.E. Watkins, X. Chen, *N*-acyldithieno[3,2-*b*:2',3'-*d*]pyrrole-based low-band-gap conjugated polymer solar cells with amine-modified [6,6]-phenyl-C₆₁-butyric acid ester cathode interlayers, *ACS Appl. Mater. Interfaces* 5 (2013) 10995-11003.
- [61] W. Vanormelingen, J. Kesters, P. Verstappen, J. Drijkoningen, J. Kudrjasova, S. Koudjina, V. Liégeois, B. Champagne, J. Manca, L. Lutsen, D. Vanderzande, W. Maes, Enhanced open-circuit voltage in polymer solar cells by dithieno[3,2-*b*:2',3'-*d*]pyrrole *N*-acylation, *J. Mater. Chem. A* 2 (2014) 7535-7545.
- [62] D. Kitazawa, N. Watanabe, S. Yamamoto, J. Tsukamoto, Quinoxaline-based *n*-conjugated donor polymer for highly efficient organic thin-film solar cells, *Appl. Phys. Lett.* 95 (2009) 053701.
- [63] E. Wang, L. Hou, Z. Wang, S. Hellström, F. Zhang, O. Inganäs, M.R. Andersson, An easily synthesized blue polymer for high-performance polymer solar cells, *Adv. Mater.* 22 (2010) 5240-5244.
- [64] Y. Kim, H.R. Yeom, J.Y. Kim, C. Yang, High-efficiency polymer solar cells with a cost-effective quinoxaline polymer through nanoscale morphology control induced by practical processing additives, *Energy Environ. Sci.* 6 (2013) 1909-1916.
- [65] W. Zhuang, H. Zhen, R. Kroon, Z. Tang, S. Hellström, L. Hou, E. Wang, D. Gedefaw, O. Inganäs, F. Zhang, M.R. Andersson, Molecular orbital energy level modulation through incorporation of selenium and fluorine into conjugated polymers for organic photovoltaic cells, *J. Mater. Chem. A* 1 (2013) 13422-13425.

- [66] Y. Zhang, J. Zou, H.-L. Yip, K.-S. Chen, D.F. Zeigler, Y. Sun, A.K.-Y. Jen, Indacenodithiophene and quinoxaline-based conjugated polymers for highly efficient polymer solar cells, *Chem Mater.* 23 (2011) 2289-2291.
- [67] L. Marin, L. Lutsen, D. Vanderzande, W. Maes, Quinoxaline derivatives with broadened absorption patterns, *Org. Biomol. Chem.* 11 (2013) 5866-5876.
- [68] G.K. Dutta, T. Kim, H. Choi, J. Lee, D.S. Kim, J.Y. Kim, C. Yang, Synthesis of fluorinated analogues of a practical polymer TQ for improved open-circuit voltages in polymer solar cells, *Polym. Chem.* 5 (2014) 2540-2547.
- [69] R.L. Danley, P.A. Caulfield, S.R. Aubuchon, A rapid-scanning differential scanning calorimeter, *Am. Lab.* 40 (2008) 9-11.
- [70] S. Wouters, F. Demir, L. Beenaerts, G. Van Assche, Calibration and performance of a fast-scanning DSC-Project RHC, *Thermochim. Acta* 530 (2012) 64.
- [71] J. Bard, L.R. Faulkner, *Electrochemical methods: fundamentals and applications*, 2nd Ed., Wiley, 2001.
- [72] S. Trasatti, The absolute electrode potential: an explanatory note, *Pure Appl. Chem.* 58 (1986) 955-966.
- [73] T. Ghoo, N. Van den Brande, M. Defour, J. Brassinne, C.-A. Fustin, J.-F. Gohy, S. Hoepfener, U.S. Schubert, W. Vanormelingen, L. Lutsen, D.J. Vanderzande, B. Van Mele, W. Maes, Amphiphilic *N*-methylimidazole-functionalized diblock copolythiophenes for organic photovoltaics, *Eur. Polym. J.* 53 (2014) 206-214.
- [74] H.J. Son, W. Wang, T. Xu, Y. Liang, Y. Wu, G. Li, L. Yu, Synthesis of fluorinated polythienothiophene-*co*-benzodithiophenes and effect of fluorination on the photovoltaic properties, *J. Am. Chem. Soc.* 133 (2011) 1885-1894.

[75] Y. Zhao, N.E. Schultz, D.G. Truhlar, Exchange-correlation functional with broad accuracy for metallic and nonmetallic compounds, kinetics, and noncovalent interactions, *J. Chem. Phys.* 123 (2005) 161103.

[76] J. Tomasi, B. Mennucci, R. Cammi, Quantum mechanical continuum solvation models, *Chem. Rev.* 105 (2005) 2999-3093.

[77] M.J. Frisch, G.W. Trucks, H.B. Schlegel, G.E. Scuseria, M.A. Robb, J.R. Cheeseman, G. Scalmani, V. Barone, B. Mennucci, G.A. Petersson, H. Nakatsuji, M. Caricato, X. Li, H.P. Hratchian, A.F. Izmaylov, J. Bloino, G. Zheng, J.L. Sonnenberg, M. Hada, M. Ehara, K. Toyota, R. Fukuda, J. Hasegawa, M. Ishida, T. Nakajima, Y. Honda, O. Kitao, H. Nakai, T. Vreven, J.A. Montgomery Jr., J.E. Peralta Jr., F. Ogliaro, M. Bearpark, J.J. Heyd, E. Brothers, K.N. Kudin, V.N. Staroverov, R. Kobayashi, J. Normand, K. Raghavachari, A. Rendell, J.C. Burant, S.S. Iyengar, J. Tomasi, M. Cossi, N. Rega, J.M. Millam, M. Klene, J.E. Knox, J.B. Cross, V. Bakken, C. Adamo, J. Jaramillo, R. Gomperts, R.E. Stratmann, O. Yazyev, A.J. Austin, R. Cammi, C. Pomelli, J.W. Ochterski, R.L. Martin, K. Morokuma, V.G. Zakrzewski, G.A. Voth, P. Salvador, J.J. Dannenberg, S. Dapprich, A.D. Daniels, Ö. Farkas, J.B. Foresman, J.V. Ortiz, J. Cioslowski, D.J. Fox, *Gaussian 09, Revision A.1*, Gaussian, Inc., Wallingford CT, 2009.

[78] G.J. Hedley, A.J. Ward, A. Alekseev, C.T. Howells, E.R. Martins, L.A. Serrano, G. Cooke, A. Ruseckas, I.D.W. Samuel, Determining the optimum morphology in high-performance polymer-fullerene organic photovoltaic cells, *Nat. Commun.* 4 (2013) 2867.

5.6 ACKNOWLEDGEMENTS

This work was supported by the project ORGANEXT (EMR INT4-1.2-2009-04/054), selected in the frame of the operational program INTERREG IV-A Euregio Maas-Rijn, and the IAP 7/05 project FS2 (Functional Supramolecular Systems), granted by the Science Policy Office of the Belgian Federal Government (BELSPO). We are also grateful for financial support by the Research Programme of the Research Foundation – Flanders (FWO) (project G.0415.14N and M.ERA-NET project RADESOL). J. Kesters and J. Drijkoningen thank Hasselt University for their PhD scholarships. P. Verstappen and T. Vangerven acknowledge the Agency for Innovation by Science and Technology in Flanders (IWT) for their PhD grants. The calculations were performed on the computing facilities of the Consortium des Équipements de Calcul Intensif (CÉCI), in particular those of the Plateforme Technologique de Calcul Intensif (PTCI) installed in the University of Namur, for which the authors acknowledge financial support of the FNRS-FRFC (Conventions No. 2.4.617.07.F and 2.5020.11) and the University of Namur. The authors are grateful to B. Van Mele and N. Van den Brande for the thermal analysis, and H. Penxten for the cyclic voltammetry measurements. We further acknowledge Hercules for providing the funding for the LTQ Orbitrap Velos Pro mass spectrometer. Hasselt University and IMO-IMOMEC are partners within the Solliance network, the strategic alliance for research and development in the field of thin-film PV energy in the Eindhoven-Leuven-Aachen region.

5.7 SUPPORTING INFORMATION

5.7.1 Synthesis and characterization

5,8-Dibromo-2,3-bis[5'-(2''-ethylhexyl)thiophen-2'-yl]quinoxaline (10a)

General Qx monomer synthesis procedure: 3,6-Dibromo-1,2-phenylenediamine (0.690 g, 2.60 mmol) and 1,2-bis[5'-(2''-ethylhexyl)thiophen-2'-yl]ethane-1,2-dione (1.160 g, 2.60 mmol) were dissolved in MeOH (50 mL) and *p*-toluenesulfonic acid monohydrate (0.050 mg, 0.26 mmol) was added. After heating under reflux for 15 h, the reaction mixture was allowed to cool down and the yellow precipitate was filtered off, washed with MeOH and purified with flash column chromatography (silica, eluent dichloromethane (20%) in petroleum ether). After recrystallization from EtOH, the pure product was obtained as yellow needles (1.370 g, 78%). ¹H NMR (400 MHz, CDCl₃): δ 7.78 (s, 2H), 7.40 (d, *J* = 3.7 Hz, 2H), 6.70 (d, *J* = 3.7 Hz, 2H), 2.80 (d, *J* = 6.9 Hz, 4H), 1.70–1.60 (m, 2H), 1.45–1.20 (m, 16H), 0.95–0.85 (m, 12H); ¹³C NMR (100 MHz, CDCl₃): δ 150.9 (2C), 147.4 (2C), 138.6 (4C), 132.7 (2C), 130.5 (2C), 126.1 (2C), 123.0 (2C), 41.6 (2C), 34.6 (2C), 32.5 (2C), 29.0 (2C), 25.7 (2C), 23.2 (2C), 14.3 (2C), 11.0 (2C); HRMS (ESI): calcd. for C₃₂H₄₁Br₂N₂S₂ [M+H]⁺: 677.1052, found: 677.1046.

5,8-Dibromo-6-fluoro-2,3-bis[5'-(2''-ethylhexyl)thiophen-2'-yl]quinoxaline (10b)

Synthesis according to the general Qx monomer synthesis procedure. Yellow solid (902 mg, 75%). ¹H NMR (400 MHz, CDCl₃): δ 7.79 (d, *J* = 8.1 Hz, 1H), 7.41 (d, *J* = 3.7 Hz, 1H), 7.39 (d, *J* = 3.7 Hz, 1H), 6.70–6.65 (m, 2H), 2.81 (d, *J* = 6.9 Hz, 4H), 1.70–1.60 (m, 2H), 1.45–1.20 (m, 16H), 0.95–0.85 (m, 12H);

^{13}C NMR (100 MHz, CDCl_3): δ 159.7 (d, $^1J_{\text{C-F}} = 252.7$ Hz, 1C), 151.9 (1C), 151.2 (1C), 148.4 (1C), 147.1 (d, $J_{\text{C-F}} = 3.0$ Hz, 1C), 139.4 (d, $J_{\text{C-F}} = 5.7$ Hz, 1C), 139.0 (1C), 138.8 (1C), 136.1 (1C), 131.3 (1C), 130.8 (1C), 126.8 (1C), 126.6 (1C), 124.0 (d, $J_{\text{C-F}} = 11.1$ Hz, 1C), 123.1 (d, $J_{\text{C-F}} = 29.2$ Hz, 1C), 108.0 (d, $J_{\text{C-F}} = 21.1$ Hz, 1C), 42.1 (2C), 35.2 (1C), 35.1 (1C), 33.1 (2C), 29.5 (2C), 26.3 (2C), 23.7 (2C), 14.8 (2C), 11.5 (2C); HRMS (ESI): calcd. for $\text{C}_{32}\text{H}_{40}\text{Br}_2\text{FN}_2\text{S}_2$ $[\text{M}+\text{H}]^+$: 695.0958, found: 695.0953.

5,8-Dibromo-6,7-difluoro-2,3-bis[5'-(2''-ethylhexyl)thiophen-2'-yl]quinoxaline (10c)

Synthesis according to the general Qx monomer synthesis procedure. Yellow solid (589 mg, 56%). ^1H NMR (400 MHz, CDCl_3): δ 7.40 (d, $J = 3.7$ Hz, 2H), 6.71 (d, $J = 3.7$ Hz, 2H), 2.81 (d, $J = 6.8$ Hz, 4H), 1.70–1.60 (m, 2H), 1.45–1.20 (m, 16H), 0.95–0.85 (m, 12H); ^{13}C NMR (100 MHz, CDCl_3): δ 151.2 (2C), 150.3 (dd, $^1J_{\text{C-F}} = 257.8$, $^2J_{\text{C-F}} = 19.8$ Hz, 2C), 147.4 (2C), 138.2 (2C), 135.2 (2C), 130.5 (2C), 126.2 (2C), 109.0 (dd, $J_{\text{C-F}} = 11.5$, 8.8 Hz, 2C), 41.6 (2C), 34.6 (2C), 32.5 (2C), 29.0 (2C), 25.8 (2C), 23.2 (2C), 14.3 (2C), 11.0 (2C); HRMS (ESI): calcd. for $\text{C}_{32}\text{H}_{39}\text{Br}_2\text{F}_2\text{N}_2\text{S}_2$ $[\text{M}+\text{H}]^+$: 713.0864, found: 713.0862.

PDTPQx

General polymerization method: A solution of N-acyl-DTP monomer **5** (213.5 mg, 0.338 mmol) in dry toluene (8 mL) was added dropwise via a syringe to a mixture of Qx monomer **10a** (228.9 mg, 0.338 mmol), $\text{Pd}_2(\text{dba})_3$ (7.7 mg, 0.0084 mmol, 2.5 mol%), and $\text{P}(o\text{-tol})_3$ (10.3 mg, 0.0338 mmol, 10 mol%) in dry DMF (2 mL). After purging with argon for 10 min, the mixture was heated to 105 °C for 1 h. The resulting crude polymer material was precipitated in methanol and purified by repetitive soxhlet extractions with methanol, acetone,

n-hexane and chloroform. The chloroform fraction was again precipitated in methanol and filtered, yielding a black solid (250 mg, 87%). ¹H NMR (CDCl₃, 400 MHz): δ = 8.80–8.10 (br, 2H), 8.00–7.55 (br, 2H), 7.50–7.10 (br, 2H), 6.90–6.50 (br, 2H), 3.70–3.40 (br, 1H), 3.05–2.55 (br, 4H), 2.10–1.85 (br, 2H), 1.80–1.60 (br, 4H), 1.55–1.15 (20H), 1.10–0.75 (br, 18H); SEC (THF, 40 °C, PS standards): M_n = 12 kg/mol, D = 2.8; After prep-SEC (**PDTPQx-H**): M_n = 33 kg/mol, D = 1.5.

PDTPQx(1F)

Similar to the procedure as outlined for **PDTPQx**: Batch **a**: DTP monomer **5** (0.257 g, 0.407 mmol), Qx monomer **10b** (0.283 g, 0.407 mmol), Pd₂(dba)₃ (9.3 mg, 10 μ mol) and P(*o*-tol)₃ (10.4 mg, 40.8 μ mol) were dissolved in 12.5 mL of dry toluene and 2.5 mL of dry DMF. The polymer was obtained as a black solid (200 mg, 57 %). Batch **b**: DTP monomer **5** (0.121 g, 0.193 mmol), Qx monomer **10b** (0.134 g, 0.193 mmol), Pd₂(dba)₃ (4.4 mg, 4.8 μ mol) and P(*o*-tol)₃ (5.9 mg, 19 μ mol) were dissolved in 6.0 mL of dry toluene and 1.2 mL of dry DMF. The polymer was obtained as a black solid (90 mg, 54%). ¹H NMR (CDCl₃, 400 MHz): δ = 9.25–8.10 (br, 1H), 8.05–7.15 (br, 3H), 7.10–6.10 (br, 3H), 3.70–3.35 (br, 1H), 3.20–2.55 (br, 3H), 2.20–1.90 (br, 3H), 1.90–1.65 (br, 4H), 1.50–0.25 (br, 38H); SEC (THF, 40 °C, PS standards): M_n = 9.9 kg/mol, D = 2.0 (for **a**) and M_n = 20 kg/mol, D = 3.1 (for **b**); After prep-SEC (**PDTPQx(1F)-H**): M_n = 18 kg/mol, D = 1.4 (for **a**) and M_n = 63 kg/mol, D = 1.9 (for **b**).

PDTPQx(2F)

Similar to the procedure as outlined for **PDTPQx**: DTP monomer **5** (0.118 g, 0.187 mmol), Qx monomer **10c** (0.134 g, 0.187 mmol), Pd₂(dba)₃ (4.3 mg, 4.7

μmol) and $\text{P}(o\text{-tol})_3$ (5.7 mg, 19 μmol) were dissolved in 4.8 mL of dry toluene and 1.2 mL of dry DMF. The polymer was obtained as a black solid (156 mg, 94%). ^1H NMR (CDCl_3 , 400 MHz): δ = 9.50–6.10 (br, 6H), 3.68–3.34 (br, 1H), 3.15–2.70 (br, 2H), 2.50–1.90 (br, 4H), 1.90–1.60 (br, 4H), 1.50–0.20 (br, 38H); SEC (THF, 40 °C, PS standards): M_n = 22 kg/mol, D = 2.8; After prep-SEC (**PDTPQx(2F)-H**): M_n = 56 kg/mol, D = 1.8.

5.7.2 Analytical size exclusion chromatograms

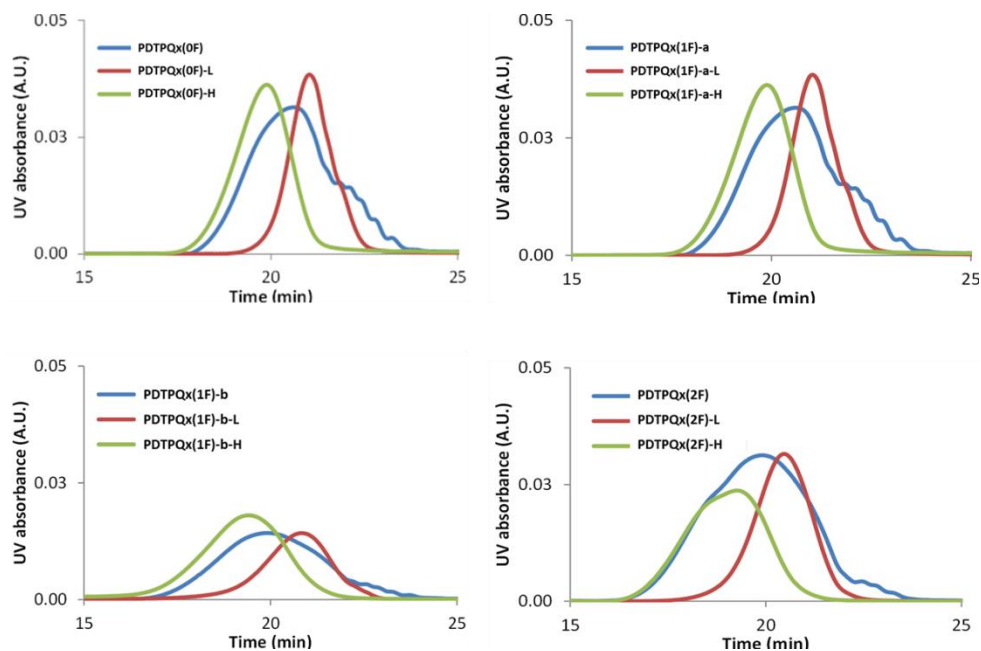


Figure S1: Analytical size exclusion chromatograms (THF, 40 °C, UV detection at 254 nm) of the crude PDTPQx copolymers (after soxhlet extractions) and their low (denoted with **-L**) and high (denoted with **-H**) molar mass fractions, as obtained after fractionation by prep-SEC (**PDTPQx**: $M_n = 12$ kg/mol, $D = 2.8$; **PDTPQx-H**: $M_n = 33$ kg/mol, $D = 1.5$; **PDTPQx(1F)-a**: $M_n = 9.9$ kg/mol, $D = 2.0$; **PDTPQx(1F)-a-H**: $M_n = 18$ kg/mol, $D = 1.4$; **PDTPQx(1F)-b**: $M_n = 20$ kg/mol, $D = 3.1$; **PDTPQx(1F)-b-H**: $M_n = 63$ kg/mol, $D = 1.9$; **PDTPQx(2F)**: $M_n = 22$ kg/mol, $D = 2.8$; **PDTPQx(2F)-H**: $M_n = 56$ kg/mol, $D = 1.8$).

5.7.3 Thermal analysis

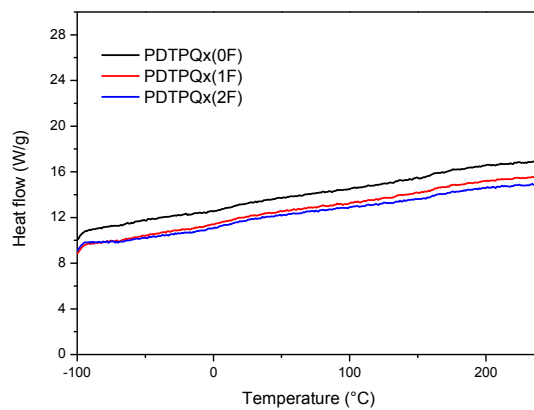


Figure S2: Rapid heat-cool calorimetry heating profiles for the PDTPQx copolymer series, revealing no visible phase transitions (curves shifted vertically for clarity).

5.7.4 Additional solar cell and mobility data

Table S1: Optimization of the polymer solar cell devices based on

PDTPQx:PC₇₁BM(1:3) blends^a

Material	Processing solvent ^b	Voc [V]	J _{sc} [mA/cm ²]	FF	Average η [%] ^c	Best η [%]
PDTPQx	CB	0.67	12.57	0.54	4.53	4.81
PDTPQx	CB + 3% CN	0.68	10.10	0.50	3.39	3.87
PDTPQx	CB + 3% DIO	0.54	2.97	0.70	1.12	1.22
PDTPQx	CF	0.62	5.42	0.39	1.30	1.40

^a Tests with a 1:1 ratio were performed as well, but best results were obtained from the 1:3 ratio. ^b CB = chlorobenzene, CN = 1-chloronaphthalene, DIO = 1,8-diiodooctane, CF = chloroform. ^c Average values over at least 4 devices.

Table S2: Optimization of the polymer solar cell devices based on

PDTPQx(1F):PC₇₁BM(1:3) blends^a

Material	Processing solvent ^b	V _{sc} [V]	J _{sc} [mA/cm ²]	FF	Average η [%] ^c	Best η [%]
PDTPQx(1F)-a	CB	0.76	6.66	0.47	2.39	2.78
PDTPQx(1F)-a	CB + 3% CN	0.71	8.88	0.37	2.31	2.45
PDTPQx(1F)-a	CB + 3% DIO	0.62	4.12	0.54	1.37	1.45
PDTPQx(1F)-a	CF + 3% CN	0.71	5.55	0.35	1.37	1.61
PDTPQx(1F)-a	CF + 10% oDCB	0.69	8.46	0.35	2.05	2.24
PDTPQx(1F)-a	oDCB	0.67	8.83	0.42	2.50	2.74
PDTPQx(1F)-a	oDCB + 3% CN	0.66	6.43	0.32	1.39	1.62
PDTPQx(1F)-a	CB:CF (2:1)	0.77	6.88	0.48	2.57	2.58
PDTPQx(1F)-b	CB	0.72	6.78	0.47	2.30	2.56
PDTPQx(1F)-b	CB + 3% DIO	0.58	7.06	0.47	1.92	2.08

^a Tests with a 1:1 ratio were performed as well, but best results were obtained from the 1:3 ratio. ^b CB = chlorobenzene, CN = 1-chloronaphthalene, DIO = 1,8-diiodooctane, CF = chloroform, oDCB = *ortho*-dichlorobenzene. ^c Average values over at least 4 devices.

Table S3: Optimization of the polymer solar cell devices based on

PDTPQx(2F):PC₇₁BM(1:3) blends^a

Material	Processing solvent ^b	V _{oc} [V]	J _{sc} [mA/cm ²]	FF	Average η [%] ^c	Best η [%]
PDTPQx(2F)	CB	0.75	4.25	0.49	1.56	1.74
PDTPQx(2F)	CB + 3% CN	0.69	4.61	0.37	1.18	1.26
PDTPQx(2F)	CB + 3% DIO	0.64	7.19	0.51	2.34	2.50
PDTPQx(2F)	CF	0.82	2.85	0.54	1.26	1.38
PDTPQx(2F)	CF + 10% oDCB	0.79	3.90	0.50	1.55	1.58
PDTPQx(2F)	CF + 3% CN	0.80	2.70	0.49	1.05	1.06
PDTPQx(2F)	oDCB ^d	/	/	/	/	/

^a Tests with a 1:1 ratio were performed as well, but best results were obtained from the 1:3 ratio. ^b CB = chlorobenzene, CN = 1-chloronaphthalene, DIO = 1,8-diiodooctane, CF = chloroform, oDCB = *ortho*-dichlorobenzene. ^c Average values over at least 4 devices. ^d No proper film attachment on the substrate.

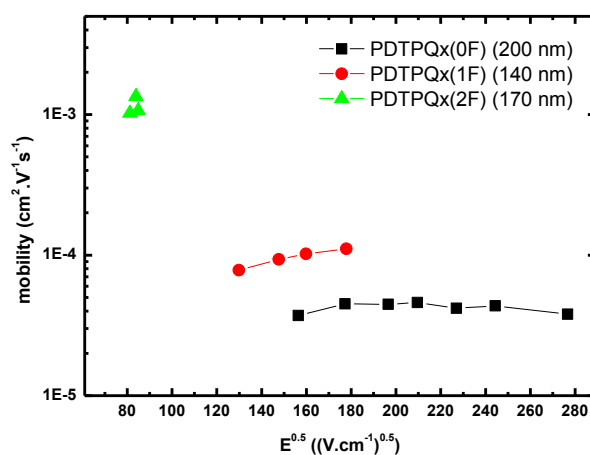
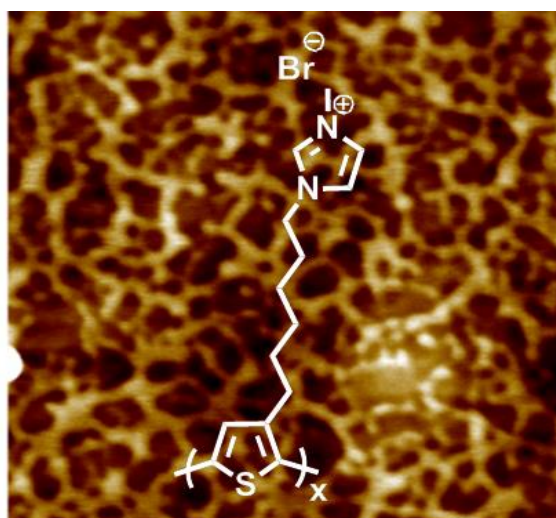


Figure S3: Photo-CELIV measurements (performed on solar cell devices) for the DTP-*alt*-quinoxaline copolymer series.

Chapter 6

Imidazolium-Substituted Polythiophenes as Efficient Electron Transport Materials Improving Photovoltaic Performance



J. Kesters, T. Ghooos, H. Penxten, J. Drijkoningen, T. Vangerven, D. M. Lyons, B. Verreet, T. Aernouts, L. Lutsen, D. Vanderzande, J. Manca, W. Maes, *Adv. Energy Mater.*, **2013**, 3, 1180.

ABSTRACT

In the field of polymer solar cells, improving photovoltaic performance has been the main driver over the past decade. To achieve high power conversion efficiencies, a plethora of new photoactive donor polymers and fullerene derivatives have been developed and blended together in bulk heterojunction active layers. Simultaneously, further optimization of the device architecture is also of major importance. In this respect, we report on the use of specific types of electron transport layers to boost the inherent I - V properties of polymer solar cell devices, resulting in a considerable gain in overall photovoltaic output. Imidazolium-substituted polythiophenes are introduced as appealing electron transport materials, outperforming the currently available analogous conjugated polyelectrolytes, mainly by an increase in short-circuit current. The molecular weight of the ionic polythiophenes has been identified as a crucial parameter influencing performance.

6.1 INTRODUCTION

The field of organic photovoltaics (OPV) has experienced a tremendous growth over the past few years. This is a direct consequence of the potential commercial value of this type of technology, exhibiting specific desirable properties such as simple preparation, novel aesthetical possibilities, reduced weight and mechanical flexibility, semi-transparency, and better performance in diffuse light, which makes OPV particularly attractive for portable or wearable electronics and building-integrated photovoltaics. Moreover, in contrast to traditional Si-based solar cells, solution-processability allows low cost large-area thin film fabrication by e.g. roll-to-roll (R2R) printing. Currently, single junction OPV power conversion efficiencies (PCEs) of up to 9.2% have been reported,^[1] and further improvements are constantly on the horizon.^[2] Up till now, the active layer materials comprising the bulk heterojunction (BHJ) have been the main focus point, with a special emphasis on low bandgap conjugated polymers and small donor molecules.^[3] However, as overall performance is determined by the entire device built-up, a closer inspection and optimization of the other cell components can also lead to noticeable improvements, e.g. better interfaces between the various layers in the solar cell stack lead to a reduction of loss-mechanisms due to an improvement of the charge extraction pathways.^[2]

At present, a number of different device architectures have been reported for BHJ polymer solar cells. Besides the standard 'sandwich' structure, inverted solar cells,^[1,4] generally leading to enhanced lifetimes, and tandem devices,^[5] in which two separate cells are stacked one upon another and connected in series or parallel (affording record efficiencies up to 10.7%), are the most effective and

widely applied architectures to date. Insertion of additional charge transporting layers has been proposed as an effective mean to further optimize device performance by diminishing detrimental factors such as leakage current, bad interface tuning, charge recombination, etc. To facilitate electron transport and collection (and block hole transport), various electron transport layers (ETLs) have been introduced at the metal/active layer (standard cell) or transparent metal oxide/active layer (inverted cell) interfaces, e.g. LiF, Cs₂CO₃, fullerene derivatives and notably conjugated polyelectrolytes (CPEs), affording remarkable improvements in device parameters (*V*_{oc}, *J*_{sc}, FF) and final PCEs.^[1,6,7] The additional layer creates a more hydrophilic surface and dipole alignment at the interface, resulting in a higher built-in potential (and hence *V*_{oc}), while electron transport and collection are facilitated (mainly causing an increase in FF) by affecting the effective work function of the cathode, providing better energy alignment and minimizing contact resistance.^[6] Hydrophilic polymers are particularly attractive as they allow low-temperature solution processing and generally afford air-stable films. Mainly inspired by parallel efforts in the field of polymer light-emitting diodes (PLEDs), the number of CPE structures explored in OPV to date is rather limited and CPE synthesis has only been exploited for a limited number of conjugated polymers. Most of the ultrathin CPE interlayers that have been reported are thiophene- or fluorene-based (co)polymers with appended polar amines or ionic ammonium moieties.^[6,7] Moreover, the influence of the chemical nature of the CPE and the underlying BHJ blend is still poorly understood, leaving lots of opportunities for improvements by interdisciplinary work of synthetic material chemists and device physicists.

In this work, we report on the implementation of a specific type of electron transport material, i.e. a CPE based on an amphiphilic polythiophene with appended ionic liquid-like polar groups, to boost the internal cell parameters of devices based on PCDTBT:PC₇₁BM and PCPDT-DTTzTz:PC₇₁BM photoactive layers (Figure 1).^[8] The addition of this CPE layer between the active layer and the electron collecting Al cathode (replacing the air-sensitive Ca layer) has a positive influence on the internal voltage as well as on the leakage current, and an efficiency increase of 20% (up to an average PCE of 6.2% for PCDTBT:PC₇₁BM devices) was achieved with one of the ETL materials. Upon comparison with an analogous polythiophene-based CPE recently reported by Bazan *et al.*^[6b] or the widely used PFN,^[9] the novel interlayer material is more effective. Additionally, the molecular weight of the hydrophilic polymer was identified as an important factor determining the overall performance.

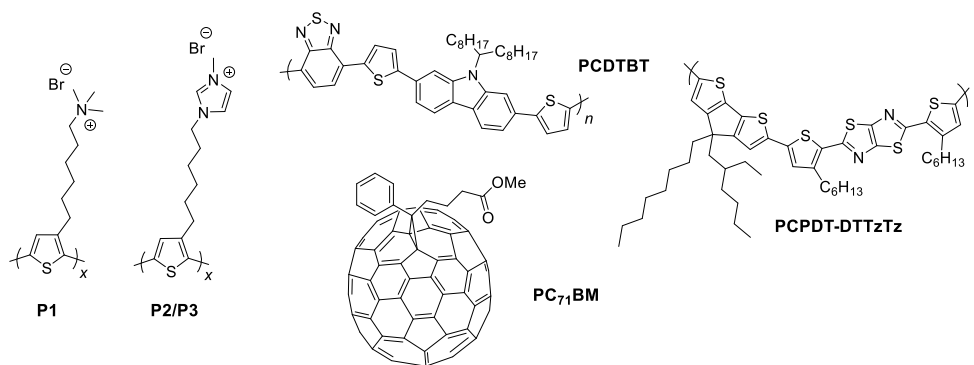


Figure 1: Trimethylamine-functionalized polythiophene **P1**, imidazole-functionalized polythiophenes **P2** and **P3**, the PCDTBT and PCPDT-DTTzTz donor polymers, and PC₇₁BM.

6.2 RESULTS AND DISCUSSION

To render conjugated polymers soluble in more environmentally benign solvents (rather than chlorobenzene etc.), which are highly desirable toward high-throughput OPV solution processing, several synthetic strategies can be adopted. Introduction of ionic moieties as side chains on the polymer backbone affords CPEs, applicable either as active light-harvesting materials or as interlayer materials in the solar cell stack. Ongoing synthetic efforts have been directed toward the preparation of a wide range of cationic polythiophene (co)polymers with appended 'ionic liquid-like' *N*-methylimidazole moieties through substitution on the bromohexyl-substituted precursor polymers and considerably facilitated by employing microwave heating.^[10,11] The versatility of the GRIM polymerization route^[12] allows straightforward tuning of the molecular weight, the built-in monomer ratio, the side chain pattern and the polymer architecture (random vs block copolymers), combined with narrow polydispersities and high regioregularities, while the counter ion can be readily exchanged on the final polymer stage.^[10]

For this interlayer work, one particular ionic imidazolium-functionalized polythiophene homopolymer (with Br⁻ counter ion) was initially selected. Two batches with varying molecular weight (**P2** and **P3**, with $M_n = 11.2$ kDa and 32.6 kDa, respectively, for the non-ionic precursor polymers) and narrow polydispersity ($D = 1.6$) were prepared (see Supporting Information). These materials were first evaluated as interlayer materials on top of an active layer comprising of PCDTBT, one of the current state-of-the-art low bandgap donor polymers,^[13] and PC₇₁BM (Figure 1). The PCDTBT:PC₇₁BM combination combines

high efficiency and long operating lifetimes. To enable comparison with the ETL material introduced by Bazan *et al.*,^[6b] trimethylamine-functionalized polythiophene **P1**^[14] was prepared as well ($M_n = 32.6$ kDa) as a reference material (Figure 1). Additionally, PFN was also included as an additional ETL material in the device set. For ionic polythiophenes **P1–P3**, complete functionalization and material purity were confirmed by ¹H NMR (Figure S1).^[10] The optical absorption spectra show typical polythiophene features, with a small red shift (in film) for **P2** and **P3** ($\lambda_{max} = 504$ nm) compared to **P1** ($\lambda_{max} = 482$ nm) (Table S1). 'P3HT-like' electrochemical behavior was observed for all three materials by cyclic voltammetry (Table S1), the main difference being located at the reduction onset. The presence of the ionic groups in these hydrophilic polymers makes them soluble in alcohols, hence enabling processing from more benign non-chlorinated solvents. Moreover, as orthogonal solvents are applied for the photoactive layer and CPE film, integrity problems due to redissolution of the underlying BHJ layer are readily avoided.

For the evaluation of the ETL features of the novel ionic polythiophenes, the standard solar cell stack glass/ITO/PEDOT-PSS/polymer:PC₇₁BM/CPE/Al was employed.^[6b] In a first experiment, the optimal concentration of the CPE materials (in methanol) was investigated for PCDTBT:PC₇₁BM active layers (data not shown). The optimum was found around 0.02 w/v% and hence all further experiments were performed using this concentration.^[6b] Next, the devices with interfacial charged polymer layers were compared to cells with traditional Ca/Al electrodes (Table 1). Ca is commonly applied as a low work function metal to optimize electrical contact but suffers from high air-sensitivity and is therefore increasingly replaced by solution-processed metal oxides (ZnO, TiO_x). The

overall increase in PCE due to the ETL materials could mainly be attributed to an increase in short-circuit current density (J_{sc}), with only minor contributions from open-circuit voltage (V_{oc}) and fill factor (FF) (Figure 2, Table 1). Comparing the three interlayer materials, the novel high- M_n ionic polythiophene **P3** afforded the best results, with a top PCE of 6.7% (average 6.2%). Compared to the reference ETL material **P1**, derived from the same precursor polymer batch, there is an increase in PCE of $\sim 0.2\%$ (both for the best and average PCE). In comparison with the device utilizing Ca, J_{sc} increased from 10.7 mA cm^{-2} to 12.1 mA cm^{-2} , which is an increase of roughly 20%. The increase in J_{sc} was confirmed by extracting the currents from external quantum efficiency (EQE) measurements (Figure S2, Table S2). The enhanced current can partly be explained by increased reflection upon removing the Ca layer (which shows some 'parasitic' absorption; Figure S3).^[15] The addition of the CPE layers seems to provide an optimal balance between improved ohmic contact and mirror effects.

Table 1: Photovoltaic performance of PCDTBT-based BHJ solar cell devices with and without the addition of CPE layers.^{a)}

Layer Sequence	V_{oc} [V]	J_{sc} [mA cm^{-2}] ^{b)}	FF	Average η [%]	Best η [%]
.../PCDTBT:PC ₇₁ BM/Al	0.73	11.36	0.41	3.39 ± 0.36	3.82
.../PCDTBT:PC ₇₁ BM/Ca/Al	0.87	10.66	0.57	5.23 ± 0.33	5.71
.../PCDTBT:PC ₇₁ BM/ P1 /Al	0.88	11.82	0.58	6.03 ± 0.46	6.48
.../PCDTBT:PC ₇₁ BM/ P2 /Al	0.84	11.67	0.55	5.32 ± 0.24	5.57
.../PCDTBT:PC ₇₁ BM/ P3 /Al	0.87	12.05	0.59	6.22 ± 0.43	6.69
.../PCDTBT:PC ₇₁ BM/PFN/Al	0.88	11.84	0.58	5.96 ± 0.42	6.33
.../PCDTBT:PC ₇₁ BM/MeOH/Al	0.88	11.68	0.57	5.81 ± 0.17	5.99

^{a)} Stack: glass/ITO/PEDOT-PSS/PCDTBT:PC₇₁BM/X/Al with X = Ca or CPE.

^{b)} Uncorrected data.

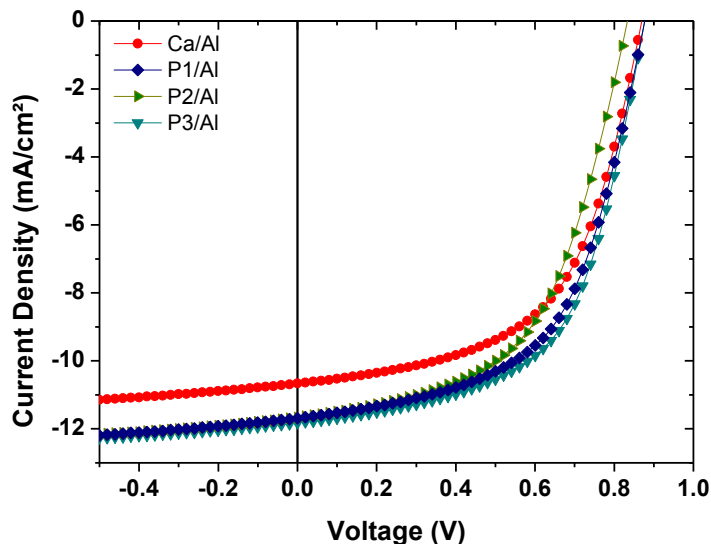


Figure 2: *J-V* curves under illumination of PCDTBT-based BHJ photovoltaic devices with and without additional CPE layers.

Utilizing the same ionic polythiophene material with a lower M_n (**P2**) resulted in a clearly lower performance, indicating that the efficiency of the interlayer is dependent on the molecular weight of the interfacial polymer. Ionic polythiophene **P3** also showed a noticeable improvement when compared with the widely used PFN interlayer material (on average 5.96% vs. 6.22%). Finally, a reference device for which pure methanol was spin-coated on top of the active layer was produced (Table 1, indicated as .../MeOH/Al, Figure S4) to investigate whether the beneficial factor leading to improved device performance could not be reproduced by the solvent only. From the data in Table 1 we can observe a noticeable improvement with respect to the reference device utilizing the traditional Ca/Al electrode. This observation has been made before, leading to the statement that the methanol treatment results in the formation of an interface dipole between the active layer and the metal layer.^[6,16] The

incorporation of the CPE layers did, however, result in further improvements in J_{sc} , resulting in higher overall PCEs. This suggests that, on top of the formation of an interface dipole, the presence of the CPE layer leads to additional beneficial factors improving charge extraction.

In a follow-up experiment, the highest performing ETL material **P3** was also tested on top of an active layer comprising of a different low bandgap polymer, i.e. PCPDT-DTTzTz.^[10] As can clearly be seen from the data in Table 2 (and the J - V curves in Figure S5), the results confirmed the beneficial effect of the novel CPE layer, with an increase in J_{sc} and FF leading to a similar overall PCE improvement. It has to be noted here that the efficiency obtained for the reference device (4.78% best, 4.50% average) is the highest PCE reported for this donor polymer (4.03% before).

Table 2: Photovoltaic performance of PCPDT-DTTzTz-based BHJ solar cell devices with and without the addition of CPE layers.^{a)}

Layer Sequence	Voc [V]	J_{sc} [mA cm ⁻²] ^{b)}	FF	Average η [%]	Best η [%]
.../PCPDT-DTTzTz:PC ₇₁ BM/Ca/Al	0.68	12.2	0.54	4.50 ± 0.20	4.78
.../PCPDT-DTTzTz:PC ₇₁ BM/ P3 /Al	0.68	12.9	0.55	4.86 ± 0.40	5.43

^{a)} Stack: glass/ITO/PEDOT-PSS/PCPDT-DTTzTz:PC₇₁BM/X/Al with X = Ca or CPE. ^{b)}

Uncorrected data.

To get a more clear view on the potential loss mechanisms in the devices, dark J - V curves were measured, revealing information on the series and shunt resistances (R_s and R_{sh}). Figure 3 shows the dark curves for the best performing CPE material **P3** and for the reference devices with solely Al and Ca/Al as top electrodes. Utilizing **P3** as a CPE resulted in a strong increase of R_{sh} in comparison to the two reference devices. As for R_s , there was a slight

improvement when comparing the CPE-containing device with the Ca/Al reference. However, compared with the Al reference, R_s was much lower. Moreover, in the negative half of the x-axis, the photovoltaic device with a **P3** ETL layer showed much less leakage current, confirming the positive influence of the interlayer on the performance of the solar cell device.

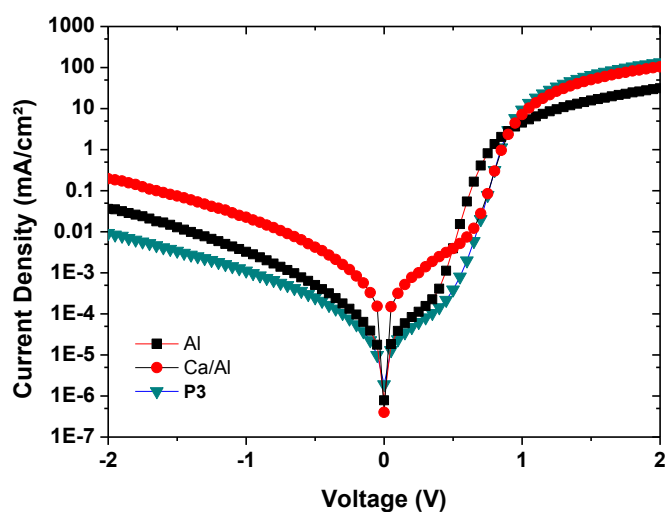


Figure 3: J - V curves of PCDTBT-based BHJ photovoltaic devices under dark conditions with and without additional CPE layers.

Atomic force microscopy (AFM) measurements were performed to investigate the interlayers when deposited on top of the PCDTBT:PC₇₁BM active layer (Figure 4). The roughness in all cases increased compared to non-covered PCDTBT:PC₇₁BM films. The ETL materials **P1–P3** did not completely cover the active layer surface. The calculated surface coverage seemed to be similar for all ETLs (~55%), but the observed morphology was noticeably different. Figure 4a–c shows the topography, whereas Figure 4d–f reveals the adhesion images, reflecting the ‘sticking’ of the AFM tip to the surface (additional images can be found in Figure S6 and S7). The topography images (a–c) show the presence of

rather large 'holes' (average diameter 110 nm) for **P1**, whereas for **P3** a much finer and more random network is formed. From the adhesion images (d-f) it can be seen that the regions with low adhesion (dark spots) correspond with the higher topography features, and the regions with high adhesion (bright spots) correspond with the lower features on the height image. From these observations, it looks like the active layer is not completely covered and is directly exposed by the presence of holes in the ETL material. The density of these holes can possibly be correlated to the final device performance.

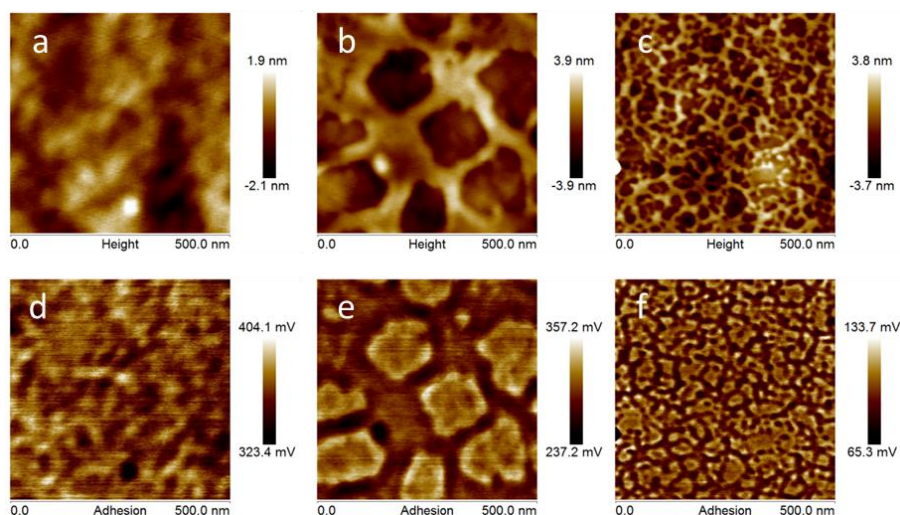


Figure 4: AFM (top row: topography; bottom row: adhesion) images (500x500 nm²) of layer stacks with and without additional CPE materials: a,d) PCDTBT:PC₇₁BM, b,e) PCDTBT:PC₇₁BM/**P1**, c,f) PCDTBT:PC₇₁BM/**P3**.

The presented study confirms that high-efficiency polymer solar cells can be prepared by insertion of appropriate ionic polymer films at the electrode/active layer interface. Interface engineering provides a simple pathway to BHJ OPV efficiency improvement, but its full potential has yet to be explored. The

imidazole-substituted ionic polythiophene introduced here combines a number of features that favor this ETL material above most competitive polymer and/or fullerene materials. It is a simple polythiophene derivative, prepared via the straightforward GRIM polymerization method – providing structural versatility and scalability – and its stability and alcohol solubility enable easy processing from environmentally acceptable solvents. The material also seems to be applicable to different polymer:fullerene active layers. Moreover, by tuning the chemical structure of the ionic polythiophene, further improvement is conceivable, e.g. by varying the density and organization of ionic groups at the surface.

6.3 EXPERIMENTAL SECTION

Synthesis of conjugated polyelectrolytes: Trimethylamine-functionalized polythiophene **P1** (**P3(TMA)HT-Br**) (Figure 1), used as a reference interlayer material, was prepared by a literature procedure as reported by Bazan *et al.*^[14] Imidazolium-substituted polythiophenes **P2** and **P3** were prepared according to a recently reported method.^[10] Details on the synthetic procedures and characterization data are provided in the Supporting Information.

Device fabrication: The reference BHJ solar cells were constructed using the traditional glass/ITO/PEDOT-PSS/active layer/Ca/Al architecture. To investigate the impact of the CPE layers, the Ca layer was replaced by a CPE. A control device without CPE or Ca layer was included as an additional reference. Before device processing, the indium tin oxide (ITO, Kintec, 100 nm, 20 Ohm/sq) containing substrates were cleaned using soap, demineralized water, acetone, isopropanol and a UV/O₃ treatment. Subsequently, the ITO substrates were covered by a ~30 nm thick layer of PEDOT-PSS [poly(3,4-ethylenedioxythiophene)-poly(styrenesulfonic acid), Heraeus Clevios] by spin-coating. Further processing was performed under nitrogen atmosphere in a glove box, starting off with an annealing step at 130 °C for 15 min to remove any residual water. The PCDTBT (poly[[9-(1-octylnonyl)-9*H*-carbazole-2,7-diyl]-2,5-thiophenediyl-2,1,3-benzothiadiazole-4,7-diyl-2,5-thiophene-diyl]) donor polymer was obtained from SolarisChem ($M_n = 79$ kDa, $D = 2.4$), and used as received. PCPDT-DTTzTz (poly([4-(2'-ethylhexyl)-4-octyl-4*H*-cyclopenta[2,1-*b*:3,4-*b'*]dithiophene-2,6-diyl]-*alt*-[2,5-di(3'-hexylthiophen-2'-yl)thiazolo[5,4-*d*]thiazole-5',5''-diyl]) was synthesized according to a previously reported

method.^[10] The active layer consisting of PCDTBT:PC₇₁BM ([6,6]-phenyl C₇₁ butyric acid methyl ester, Solenne) was spin-coated with a thickness of ~65 nm (as confirmed by DEKTAK). Blend solutions were prepared in a 1:4 ratio, with PCDTBT concentrations of 5 mg/mL, using chlorobenzene:1,2-dichlorobenzene (1:3) as a solvent mixture.^[6b] For the devices containing PCPDT-DTTzTz:PC₇₁BM as the active layer, a thickness of ~70 nm was obtained through spin-coating. Blend solutions were prepared in a 1:3 ratio, with PCPDT-DTTzTz concentrations of 5 mg/mL, using chlorobenzene as a solvent.^[10] The active layer deposition step was followed by spin-coating of the CPE interlayers, aiming for thicknesses of ~5-10 nm. The CPE solutions were prepared in concentrations of 0.01, 0.02 and 0.04 w/v% in methanol. Finally, the devices were finished off with Al as the top electrode, with a thickness of ~80 nm. Thicknesses of the top electrodes of the reference device containing Ca/Al were ~20 and 80 nm, respectively. In the standard cell configuration, an active area of 25 mm² was obtained. To provide a better assessment of the value of the in-house prepared CPE's, the more commonly used interlayer material PFN (poly[(9,9-bis(3'-(N,N-dimethylamino)propyl)-2,7-fluorene)]) was used as well.

Device characterization: The PCEs of the BHJ solar cells were measured using a Newport class A solar simulator (model 91195A) calibrated with a silicon solar cell to give an AM 1.5g spectrum. For AFM imaging, a Bruker Multimode 8 AFM was used in PeakForce tapping mode, employing ScanAsyst. The images were produced with a silicon tip on a nitride lever with a spring constant of 4 N m⁻¹.

EQE and reflection measurements: A commercial set-up (Bentham) was used to measure the EQE. Light from a Xe arc lamp (300–670 nm) and a quartz halogen lamp (670–900 nm) is chopped, coupled into a monochromator and aimed at

the device. The resulting current is sent through a Bentham477 current pre-amplifier, then arriving in the Bentham485 lock-in amplifier. Calibration is done with a certificated Si cell. The integration of these EQEs over the solar spectrum is listed in Table S2 as J_{EQE} . The same optics and measurement setup is used with a DTR6 integrating sphere to determine the reflection.

6.4 CONCLUSIONS

In conclusion, we have shown that the device performance of polymer solar cells can be remarkably improved by incorporation of a thin electron transport layer based on an imidazolium-substituted ionic polythiophene (20% increase in PCE up to an average value of 6.2% for PCDTBT:PC₇₁BM). The beneficial effect is notably higher than for previously reported materials such as an analogous trimethylamine-functionalized ionic polythiophene or PFN. Best results were obtained for the highest molecular weight ETL material, pointing to an important influence of polymer chain length on ETL performance. Remaining questions on the exact influence of polymer molecular weight (and its relation to active layer coverage) and the polythiophene backbone need to be addressed in future work.

6.5 REFERENCES

- [1] Z. He, C. Zhong, S. Su, M. Xu, H. Wu, Y. Cao, *Nat. Photonics* **2012**, *6*, 591.
- [2] a) C. J. Brabec, S. Gowrisanker, J. J. M. Halls, D. Laird, S. Jia, S. P. Williams, *Adv. Mater.* **2010**, *22*, 3839; b) J. Nelson, *Mater. Today* **2011**, *14*, 462; c) L. J. A. Koster, S. E. Shaheen, J. C. Hummelen, *Adv. Energy Mater.* **2012**, *2*, 1246; d) P. Kumar, S. Chand, *Prog. Photovoltaics*, **2012**, *20*, 377; e) G. Li, R. Zhu, Y. Yang, *Nat. Photonics* **2012**, *6*, 153; f) M. Jørgensen, K. Norrman, S. Gevorgyan, T. Tromholt, B. Andreasen, F. C. Krebs, *Adv. Mater.* **2012**, *24*, 580.
- [3] a) A. J. Heeger, *Chem. Soc. Rev.* **2010**, *39*, 2354; b) J. L. Delgado, P.-A. Bouit, S. Filippone, M. A. Herranz, N. Martín, *Chem. Commun.* **2010**, *46*, 4853; c) P.-L. T. Boudreault, A. Najari, M. Leclerc, *Chem. Mater.* **2011**, *23*, 456; d) A. Facchetti, *Chem. Mater.* **2011**, *23*, 733; e) L. Bian, E. Zhu, J. Tang, W. Tang, F. Zhang, *Prog. Polym. Sci.* **2012**, *37*, 1292; f) H. Zhou, L. Yang, W. You, *Macromolecules* **2012**, *45*, 607; g) A. Mishra, P. Bäuerle, *Angew. Chem. Int. Ed.* **2012**, *51*, 2020.
- [4] a) S. R. Ferreira, R. J. Davis, Y. Lee, P. Lu, J. W. P. Hsu, *Org. Electron.* **2011**, *12*, 1258; b) Y. Sun, C. J. Takacs, S. R. Cowan, J. H. Seo, X. Gong, A. Roy, A. J. Heeger, *Adv. Mater.* **2011**, *23*, 2226; c) F. Zhang, X. Xu, W. Tang, J. Zhang, Z. Zhuo, J. Wang, J. Wang, X. Zheng, Y. Wang, *Sol. Energy Mater. Sol. Cells* **2011**, *95*, 1785; d) J. Liu, S. Shao, G. Fang, B. Meng, Z. Xie, L. Wang, *Adv. Mater.* **2012**, *24*, 2774.
- [5] a) S. Sista, Z. Hong, L.-M. Chen, Y. Yang, *Energy Environ. Sci.* **2011**, *4*, 1606; b) L. Dou, J. You, J. Yang, C. Chen, Y. He, S. Murase, T. Moriarty, K.

Emery, G. Li, Y. Yang, *Nat. Photonics* **2012**, *6*, 356; c) V. S. Gevaerts, A. Furlan, M. M. Wienk, M. Turbiez, R. A. J. Janssen, *Adv. Mater.* **2012**, *24*, 2130. d) S. Kouijzer, S. Esiner, C. H. Frijters, M. Turbiez, M. M. Wienk, R. A. J. Janssen, *Adv. Energy Mater.* **2012**, *2*, 945.

[6] a) F. Huang, H. Wu, Y. Cao, *Chem. Soc. Rev.* **2010**, *39*, 2500; b) J. H. Seo, A. Gutacker, Y. Sun, H. Wu, F. Huang, Y. Cao, U. Scherf, A. J. Heeger, G. C. Bazan, *J. Am. Chem. Soc.* **2011**, *133*, 8416; c) H. Choi, J. S. Park, E. Jeong, G.-H. Kim, B. R. Lee, S. O. Kim, M. H. Song, H. Y. Woo, J. Y. Kim, *Adv. Mater.* **2011**, *23*, 2759; d) E. Ratcliff, B. Zacher, N. R. Armstrong, *J. Phys. Chem. Lett.* **2011**, *2*, 1337; e) H.-L. Yip, A. K.-Y. Jen, *Energy Environ. Sci.* **2012**, *5*, 5994; f) Y. Chen, Z. Jiang, M. Gao, S. E. Watkins, P. Lu, H. Wang, X. Chen, *Appl. Phys. Lett.* **2012**, *100*, 203304; g) T. Yang, M. Wang, C. Duan, X. Hu, L. Huang, J. Peng, F. Huang, X. Gong, *Energy Environ. Sci.* **2012**, *5*, 8208; h) C. Duan, C. Zhong, C. Liu, F. Huang, Y. Cao, *Chem. Mater.* **2012**, *24*, 1682; i) L. Ying, P. Zalar, S. D. Collins, Z. Chen, A. A. Mikhailovsky, T.-Q. Nguyen, G. C. Bazan, *Adv. Mater.* **2012**, *24*, 6496.

[7] a) A. Duarte, K. -Y. Pu, B. Liu, G. C. Bazan, *Chem. Mater.* **2011**, *23*, 501; b) J. Fang, B. H. Wallikewitz, F. Gao, G. Tu, C. Müller, G. Pace, R. H. Friend, W. T. S. Huck, *J. Am. Chem. Soc.* **2011**, *133*, 683; c) Y. Zhou, C. Fuentes-Hernandez, J. Shim, J. Meyer, A. J. Giordano, H. Li, P. Winget, T. Papadopoulos, H. Cheun, J. Kim, M. Fenoll, A. Dindar, W. Haske, E. Najafabadi, T. M. Khan, H. Sojoudi, S. Barlow, S. Graham, J.-L. Brédas, S. R. Marder, A. Kahn, B. Kippelen, *Science* **2012**, *336*, 327.

[8] S. Van Mierloo, A. Hadipour, M. Spijkman, N. Van den Brande, B. Ruttens, J. Kesters, J. D'Haen, G. Van Assche, D. M. de Leeuw, T. Aernouts, J. Manca, L. Lutsen, D. J. Vanderzande, W. Maes, *Chem. Mater.* **2012**, *24*, 587.

- [9] Z. He, C. Zhong, X. Huang, W.-Y. Wong, H. Wu, L. Chen, S. Su, Y. Cao, *Adv. Mater.* **2011**, *23*, 4636.
- [10] T. Ghoo, O. Malinkiewicz, L. Lutsen, D. Vanderzande, H. J. Bolink, W. Maes, *RSC Adv.* **2013**, *3*, 25197.
- [11] a) D. Bondarev, J. Zedník, *J. Polym. Sci., Part A: Polym. Chem.* **2010**, *48*, 3073; b) M. Knaapila, R. C. Evans, A. Gutacker, V. M. Garamus, N. K. Székely, U. Scherf, H. D. Burrows, *Soft Matter* **2011**, *7*, 6863.
- [12] a) R. S. Loewe, P. C. Ewbank, J. Liu, L. Zhai, R. D. McCullough, *Macromolecules* **2001**, *34*, 4324; b) L. Zhai, R. L. Pilston, K. L. Zaiger, K. K. Stokes, R. D. McCullough, *Macromolecules* **2003**, *36*, 61; c) M. C. Iovu, E. E. Sheina, R. R. Gil, R. D. McCullough, *Macromolecules* **2005**, *38*, 8649.
- [13] a) N. Blouin, A. Michaud, M. Leclerc, *Adv. Mater.* **2007**, *19*, 2295; b) N. Blouin, A. Michaud, D. Gendron, S. Wakim, E. Blair, R. Neagu-Plesu, M. Belletête, G. Durocher, Y. Tao, M. Leclerc, *J. Am. Chem. Soc.* **2008**, *130*, 732; c) S. H. Park, A. Roy, S. Beaupré, S. Cho, N. Coates, J. S. Moon, D. Moses, M. Leclerc, K. Lee, A. J. Heeger, *Nat. Photonics* **2009**, *3*, 297; d) C. H. Peters, I. T. Sachs-Quintana, J. P. Kastrop, S. Beaupré, M. Leclerc, M. D. McGehee, *Adv. Energy Mater.* **2011**, *1*, 491.
- [14] S. Wang, G. C. Bazan, *Chem. Commun.* **2004**, 2508.
- [15] A. Hadipour, D. Cheyng, P. Heremans, B. P. Rand, *Adv. Energy Mater.* **2011**, *1*, 930.
- [16] Q. Wang, Y. Zhou, H. Zheng, J. Shi, C. Li, C. Q. Su, L. Wang, C. Luo, D. Hu, J. Pei, J. Wang, J. Peng, Y. Cao, *Org. Electron.* **2011**, *12*, 1858.

6.6 ACKNOWLEDGEMENTS

The authors acknowledge Hasselt University for a PhD fellowship to J. K., and BELSPO in the frame of the IAP P6/27 and IAP 7/05 networks. The reported activity is partly supported by the European Community Framework Program 7 - Large-scale integrating project - ORION ("Ordered Inorganic-Organic Hybrids Using Ionic Liquids For Emerging Applications", contract n° CP-IP 229036-2) and by the project ORGANEXT (EMR. INT4-1.2.-2009-04/054), selected in the frame of the operational program INTERREG IV-A Euregio Maas-Rijn.

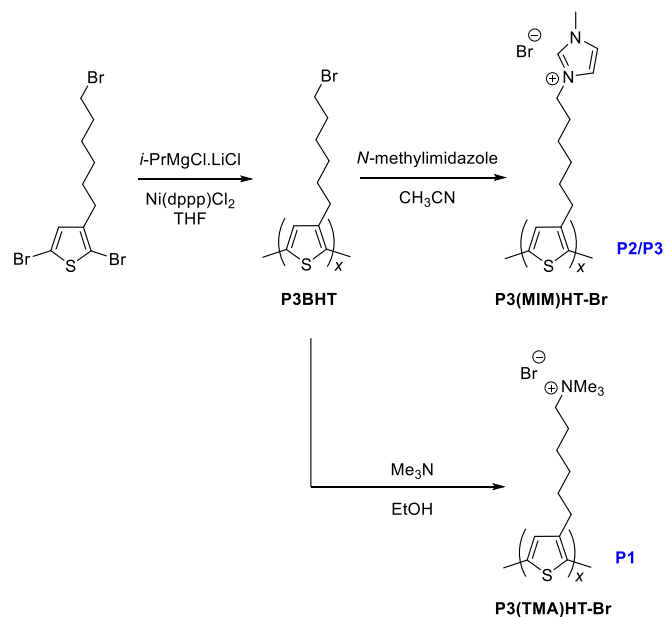
6.7 SUPPORTING INFORMATION

6.7.1 CPE synthesis and characterization data

General experimental procedures

Unless stated otherwise, all reagents and chemicals were obtained from commercial sources and used without further purification. Tetrahydrofuran (THF) was dried using an MBraun MB-SPS 800 solvent purification system. NMR chemical shifts (δ , in ppm) were determined relative to the residual ^1H absorption of CHCl_3 (7.26 ppm) or the ^{13}C resonance shift of CDCl_3 (77.16 ppm). Analysis of the molecular weights and molecular weight distributions of the polymer samples was performed on a Tosoh EcoSEC System, comprising of an autosampler, a PSS guard column SDV (50 x 7.5 mm), followed by three PSS SDV analytical linear XL columns (5 μm , 300 x 7.5 mm), and a differential refractive index (Tosoh EcoSEC RI) and UV detector using THF as the eluent at 40 °C with a flow rate of 1.0 mL min^{-1} . The SEC system was calibrated using linear narrow polystyrene standards ranging from 474 to 7.5×10^6 g mol^{-1} ($K = 14.1 \times 10^{-5}$ dL g^{-1} and $\alpha = 0.70$). Microwave synthesis was performed using a CEM Discover SP synthesis platform. Optical absorption measurements were performed on a Cary500 UV-Vis-NIR instrument from Agilent. The optical bandgap was calculated from the intersection between the X-axis and the tangent line to the (film) absorption spectrum at the low energy side. Electrochemical measurements were performed with an Eco Chemie Autolab PGSTAT 30 potentiostat/galvanostat using a three-electrode microcell [Ag/AgNO₃ reference electrode (silver wire/0.01 M AgNO₃/0.1 M NBu₄PF₆/MeCN); Pt counter electrode; Pt working electrode]. Freshly distilled anhydrous MeCN containing 0.1 M NBu₄PF₆ was used as the electrolyte. To

prevent air from entering the system, solutions were degassed with argon prior to each measurement and experiments were carried out under a curtain of argon. Films of the polymers on the working electrode were prepared by dipping the electrode in the polymer solution (solvent details can be found in Table S1) and waiting until the solvent had evaporated. All films were prepared in air. Cyclic voltammograms were recorded at a scan rate of 100 to 300 mV s^{-1} . The HOMO and LUMO energy levels were calculated from the onset oxidation and the onset reduction potential, respectively, and by assuming that the energy level of ferrocene/ferrocenium (Fc/Fc^+) has a value of -4.98 eV below the vacuum level.



Scheme S1: Synthesis of ionic polythiophenes **P1–P3**.

Poly[3-(6-bromohexyl)thiophene] (P3BHT) precursor polymers^[1]

The monomer, 2,5-dibromo-3-(6-bromohexyl)thiophene^[1,2] (0.500 g, 1.2 mmol), was added to a flame-dried three-neck flask and dissolved in dry THF (15 mL). The reaction mixture was put under inert atmosphere and cooled to 0 °C. An *i*-PrMgCl.LiCl solution (1.3 M in THF, 0.923 mL, 1.2 mmol, 1 equiv) was added and the mixture was stirred for 30 min at 0 °C. To start the polymerization, 0.8 mol% of Ni(dppp)Cl₂ (5 mg, 0.01 mmol) was added and the mixture was stirred for 2 h at 40 °C and 12 h at room temperature. The polymer was precipitated into an ice-cold HCl/MeOH (5%) mixture filtered off on a PTFE membrane (47 mm/0.45 μm). The polymer was purified using Soxhlet extraction for 24 h with methanol, *n*-hexane and chloroform, respectively. After evaporation of the solvent, the residue was redissolved in chloroform and precipitated again from methanol, filtered, washed with methanol and dried, affording high-*M_n* polythiophene precursor **P3BHT-HMn** as a black powder (0.141 g, 48%). ¹H NMR (300 MHz, CDCl₃, δ): 6.96 (s, 1H), 3.41 (t, *J* = 6.7 Hz, 2H), 2.81 (t, *J* = 7.3 Hz, 2H), 1.88 (q, *J* = 6.8 Hz, 2H), 1.71 (br, 2H), 1.56–1.41 (m, 4H); UV-vis (CHCl₃): λ_{max} = 447 nm; SEC (THF, PS standards): *M_n* = 3.2 × 10⁴ g mol⁻¹, *M_w* = 5.1 × 10⁴ g mol⁻¹, *D* = 1.6.

When 1.6 mol% of Ni(dppp)Cl₂ catalyst (10 mg, 0.02 mmol) was added in the same polymerization procedure, a lower molecular weight precursor polymer **P3BHT-LMn** was obtained (0.102 g, 34%). ¹H NMR (300 MHz, CDCl₃, δ): 6.96 (s, 1H), 3.41 (t, *J* = 6.9 Hz, 2H), 2.80 (t, *J* = 8.2 Hz, 2H), 1.88 (br, 2H), 1.71 (br, 2H), 1.58–1.38 (m, 4H); UV-vis (CHCl₃): λ_{max} = 447 nm; SEC (THF, PS standards): *M_n* = 1.1 × 10⁴ g mol⁻¹, *M_w* = 1.8 × 10⁴ g mol⁻¹, *D* = 1.6.

[1] S. Miyanishi, K. Tajima, K. Hashimoto, *Macromolecules* **2009**, *42*, 1610.

[2] P. Bäuerle, F. Würthner, S. Heid, *Angew. Chem. Int. Ed.* **1990**, *29*, 419

Polymer functionalization with trimethylamine: poly[3-(6-trimethylammoniumhexyl)-thiophene] P3(TMA)HT-Br (P1)

P3BHT-HMn (0.040 g) was suspended in a solution of trimethylamine in EtOH (4.2 M, 2 mL) and added to a 10 mL microwave vial, which was then filled with Ar and closed. The reaction mixture was heated in the microwave at 100 °C for 3 h (with maximum power of 200 W and maximum pressure of 250 psi). After cooling down, the dark purple and viscous reaction mixture was added dropwise to Et₂O and a dark precipitate was obtained. The precipitated polymer was filtered off using a PTFE membrane (47 mm/0.45 μm) and dried carefully, affording **P3(TMA)HT-HMn** or **P1** as a purple-black powder (0.049 g, 99%). ¹H NMR (300 MHz, DMSO-*d*₆, δ): 7.25 (s, 1H), 3.09 (s, 9H), 2.81 (br, 2H), 1.70 (br, 4H), 1.55–1.21 (m, 4H) (2 protons are hidden under the H₂O signal); UV-vis (MeOH): λ_{max} = 443 nm.

Polymer functionalization with N-methylimidazole: P3(MIM)HT-Br (P2/P3)

P3BHT-HMn (0.086 g) was suspended in acetonitrile (1 mL) in a 10 mL microwave vial and *N*-methylimidazole (1 mL) was added. The vial was filled with argon and closed. The reaction mixture was heated in the microwave at 100 °C for 3 h (maximum power 200 W, maximum pressure 250 psi). After cooling down, the reaction mixture was added dropwise to Et₂O and a dark precipitate was obtained. The precipitated polymer was filtered off using a PTFE membrane (47 mm/0.45 μm) and (freeze-)dried carefully, affording **P3(MIM)HT-Br-HMn** or **P3** as a purple-black powder (0.109 g, 95%). ¹H NMR (300 MHz, DMSO-*d*₆, δ): 9.30 (s, 1H), 7.83 (s, 1H), 7.72 (s, 1H), 7.18 (s, 1H), 4.18 (br, 2H), 3.84 (s,

3H), 2.76 (br, 2H), 1.79 (br, 2H), 1.68–1.55 (m, 2H), 1.44–1.22 (m, 4H); UV-vis (MeOH): $\lambda_{\text{max}} = 443 \text{ nm}$.

P3BHT-LMn (0.090 g) was reacted in the same way, affording **P3(MIM)HT-Br-LMn** or **P2** as a purple-black powder (0.108 g, 94%). ^1H NMR (300 MHz, DMSO- d_6 , δ): 9.39 (s, 1H), 7.85 (s, 1H), 7.75 (s, 1H), 7.21 (s, 1H), 4.21 (br, 2H), 3.87 (s, 3H), 2.78 (br, 2H), 1.81 (br, 2H), 1.64 (br, 2H), 1.46–1.24 (m, 4H); UV-vis (MeOH): $\lambda_{\text{max}} = 442 \text{ nm}$.

6.7.2 Optical and electrochemical characterization data

Table S1: Cyclic voltammetry and UV-vis data (both in film) of the **P1–P3** ionic polythiophenes (and P3HT/PCDTBT under the same conditions).

Polymer	λ_{max} [nm] ^{a)}	$E_{\text{onset}}^{\text{ox}}$ [V]	$E_{\text{onset}}^{\text{red}}$ [V]	HOMO [eV]	LUMO ^{b)} [eV]	E_{g}^{EC} [eV]	E_{g}^{OP} [eV] ^{a)}
P1	482	0.34	-1.98	-5.20	-2.88 (-3.19) ^{c)}	2.32	2.01
P2	504	0.33	-1.91	-5.19	-2.95 (-3.25) ^{c)}	2.24	1.94
P3	504	0.10	-1.93	-4.96	-2.93 (-3.00) ^{c)}	2.03	1.96
P3HT^{d)}	519	0.27	-2.24	-5.13	-2.62 (-3.23) ^{c)}	2.51	1.90
PCDTBT	579	0.47	-1.63	-5.43	-3.33 (-3.57) ^{c)}	2.10	1.86

^{a)} In film (**P1–P3** from tetrafluoropropanol, P3HT from chlorobenzene, PCDTBT from chlorobenzene/dichlorobenzene 70/30); ^{b)} Based on the onset of reduction; ^{c)} Values between brackets are based on: LUMO = HOMO + E_{g}^{OP} ; ^{d)} $M_n = 2.5 \times 10^4$ g/mol, $D = 2.1$.

6.7.3 EQE and reflection measurements

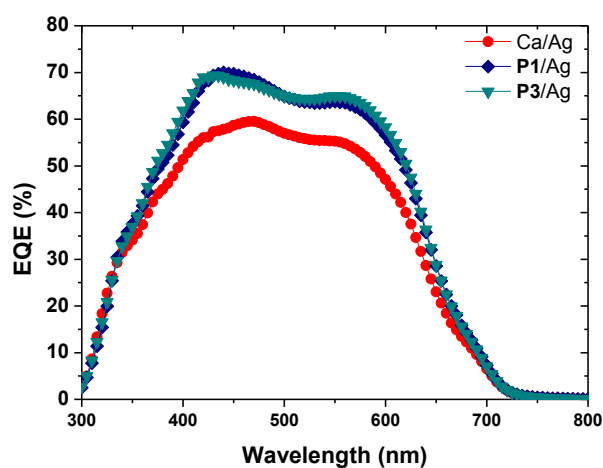


Figure S2: EQE spectra for devices containing the **P1** and **P3** CPEs (compared to a reference Ca/Ag device).^[3]

Table S2: Photovoltaic performance of PCDTBT-based BHJ solar cell devices with and without the addition of CPE layers, as applied for the EQE measurements.^{[3,4] a)}

Layer Sequence	Voc [V]	Jsc [mA cm ⁻²] ^{b)}	FF	Best η [%]	J _{EQE}
.../PCDTBT:PC ₇₁ BM/Ca/Ag	0.81	9.26	0.62	4.66	9.05
.../PCDTBT:PC ₇₁ BM/ P1 /Ag	0.87	10.2	0.65	5.79	10.6
.../PCDTBT:PC ₇₁ BM/ P3 /Ag	0.85	10.4	0.67	5.90	10.7

^{a)} Stack: glass/ITO/PEDOT-PSS/PCDTBT:PC₇₁BM/X/Ag with X = Ca or CPE.

^{b)} Uncorrected data.

[3] Due to the different facilities that were used to produce these devices and the slightly different solar cell stack (Ag instead of Al), non-optimized results were obtained.

[4] Global tilt ASTM G173-03 reference spectrum: <http://rredc.nrel.gov/solar/spectra/am1.5/>

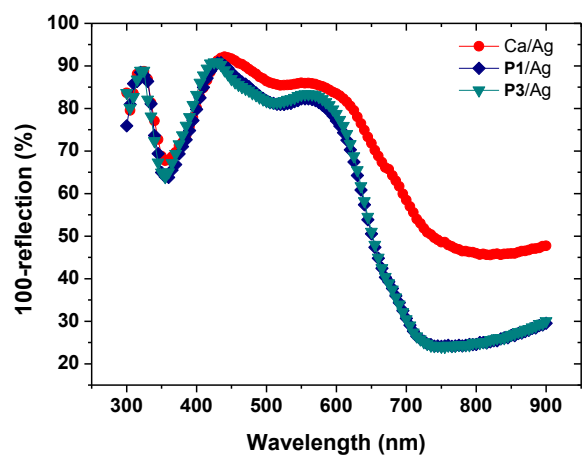


Figure S3: Reflectivity spectra for devices containing the **P1** and **P3** CPEs (compared to a reference Ca/Ag device).^[3]

6.7.4 J-V curves

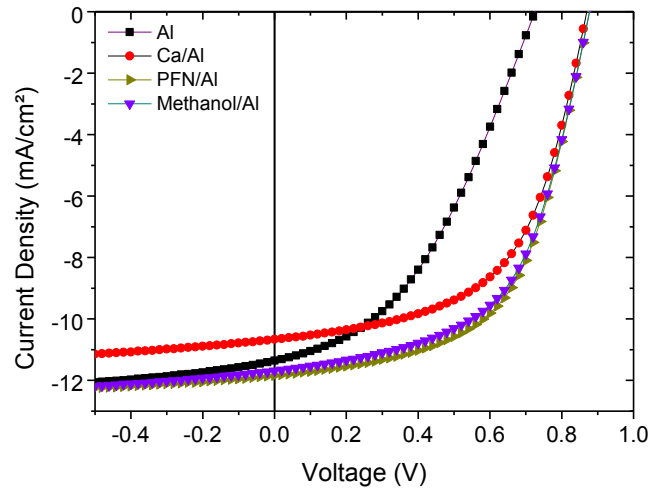


Figure S4: J-V curves under illumination of PCDTBT:PC₇₁BM BHJ photovoltaic devices with and without additional CPE layers.

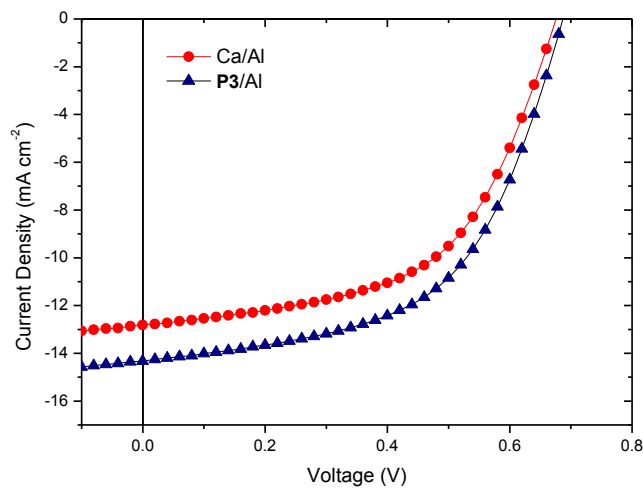


Figure S5: J-V curves under illumination of PCPDT-DTTzTz:PC₇₁BM BHJ photovoltaic devices with and without additional CPE layers.

6.7.5 Atomic force microscopy images

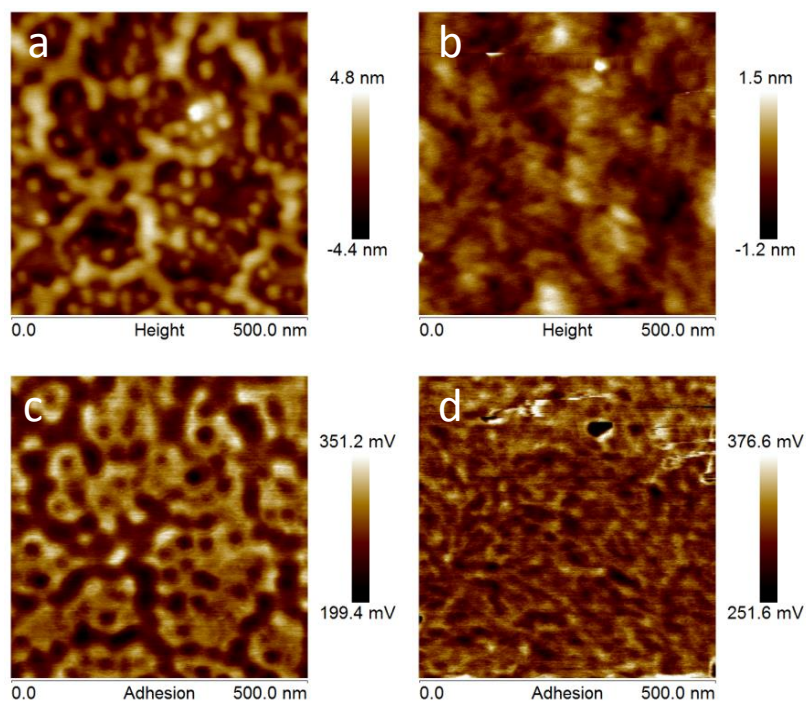


Figure S6: AFM (a,b: topography; c,d: adhesion) images (500x500 nm²) of layer stacks with and without additional CPE layer: a,c) PCDTBT:PC₇₁BM/P₂, b,d) PCDTBT:PC₇₁BM/MeOH.

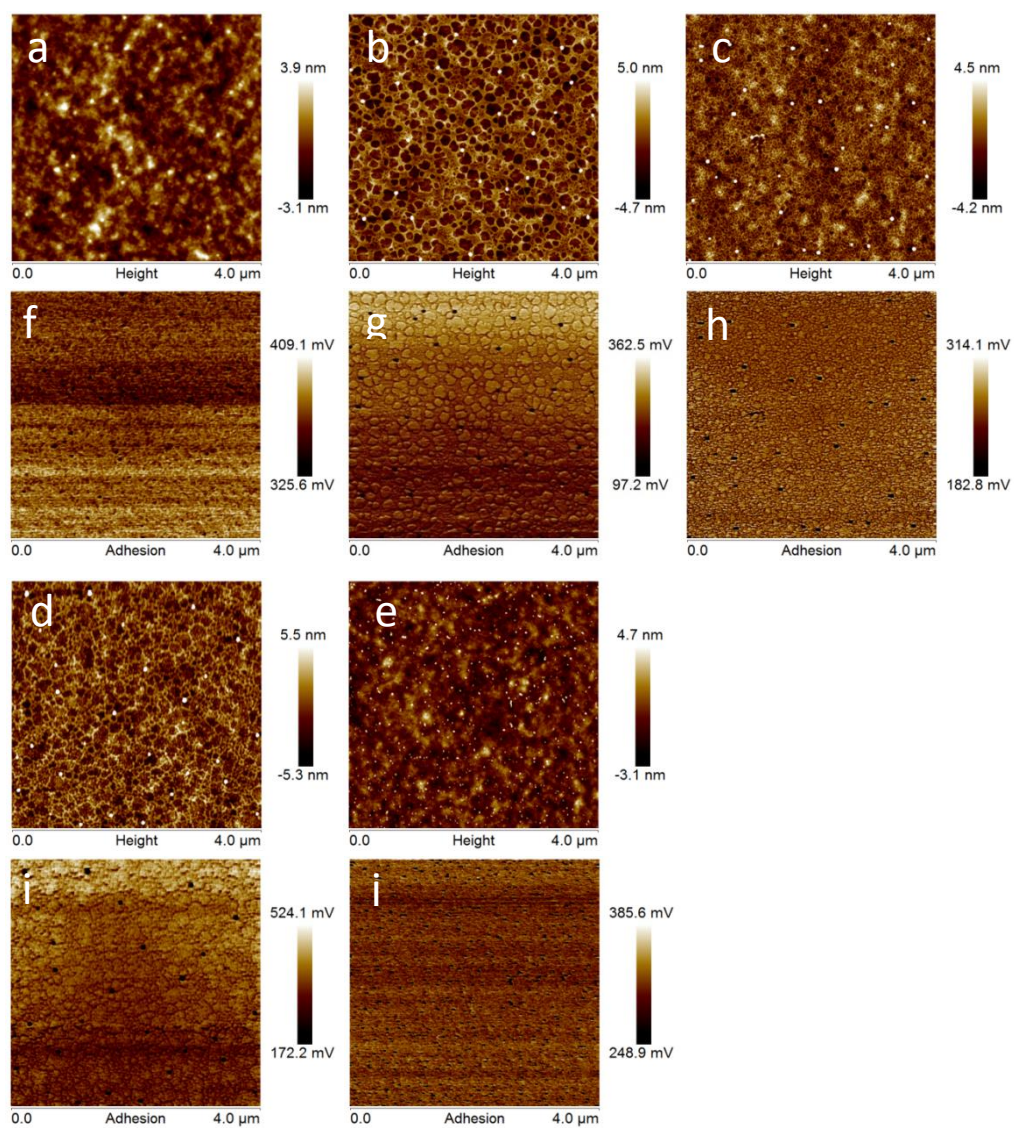
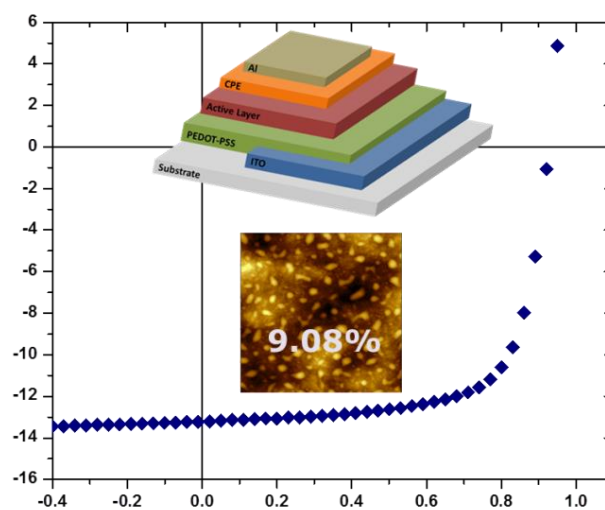


Figure S7: AFM (a-e: topography; f-j: adhesion) images ($4 \times 4 \mu\text{m}^2$) of layer stacks with and without additional CPE layers: a,f) PCDTBT:PC₇₁BM; b,g) PCDTBT:PC₇₁BM/**P1**; c,h) PCDTBT:PC₇₁BM/**P2**; d,i) PCDTBT:PC₇₁BM/**P3**; e,j) PDCTBT:PC₇₁BM/MeOH

Chapter 7

Exploring the Scope of Polythiophene-Based Conjugated Polyelectrolytes as Cathode Interlayer Materials for Polymer Solar Cells



J. Kesters, G. Pirotte, S. Govaerts, J. Drijkoningen, S. Clément, N. Van den Brande, B. Van Mele, L. Lutsen, D. Vanderzande, J. Manca, W. Maes, ...

7.1 INTRODUCTION

Organic photovoltaics (OPV) have demonstrated strong potential as renewable energy sources, adding appealing features to the classical solar cell technology, such as flexibility, light-weight, semi-transparency, and the potential for low-cost production.^[1] Polymer solar cells comprised of intimate blends of conjugated polymers and (methano)fullerenes have recently demonstrated power conversion efficiencies (PCE's) exceeding 10%, mainly through extensive structural optimization of the polymer donor material.^[2] Simultaneously, interface optimization through the use of dedicated interfacial layers has afforded significant enhancements of one or more of the *I-V* parameters. Conjugated polyelectrolytes (CPE's), conjugated polymers with substituents bearing ionic moieties, are frequently employed as cathodic or anodic interlayers, as the nature of the ionic side chains allows for processing from orthogonal solvents (often alcohols).^[3] One particular CPE material that stands out is PFN ($\{[9,9\text{-bis}(3'\text{-}N,N\text{-dimethylamino)propyl}]2,7\text{-fluorene}\}\text{-}alt\text{-}2,7\text{-(}9,9\text{-dioctylfluorene)}\}$), which is widely used as a powerful interfacial layer with a reported top efficiency of 9.2% when applied in an inverted solar cell in combination with PTB7:PC₇₁BM.^[2a] Apart from polymer-based interfaces, also alternative materials are considered, such as the non-conjugated PEIE (polyethylenimine ethoxylated) and small molecule porphyrin and C₆₀ derivatives.^[4-6]

The detailed working mechanism of these interlayers, in particular with respect to the structural properties of the employed materials, is not fully understood at this stage. The generally accepted understanding involves the formation of an

interfacial dipole, as analyzed through Kelvin probe force microscopy (KPFM) or ultraviolet photoelectron spectroscopy (UPS).^[3,5] By deposition of a charged species on top of a non-polar (active layer) or metallic (electrode) substrate, preferred orientation of the ionic moieties will result in a shift in the vacuum level.^[7] Other hypotheses comment the energy-level alignment at the organic/metal interface^[8] or active layer doping^[9]. Extensive investigation on the influence of different interlayer materials (on top of various substrates) was recently performed in the group of Janssen.^[10] The proposed mechanism involves the formation of an image charge, causing alterations in the work functions (as determined by KPFM). From these findings, a model was postulated involving the formation of dipoles depending on the ability of the charged constituents to move. Additionally, it was shown that the size of the counterion determined the extent to which the work function could be manipulated. No definite translations toward photovoltaic performances were made though.

In 2011, Bazan *et al.* reported on polythiophene-based interfacial materials with pendant trimethylammonium groups (P3TMAHT). In standard architecture solar cells based on PCDTBT:PC₇₁BM, a PCE of 6.3% was obtained (compared to 5.3% without interlayer).^[3d] In previous work, we have replaced the trimethylammonium end groups by imidazolium functionalities. Application of this material as cathodic interlayer in standard architecture PCDTBT:PC₇₁BM solar cells resulted in a PCE of 6.69%, a clear enhancement in comparison to the reference device (5.71%) and devices with P3TMAHT as interfacial layer (6.48%).^[11] In the present work, we have examined a broad array of potential cathode interlayer materials based on a common polythiophene backbone

decorated with different pendant side chains bearing various ionic end groups, as a possible means to analyze the effect of structural modifications. To this extent, we have investigated homopolymers containing imidazolium, pyridinium and phosphonium ionic species as well as a specific random (50/50) copolythiophene with triethylene glycol and imidazolium-substituted hexyl side chains (Figure 1).^[12] The corresponding counterions were limited to bromine and bis(trifluoromethylsulfonyl)imide (TFSI). As a donor polymer, PBDTTPD (poly[bis(2'-ethylhexyloxy)benzo[1,2-*b*:4,5-*b'*]dithiophene-*alt*-octylthieno[3,4-*c*]pyrrole-4,6-dione]) (Figure S1) was chosen, which, in combination with PC₇₁BM, has been reported to deliver PCE's up to 8.3%.^[2c,13]

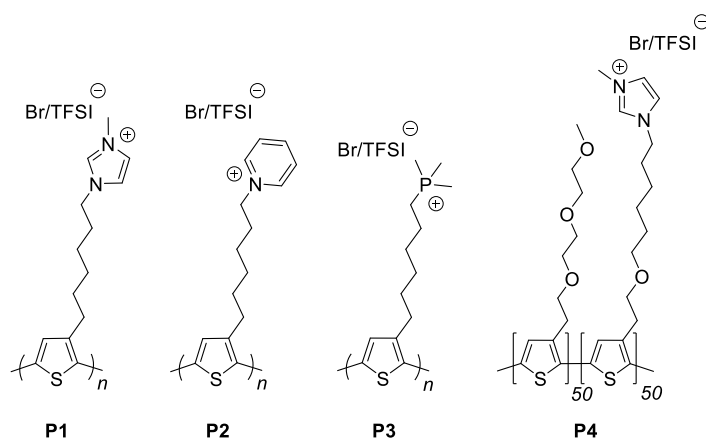


Figure 1: Chemical structures of the employed conjugated polythiophene-based polyelectrolytes **P1–P4**.

7.2 RESULTS AND DISCUSSION

Ionic (co)polythiophenes **P1–P4** were prepared according to previously reported procedures.^[12] Grignard metathesis (GMIM) polymerization was employed to prepare bromoalkyl-functionalized polythiophene precursors and

post-polymerization functionalization afforded the ionic derivatives. Finally, the bromine counter ions were exchanged for more hydrophobic TFSI ions to expand the structural diversity and avoid the hygroscopic features imposed by the Br⁻ ions (*vide infra*). Experimental data on the interlayer materials are gathered in the experimental section.

Prior to evaluation of the interlayer materials in organic solar devices, rapid heat-cool calorimetry (RHC) was performed on these materials, mainly aiming at the determination of the glass transition temperatures (T_g 's) (Figure 2, Figure S2 and Table S1). Exchanging the bromine ion for TFSI resulted in considerably lower T_g 's and a strong plasticizing effect was observed. As illustrated in Figure 2, the polythiophene-based polyelectrolytes containing bromine counter ions showed a strong hygroscopic behavior, indicated by the broad temperature range to remove residual water during the first heating in the RHC measurements. Considering the hypothesis on the vacuum level shift due to the formation of dipoles at the interface, the (unavoidable) presence of water risks to obscure underlying mechanisms, hindering comparison of the different interfacial materials. Therefore, it was decided to focus mainly on the CPE's containing TFSI counter ions, for which no hygroscopic behavior was observed (Figure 2).

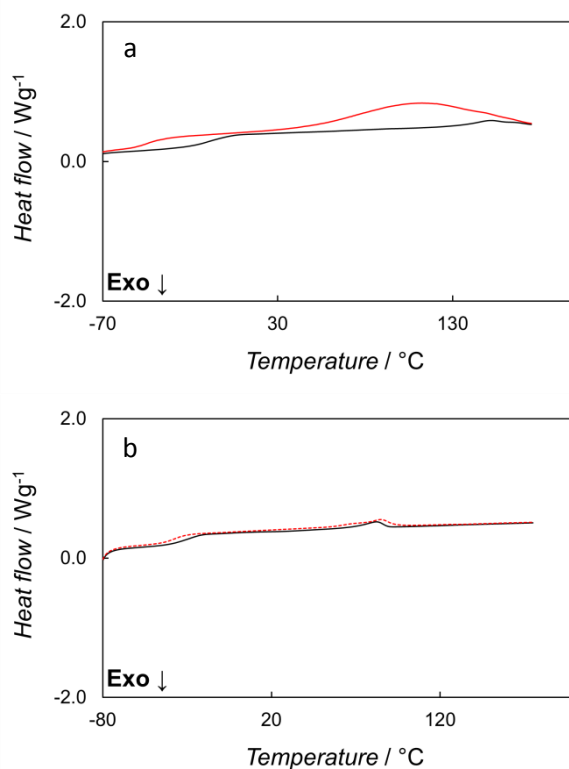


Figure 2: RHC measurements for **P4** with a) bromine and b) TFSI counter ions.

The red line corresponds to the 1st heating (demonstrating the hygroscopic behavior of the bromine containing CPE). The black line corresponds to the 2nd heating.

The PBDTPD copolymer (M_n : 43 kDa, D : 2.3) was prepared by Stille polycondensation, as previously reported by Beaujuge and co-workers.^[2c] To evaluate the different polythiophene-based interlayers, organic solar cells based on a standard architecture glass/ITO/PEDOT:PSS/PBDTPD:PC₇₁BM/interlayer/Al were prepared. For the photoactive layer (PAL), a total concentration of 10 mg/mL was utilized (1:1.5 polymer:PC₇₁BM ratio) and the reference device employed calcium instead of a CPE affording an average PCE of 7.32% (with a

top efficiency of 7.91%). Table 1 and Figure 3 show the improvements in photovoltaic performance of the polymer solar cells upon incorporation of the various cathode interlayers. The higher PCE's can mostly be ascribed to enhanced short-circuit currents (J_{sc}). Utilization of **P4** resulted in an additional small gain in fill factor (FF), consequently resulting in a top PCE of 9.08% (average 8.18%). The best performing material, **P4**, was also deposited on top of PCDTBT:PC₇₁BM (1:4 polymer:PC₇₁BM ratio), showing a similar rise in efficiency, but this time affecting all I - V parameters (Table 1). The lower PCE of these PCDTBT:PC₇₁BM devices in comparison to the values obtained in Chapter 6 are due to the use of a new (inferior) batch of PCDTBT.

Table 1: Photovoltaic performances of PBDTTPD:PC₇₁BM and PCDTBT:PC₇₁BM polymer solar cells with or without the incorporation of cathode interfacial layers.

PAL donor material	Interfacial material	Voc [V]	J_{sc} [mA/cm ²]	FF	Average η [%] ^{a)}	Best η [%]
PBDTTPD	Ca	0.92	11.28	0.71	7.32	7.91
PBDTTPD	P1	0.92	11.57	0.70	7.44	8.08
PBDTTPD	P2	0.93	12.12	0.70	7.90	8.53
PBDTTPD	P3	0.92	11.73	0.71	7.72	8.30
PBDTTPD	P4	0.92	12.26	0.72	8.18	9.08
PCDTBT	Ca	0.85	10.15	0.53	4.54	5.11
PCDTBT	P4	0.89	11.55	0.59	6.01	6.42

^{a)}Average efficiencies gathered over 16-20 devices.

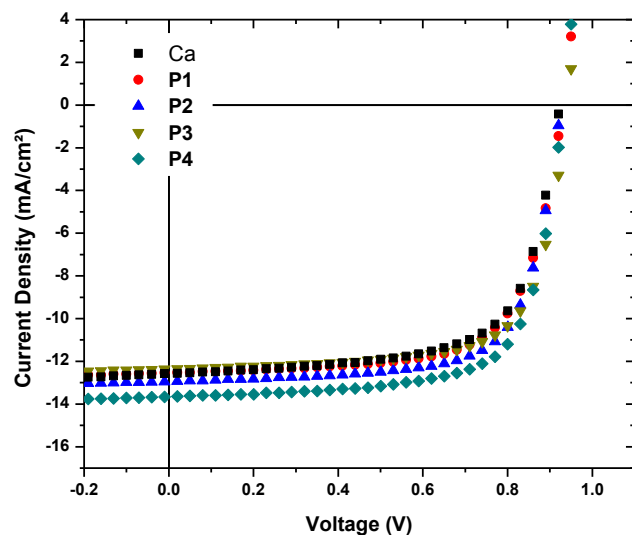


Figure 3: J - V curves for the best PBDTTPD:PC₇₁BM solar cell devices produced with and without interlayers **P1–P4**.

To investigate if the varying PCE enhancements are originating from differences in active layer coverage of the interfacial layers, atomic force microscopy (AFM) measurements were performed on the devices containing the CPE's spincoated on top of PBDTTPD:PC₇₁BM from solutions with the same concentration (0.25 mg/mL) in methanol (Figure 4). These images clearly indicate an incomplete coverage with the formation of stain-like structures on top of the PAL (adhesion images in Figure S3). **P4** shows a higher compatibility with the underlying active layer, as indicated by a slightly higher coverage and more homogeneously distributed domains, possibly related to the slight enhancement in FF and the top efficiency. Comparison with the AFM image of the device containing **P4** on top of PCDTBT:PC₇₁BM demonstrates a lower wettability of this interlayer material on top of PBDTTPD:PC₇₁BM, illustrating the strong dependence of the underlying active layer on the deposition of the interlayer material (Figure S4).

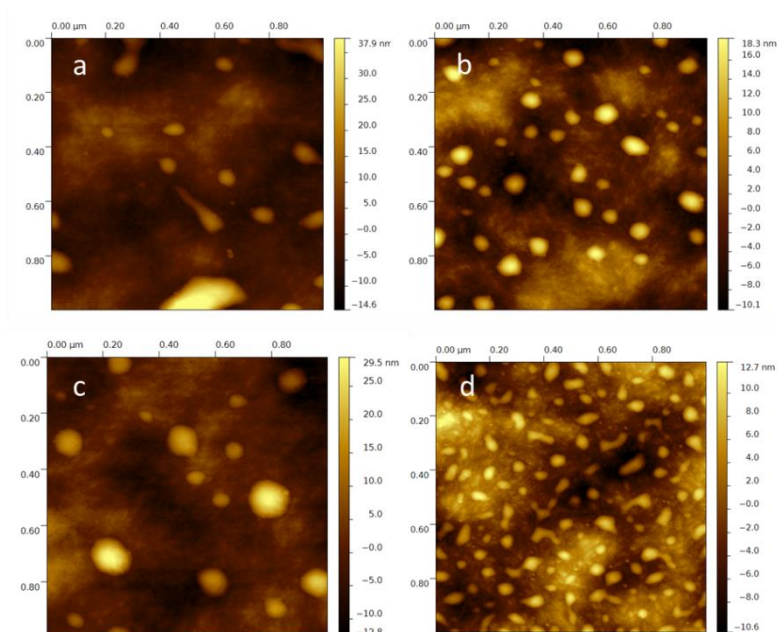


Figure 4: AFM topography images of the polymer solar cells (PBDTTPD:PC₇₁BM) based on a) **P1** b) **P2** c) **P3** d) **P4**.

Inspection of the dark curves for the devices based on **P4** on top of either PBDTTPD:PC₇₁BM or PCDTBT:PC₇₁BM reveals some indicative results toward the observed differences in the enhancement of the *I-V* parameters (Figure 5). Devices constructed with PBDTTPD:PC₇₁BM show little deviation in R_s and R_{sh} upon application of **P4**. In contrast, the PCDTBT:PC₇₁BM devices with **P4** exhibit a turn-on voltage of 1.2–1.3 V, while it is only 0.9–1.0 V for the reference device, implying that V_{bi} is enlarged upon insertion of **P4**. These differences are possibly linked with the obtained changes in V_{oc} and support the fact that a certain CPE interlayer will behave differently on various PAL's.

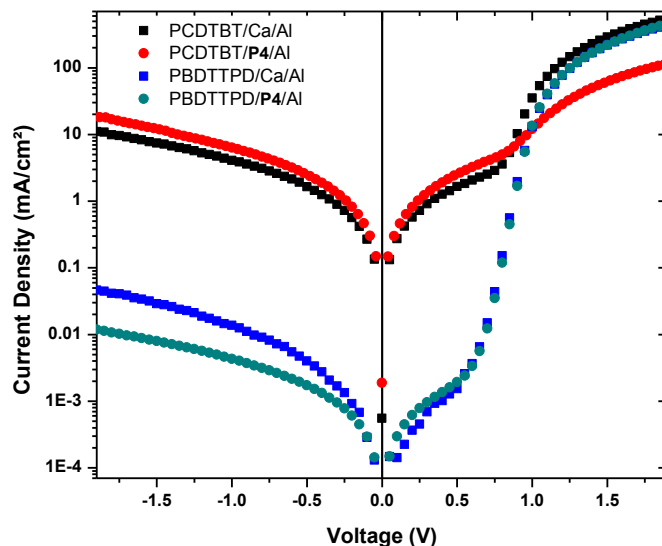


Figure 5: Dark curves of PCDTBT:PC₇₁BM and PBDTTPD:PC₇₁BM based polymer solar cells with and without **P4** as an interfacial layer.

7.3 CONCLUSIONS

In conclusion, we have demonstrated a considerable improvement in device performance upon insertion of various CPE interlayers. For PBDTTPD:PC₇₁BM devices, application of **P4** resulted in a significant gain in J_{sc} , affording a record efficiency of 9.08% for this photoactive material (in comparison to a top PCE of 7.91% for the reference device). A similar approach on PCDTBT:PC₇₁BM devices showed improvements in all I - V parameters, possibly linked to a difference in compatibility of the CPE material with the underlying photoactive layer, as indicated also by AFM imaging. Additionally, dark curve measurements revealed a difference in R_s when comparing the different polymer solar cells. Further investigation of alternative active layer material systems is required to establish

more insights into the working mechanism of specific interlayers on top of the different polymer:fullerene systems.

7.4 EXPERIMENTAL SECTION

Synthesis: The conjugated polyelectrolytes **P1–P3** (M_n : 40 kDa, D : 1.4) and **P4** (M_n : 29 kDa, D : 1.15) were prepared as previously reported.^[12] The active layer material PBDTTPD (M_n : 43 kDa, D : 2.3) was prepared by Stille polycondensation, according to a previously reported synthesis by Beaujuge and co-workers.^[2c] PCDTBT was purchased from SolarisChem (M_n : 79 kDa, D : 2.4) and used as received.

Device Fabrication: Bulk heterojunction polymer solar cells were constructed using the traditional glass/ITO/PEDOT:PSS/photoactive layer/Ca/Al architecture. To investigate the influence of the various CPE interlayers, Ca was replaced by a CPE. Prior to device processing, the indium tin oxide (ITO, Kintec, 100 nm, 20 Ohm/sq) covered glass substrates were cleaned using soap, demineralized water, acetone, isopropanol and a UV/O₃ treatment. In a following step, PEDOT:PSS [poly(3,4-ethylenedioxythiophene)-poly(styrenesulfonic acid), Heraeus Clevis] was deposited at a thickness of ~30 nm. Further processing was performed under nitrogen atmosphere in a glovebox, initialized with an annealing step at 130 °C for 15 min to remove any residual water. Consequently, blend solutions (PBDTTPD:PC₇₁BM or PCDTBT:PC₇₁BM) were spincoated on top of PEDOT:PSS. For PBDTTPD:PC₇₁BM, a ratio of 1:1.5 was utilized with a total concentration of 10 mg/mL, using a combination of chlorobenzene and 5 v/v% chloronaphthalene as a solvent. For PCDTBT:PC₇₁BM, an optimized blend ratio of 1:4 was prepared with a total concentration of 20

mg/mL, using 1,2-dichlorobenzene as a solvent. In a next step, the CPE materials, with a concentration of 0.25 mg/mL in methanol, were deposited on top of the active layer. Finally, the devices were finished off with Al (~80 nm) as a top electrode. In the case of the reference device, the top electrode consisted of Ca/Al, with thicknesses of 30 and 80 nm, respectively. This way, an active area of 3 mm² was obtained.

Device characterization: The PCE's of the polymer solar cells (employing CPE interlayers) were measured using a Newport class A solar simulator (model 91195A) calibrated with a silicon solar cell to give an AM 1.5g spectrum. AFM imaging was performed with a Bruker Multimode 8 AFM in PeakForce tapping mode, employing ScanAsyst. The images were produced with a silicon tip on a nitride lever with a spring constant of 4 N m⁻¹.

7.5 REFERENCES

- [1] a) Kippelen, B.; Brédas, J.-L. *Energy Environ. Sci.* **2009**, *2*, 251; b) Su, Y.; Lan, S.; Wei, K. *Mater. Today* **2012**, *15*, 554; c) Dou, L.; You, J.; Hong, Z.; Xu, Z.; Li, G.; Street, R. A.; Yang, Y. *Adv. Mater.* **2013**, *25*, 6642; d) Lizin, S.; Van Passel, S.; De Schepper, E.; Maes, W.; Lutsen, L.; Manca, J.; Vanderzande, D. *Energy Environ. Sci.* **2013**, *6*, 3136.
- [2] a) He, Z. C.; Zhong, C. M.; Su, S. J.; Xu, M.; Wu, H. B.; Cao, Y. *Nat. Photonics* **2012**, *6*, 591; b) Hendriks, K. H.; Heintges, G. H. L.; Gevaerts, S.; Wienk, M. M.; Janssen, R. A. J. *Angew. Chem. Int. Ed.* **2013**, *52*, 8341; c) Cabanetos, C.; Labban, A. E.; Bartelt, J. A.; Douglas, J. D.; Mateker, W. M.; Fréchet, J. M.; McGehee, M. D.; Beaujuge, P. M. *J. Am. Chem. Soc.* **2013**, *135*, 4656; d) Zhang, W.; Wu, Y.; Bao, Q.; Gao, F.; Fang, J. *Adv. Energy Mater.* **2014**, *4*, 1400359; e) Liu, Y.; Zhao, J.; Li, Z.; Mu, C.; Ma, W.; Hu, H.; Jiang, K.; Lin, H.; Ade, H.; Yan, H. *Nat. Commun.* **2014**, *5*, 5293.
- [3] a) Oh, S.-H.; Na, S.-I.; Jo, J.; Lim, B.; Vak, D.; Kim, D.-Y. *Adv. Funct. Mater.* **2010**, *20*, 1977; b) Huang, F.; Wu, H.; Cao, Y. *Chem. Soc. Rev.* **2010**, *39*, 2500; c) He, Z.; Zhong, C.; Huang, X.; Wong, W.-Y.; Wu, H.; Chen, L.; Su, S.; Cao, Y. *Adv. Mater.* **2011**, *23*, 4636; d) Seo, J. H.; Gutacker, A.; Sun, Y.; Wu, H.; Huang, F.; Cao, Y.; Scherf, U.; Heeger, A. J.; Bazan, G. C. *J. Am. Chem. Soc.* **2011**, *133*, 8416; e) Chen, L.; Xie, C.; Chen, Y. *Org. Electron.* **2013**, *14*, 1551; f) Liu, S.; Zhang, K.; Lu, J.; Zhang, J.; Yip, H.-L.; Huang, F.; Cao, Y. *J. Am. Chem. Soc.* **2013**, *135*, 15326; g) Lee, B. H.; Jung, I. H.; Woo, H. Y.; Shim, H.-K.; Kim, G.; Lee, K. *Adv. Funct. Mater.* **2014**, *24*, 1100.

[4] a) Zhou, Y. H.; Fuentes-Hernandez, C.; Shim, J.; Meyer, J.; Giordano, A. J.; Li, H.; Winget, P.; Papadopoulos, T.; Cheun, H.; Kim, H.; Fenoll, M.; Dindar, A.; Haske, W.; Najafabadi, E.; Khan, T. M.; Sojoudi, H.; Barlow, S.; Graham, S.; Brédas, J. L.; Marder, S. R.; Kahn, A.; Kippelen, B. *Science* **2012**, *336*, 327; b) Li, P.; Wang, G.; Cai, L.; Ding, B.; Zhou, D.; Hu, Y.; Zhang, Y.; Xiang, J.; Wan, K.; Chen, L.; Alameh, K.; Song, Q. *Phys. Chem. Chem. Phys.* **2014**, *16*, 23792.

[5] a) Vasilopoulou, M.; Georgiadou, D. G.; Douvas, A. M.; Soultati, A.; Constantoudis, V.; Davazoglou, D.; Gardelis, S.; Palilis, L. C.; Fakis, M.; Kennou, S.; Lazarides, T.; Coutsolelos, A. G.; Argitis, P. *J. Mater. Chem. A* **2014**, *2*, 182; b) Vasilopoulou, M.; Douvas, A. M.; Georgiadou, D. G.; Constantoudis, V.; Davazoglou, D.; Kennou, S.; Palilis, L. C.; Daphnomili, D.; Coutsolelos, A. G.; Argitis, P. *Nano Research* **2014**, *7*, 679.

[6] a) O'Malley, K. M.; Li, C.-Z.; Yip, H.-L.; Jen, A. K.-Y. *Adv. Energy Mater.* **2012**, *2*, 82; b) Duan, C.; Zhong, C.; Liu, C.; Huang, F.; Cao, Y. *Chem. Mater.* **2012**, *24*, 1682.

[7] a) Seo, J. H.; Nguyen, T.-Q. *J. Am. Chem. Soc.* **2008**, *130*, 10042; b) Seo, J. H.; Yang, R.; Brzezinski, J. Z.; Walker, B.; Bazan, G. C.; Nguyen, T.-Q. *Adv. Mater.* **2009**, *21*, 1006

[8] a) Ishii, H.; Sugiyama, K.; Ito, E.; Seki, K. *Adv. Mater.* **1999**, *11*, 605; b) Braun, S.; Salaneck, W. R.; Fahlman, M. *Adv. Mater.* **2009**, *21*, 1450.

[9] Li, C.-Z.; Chueh, C.-C.; Ding, F.; Yip, H.-L.; Liang, P.-W.; Li, X.; Jen, A. K.-Y. *Adv. Mater.* **2013**, *25*, 4425.

[10] van Reenen, S.; Kouijzer, S.; Janssen, R. A. J.; Wienk, M. M.; Kemerink, M. *Adv. Mater. Interfaces* **2014**, 1400189.

[11] Kesters, J.; Ghoo, T.; Penxten, H.; Drijkoningen, J.; Vangerven, T.; Lyons, D. M.; Verreert, B.; Aernouts, T.; Lutsen, L.; Vanderzande, D.; Manca, J.; Maes, W. *Adv. Energy Mater.* **2013**, 3, 1180.

[12] a) Rubio-Magnieto, J.; Thomas, A.; Richeter, S.; Mehdi, A.; Dubois, P.; Lazzaroni, R.; Clément, S.; Surin, M. *Chem. Commun.* **2013**, 49, 5483; b) Ghoo, T.; Brassinne, J.; Fustin, C.-A.; Gohy, J.-F.; Defour, M.; Van den Brande, N.; Van Mele, B.; Lutsen, L.; Vanderzande, D. J.; Maes, W. *Polymer* **2013**, 54, 6293; c) Ghoo, T.; Malinkiewicz, O.; Conings, B.; Manca, J.; Lutsen, L.; Vanderzande, D.; Bolink, H. J.; Maes, W. *RSC Adv.* **2013**, 3, 25197; d) Ghoo, T.; Van den Brande, N.; Defour, M.; Brassinne, J.; Fustin, C.-A.; Gohy, J.-F.; Hoepfener, S.; Schubert, U. S.; Vanormelingen, W.; Lutsen, L.; Vanderzande, D. J.; Van Mele, B.; Maes, W. *Eur. Polym. J.* **2014**, 53, 206.

[13] Bartelt, J. A.; Douglas, J. D.; Mateker, W. R.; El Labban, A.; Tassone, C. J.; Toney, M. F.; Fréchet, J. M. J.; Beaujuge, P. M.; McGehee, M. D. *Adv. Energy Mater.* **2014**, 4, 1301733.

7.6 SUPPORTING INFORMATION

7.6.1 Chemical structure of donor polymer

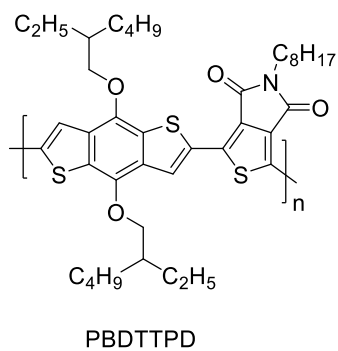


Figure S1: Chemical structure of the donor polymer material PBDTTPD.

7.6.2 Thermal analysis

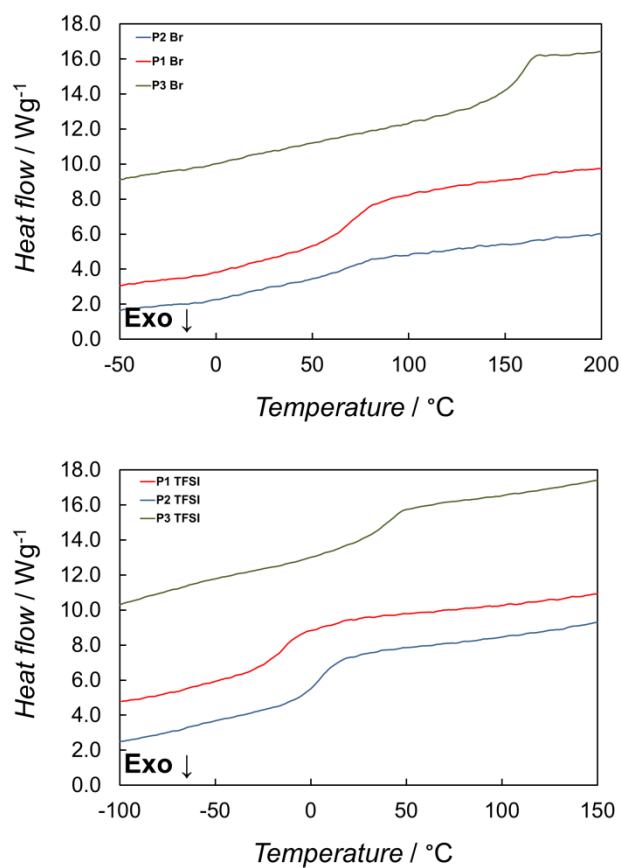


Figure S2: Rapid heat-cool calorimetry heating profiles for **P1–P3**, revealing a lowering of the T_g upon exchange of the bromine for a TFSI counter ion.

Table S1: Glass transition temperatures for the ionic (co)polythiophenes **P1–P4** with either a bromine or a TFSI counter ion.

Conjugated polythiophene	Counter ion	T_g (°C)
P1	Br	63
P1	TFSI	-14
P2	Br	87
P2	TFSI	6
P3	Br	154
P3	TFSI	39
P4	Br	-11
P4	TFSI	-29

7.6.3 Additional atomic force microscopy images

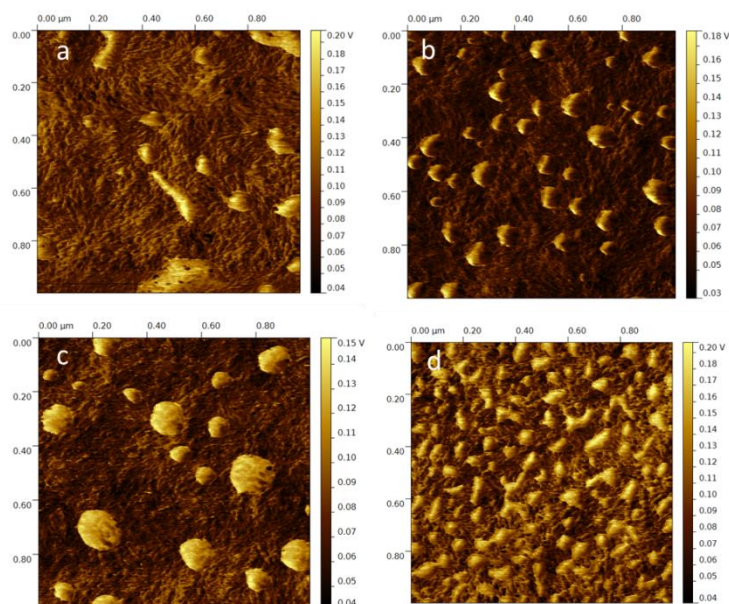


Figure S3: AFM adhesion images of **P1–P4** showing the difference in coverage of the various ionic copolythiophene interlayers after deposition on PBDTTPD:PC₇₁BM

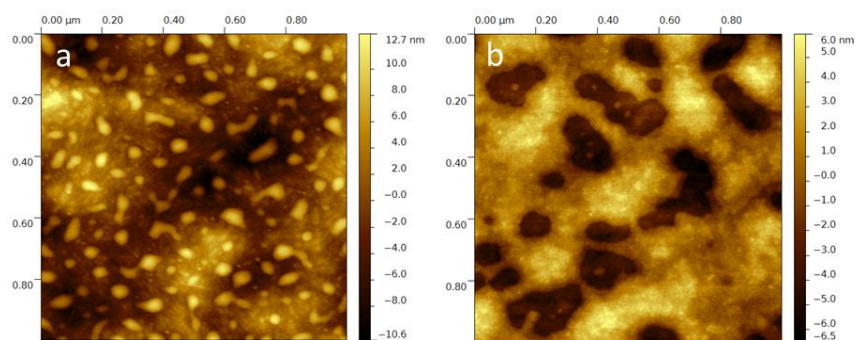
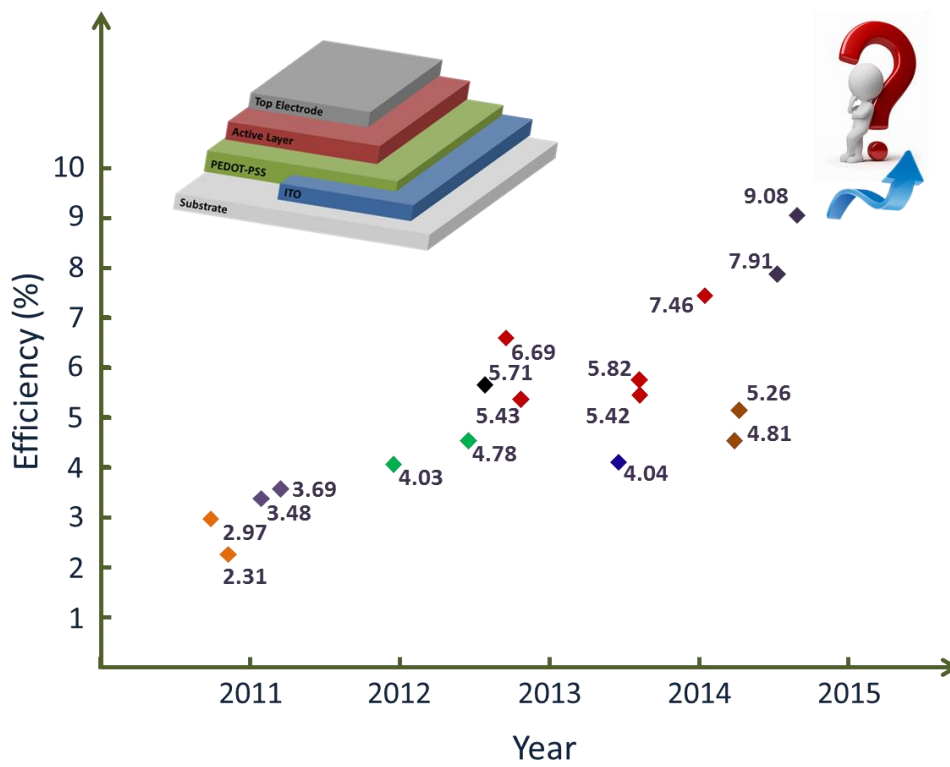


Figure S4: AFM topography images of **P4** on top of a) PBDTTPD:PC₇₁BM and b) PCDTBT:PC₇₁BM.

Chapter 8

Summary and Outlook



8.1 SUMMARY

Organic photovoltaics (OPV) have seen a strong growth over the past decade, attracting researchers worldwide by their appealing features such as flexibility, transparency, light-weight, and the ability to fine-tune the color. This aesthetically attractive nature inspires for instance building, automotive and textile integration. However, device efficiency, stability and production cost are key parameters that need to be addressed further to enable a successful commercialization of this thin film PV technology. In this thesis we have worked on the optimization of two of these parameters, i.e. efficiency and stability, through the design and development of specific conjugated polymers and their evaluation in bulk heterojunction polymer solar cells.

In first instance, we have focused on the stability aspect and demonstrated the enhanced thermal durability of P3AT:PC₆₁BM solar cell devices through the implementation of side chain functionalization (ester, alcohol, cinnamoyl). Even though polythiophenes have been outperformed by low bandgap push-pull conjugated polymers, they provided an ideal test-case to investigate the side chain strategy. Upon exposure of the devices to a continuous stress of 85 °C for 700 hours, it was shown that the solar cells based on the functionalized P3AT materials exerted only a small reduction in PCE, whereas the reference P3HT:PC₆₁BM device only maintained 35% of its initial performance. This large difference could be attributed to changes in the (nano)morphology of the blends. Transmission electron microscopy (TEM) revealed the formation of microcrystalline structures for the reference device, assigned to PC₆₁BM-rich

domains. Through the presence of the functional side chains, enlarged resistivity against this phase separation phenomenon resulted in more durable devices.

In a next step, this strategy was extended to a particular low bandgap copolymer, PCPDTBT. Thermal analysis of the functionalized (alcohol, ester) PCPDTBT materials revealed inherently higher T_g 's, strongly reducing the phase separation tendency. Possible degradation upon thermal stress hence had to originate from different processes. Once again, more stable photovoltaic devices were procured for the functionalized copolymers, with PCE's up to 55% of the starting value after exposure to a temperature of 85 °C for 650 hours, whereas the performance of the reference device lowered to 26%. The degradation profile was characterized by a strong initial (burn-in) decay, followed by a more linear regime. Through deconvolution of the various degradation pathways, it was found that upon insertion of an alcohol or ester function, a higher resistivity toward reduced interface (active layer–top electrode) quality could be obtained.

In a second part of the thesis, we have focused on the improvement of the photovoltaic performance by dedicated material design. More specifically, work was done on particular low bandgap donor copolymers. As the electron-rich component, dithieno[3,2-*b*;2',3'-*d*]pyrrole (DTP) has been moderately successful, with a recently reported OPV performance up to 4.8%. However, the maximum obtainable V_{oc} is limited when using standard N-alkylated DTP derivatives. To overcome this issue, we have employed DTP N-acylation. Through linkage with the strongly electron accepting TPD unit, a PDTTPD:PC₇₁BM polymer solar cell with a record V_{oc} of 0.8 V was obtained, with a corresponding PCE of 4.0%. Upon insertion of a specific conjugated polyelectrolyte interlayer, the performance could be enhanced further to 5.8%.

The same N-acylated DTP was then also combined with quinoxaline acceptor units. This building block was chosen for its ability to allow the incorporation of additional fluorine atoms. In this way, a PCE of 4.81% was obtained (with a Voc of 0.67 V) for a BHJ PDTPQx:PC₇₁BM polymer solar cell. Unfortunately, the fluorination strategy was not really successful. By atomic force microscopy (AFM) imaging it was shown that fluorination of the polymer promotes the formation of (PC₇₁BM-rich) domains in the photoactive layers during film formation.

In the final part of this work, a different approach was investigated toward organic solar cell optimization through the implementation of conjugated polyelectrolyte (CPE) (cathodic) interlayers between the photoactive layer and the top electrode. Ionic polythiophene based materials were used to replace calcium, which is sensitive to oxidation, and they simultaneously enhanced the photovoltaic performance. When applied between PCDTBT:PC₇₁BM and Al, the device performance increased from 5.71% (for a reference device employing Ca/Al) to 6.69%. This enhancement was found to be due to a lowering of the series resistance, facilitating electron injection. Similarly, when applied on top of PCPDT-DTTzTz:PC₇₁BM, an increase from 4.78 to 5.43% was observed.

In a similar approach, a set of different CPE (cathodic) interlayers was applied in PBDTTPD:PC₇₁BM devices and their influence on the photovoltaic performance was investigated. One specific CPE material performed really well, affording devices with a PCE of 9.08% (7.91% reference device), a record efficiency for this photoactive material. Application of the same CPE on top of PCDTBT:PC₇₁BM, however, revealed different results in respect to the *I-V* parameters. For PBDTTPD:PC₇₁BM devices, the increased performance originated

mainly from a gain in J_{sc} , whereas for the PCDTBT:PC₇₁BM system, all parameters (V_{oc} , J_{sc} , FF) showed improvement upon insertion of the CPE interlayer. By AFM imaging, a difference in compatibility of the ionic (co)polythiophene and the different underlying polymer:fullerene active layers was observed.

8.2 OUTLOOK

In this work we have focused on three major aspects of high relevance in the OPV field, i.e. (i) the (thermal) stability of bulk heterojunction organic solar cells, (ii) active layer material development and (iii) interface engineering for improved photovoltaic performance. In this section, some recommendations for further research are postulated.

8.2.1 Stability

In Chapters 2 and 3, we have demonstrated the positive influence of the incorporation of functional moieties on the thermal durability of both P3HT- and PCPDTBT-based polymer solar cells. However, the approach remained limited to rather low performance polymer materials and a logical recommendation for future work would involve the translation to higher efficiency materials. It was shown that this side chain strategy has a minor influence on the power conversion efficiency, whenever the built-in ratio is sufficiently low, therefore proving to be a powerful and versatile tool for more (thermally) stable (yet efficient) OPV devices.

For P3HT (which exhibits a rather low T_g), we observed hindered diffusion of PC₆₁BM to form microcrystals upon incorporation of functional side chain

moieties. On the other hand, the major impact for PCPDTBT (due to the higher T_g) was found at the active layer–top electrode interface. It would be interesting to study a material set with a larger distinction in T_g 's, allowing the simultaneous investigation of both phase separation and interface degradation. To this extent, recent work on difluorinated PCPDTQx low bandgap copolymers with different amounts of alkyl side chains revealed a large increase in T_g upon removal of the side chains. Polymers containing 100, 50 or 0% of side chains on the Qx building block exhibited T_g 's of 65 (and 170), 135 and 175 °C, respectively, and initial thermal degradation studies at 85 °C revealed a lowered tendency for phase separation for the higher- T_g materials. In combination with the incorporation of functional side chains on the CPDT component, this material set could provide further valuable information on the routes to follow toward improved thermal stability of polymer solar cells.

With recent observations pointing to the formation of light-induced charge traps at the interface (with a lowering of the V_{oc} as a consequence), further exploration of the photostability of either the interfaces or the photoactive layer (materials) of organic solar cell devices is certainly also worthwhile and complementary to the thermal stability studies done so far. In this respect, collaborations with expert groups on photostability should be established.

As mentioned before, the introduction of CPE interlayers is a viable tool to boost the performance of photovoltaic cells. However, the longterm stability of the solar cells constructed with CPE interlayers is a topic yet to be investigated. Such efforts can possibly also provide additional insights into the working principle of these interlayers as well as on the specific degradation mechanisms occurring at the active layer–top electrode interface.

8.2.2. Material development

Apart from synthesizing new high-performance materials for organic photovoltaic applications, the fine-tuning of existing semiconducting materials is an alternative versatile strategy toward high-efficiency solar cell devices. Two examples were demonstrated in this PhD dissertation. DTP N-acylation was applied to improve the V_{oc} of DTP-based polymer solar cells and this approach was extended by fluorination of the second (Qx) building block, a common practice to enhance the V_{oc} of organic solar cells. However, upon fluorination of the low bandgap copolymers, the active layer films exhibited aggregated domains (possibly induced by the fluorophobicity of the fullerene component), decreasing the donor-acceptor interfacial area and consequently limiting the obtainable J_{sc} and PCE. A possible approach to solve this issue involves fine-tuning of the side chains of the polymer materials. Reducing the density of side chains on the quinoxaline monomer of a difluorinated PCPDTQx copolymer has already been shown to provide much more homogeneous donor-acceptor distributions, as observed by AFM and TEM. Despite a significant improvement in active layer morphology, the impact on the PCE was rather limited though. It would be worthwhile to investigate alternative side chain patterns, enhancing the stacking properties of the polymer materials and granting better performing solar cells. Upon altering the side chains, it would be preferable to bear in mind the consequences for the (thermal and photo) stability of the devices as well.

8.3.3 Interface engineering

Optimization of the active layer–electrode interfaces has become an important topic during the past years. Through incorporation of suitable interlayer materials, often conjugated polyelectrolytes, enhanced electron injection (hole

blocking) can be induced and improvements in the photovoltaic response can be achieved. However, as most research groups focus on one particular type of interlayer material, the basic knowledge on their working mechanism and the structural influence on solar cell performance remains limited. To gain a more thorough understanding, a more diverse pallet of interlayer materials (e.g. low bandgap copolymer based CPE's with a variety of counter ions) would be beneficial. Moreover, considering the quickly rising popularity of perovskite based solar cells, one can easily envision the possibilities when translating the interlayer approach – optimizing both electron and hole extraction – to these types of hybrid photovoltaics.

8.3 NEDERLANDSE SAMENVATTING

De technologie van de organische zonnecellen heeft de afgelopen jaren een sterke vooruitgang geboekt, gedreven door een aantal aantrekkelijke karakteristieken zoals flexibiliteit, transparantie, de mogelijkheid tot afstemming van de kleur en een gering gewicht. Daarnaast kunnen ze door middel van allerhande depositietechnieken in verschillende maten en vormen geproduceerd worden, waardoor ze een (esthetische) meerwaarde kunnen bieden bij integratie in bv. energie-neutrale gebouwen, auto's en textiel. Desalniettemin zijn er drie belangrijke voorwaarden waaraan de technologie moet voldoen om commercieel succesvol te kunnen zijn, nl. hoge efficiëntie, lange levensduur en geringe productiekost. Met het oog op deze doelstellingen hebben we ons in deze thesis gericht op twee van deze aspecten, efficiëntie en stabiliteit, door middel van de ontwikkeling van specifieke geconjugeerde polymeren en hun toepassing in bulk heterojunctie polymere zonnecellen.

In een eerste fase hebben we ons toegelegd op de (thermische) stabiliteit van organische zonnecellen door middel van de invoer van specifieke functionele groepen (ester, alcohol, cinnamoyl) op de zijketens van poly(3-alkylthiofenen). Op deze manier hebben we kunnen vaststellen dat, na blootstelling aan een temperatuur van 85 °C gedurende 700 uur, de zonnecellen op basis van gefunctionaliseerde polythiofenen slechts een kleine daling vertoonden in efficiëntie, terwijl de referentiestalen aanzienlijk sneller degradeerden. Met behulp van *transmission electron microscopy* (TEM) kon aangetoond worden dat de grootste veranderingen plaatsvonden in de (nano)morfologie van de fotoactieve laag. Het referentiedevice vertoonde microkristallijne structuren, die

toegeschreven konden worden aan (lokale hogere concentraties van) PC₆₁BM. Door het invoeren van de functionele groepen verkregen de zonnecellen een grotere weerstand tegen deze (nefaste) fasescheiding, hetgeen bijgevolg resulteerde in stabielere devices.

Een volgende (logische) stap was dan de vertaling van deze strategie naar *low bandgap* polymeren, meer specifiek PCPDTBT. Na synthese van de alcohol- en estergerfunctionaliseerde copolymeren bleek dat deze materialen een verhoogde T_g vertoonden. Daardoor zal fasescheiding veel moeilijker (d.w.z. bij veel hogere temperatuur) plaatsvinden en de degradatie onder invloed van de temperatuur dient dus toegeschreven te worden aan andere degradatieprocessen. Net zoals voor het P3HT:PC₆₁BM systeem konden stabielere fofovoltaïsche cellen bekomen worden voor de gefunctionaliseerde PCPDTBT's, met efficiënties tot 55% van de startwaarden na blootstelling aan een temperatuur van 85 °C voor 650 uur. Tijdens dezelfde periode verminderde de efficiëntie van de referentiecel (op basis van ongesubstitueerd PCPDTBT) tot slechts 26% van de initiële waarde. Het degradatieprofiel vertoonde een sterk initieel verval gedurende de eerst 40–50 uren, gevolgd door een meer lineair regime voor de rest van het experiment. Een meer gedetailleerd beeld kon verkregen worden door het ontleden van de verschillende zonnecelparameters. Hieruit bleek dat de weerstand ten opzigt van degradatie van de interfase tussen de actieve laag en de top-elektrode verhoogd werd door het gebruik van de gefunctionaliseerde polymeren.

Het tweede deel van deze thesis handelde over de verbetering van de zonnecelkarakteristieken door middel van specifiek ontworpen donorpolymeren. Uit literatuuronderzoek bleek dat polymere zonnecellen op basis van N-

gealkyleerde dithiëno[3,2-*b*;2',3'-*d*]pyrrolen (DTP's) (als elektronenrijke bouwstenen voor low bandgap copolymeren) zonnecefficiënties gaven tot 2.8%. Het voornaamste probleem bij het gebruik van N-gealkyleerd DTP is de gelimiteerde openklemspanning (V_{oc} waarden rond 0.5 V) van de resulterende polymere zonnecellen. Om dit te verbeteren werd overgeschakeld op N-geacyleerde DTP varianten, hetgeen resulteerde in een V_{oc} van 0.8 V wanneer deze component gecombineerd werd met TPD (thiëno[3,4-*c*]pyrrool-4,6-dion) als elektronenarme bouwsteen. In een standaard polymeer:fullereen-zonnecel gaf dit vervolgens een efficiëntie van 4.0%, en door toevoeging van een geconjugeerde polyelektroliet-interlaag kon de efficiëntie opgevoerd worden tot 5.8%. In tweede instantie werd N-geacyleerd DTP ook gecombineerd met quinoxaline, waarop ook één of twee fluoratomen geïntroduceerd konden worden. Op deze manier kon een zonnecefficiëntie van 4.8% bekomen worden (met een V_{oc} van 0.67 V) op basis van het niet-gefluoreerde PDTPQx-polymeer. Jammer genoeg kon de efficiëntie niet verder verhoogd worden voor de gefluoreerde derivaten. Met behulp van *atomic force microscopy* (AFM) kon worden aangetoond dat de fluorering leidde tot de vorming van aparte domeinen in de fotoactieve laag, een fenomeen dat niet kon worden verholpen, ondanks de intensieve optimalisatiepogingen.

In het laatste deel van de thesis hebben we een alternatieve strategie onderzocht om de efficiëntie van organische zonnecellen te verbeteren, nl. via de implementatie van specifieke kathode-interlagen gebaseerd op polythiofeen. Deze geconjugeerde polyelektrolieten werden afgezet uit methanol bovenop de actieve laag, ter vervanging van het snel oxiderende calcium, en zorgden voor een aanzienlijke verhoging van de efficiëntie. Wanneer ze toegepast werden

tussen PCDTBT:PC₇₁BM en aluminium kon de zonneefficiëntie verhoogd worden tot 6.69% (in vergelijking met 5.71% voor Ca/Al). Deze verbetering werd gerealiseerd door een verlaging van de serieweerstand, wat op zijn beurt aanleiding gaf tot een gemakkelijker injectie van elektronen. Op dezelfde manier werd deze interlaag ook toegepast op een fotoactieve laag bestaande uit PCPDT-DTTzTz en PC₇₁BM, hetgeen aanleiding gaf tot een vergelijkbare efficiëntieverhoging van 4.78 naar 5.43%.

In een volgende stap hebben we een reeks verschillende kathode-interlagen onderzocht in zonnecellen gebaseerd op PBDTPD:PC₇₁BM. De invloed van de verschillende interlagen was voornamelijk zichtbaar in de J_{sc} en voor één van deze materialen werd een efficiëntieverhoging van 7.91 naar 9.08% bekomen, hetgeen een recordwaarde is voor dit materiaal. Toepassing van deze interlaag op het PCDTBT:PC₇₁BM systeem gaf aanleiding tot een verschillend gedrag in, met name een verbetering van alle $I-V$ parameters. Met behulp van AFM kon ook een verschil in compatibiliteit worden aangetoond tussen de interlaag en de verschillende polymeer:fullereen actieve lagen.

